The Dissertation Committee for Laura Michelle Ricles Certifies that this is the approved version of the following dissertation:

Investigating Mesenchymal Stem Cell Therapy for Ischemic Repair

Committee:

Laura J. Suggs, Co-Supervisor

Stanislav Y. Emelianov, Co-Supervisor

Aaron B. Baker

Roger P. Farrar

Janeta Zoldan

Investigating Mesenchymal Stem Cell Therapy for Ischemic Repair

by

Laura Michelle Ricles, B.S.

Dissertation

Presented to the Faculty of the Graduate School of

The University of Texas at Austin

in Partial Fulfillment

of the Requirements

for the Degree of

Doctor of Philosophy

The University of Texas at Austin

August 2014

Dedication

To my family, for their never-ending love, support, and encouragement.

Acknowledgements

I sincerely thank my advisors, Dr. Laura Suggs and Dr. Stanislav Emelianov, for their guidance and support during my PhD. Without your mentorship and advice, none of this would have been possible. You were instrumental in my growth as a researcher and scientist, and provided me with invaluable skills for the future. I would also like to thank my committee members who were a tremendous help during my graduate career by providing advice and access to their lab equipment: Dr. Aaron Baker, Dr. Roger Farrar, and Dr. Janeta Zoldan.

I had the privilege of collaborating with many wonderful people during my graduate study and I am very grateful to my colleagues and labmates for providing insightful discussions and moral support. I would especially like to thank my co-workers: Pei-Ling Hsieh, Dr. Seung Yun Nam, and Dr. Eunna Chung. Pei-Ling was extremely helpful with the *in vivo* experiments and helping me learn animal surgeries. Seung Yun was one of the first people I met at UT and we started our journey together into the field of stem cell research. It has been a wonderful experience working with you and I appreciate your friendship and willingness to always give a lending hand. I would especially like to thank Eunna for all of her wonderful advice and her cheerful and upbeat attitude that she brought to the lab every day, even when we had to work on the weekends. You were a great co-worker, mentor, and friend. I truly appreciate your guidance and support, both professionally and personally, and I am so glad we were able to share our experience at UT together. I am also thankful to the wonderful undergraduate students who I had the opportunity to work with, including Elda Treviño, Noah Kopcho, Esteban Esquivel, and Ally Willauer.

I would also like to thank several facilities and staff members at UT for their assistance: Dwight Romanovicz and Richard Salinas in the Microscopy and Imaging Facility of the Institute for Cellular and Molecular Biology, the Holcombe Laboratory in the Department of Chemistry and Biochemistry, Nathan Miller in the Quadropole ICP-MS Laboratory in the Jackson School of Geosciences, and the Center for Nano- and Molecular Science.

Finally, I would like to express my love and appreciation to my family for their unending support. My mom has always been there for me to offer an empathetic ear and encourage me to pursue my dreams, no matter how big or small or where they might take me. My dad inspired me to go into science and it was through his example that I learned to always strive to be my best. Both of my parents instilled in me the importance of hard work and higher education. My brother, Jason, and sisters, Victoria and Hannah, entertained me with their never-ending questions about my research and always had the ability to make me laugh, even on my toughest days. I am truly grateful for all of your support during this journey.

Investigating Mesenchymal Stem Cell Therapy for Ischemic Repair

Laura Michelle Ricles, Ph.D.

The University of Texas at Austin, 2014

Supervisors: Laura J. Suggs and Stanislav Emelianov

Cardiovascular diseases are the leading cause of death globally and continue to be a growing health concern. The currently available therapies are not suitable or effective for all patients, which has prompted investigation into stem cell-based therapies for vascular regeneration and ischemic repair. Clinical trials using stem cell therapy have shown promising outcomes for patients with cardiovascular diseases. However, the mechanisms of repair, and the contribution of stem cells to wound healing, are poorly understood. The objective of this dissertation is to evaluate the use of bone marrow-derived mesenchymal stem cells (MSCs) delivered within a PEGylated fibrin gel for revascularization therapies. Demonstrated in this dissertation is the design of nanoparticle contrast agents which are capable of labeling and tracking stem cells and infiltrating macrophages *in vivo*. In addition, the effect of hypoxia on MSC function and the resulting interaction with macrophages was studied. Hypoxia was shown to modulate MSCs to have pro-regenerative and angiogenic-promoting properties, which subsequently affected the interaction with macrophages. Lastly, functional recovery and vascular regeneration in an *in vivo* ischemia model were shown to be enhanced in response to MSCs delivered within PEGylated fibrin gels. The results of this work provide insights into the mechanisms of stem cell therapy in combination with PEGylated fibrin matrices and can contribute to the advancement of the field of regenerative medicine.

Table of Contents

List of Tables

List of Figures

Chapter 1: Introduction

1.1 Background and motivation

1.1.1 Cardiovascular diseases

Cardiovascular diseases (CVDs) are a group of disorders of the heart and blood vessels and are the number one cause of death globally.[1] An estimated 17.3 million people died from CVDs in 2008 (30% of all global deaths),[2] and this number is expected to reach 23.3 million by 2030[2,3]. Common causes and risk factors for CVDs include diabetes, smoking, high cholesterol, obesity, and high blood pressure.[2] CVDs are most commonly the result of atherosclerotic plaque buildup, leading to narrowing of the arteries and ischemia of the downstream tissue.[4] CVDs include coronary heart disease, cerebrovascular disease, and peripheral artery disease.

Peripheral artery disease (PAD), which is characterized by reduced blood flow in the extremities, affects 8-10 million people in the United States and is characterized by intermittent claudication, leg pain and muscle weakness, and foot ulcers.[5] The disease can further progress to critical limb ischemia, in which the resting metabolic needs of the limb are not met by the available blood supply.[5] If the blockages are left untreated, tissue infection or death, and possibly amputation, could occur. Current therapies include antiplatelet medication, angioplasty, and bypass grafting, all of which aim to promote revascularization of the ischemic tissue. However, approximately 50% of patients with critical limb ischemia are not eligible for revascularization procedures[6] and thus will either die or require amputation of the affected limb within one year of diagnosis[7]. Of those patients who undergo revascularization procedures, about 50% will require an additional surgery within 6 months and <50% will achieve complete wound healing at 3 months.[8] In addition, limb amputation (30% of cases) and death are still frequent

complications.[9] As a result, it is imperative to explore new revascularization strategies for PAD. Regenerative medicine and cell-based therapies are widely being investigated as alternative strategies for the currently available revascularization techniques. In particular, bone marrow-derived mesenchymal stem cells have shown great promise in preclinical and clinical trials for patients with PAD.[9]

1.1.2 Stem cell therapy and biomaterial matrices for vascular repair

Mesenchymal stem cells (MSCs) are an adult stem cell population found within multiple regions of the body (including the bone marrow and adipose, placental, and vascular tissues[1,10]) and which can terminally differentiate into mesodermal lineages. MSCs are typically positive for CD44, CD90, and CD105 and negative for CD45 (hematopoietic), CD31 (endothelial) and CD11b (macrophage) markers.[1] Transplanted MSCs have also been demonstrated to differentiate into bone marrow stromal cells, pericytes, myofibroblasts, and endothelial cells.[10] MSCs do not have any MHC class II surface markers, essentially rendering them invisible to the host's immune system.[11] Thus, MSCs are an ideal candidate cell type for therapeutic revascularization, and many research groups have demonstrated blood vessel formation and increased reperfusion of ischemic areas following delivery of MSCs or other stem cells,[12-14] either through direct cell differentiation or paracrine effects[1,14,15]. In addition, as shown in Table 1.1, clinical trials involving therapeutic delivery of MSCs to ischemic skeletal muscle have demonstrated improved muscle function and vascular regeneration.[9] While MSCs have the potential to differentiate to endothelial and skeletal muscle cell types, the low MSC survival rate following delivery *in vivo* suggest that delivered cells may play a primarily paracrine role in healing.[16] MSCs have been shown to secrete factors which are pro-angiogenic and promote wound healing (*e.g.* vascular endothelial growth factor (VEGF),

fibroblast growth factor (FGF), angiopoietin, platelet-derived growth factor (PDGF), stromal cell-derived factor (SDF)-1, interleukin-6, matrix metalloproteinase (MMP)-9, transforming growth factor (TGF)-β, macrophage inflammatory protein (MIP), and monocyte chemoattractant protein (MCP)) through interactions with other cell types, including endothelial cells and macrophages.[1,14,15,17] In addition, secretion of these factors by MSCs has been shown to be upregulated under hypoxic conditions.[18,19] However, the mechanisms by which MSCs contribute to vascular repair are poorly understood, and the advancement of stem cell therapies and clinical trials are hindered by the limited information concerning cell function *in vivo* and the inability to monitor the cells following delivery.

Biomaterial delivery systems can assist in cell-based revascularization therapies by increasing the rate of cell retention at the delivery site and altering the cellular microenvironment, leading to changes in cell function. Fibrin-based matrices are an attractive biomatrix material for wound healing purposes because fibrin is biocompatible, has high affinity to various biological surfaces, supports angiogenesis and tissue repair, contains sites for cellular binding, and is FDA approved.[20] Fibrin is also a natural component of the wound healing response and is formed naturally in the body after thrombin cleavage of fibrinopeptide A from fibrinogen Aα.[21] Fibrin gels can be made as an injectable system,[22] and the rate of fibrin matrix degradation can be controlled by cross-linking with synthetic polymers,[20] such as polyethylene glycol (PEG)[23-25]. PEGylation also serves to overcome the limitation of poor mechanical properties of the gel.[26,27]

1.1.3 Cell tracking and vascular imaging

1.1.3.1 Contrast agents for cell tracking

Tracking cell fate *in vivo* is critical in order to better understand the biological mechanisms underlying disease states and potential therapies. Monitoring cells following *in vivo* delivery would provide important information concerning cell persistence and engraftment, cell localization, cell survival, and the participation and role of administered cells in wound healing processes. Conventional methods for assessing these mechanisms rely on postmortem histology,[28] which only offers endpoint measurements and requires a large number of animals to be sacrificed in order to produce statistically significant results. A more ideal cell tracking method would involve noninvasive longitudinal imaging to monitor cells. Towards this end, many contrast agents are available and currently being investigated to label cells for longitudinal imaging purposes. The ideal contrast agent should be safe and biocompatible, not affect cell function, allow for longitudinal imaging with high sensitivity and cell quantification, have minimal decrease in signal over time (due to contrast dilution as a result of cell division), and not be transferred to non-stem cells *in vivo*.[29,30]

Some of the most common labeling techniques include radionuclides, reporter genes, fluorescent probes, and nanoparticles. Radionuclides are radiolabeled markers and include ^{111}indium oxine, 18F-flurodeoxygluocse (FDG), and ^{99}mtechnetrium exametazine. Radionuclide contrast agents are commonly used for single-photon emission computed tomography (SPECT) imaging. While SPECT imaging can provide quantitative and spatial information concerning cell distribution following administration, the short half-lives of radionuclides limit long-term imaging.[31] In fact, the longest reported imaging time was 120 hours following delivery of cells labeled with ^{111}In.[31]

Thus, only early biodistribution following cell delivery can be observed[32] and long-term monitoring is not capable with radionuclide labeling.

Reporter gene labeling involves genetically manipulating the cell by introducing a reporter gene construct. A reporter protein is produced and detected by an imaging probe introduced into the subject, resulting in production of a signal which is detected by an imaging modality, such as positron emission tomography (PET) or SPECT. Reporter gene labeling allows for stable imaging of cell migration, proliferation, and viability, but cell function can be compromised as a result of transfection.[33,34] In addition, nuclear medicine imaging modalities (PET and SPECT) can be harmful to patients because of the ionizing radiation.

Fluorescent probes are compounds which are excited to a higher energy state by light, and then re-emit energy in the form of light as a result of returning to the ground state. They can be imaged using optical imaging techniques with high sensitivity and resolution, but suffer from loss of signal over time due to photobleaching and limited penetration depth.[31,33]

Nanoparticles (such as quantum dots, iron oxide nanoparticles, and plasmonic noble metal nanoparticles (gold and silver)) can be optimized to promote cellular uptake and allow for long term monitoring.[35-39] Nanoparticles can be imaged with a variety of imaging modalities, including magnetic resonance imaging, radionuclide imaging (PET and SPECT), optical imaging, and hybrid imaging (photoacoustic). Quantum dots are semiconductor nanoparticles (usually 2-10 nm) which can be excited by a wide range of wavelengths, exhibit size-dependent tunable emission, and are relatively photostable.[40-43] However, most of the currently available quantum dots contain toxic core substances,[31,44] and need to be tuned to emit and excite within the near-infrared region to allow for deep tissue imaging.[31] Iron oxide nanoparticles are commonly used as magnetic resonance

imaging contrast agents. Superparamagnetic iron oxide (SPIO) nanoparticles consist of an iron oxide core (as small as 5 nm[45,46]) and are FDA approved. Polymers such as dextran, carboxydextran, or polylysine are often used to coat SPIO nanoparticles in order to prevent nanoparticle aggregation[45-47] and increase cell labeling efficiency[46,47]. Gold nanoparticles can be made in a variety of sizes and shapes (*e.g.* spheres, rods, shells, and cages), and these intrinsic properties determine the wavelengths at which gold nanoparticles maximally absorb and resonantly scatter light.[48-50] In addition, the core of gold nanoparticles is inert and non-toxic to cells,[48,51] and various surface coatings can be conjugated to the gold surface via thiol or amine moieties, which have well defined surface chemistries with gold[47,48]. Gold nanoparticles are commonly used as contrast agents for cell labeling in applications related to cancer imaging, diagnosis, and therapy.[52-54] However, the use of gold nanoparticles is also being extended to stem cell labeling and *in vivo* tracking. Gold nanoparticles exhibit surface plasmon resonance, which contributes to their superior optical absorption properties,[55,56] making them ideal contrast agents for photoacoustic imaging.

1.1.3.2 Photoacoustic imaging

Photoacoustic imaging is based on the photoacoustic effect, in which light energy is transformed into sound energy. Photoacoustic imaging involves irradiating a biological tissue source of interest with a nanosecond laser pulse. The photon energy is absorbed by the tissue, leading to a temporary temperature increase and thermoelastic expansion of the tissue.[57] Acoustic waves are then emitted and detected using an ultrasound transducer. Due to the fact that an ultrasound transducer is used to collect photoacoustic signals, photoacoustic imaging can easily be combined with ultrasound imaging in order to provide both functional and structural information, respectively. As a result,

photoacoustic imaging combines the benefits of ultrasound (penetration depth) with optical imaging (molecular specificity).[58,59] In order to efficiently generate photoacoustic signals, the laser pulse needs to be short enough to satisfy both thermal and stress confinement conditions.[57,59] Under these conditions, the photoacoustic signal is linearly proportional to the laser fluence, optical absorption coefficient of the material, and the Grüneisen coefficient.[57] Thus, contrast in photoacoustic imaging is largely dependent upon the optical absorption coefficient. The optical absorption properties of various tissues are shown in Figure 1.1. The range of wavelengths from 700-1000 nm is known as the tissue optical window, in which absorption from endogenous tissue is dramatically decreased and light is able to penetrate deeply (several centimeters) into biological tissue.[59] As a result, designing contrast agents, such as gold nanoparticles, which have high optical absorption properties within the tissue optical window is advantageous.

1.1.4 The role of hypoxia in wound healing and vascular regeneration

The percentage of stem cell death following therapeutic delivery is quite significant,[16,60] due primarily to the harsh, ischemic environment at the delivery site. This means that studies tracking cell fate using biomedical imaging may actually be monitoring cells which are primarily dead. However, hypoxia-induced cell death can be mitigated using cell priming techniques and altering the cellular microenvironment.[18] In order to optimize such techniques, there is a need to understand the response of stem cells to hypoxia, both *in vitro* and *in vivo*, and the implications of hypoxia on stem cell function.

Bone marrow-derived mesenchymal stem cells reside in a hypoxic niche (2-6% oxygen) within the bone marrow cavity.[61-64] Under ischemic conditions (1-2% oxygen), MSCs have been shown to produce improved angiogenic responses.[18,19,62,65,66] MSCs

cultured under hypoxia also maintain a more multipotent, undifferentiated state.[67] In order to adapt to low oxygen tensions, stem cells upregulate the production of hypoxia inducible factor (HIF).[19] HIFs are transcription factors which activate pathways that are pro-angiogenic and anti-apoptotic. Under normoxic (20% oxygen) conditions, HIF-1α is hydroxylated at proline residues, labeling them for rapid degradation.[19] However, when oxygen tension is low, HIF-1α is hydroxylated and is thus stabilized, leading to the modulation of up to 200 genes involved in processes including angiogenesis, production of erythropoietin, cell proliferation, and apoptosis.[19] Furthermore, the degree of HIF-1 stabilization is inversely proportional to the oxygen concentration.[68] Thus, in order to improve the survival of stem cells following delivery within an ischemic site, many have implemented hypoxic pre-conditioning methods so as to protect the transplanted cells during the initial critical period after transplantation.[18] Hypoxic pre-conditioned stem cells have shown improvements in heart functional recovery and skeletal muscle and liver regeneration.[18,65,69]

The enhanced regenerative potential of MSCs within a hypoxic environment can potentially be attributed to the fact that MSCs show increased expression and secretion of pro-angiogenic and pro-survival factors, including HIF, angiopoietin 1, VEGF, Flk-1, erythropoietin, FGF, and MMP-2.[18,19,65,70,71] Stem cells have also been shown to secrete immunomodulatory factors, including indoleamine 2,3-dioxygenase (IDO),[72] interferon-gamma (IFN-γ),[72] tumor necrosis factor-alpha (TNF-α),[72,73] macrophage inflammatory protein (MIP),[17] and interleukins[71,73] when exposed to hypoxia. As a result, the paracrine action of MSCs can modulate surrounding host cells, such as endothelial cells and macrophages.[17,74] In fact, recent literature has suggested that macrophages may be altered through the interaction with MSCs, leading to accelerated and more improved tissue regeneration.[75-77]

1.1.5 The role of macrophages in wound healing

Effective wound healing and tissue repair requires the orchestrated actions of many cell types. Following an injury, macrophages quickly infiltrate the area and are instrumental in initiating the immune response. Macrophages have been shown to have key roles in wound healing, angiogenesis, and skeletal muscle repair. Thus, understanding the contribution of macrophages to these processes, as well as the influence of the environment on macrophage function, is essential for monitoring wound healing and optimizing therapies.

Dynamic changes in macrophage populations are essential for efficient wound healing.[78] Specifically in skeletal muscle injuries, recruitment of pro-inflammatory monocytes within the first few days following injury is required in order to clear debris and release cytokines that stimulate myoblast proliferation.[75,77,79,80] Furthermore, impairment of monocyte/macrophage recruitment during the early stages prevents muscle repair.[75,77,79] However, conversion into an anti-inflammatory macrophage population is necessary for complete wound repair, as anti-inflammatory macrophages promote myoblast differentiation and fusion in skeletal muscle.[75-77,80] In ischemic tissues following myocardial infarction, the phenotypic changes of macrophages in response to the interactions with stem cells can be a critical factor, with the external environment dictating the transition from pro- (M1) to anti-inflammatory (M2) macrophages.[76,77,79,80] M2 macrophages are known to have a more "regenerative" role compared to M1 pro-inflammatory macrophages.[81] Differentiation stimuli include cytokine secretion by surrounding cells and by macrophages themselves, as well as phagocytosis of debris and apoptotic cells by macrophages. In particular, interferon-γ (IFN-γ) and TNF-α polarize macrophages to an M1 phenotype, while interleukin (IL)-4, IL-10, and IL-13 polarize macrophages to an M2 phenotype.[76,80] Thus altering these factors may influence

macrophage phenotype and wound healing. Figure 1.2 outlines the different macrophage phenotypes, including stimulating factors, secreted cytokines and chemokines, and expressed surface markers.

It has been demonstrated that MSC therapy significantly affects macrophage subpopulations and, subsequently, wound repair.[82] The mechanisms responsible for this could potentially be attributed to the pro-angiogenic role of macrophages, including physically interacting with sprouting blood vessels, facilitating the growth of blood vessels by degrading the extracellular matrix, and promoting vascular remodeling via VEGF-independent angiogenic pathways.[83] In addition, macrophages have been suggested to have different pro-angiogenic mechanisms depending on their phenotype (M1 vs M2).[83,84]

1.2 OVERALL RESEARCH GOALS

The overall goal of this research is to evaluate the use of bone marrow-derived mesenchymal stem cells delivered within a PEGylated fibrin gel biomatrix for revascularization therapies. The hypothesis is that (1) MSCs delivered via an injectable PEGylated fibrin matrix will contribute to increased vascularization and regeneration of ischemic tissue and (2) this repair mechanism can be attributed to paracrine effects of MSCs and the interaction with macrophages.

The research presented here addresses the overall hypothesis by (1) determining the feasibility of nanoparticle labeling of MSCs *in vitro*, (2) optimizing the nanoparticle system for *in vivo* monitoring of MSCs and infiltrating macrophages, (3) assessing the influence of a hypoxic environment on MSC function and the interaction with macrophages, and (4) demonstrating the extent of neovascularization and muscle function improvement *in vivo* following delivery of MSCs within a PEGylated fibrin biomatrix.

Chapter 2 outlines the initial studies in investigating nanoparticle labeling of MSCs with various spherical nanoparticle formulations. Nanoparticle uptake and the resulting effects on cell viability and function were assessed for different nanoparticle sizes and surface coatings. Chapter 3 investigates the design of a dissociative nanoparticle system in order to evade macrophage uptake and accumulation in organs and tissues *in vivo*. Chapter 4 expands upon the work in Chapter 3 by developing a dual nanoparticle system to label both MSCs and macrophages. Characterization of the nanoparticles was performed, as well as assessing the specificity of nanoparticle labeling of the cell types *in vitro* and *in vivo.* Chapter 5 attempts to understand the role of hypoxia on stem cell function and the resulting implications for wound healing in terms of immunomodulation. Chapter 6 presents the investigation of MSC therapy within an *in vivo* hind limb ischemia model. The contribution of MSCs delivered within a PEGylated fibrin gel to functional recovery of the tissue and vascular regeneration were evaluated. Chapter 7 outlines overall conclusions, recommendations for future work, and the broad implications of this research.

Study	Cell Type (delivery route)	Clinical Outcome
Bartsch[85]	Bone marrow mononuclear cells (IM and IA)	2 months: improvements in ABI, capillary-venous oxygen saturation, mean reactive hyperemia, and pain free walking distance
Cobellis[86]	Bone marrow mononuclear cells (IA)	12 months: substantial improvement of blood flow and increased capillary densities; ABI and pain free walking distance improved significantly
Walter[87]	Bone marrow mononuclear cells (IA)	3 months: no significant improvements in ABI; significantly improved ulcer healing and reduced rest pain; limb salvage and amputation free survival rates did not differ between groups
Idei[88]	Bone marrow mononuclear cells (IM)	4 years: improvements in amputation free rates and survival rates; ABI and $tcpO_2$ significantly increased after 1 month and gradually decreased during 3 year follow up and returned to baseline
Benoit[89]	Bone marrow-derived stem cells (IM)	6 months: lower amputation rate; no differences in ABI
Powell[90]	Bone marrow tissue repair cells (IM)	12 months: decreased amputation rate, and improved wound healing
Losordo[91]	CD34+ cells (IM)	6 and 12 months: decreased amputation rate
Amann[92]	Bone marrow cells (IM)	3 and 6 months: increased ABI, $tcpO_2$, and total walking distance
Iafrati[93]	Bone marrow aspirate concentrate (IM)	1, 4, 8, and 12 weeks: Decreased amputation rate and improved pain, ABI, Rutherford classification, and quality of life scoring
Highashi[94]	Bone marrow mononuclear cells (IM)	4 and 24 weeks: improved ABI, $tcpO_2$, and pain-free walking time
Ishida[95]	Peripheral blood mononuclear cells (IM)	4 weeks: improvement in ABI, ischemic ulcers, mean walking distance, and physiological functioning
Chochola[96]	Bone marrow mononuclear cells (IM)	1 year: decreased amputation rate and improvements in grade of ischemia and wound healing
Durdu[97]	Bone marrow mononuclear cells (IM)	6 months: improvements in ABI, rest pain scores, quality of life, wound healing, and collateral network formation across affected arteries
Saito[98]	Bone marrow mononuclear cells (IM)	4 and 24 weeks: rest pain significantly reduced and ulcers healed and diminished in size

Table 1.1: Summary of clinical trials investigating therapeutic delivery of mesenchymal stem cells to ischemic skeletal muscle. Abbreviations: intraarterial (IA), intramuscular (IM), ankle-brachial index (ABI), transcutaneous oxygen pressure (tcpO2).

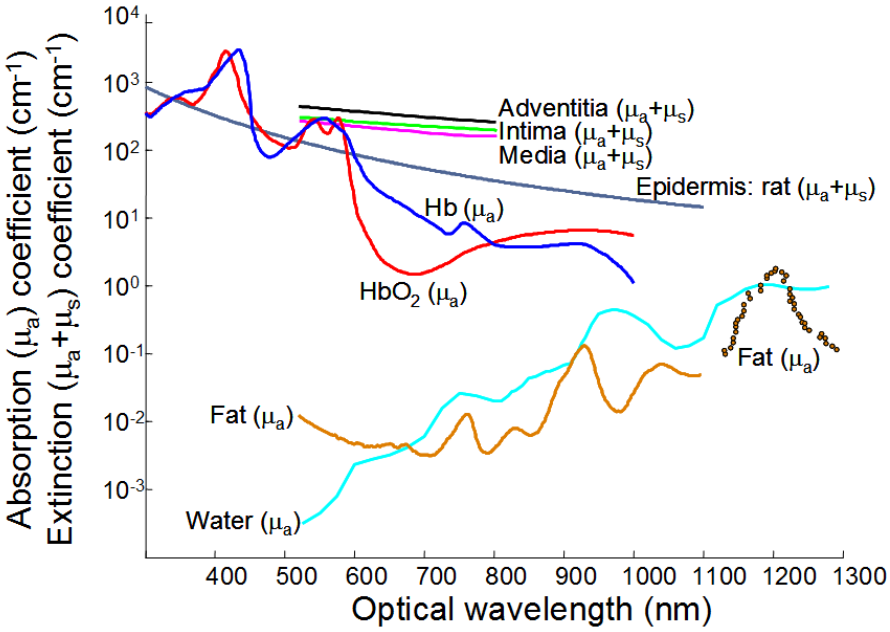

Figure 1.1: Optical absorption and extinction coefficients of various endogenous tissues. Abbreviations: deoxygenated hemoglobin (Hb), oxygenated hemoglobin (HbO_2).

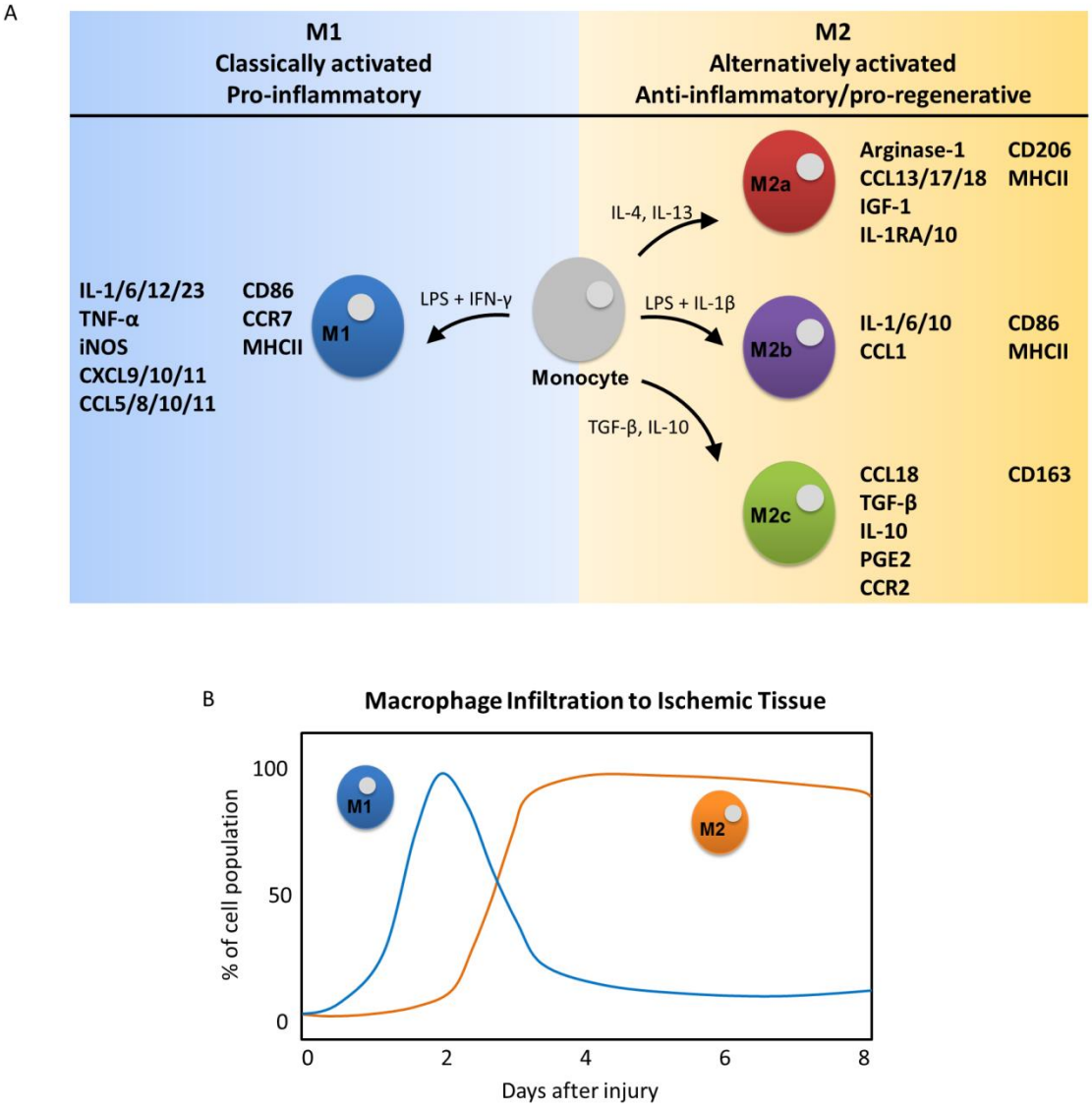

Figure 1.2: (A) The spectrum of macrophage phenotypes, including stimulating factors, secreted cytokines and chemokines, and expressed surface markers. (B) Time course of macrophage infiltration and phenotype expression following an ischemic injury.

1.3 REFERENCES

1. Copland, I.B. Mesenchymal stromal cells for cardiovascular disease. *J Cardiovasc Dis Res* **2**, 3-13 (2011).

2. Organization, W.H. (World Health Organization, Geneva, Switzerland; 2011).

3. Mathers, C.D., Loncar, D. Projections of global mortality and burden of disease from 2002 to 2030. *PLoS medicine* **3**, e442 (2006).

4. Robbins, S.L., Kumar, V., Cotran, R.S. Robbins and Cotran pathologic basis of disease, Edn. 8th. (Saunders/Elsevier, Philadelphia, PA; 2010).

5. Creager, M.A. Medical management of peripheral arterial disease. *Cardiol Rev* **9**, 238-245 (2001).

6. Taghavi, S., Duran, J.M., George, J.C. Stem cell therapy for peripheral arterial disease: a review of clinical trials. *Stem Cell Studies* **1**, 105-114 (2011).

7. Hunt, S.A., Abraham, W.T., Chin, M.H., Feldman, A.M., Francis, G.S., Ganiats, T.G., Jessup, M., Konstam, M.A., Mancini, D.M., Michl, K., Oates, J.A., Rahko, P.S., Silver, M.A., Stevenson, L.W., Yancy, C.W., Antman, E.M., Smith, S.C., Jr., Adams, C.D., Anderson, J.L., Faxon, D.P., Fuster, V., Halperin, J.L., Hiratzka, L.F., Jacobs, A.K., Nishimura, R., Ornato, J.P., Page, R.L., Riegel, B. ACC/AHA 2005 Guideline Update for the Diagnosis and Management of Chronic Heart Failure in the Adult: a report of the American College of Cardiology/American Heart Association Task Force on Practice Guidelines (Writing Committee to Update the 2001 Guidelines for the Evaluation and Management of Heart Failure): developed in collaboration with the American College of Chest Physicians and the International Society for Heart and Lung Transplantation: endorsed by the Heart Rhythm Society. *Circulation* **112**, e154-235 (2005).

8. Goshima, K.R., Mills, J.L., Hughes, J.D. A new look at outcomes after infrainguinal bypass surgery: Traditional reporting standards systematically underestimate the expenditure of effort required to attain limb salvage. *J Vasc Surg* **39**, 330-335 (2004).

9. Lawall, H., Bramlage, P., Amann, B. Stem cell and progenitor cell therapy in peripheral artery disease. A critical appraisal. *Thromb Haemost* **103**, 696-709 (2010).

10. Appasani, K., Appasani, R.K. Stem cells & regenerative medicine : from molecular embryology to tissue engineering. (Humana Press, New York; 2011).

11. Caplan, A.I. Why are MSCs therapeutic? New data: new insight. *Journal of Pathology* **217**, 318-324 (2009).

12. Ikenaga, S., Hamano, K., Nishida, M., Kobayashi, T., Li, T.S., Kobayashi, S., Matsuzaki, M., Zempo, N., Esato, K. Autologous bone marrow implantation induced angiogenesis and improved deteriorated exercise capacity in a rat ischemic hindlimb model. *The Journal of surgical research* **96**, 277-283 (2001).

13. Aranguren, X.L., McCue, J.D., Hendrickx, B., Zhu, X.H., Du, F., Chen, E., Pelacho, B., Penuelas, I., Abizanda, G., Uriz, M., Frommer, S.A., Ross, J.J., Schroeder, B.A., Seaborn, M.S., Adney, J.R., Hagenbrock, J., Harris, N.H., Zhang, Y., Zhang, X., Nelson-Holte, M.H., Jiang, Y., Billiau, A.D., Chen, W., Prosper, F., Verfaillie, C.M., Luttun, A. Multipotent adult progenitor cells sustain function of ischemic limbs in mice. *J Clin Invest* **118**, 505-514 (2008).

14. Kinnaird, T., Stabile, E., Burnett, M.S., Shou, M., Lee, C.W., Barr, S., Fuchs, S., Epstein, S.E. Local delivery of marrow-derived stromal cells augments collateral perfusion through paracrine mechanisms. *Circulation* **109**, 1543-1549 (2004).

15. Kinnaird, T., Stabile, E., Burnett, M.S., Epstein, S.E. Bone-marrow-derived cells for enhancing collateral development: mechanisms, animal data, and initial clinical experiences. *Circulation research* **95**, 354-363 (2004).

16. Suga, H., Glotzbach, J., Sorkin, M., Longaker, M., Gurtner, G. Paracrine mechanism of angiogenesis in adipose-derived stem cell transplantation. *Annals of Plastic Surgery* **72**, 234-241 (2014).

17. Chen, L., Tredget, E.E., Wu, P.Y., Wu, Y. Paracrine factors of mesenchymal stem cells recruit macrophages and endothelial lineage cells and enhance wound healing. *PLoS One* **3**, e1886 (2008).

18. Hu, X., Yu, S.P., Fraser, J.L., Lu, Z., Ogle, M.E., Wang, J.A., Wei, L. Transplantation of hypoxia-preconditioned mesenchymal stem cells improves infarcted heart function via enhanced survival of implanted cells and angiogenesis. *J Thorac Cardiov Sur* **135**, 799-808 (2008).

19. Muscari, C., Giordano, E., Bonafe, F., Govoni, M., Pasini, A., Guarnieri, C. Priming adult stem cells by hypoxic pretreatments for applications in regenerative medicine. *Journal of biomedical science* **20**, 63 (2013).

20. Shaikh, F.M., Callanan, A., Kavanagh, E.G., Burke, P.E., Grace, P.A., McGloughlin, T.M. Fibrin: a natural biodegradable scaffold in vascular tissue engineering. *Cells Tissues Organs* **188**, 333-346 (2008).

21. Mosesson, M.W. Fibrinogen and fibrin structure and functions. *J Thromb Haemost* **3**, 1894-1904 (2005).

22. Hammers, D.W., Sarathy, A., Pham, C.B., Drinnan, C.T., Farrar, R.P., Suggs, L.J. Controlled release of IGF-I from a biodegradable matrix improves functional recovery of skeletal muscle from ischemia/reperfusion. *Biotechnol Bioeng* **109**, 1051-1059 (2012).

23. Dikovsky, D., Bianco-Peled, H., Seliktar, D. The effect of structural alterations of PEG-fibrinogen hydrogel scaffolds on 3-D cellular morphology and cellular migration. *Biomaterials* **27**, 1496-1506 (2006).

24. Zhang, G., Drinnan, C.T., Geuss, L.R., Suggs, L.J. Vascular differentiation of bone marrow stem cells is directed by a tunable three-dimensional matrix. *Acta Biomater* **6**, 3395-3403 (2010).

25. Zhang, G., Wang, X., Wang, Z., Zhang, J., Suggs, L. A PEGylated fibrin patch for mesenchymal stem cell delivery. *Tissue Engineering* **12**, 9-19 (2006).

26. Almany, L., Seliktar, D. Biosynthetic hydrogel scaffolds made from fibrinogen and polyethylene glycol for 3D cell cultures. *Biomaterials* **26**, 2467-2477 (2005).

27. Taylor, P.M. Biological matrices and bionanotechnology. *Philosophical transactions of the Royal Society of London. Series B, Biological sciences* **362**, 1313-1320 (2007).

28. Sheikh, A., Wu, J. Molecular Imaging of Cardiac Stem Cell Transplantation. *Current Cardiology Reports* **8**, 147-154 (2006).

29. Frangioni, J.V., Hajjar, R.J. In vivo tracking of stem cells for clinical trials in cardiovascular disease. *Circulation* **110**, 3378-3383 (2004).

30. Li, S.C., Tachiki, L.M., Luo, J., Dethlefs, B.A., Chen, Z., Loudon, W.G. A biological global positioning system: considerations for tracking stem cell behaviors in the whole body. *Stem Cell Rev* **6**, 317-333 (2010).

31. Kraitchman, D.L., Wu, J.C.-M. Stem cell labeling for delivery and tracking using noninvasive imaging. (CRC Press/Taylor & Francis, Boca Raton; 2012).

32. Zhang, Y., Thorn, S., DaSilva, J.N., Lamoureux, M., DeKemp, R.A., Beanlands, R.S., Ruel, M., Suuronen, E.J. Collagen-based matrices improve the delivery of transplanted circulating progenitor cells: development and demonstration by ex vivo radionuclide cell labeling and in vivo tracking with positron-emission tomography. *Circulation. Cardiovascular imaging* **1**, 197-204 (2008).

33. Bhirde, A., Xie, J., Swierczewska, M., Chen, X. Nanoparticles for cell labeling. *Nanoscale* **3**, 142 (2011).

34. Schroeder, T. Imaging stem-cell-driven regeneration in mammals. *Nature* **453**, 345-351 (2008).

35. Chithrani, B.D., Ghazani, A.A., Chan, W.C. Determining the size and shape dependence of gold nanoparticle uptake into mammalian cells. *Nano Lett* **6**, 662-668 (2006).

36. Horák, D., Babič, M., Jendelová, P., Herynek, V., Trchova, M., Likavanova, K., M, K., Hajek, M., Sykova, E. Effect of different magnetic nanoparticle coatings on the efficiency of stem cell labeling. *Journal of Magnetism and Magnetic Materials* **321**, 1539-1547 (2009).

37. Suh, J.S., Lee, J.Y., Choi, Y.S., Yu, F., Yang, V., Lee, S.J., Chung, C.P., Park, Y.J. Efficient labeling of mesenchymal stem cells using cell permeable magnetic nanoparticles. *Biochemical and Biophysical Research Communications* **379**, 669-675 (2009).

38. Alkilany, A.M., Nagaria, P.K., Hexel, C.R., Shaw, T.J., Murphy, C.J., Wyatt, M.D. Cellular Uptake and Cytotoxicity of Gold Nanorods: Molecular Origin of Cytotoxicity and Surface Effects. *Small* **5**, 701-708 (2009).

39. Chithrani, B.D., Chan, W.C. Elucidating the mechanism of cellular uptake and removal of protein-coated gold nanoparticles of different sizes and shapes. *Nano Lett* **7**, 1542-1550 (2007).

40. Lin, S., Xie, X., Patel, M.R., Yang, Y.H., Li, Z., Cao, F., Gheysens, O., Zhang, Y., Gambhir, S.S., Rao, J.H., Wu, J.C. Quantum dot imaging for embryonic stem cells. *BMC Biotechnol* **7**, 67 (2007).

41. Michalet, X. Quantum Dots for Live Cells, in Vivo Imaging, and Diagnostics. *Science* **307**, 538-544 (2005).

42. Muller-Borer, B.J., Collins, M.C., Gunst, P.R., Cascio, W.E., Kypson, A.P. Quantum dot labeling of mesenchymal stem cells. *J Nanobiotechnology* **5**, 9 (2007).

43. So, M.K., Xu, C., Loening, A.M., Gambhir, S.S., Rao, J. Self-illuminating quantum dot conjugates for in vivo imaging. *Nat Biotechnol* **24**, 339-343 (2006).

44. Hardman, R. A toxicologic review of quantum dots: toxicity depends on physicochemical and environmental factors. *Environmental health perspectives* **114**, 165-172 (2006).

45. Ferreira, L., Karp, J., Nobre, L., Langer, R. New Opportunities: The Use of Nanotechnologies to Manipulate and Track Stem Cells. *Cell Stem Cell* **3**, 136-146 (2008).

46. Kubinová, Š., Syková, E. Nanotechnologies in regenerative medicine. *Minimally Invasive Therapy & Allied Technologies* **19**, 144-156 (2010).

47. Solanki, A., Kim, J., Lee, K.-B. Nanotechnology for Regenerative Medicine: Nanomaterials for Stem Cell Imaging. *Nanomedicine* **3**, 567-578 (2008).

48. Lévy, R., Shaheen, U., Cesbron, Y., Sée, V. Gold nanoparticles delivery in mammalian live cells: a critical review. *Nano Reviews* **1** (2010).

49. Chen, P., Mwakwari, S., Oyeler, A. Gold nanoparticles: From nanomedicine to nanosensing. *Nanotechnology, Science and Applications*, 45-66 (2008).

50. Alkilany, A.M., Murphy, C.J. Toxicity and cellular uptake of gold nanoparticles: what we have learned so far? *J Nanopart Res* **12**, 2313-2333 (2010).

51. Ghosh, P., Han, G., De, M., Kim, C., Rotello, V. Gold nanoparticles in delivery applications. *Advanced Drug Delivery Reviews* **60**, 1307-1315 (2008).

52. Mallidi, S., Larson, T., Tam, J., Joshi, P.P., Karpiouk, A., Sokolov, K., Emelianov, S. Multiwavelength Photoacoustic Imaging and Plasmon Resonance Coupling of Gold Nanoparticles for Selective Detection of Cancer. *Nano Lett* **9**, 2825-2831 (2009).

53. Durr, N.J., Larson, T., Smith, D.K., Korgel, B.A., Sokolov, K., Ben-Yakar, A. Two-photon luminescence imaging of cancer cells using molecularly targeted gold nanorods. *Nano Lett* **7**, 941-945 (2007).

54. Homan, K., Shah, J., Gomez, S., Gensler, H., Karpiouk, A., Brannon-Peppas, L., Emelianov, S. Silver nanosystems for photoacoustic imaging and image-guided therapy. *Journal of Biomedical Optics* **15**, 021316 (2010).

55. Jain, P.K., El-Sayed, M.A. Plasmonic coupling in noble metal nanostructures. *Chemical Physics Letters* **487**, 153-164 (2010).

56. Hore, M.J.A., Composto, R.J. Nanorod Self-Assembly for Tuning Optical Absorption. *Acs Nano* **4**, 6941-6949 (2010).

57. Wang, L.V., Hu, S. Photoacoustic tomography: in vivo imaging from organelles to organs. *Science* **335**, 1458-1462 (2012).

58. Emelianov, S.Y., Li, P.C., O'Donnell, M. Photoacoustics for molecular imaging and therapy. *Phys Today* **62**, 34-39 (2009).

59. Xu, M.H., Wang, L.H.V. Photoacoustic imaging in biomedicine. *Rev Sci Instrum* **77** (2006).

60. Robey, T.E., Saiget, M.K., Reinecke, H., Murry, C.E. Systems approaches to preventing transplanted cell death in cardiac repair. *J Mol Cell Cardiol* **45**, 567-581 (2008).

61. Das, R., Jahr, H., van Osch, G.J., Farrell, E. The role of hypoxia in bone marrow-derived mesenchymal stem cells: considerations for regenerative medicine approaches. *Tissue engineering. Part B, Reviews* **16**, 159-168 (2010).

62. Grayson, W.L., Zhao, F., Izadpanah, R., Bunnell, B., Ma, T. Effects of hypoxia on human mesenchymal stem cell expansion and plasticity in 3D constructs. *Journal of cellular physiology* **207**, 331-339 (2006).

63. Lonne, M., Lavrentieva, A., Walter, J.G., Kasper, C. Analysis of oxygen-dependent cytokine expression in human mesenchymal stem cells derived from umbilical cord. *Cell and tissue research* **353**, 117-122 (2013).

64. Dos Santos, F., Andrade, P.Z., Boura, J.S., Abecasis, M.M., da Silva, C.L., Cabral, J.M. Ex vivo expansion of human mesenchymal stem cells: a more effective cell proliferation kinetics and metabolism under hypoxia. *Journal of cellular physiology* **223**, 27-35 (2010).

65. Hoffmann, J., Glassford, A.J., Doyle, T.C., Robbins, R.C., Schrepfer, S., Pelletier, M.P. Angiogenic effects despite limited cell survival of bone marrow-derived mesenchymal stem cells under ischemia. *The Thoracic and cardiovascular surgeon* **58**, 136-142 (2010).

66. Yang, D., Wang, W., Li, L., Peng, Y., Chen, P., Huang, H., Guo, Y., Xia, X., Wang, Y., Wang, H., Wang, W.E., Zeng, C. The relative contribution of paracine effect versus direct differentiation on adipose-derived stem cell transplantation mediated cardiac repair. *PLoS One* **8**, e59020 (2013).

67. Basciano, L., Nemos, C., Foliguet, B., de Isla, N., de Carvalho, M., Tran, N., Dalloul, A. Long term culture of mesenchymal stem cells in hypoxia promotes a genetic program maintaining their undifferentiated and multipotent status. *BMC cell biology* **12**, 12 (2011).

68. Ivanovic, Z. Hypoxia or in situ normoxia: The stem cell paradigm. *Journal of cellular physiology* **219**, 271-275 (2009).

69. Yu, J., Yin, S., Zhang, W., Gao, F., Liu, Y., Chen, Z., Zhang, M., He, J., Zheng, S. Hypoxia preconditioned bone marrow mesenchymal stem cells promote liver regeneration in a rat massive hepatectomy model. *Stem cell research & therapy* **4**, 83 (2013).

70. Meirelles Lda, S., Fontes, A.M., Covas, D.T., Caplan, A.I. Mechanisms involved in the therapeutic properties of mesenchymal stem cells. *Cytokine & growth factor reviews* **20**, 419-427 (2009).

71. Chen, L., Xu, Y.B., Zhao, J.L., Zhang, Z.Q., Yang, R.H., Xie, J.L., Liu, X.S., Qi, S.H. Conditioned Medium from Hypoxic Bone Marrow-Derived Mesenchymal Stem Cells Enhances Wound Healing in Mice. *PLoS One* **9** (2014).

72. Roemeling-van Rhijn, M., Mensah, F.K., Korevaar, S.S., Leijs, M.J., van Osch, G.J., Ijzermans, J.N., Betjes, M.G., Baan, C.C., Weimar, W., Hoogduijn, M.J. Effects of Hypoxia on the Immunomodulatory Properties of Adipose Tissue-Derived Mesenchymal Stem cells. *Frontiers in immunology* **4**, 203 (2013).

73. Li, Z., Wei, H., Deng, L., Cong, X., Chen, X. Expression and secretion of interleukin-1beta, tumour necrosis factor-alpha and interleukin-10 by hypoxia- and serum-deprivation-stimulated mesenchymal stem cells. *The FEBS journal* **277**, 3688-3698 (2010).

74. Kim, J., Hematti, P. Mesenchymal stem cell-educated macrophages: a novel type of alternatively activated macrophages. *Exp Hematol* **37**, 1445-1453 (2009).

75. Chazaud, B., Brigitte, M., Yacoub-Youssef, H., Arnold, L., Gherardi, R., Sonnet, C., Lafuste, P., Chretien, F. Dual and beneficial roles of macrophages during skeletal muscle regeneration. *Exercise and sport sciences reviews* **37**, 18-22 (2009).

76. Kharraz, Y., Guerra, J., Mann, C.J., Serrano, A.L., Munoz-Canoves, P. Macrophage Plasticity and the Role of Inflammation in Skeletal Muscle Repair. *Mediators of Inflammation* (2013).

77. Novak, M.L., Koh, T.J. Phenotypic transitions of macrophages orchestrate tissue repair. *Am J Pathol* **183**, 1352-1363 (2013).

78. Ploeger, D.T., Hosper, N.A., Schipper, M., Koerts, J.A., de Rond, S., Bank, R.A. Cell plasticity in wound healing: paracrine factors of M1/ M2 polarized macrophages influence the phenotypical state of dermal fibroblasts. *Cell communication and signaling : CCS* **11**, 29 (2013).

79. Arnold, L., Henry, A., Poron, F., Baba-Amer, Y., van Rooijen, N., Plonquet, A., Gherardi, R.K., Chazaud, B. Inflammatory monocytes recruited after skeletal muscle injury switch into antiinflammatory macrophages to support myogenesis. *The Journal of experimental medicine* **204**, 1057-1069 (2007).

80. Tidball, J.G. Inflammatory processes in muscle injury and repair. *American journal of physiology. Regulatory, integrative and comparative physiology* **288**, R345-353 (2005).

81. Swirski, F.K., Nahrendorf, M. Macrophage-stem cell crosstalk after myocardial infarction. *J Am Coll Cardiol* **62**, 1902-1904 (2013).

82. Ben-Mordechai, T., Holbova, R., Landa-Rouben, N., Harel-Adar, T., Feinberg, M.S., Abd Elrahman, I., Blum, G., Epstein, F.H., Silman, Z., Cohen, S., Leor, J. Macrophage Subpopulations Are Essential for Infarct Repair With and Without Stem Cell Therapy. *J Am Coll Cardiol* **62**, 1890-1901 (2013).

83. Nucera, S., Biziato, D., De Palma, M. The interplay between macrophages and angiogenesis in development, tissue injury and regeneration. *International Journal of Developmental Biology* **55**, 495-503 (2011).

84. Spiller, K.L., Anfang, R.R., Spiller, K.J., Ng, J., Nakazawa, K.R., Daulton, J.W., Vunjak-Noyakovic, G. The role of macrophage phenotype in vascularization of tissue engineering scaffolds. *Biomaterials* **35**, 4477-4488 (2014).

85. Bartsch, T., Brehm, M., Zeus, T., Kogler, G., Wernet, P., Strauer, B.E. Transplantation of autologous mononuclear bone marrow stem cells in patients with peripheral arterial disease (the TAM-PAD study). *Clin Res Cardiol* **96**, 891-899 (2007).

86. Cobellis, G., Silvestroni, A., Lillo, S., Sica, G., Botti, C., Maione, C., Schiavone, V., Rocco, S., Brando, G., Sica, V. Long-term effects of repeated autologous transplantation of bone marrow cells in patients affected by peripheral arterial disease. *Bone Marrow Transplant* **42**, 667-672 (2008).

87. Walter, D.H., Krankenberg, H., Balzer, J.O., Kalka, C., Baumgartner, I., Schluter, M., Tonn, T., Seeger, F., Dimmeler, S., Lindhoff-Last, E., Zeiher, A.M. Intraarterial administration of bone marrow mononuclear cells in patients with critical limb ischemia: a randomized-start, placebo-controlled pilot trial (PROVASA). *Circ Cardiovasc Interv* **4**, 26-37 (2011).

88. Idei, N., Soga, J., Hata, T., Fujii, Y., Fujimura, N., Mikami, S., Maruhashi, T., Nishioka, K., Hidaka, T., Kihara, Y., Chowdhury, M., Noma, K., Taguchi, A., Chayama, K., Sueda, T., Higashi, Y. Autologous bone-marrow mononuclear cell implantation reduces long-term major amputation risk in patients with critical limb ischemia: a comparison of atherosclerotic peripheral arterial disease and Buerger disease. *Circ Cardiovasc Interv* **4**, 15-25 (2011).

89. Benoit, E., O'Donnell, T.F., Jr., Iafrati, M.D., Asher, E., Bandyk, D.F., Hallett, J.W., Lumsden, A.B., Pearl, G.J., Roddy, S.P., Vijayaraghavan, K., Patel, A.N. The role of amputation as an outcome measure in cellular therapy for critical limb ischemia: implications for clinical trial design. *J Transl Med* **9**, 165 (2011).

90. Powell, R.J., Comerota, A.J., Berceli, S.A., Guzman, R., Henry, T.D., Tzeng, E., Velazquez, O., Marston, W.A., Bartel, R.L., Longcore, A., Stern, T., Watling, S. Interim analysis results from the RESTORE-CLI, a randomized, double-blind multicenter phase II trial comparing expanded autologous bone marrow-derived tissue repair cells and placebo in patients with critical limb ischemia. *J Vasc Surg* **54**, 1032-1041 (2011).

91. Losordo, D.W., Kibbe, M.R., Mendelsohn, F., Marston, W., Driver, V.R., Sharafuddin, M., Teodorescu, V., Wiechmann, B.N., Thompson, C., Kraiss, L., Carman, T., Dohad, S., Huang, P., Junge, C.E., Story, K., Weistroffer, T., Thorne, T.M., Millay, M., Runyon, J.P., Schainfeld, R. A randomized, controlled pilot study of autologous CD34+ cell therapy for critical limb ischemia. *Circ Cardiovasc Interv* **5**, 821-830 (2012).

92. Amann, B., Luedemann, C., Ratei, R., Schmidt-Lucke, J.A. Autologous bone marrow cell transplantation increases leg perfusion and reduces amputations in patients with advanced critical limb ischemia due to peripheral artery disease. *Cell Transplant* **18**, 371-380 (2009).

93. Iafrati, M.D., Hallett, J.W., Geils, G., Pearl, G., Lumsden, A., Peden, E., Bandyk, D., Vijayaraghava, K.S., Radhakrishnan, R., Ascher, E., Hingorani, A., Roddy, S. Early results and lessons learned from a multicenter, randomized, double-blind trial of bone marrow aspirate concentrate in critical limb ischemia. *J Vasc Surg* **54**, 1650-1658 (2011).

94. Higashi, Y., Kimura, M., Hara, K., Noma, K., Jitsuiki, D., Nakagawa, K., Oshima, T., Chayama, K., Sueda, T., Goto, C., Matsubara, H., Murohara, T., Yoshizumi, M. Autologous bone-marrow mononuclear cell implantation improves endothelium-dependent vasodilation in patients with limb ischemia. *Circulation* **109**, 1215-1218 (2004).

95. Ishida, A., Ohya, Y., Sakuda, H., Ohshiro, K., Higashiuesato, Y., Nakaema, M., Matsubara, S., Yakabi, S., Kakihana, A., Ueda, M., Miyagi, C., Yamane, N., Koja, K., Komori, K., Takishita, S. Autologous peripheral blood mononuclear cell implantation for patients with peripheral arterial disease improves limb ischemia. *Circ J* **69**, 1260-1265 (2005).

96. Chochola, M., Pytlik, R., Kobylka, P., Skalicka, L., Kideryova, L., Beran, S., Varejka, P., Jirat, S., Koivanek, J., Aschermann, M., Linhart, A. Autologous intra-arterial infusion of bone marrow mononuclear cells in patients with critical leg ischemia. *Int Angiol* **27**, 281-290 (2008).

97. Durdu, S., Akar, A.R., Arat, M., Sancak, T., Eren, N.T., Ozyurda, U. Autologous bone-marrow mononuclear cell implantation for patients with Rutherford grade II-III thromboangiitis obliterans. *J Vasc Surg* **44**, 732-739 (2006).

98. Saito, Y., Sasaki, K., Katsuda, Y., Murohara, T., Takeshita, Y., Okazaki, T., Arima, K., Katsuki, Y., Shintani, S., Shimada, T., Akashi, H., Ikeda, H., Imaizumi, T. Effect of autologous bone-marrow cell transplantation on ischemic ulcer in patients with Buerger's disease. *Circ J* **71**, 1187-1192 (2007).

Chapter 2: *In vitro* evaluation of nanoparticle labeling of mesenchymal stem cells

2.1 INTRODUCTION

Stem cells are advantageous in that they can potentially be used for cellular therapies due to the fact that they can differentiate into multiple cell types,[1] including cardiovascular cell types.[2-5] Previous work by our group demonstrated that PEGylated fibrin gels promote mesenchymal stem cell (MSC) tubulogenesis and differentiation towards a vascular cell type.[4] These findings suggest MSCs could potentially be delivered to an injury site after an ischemic event in order to assist in neovascularization and tissue repair.[3-7] However, the exact mechanisms of vascular repair, as well as the role and extent of participation of MSCs in neovascularization, are not well understood.

To this end, there have been numerous proposed approaches for long-term tracking of stem cells *in vivo*. A majority of this research has focused on labeling MSCs *in vitro*, delivering the MSCs *in vivo*, and sacrificing the animals at various time points and performing histology.[8] However, a major issue with this methodology is the inability to track the cells within a single, live animal model over time. As a result, many investigators have turned to noninvasive imaging modalities which are capable of longitudinally monitoring and tracking stem cells within a single model.[9-11]

The imaging approaches previously investigated require the use of contrast agents to label the cells. Efficient cell labeling with contrast agents is necessary in order to adequately image and track MSCs. For long-term imaging, it is desirable to have contrast agents which have long-term stability, are not toxic to the cells, and do not affect cell function. Radionuclides have short half-lives,[12] and thus are not ideal for long-term imaging studies. Reporter genes indirectly label cells and are not diluted as a result of cell

division.[13] However, the cells need to be genetically manipulated, which could alter cell function, and a substrate must be administered intravenously for each imaging session.[13] Nanoparticles provide an advantage over radionuclides, in that they can be used for long-term imaging and allow for repeated imaging over time.[12,14-17] Although nanoparticle labeling can decrease over time due to cell division, certain nanoparticle materials, such as gold, are not toxic to the cells and do not alter cell function.[16]

Taking into account the advantages and disadvantages of the various contrast agents which can be employed, gold nanoparticles were investigated as a contrast agent for stem cell tracking. Gold nanoparticles offer many advantages, including their optically tunable properties and inert characteristics. In addition, photoacoustic imaging can be used to image cells labeled with gold nanoparticles.[18,19] Photoacoustic imaging can be used for i*n vivo* imaging at reasonable depths,[20] as well as for longitudinal studies.[21,22] Specifically, the long term goal of this study is to optically assess how MSCs delivered *in vivo* via a PEGylated fibrin gel participate in the process of neovascularization. In this study, the efficiency of MSC labeling with gold nanoparticles and the effects of nanoparticle loading on cell function were assessed. Initial nanoparticle loading and retention over time were determined in order to evaluate the feasibility of long-term imaging of MSCs. This study provides a first step in achieving the goal of tracking the migration of MSCs delivered *in vivo* using PEGylated fibrin gels in order to assess the role of MSCs in the process of neovascularization and tissue repair. A better understanding of the process of neovascularization, and the extent to which MSCs participate in this process, can potentially lead to the development of better therapies for tissue repair.

2.2 MATERIALS AND METHODS

2.2.1 Human MSC culture

Human mesenchymal stem cells (hMSCs) (Lonza, Walkersville, MD) were cultured in Dulbecco's Modified Eagle Medium (DMEM) (Invitrogen, Carlsbad, CA) supplemented with 10% fetal bovine serum (FBS), 1% glutamax, and 1% penicillin-streptomycin. The cell culture media was changed every 2-3 days. Cells were passaged using 0.25% trypsin/EDTA (Lonza), collected by centrifugation at 600 x g for 7 minutes, and counted with trypan blue exclusion. For all experiments, cells were seeded at a density of 5,000 cells/cm^2. Cells were grown under standard cell culture conditions (37°C, 5% CO_2). Passage 5-8 hMSCs were used in this study.

2.2.2 Nanoparticle synthesis

Gold nanoparticles were synthesized via citrate reduction of tetrachloroauric (III) acid ($HAuCl_4$) under reflux. Gold nanoparticles of various sizes (20 nm, 40 nm, and 60 nm) were synthesized by varying the percentage of sodium citrate. Gold nanoparticles were coated with poly-L-lysine (1-5 kD) by adding 120 μL of poly-L-lysine/mL of nanoparticle solution and allowed to mix for 30 minutes. Poly-L-lysine hydrobromide (Sigma-Aldrich, St. Louis, MO) was dissolved in distilled water prior to use.

2.2.3 Nanoparticle characterization

A DelsaNano (Beckman Coulter, Inc., Brea, CA) was used to determine the size and zeta potential of citrate-stabilized (CS) and poly-L-lysine (PLL) coated gold nanoparticles in water and in cell culture media. Briefly, nanoparticle solutions were loaded into a glass cuvette and readings were taken at a temperature of 25°C. For size measurements, 5 repetitions were performed for each nanoparticle solution with 60

readings per repetition. For zeta potential measurements, 3 repetitions were performed for each nanoparticle solution with 5 readings per repetition.

An FEI Tecnai transmission electron microscope operating at 80 kV and fitted with a top mount AMT Advantage HR 1kX1k digital camera was used to determine the size and shape of citrate-stabilized and poly-L-lysine coated gold nanoparticles in water and in cell culture media. Images were taken at 135kx magnification. Prior to imaging, carbon coated copper 300 mesh grids (Electron Microscopy Sciences, Hatfield, PA) were placed in the nanoparticle solutions and allowed to incubate for approximately 2 minutes. The grids were then removed from the solution and allowed to dry.

2.2.4 Nanoparticle incubation and assessment of cell uptake

Cells were cultured as described in section 2.2.1. Nanoparticle media was made by centrifuging the nanoparticle solutions (5000 x g for 15 minutes for 20 nm citrate-stabilized nanoparticles and 3220 x g for 30 minutes for all other nanoparticle solutions) and resuspending the pellet in phenol red free media at a concentration of approximately 10^{12} nanoparticles/mL. MSC growth media was aspirated from the flasks and 200 $\mu L/cm^2$ of nanoparticle media was added to the cell culture and allowed to incubate for 24 hours. After 24 hours, the nanoparticle media was removed and the cells were washed with phosphate-buffered saline (PBS). A Leica DMI2000B microscope equipped with a Leica DFC290 camera was used to obtain dark field images in order to assess nanoparticle uptake.

2.2.5 LIVE/DEAD staining

In order to assess cell viability after nanoparticle uptake, a LIVE/DEAD stain was performed. Briefly, stock solutions of calcein AM (4 mM) and ethidium homodimer-1 (2 mM) were diluted in PBS to a final working concentration of 4 μM and 1 μM,

respectively. MSC growth media was removed from the wells and the cells were washed two times in PBS. The cells were then incubated in the LIVE/DEAD stain for 45 minutes at 37°C, after which they were washed two times in PBS. The stained cells were then imaged using fluorescence microscopy (Leica DMI2000B microscope equipped with a Leica DFC290 camera). Control cells consisted of cells not incubated with nanoparticles. Cell viability was assessed at various time points over a two week period.

2.2.6 MTT assay

A Sigma-Aldrich MTT Cell Proliferation Assay kit was used to perform the MTT assay. Briefly, MTT reagent was added to cells at a ratio of 100 μL/mL of media. The samples were incubated for 3 hours at 37°C. The detergent reagent was then used to lyse the cells. A universal microplate reader ELX800 (Bio-Tek Instruments Inc., Winooski, VT) was used to measure the absorbance values of the samples at 562 nm and a reference wavelength of 630 nm. Control cells consisted of cells not incubated with nanoparticles. A blank sample containing no cells was used and subtracted from all measurements. Cytotoxicity was assessed over a one week period at various time points. Triplicate samples were used and the assay was performed twice.

The number of cells was calculated using a standard curve. A one-way ANOVA, followed by t-tests for multiple comparisons, was used to statistically compare the experimental conditions to the control condition at the same time point ($p<0.01$).

2.2.7 MSC differentiation

The ability of the cells to exhibit bipotent differentiation (*i.e.* adipogenic and osteogenic) after nanoparticle uptake was assessed for all nanoparticle conditions. Control cells consisted of cells not incubated with nanoparticles and which were induced to differentiate into the specified lineages. Negative control cells consisted of cells not

incubated with nanoparticles and which were not induced to differentiate into the specified lineages.

Briefly, adipogenesis was induced by plating cells at a density of 2.1 x 10^4 cells/cm^2 and allowing the cells to grow to confluency. After the cultures reached 100% confluence, the growth media was replaced with adipogenic induction media (DMEM, 10% FBS, 1% penicillin-streptomyocin, 1% glutamax, 1 µM dexamethasone (Sigma-Aldrich, St. Louis, MO), 10 µg/mL 3-isobutyl-1-methylxanthine (Sigma-Aldrich, St. Louis, MO), 10 µg/mL insulin (Sigma-Aldrich, St. Louis, MO), and 100 µM indomethacin (Sigma-Aldrich, St. Louis, MO)). After three days, the adipogenic induction media was replaced with adipogenic maintenance media for one day (DMEM, 10% FBS, 1% penicillin-streptomyocin, 1% glutamax, 10 µg/mL insulin). Three cycles of induction/maintenance were performed, after which the cells were incubated in adipogenic maintenance media for seven days. Control cells were supplemented only with adipogenic maintenance media. Oil red O (Sigma-Aldrich, St. Louis, MO) staining was used to assess adipogenesis. The cells were fixed in 10% formalin and then incubated in 60% isopropanol for 4 minutes. The cells were then incubated in oil red O staining solution for 5 minutes, rinsed in tap water, and counterstained in hematoxylin for 1 minute. After washing with tap water, the slides were mounted and viewed under phase contrast using a Leica DMI2000B microscope equipped with a Leica DFC290 camera.

Osteogenesis was induced by plating cells at a density of 3.1 x 10^3 cells/cm^2. The cells were allowed to adhere for 24 hours, after which the media was replaced with osteogenic induction media (DMEM, 10% FBS, 1% pencillin-streptomyocin, 1% glutamax, 50 µg/mL ascorbic acid, 100 nM dexamethsone (Sigma-Aldrich, St. Louis, MO), and 10 mM beta-glycerophosphate disodium salt hydrate (Sigma-Aldrich, St. Louis, MO)). Osteogenesis was induced over a period of two weeks, after which a von

Kossa staining kit (Fisher Scientific) was used to assess osteogenesis. The cells were fixed in 10% formalin and then incubated in 5% silver nitrate for 40 minutes with exposure to an ultraviolet light. The cells were washed in distilled water and then placed in 5% sodium thiosulfate for 2 minutes, after which they were rinsed in tap water and placed in nuclear fast red stain for 5 minutes. After washing with tap water, the slides were mounted and viewed under bright field using a Leica DMI2000B microscope equipped with a Leica DFC290 camera.

2.2.8 Inductively coupled plasma mass spectrometry

Initial nanoparticle loading and retention over a two week period were assessed for cells incubated with 20 nm citrate-stabilized nanoparticles using inductively coupled plasma mass spectrometry (ICP-MS). Cells were cultured and incubated with nanoparticles for 24 hours as described in section 2.2.3. After 24 hours, the nanoparticle media was removed and the cells were washed two times with PBS. The cells were then incubated in growth media without nanoparticles and collected at the designated time points. Cell media was changed every 2-3 days and the cells were passaged after reaching ~80% confluence.

At the designated time points the cells were collected, centrifuged, and resuspended in 300 μL of 70% nitric acid and incubated at 60°C for 14 hours, after which the cells were diluted 100x in nanopure water. A standard curve was used to quantify the amount of gold in the cells. Briefly, standard solutions were made by diluting AAS gold standard (Sigma-Aldrich, St. Louis, MO) in the same background solution as that of the cell solutions. All measurements were made using triplicate samples.

2.3 RESULTS AND DISCUSSION

2.3.1 Nanoparticle characterization

Nanoparticle size was analyzed using transmission electron microscopy (TEM) and dynamic light scattering (DLS). In addition, nanoparticle shape and zeta potential were assessed using TEM and DLS, respectively. Using DLS, the average size of the three nanoparticle formulations (*i.e.* citrate-stabilized nanoparticles in water) were determined to be 23.1 ± 4.14 nm, 49.78 ± 9.18 nm, and 57.58 ± 10.72 nm (Table 2.1), and were designated as 20 nm, 40 nm, and 60 nm, respectively. In addition, representative TEM images of 20 nm, 40 nm, and 60 nm citrate-stabilized (CS) nanoparticles in water are shown in Figures 2.1A, B, and C, respectively.

Coating the gold nanoparticles with poly-L-lysine (PLL) caused the zeta potential of the nanoparticles in water to go from negatively charged (approximately -30 mV) to positively charged (approximately +30 mV), as determined using a DelsaNano. There was also a slight increase in the average size of the nanoparticles after coating with PLL (Table 2.1). It should be noted that 20 nm particles most likely undergo aggregation in the presence of PLL.

2.3.2 MSC nanoparticle loading

MSC nanoparticle loading was assessed using dark field microscopy. Control cells were not incubated with nanoparticles and appear as a faint blue (Figure 2.2A). Due to the faint appearance of the control cells under dark field, a phase contrast image of the control cells is provided in Figure 2.2A1 to verify the presence of cells.

Nanoparticle loaded cells appear a yellow-orange color when observed under dark field microscopy, as compared to cells not loaded with nanoparticles, which appear blue. The dark field images show that cells were loaded with 20 nm, 40 nm, and 60 nm CS

nanoparticles after 24 hour incubation (Figures 2.2B, D, and F, respectively), as evidenced by the yellow-orange appearance of the cells. In addition, cells were loaded with 20 nm, 40 nm, and 60 nm PLL coated nanoparticles after 24 hour incubation (Figures 2.2C, E, and G, respectively), as evidenced by the yellow-orange appearance of the cells.

Cells were also incubated with 20 nm, 40 nm, and 60 nm gold nanoparticles coated with polyethylene glycol (PEG), but did not exhibit nanoparticle uptake. Instead, cells incubated with PEGylated nanoparticles more closely resembled the control cells. However, MSC nanoparticle loading was not expected for cells incubated with PEGylated nanoparticles because of the well-documented evidence of PEG as a stealthing agent.[23,24] Due to the fact that the nanoparticle formulations used in this study did not incorporate targeting agents (*e.g.* targeting antibodies), nanoparticle uptake by cells was passive, and thus MSCs were unable to detect and passively uptake PEGylated nanoparticles.

2.3.3 MSC viability and cytotoxicity

MSC viability and cytotoxicity after nanoparticle loading was assessed using a LIVE/DEAD stain and an MTT assay. The effect of nanoparticle loading on MSC viability was assessed over a two week period at various time points. The time points (day 1, day 7, and day 14) correspond to the number of days after initial nanoparticle incubation. The results of the LIVE/DEAD assay are shown in Figure 2.3A. Green cells were considered live and red cells were considered dead. Control cells were not incubated with nanoparticles. As evident from the representative LIVE/DEAD images in Figure 2.3A, the cells remained viable for all nanoparticle formulations over a two week period, and there was minimal cell death present (indicated by white arrows).

Nanoparticle cytotoxicity was assessed at various time points over a one week period using an MTT proliferation assay. The time points (day 1, day 4, and day 7) correspond to the number of days after initial nanoparticle incubation. The cell numbers were quantified using a spectrophotometer and a standard curve. Control cells were not incubated with nanoparticles. The results for the MTT assay are shown in Figure 2.3B. It should be noted that the nanoparticles loaded within the cells did not contribute to the absorbance readings. Cell numbers for the various nanoparticle formulations were statistically compared to the control condition for the corresponding day. It was found for day 1 that cells loaded with 20 nm CS and 60 nm CS nanoparticles had a significantly lower cell number compared to control cells ($p<0.01$). In addition, on day 7, cells loaded with 60 nm PLL nanoparticles had a significantly lower cell number compared to control cells ($p<0.01$).

2.3.4 MSC differentiation

The bipotent ability of MSCs to differentiate to adipogenic and osteogenic lineages after nanoparticle loading was assessed in order to determine if MSC function was maintained after nanoparticle loading. Control (+) cells were not incubated with nanoparticles and were induced to differentiate and Control (-) cells were not incubated with nanoparticles and were not induced to differentiate.

Figure 2.4A shows the results of oil red O staining for assessing adipogenesis. Fatty, lipid deposits were stained red (indicated by white arrows) and are indicative of adipogenesis. The ability of MSCs to differentiate into adipocytes was maintained for all nanoparticle formulations, as qualitatively assessed by comparing the control images to the nanoparticle loaded MSC images. As expected, Control (-) cells did not exhibit any lipid deposits, as indicated by the negative staining.

Figure 2.4B shows the results of von Kossa staining for assessing osteogenesis. Calcium deposits were stained black (indicated by red arrows) and are indicative of osteogenesis. The ability of MSCs to differentiate into osteocytes was maintained for all nanoparticle formulations, as qualitatively assessed by comparing the control images to the nanoparticle loaded MSC images. Control (-) cells did not exhibit any calcium deposits.

2.3.5 MSC nanoparticle uptake and retention

Initial nanoparticle loading and retention over a two week period were determined for MSCs loaded with 20 nm CS gold nanoparticles using ICP-MS (Figure 2.5A). The average number of nanoparticles/cell decreased by approximately an order of magnitude over a two week period from $4.53 \times 10^5 \pm 3.98 \times 10^3$ nanoparticles/cell to $2.00 \times 10^4 \pm 2.18 \times 10^2$ nanoparticles/cell. Also, the number of nanoparticles/cell decreased exponentially over a two week period. Figure 2.5B compares the average number of nanoparticles/cell and cell proliferation rate for cells loaded with 20 nm CS nanoparticles. The data was normalized to the maximum value for the corresponding data set. Day 7 was the only data point that had a significant difference between the ICP-MS and cell proliferation data ($p<0.01$), as determined using a Student's t-test.

2.4 CONCLUSIONS

Previous work has demonstrated that PEGylated fibrin gels promote MSC differentiation and tubulogenesis.[4] Many investigators have suggested delivering stem cells to an injury site (*e.g.* myocardial infarction) in order to promote wound healing and retain normal physiological function.[2-4,25,26] However, it is not clear if the MSCs implanted within the gels are actively participating in neovascularization *in vivo*, and, if so, what the specific role of the delivered MSCs is in neovascularization. Thus, this study

evaluated labeling MSCs with gold nanoparticles in order to track and monitor MSCs over time *in vivo* after delivery. The specific aims of this study were to determine if nanoparticle loading of MSCs with gold nanoparticles was possible, and also to assess if MSC function was compromised as a result of nanoparticle loading. To this end, the results of this study demonstrate the feasibility of loading MSCs with gold nanoparticles in order to track the MSCs *in vivo*. Specifically, MSCs were loaded with 20 nm, 40 nm, and 60 nm CS and PLL coated gold nanoparticles. In addition, nanoparticle loading did not substantially affect MSC viability or proliferation and MSCs were still able to differentiate into adipogenic and osteogenic lineages.

MSC nanoparticle loading was accomplished via passive uptake of the nanoparticles by the cells because no targeting agents were used to promote nanoparticle uptake. The nanoparticles aggregated when resuspended in cell culture media, as evident from the change in color of the nanoparticle solution from deep red to light blue, as well as the presence of peak broadening in the absorbance spectrum. Nanoparticle aggregation can most likely be attributed to the adsorption of serum proteins onto the nanoparticle surface. It is possible that protein adsorption could promote nanoparticle uptake by the cell.

It is interesting to note that the PLL nanoparticles did not have a negative effect on MSC function. Other investigators have found that high concentrations of PLL induce cell toxicity.[27] However, PLL is commonly used to coat substrates in low concentrations in order to promote cell adhesion, with no negative effects on cell viability. In this study, the cells were exposed to a low concentration of PLL coating the nanoparticles, and, as a result, cell toxicity was not induced. In fact, previous investigators have also found that PLL in low concentrations, such as that used for coating nanoparticles, is not toxic to cells.[28,29]

The results of this study also demonstrate that nanoparticle loading decreased exponentially over time. The decrease in nanoparticle loading over time could be attributed to both cell division and exocytosis of the nanoparticles by the cells. The normalized data for the average number of nanoparticles/cell and the inverse of the cell number over time exhibit a similar trend, with what appears to be an exponential decrease over time. Of the three time points analyzed, only day 7 had a statistically significant difference between the ICP-MS and cell proliferation data. Thus, it was concluded that at the later time points, cell division was not the only factor responsible for the decrease in nanoparticle retention over time, and additional mechanisms, such as nanoparticle exocytosis, also significantly contributed to the observed results. However, as evidenced by the results, a majority of the decrease in nanoparticle retention over time was due to cell division.

Regardless of the mechanisms responsible for the decrease in the number of nanoparticles/cell, the decrease in nanoparticle retention over time has implications on the ability to image cells over long time periods. That is, a significant decrease in nanoparticle loading over time corresponds to a substantial decrease in signal when imaging. However, previous investigators have demonstrated the ability to use photoacoustic imaging, which is a noninvasive imaging approach that is capable of imaging cells at sufficient depths *in vivo*, to image human epithelial carcinoma cells.[18] The cells were also imaged *in vitro* and loaded with 50 nm EGFR-targeted gold nanospheres at a concentration almost an order of magnitude lower than that exhibited by MSCs after two weeks.[18] Thus, longitudinally imaging MSCs loaded with gold nanoparticles using photoacoustic imaging should be feasible.

The end goal of this study is to develop an imaging technique which can visualize and track MSCs at sufficient depths and spatial/temporal resolutions. Specifically, using a

noninvasive imaging approach which is capable of optically tracking MSCs *in vivo* over long time periods within a single animal model is ideal. Optical imaging modalities which could be employed to monitor and track MSCs include photoacoustic imaging,[18,19] confocal microscopy,[30] two-photon microscopy,[31] and optical coherence tomography.[32,33]

In summary, the presented work demonstrates the ability to load MSCs with gold nanoparticles of various sizes and surface coatings. In addition, this study also demonstrates that MSC function is not altered by nanoparticle loading. Furthermore, these findings lend to the possibility of longitudinal imaging MSCs *in vivo* in order to better understand the participation and role of MSCs in neovascularization.

	Average Diameter
20 nm CS (water)	23.1 ± 4.14 nm
20 nm PLL (water)	1128.1 ± 226.64 nm
40 nm CS (water)	49.78 ± 9.18 nm
40 nm PLL (water)	52.02 ± 9.73 nm
60 nm CS (water)	57.58 ± 10.72 nm
60 nm PLL (water)	61.04 ± 11.65 nm

Table 2.1: Dynamic light scattering was used to determine the average size of the nanoparticle formulations. Results are shown as average nanoparticle size ± standard deviation. Reprinted with permission from Ricles *et al.*[34] Copyright 2011 Dove Medical Press.

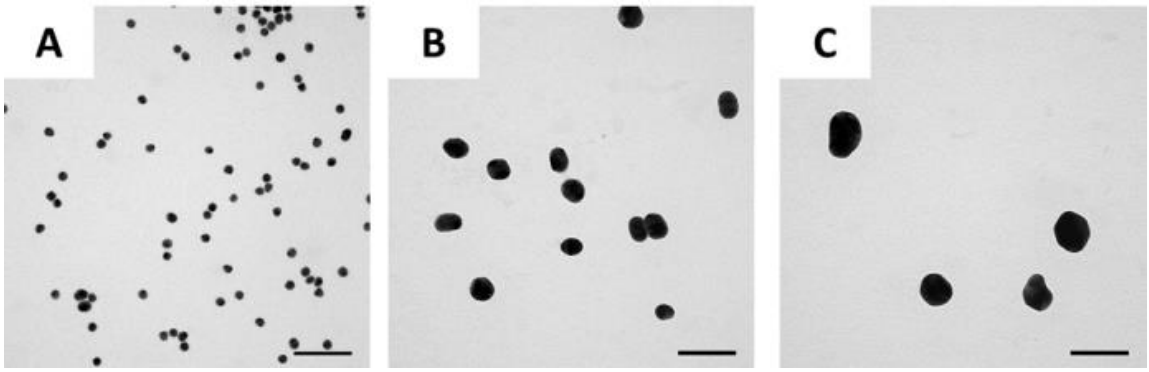

Figure 2.1: Representative TEM images of (A) 20 nm, (B) 40 nm, and (C) 60 nm citrate-stabilized gold nanoparticles in water. Scale bars = 100 nm. Reprinted with permission from Ricles *et al.*[34] Copyright 2011 Dove Medical Press.

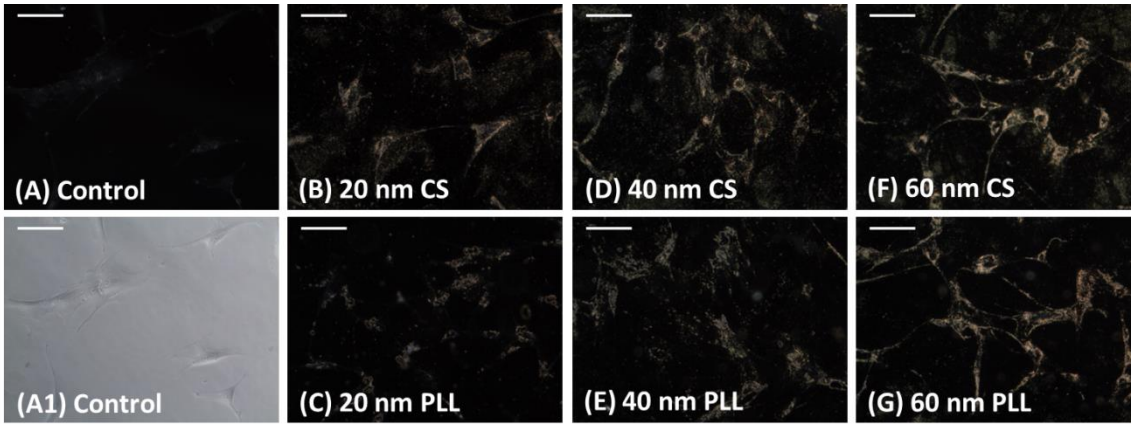

Figure 2.2: Dark field images of MSCs incubated for 24 hours with (B) 20 nm citrate-stabilized, (C) 20 nm poly-L-lysine, (D) 40 nm citrate-stabilized, (E) 40 nm poly-L-lysine, (G) 60 nm citrate-stabilized, and (G) 60 nm poly-L-lysine media. (A) A control dark field image and (A1) phase contrast image of MSCs not incubated with nanoparticles is shown for comparison. Scale bars = 100 μm. Abbreviations: citrate-stabilized (CS), poly-L-lysine (PLL). Reprinted with permission from Ricles *et al.*[34] Copyright 2011 Dove Medical Press.

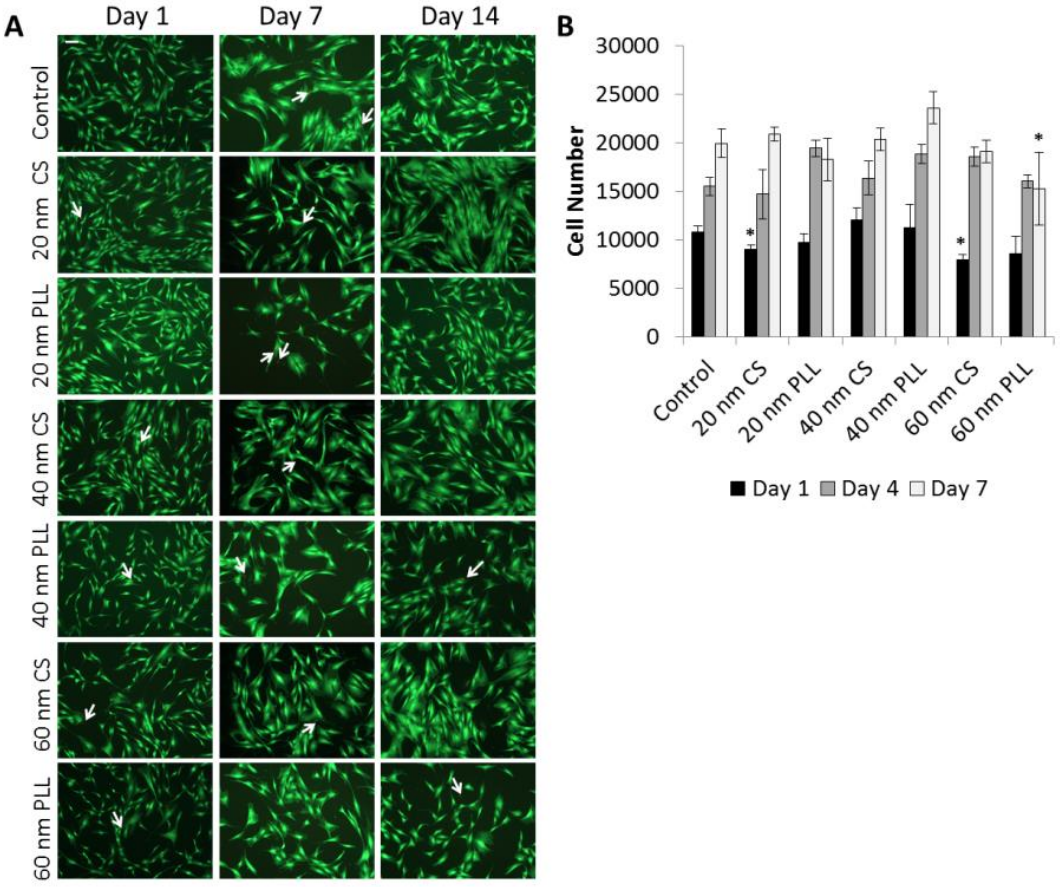

Figure 2.3: (A) Representative LIVE/DEAD images of cells incubated with nanoparticles for 24 hours and assessed at various time points after nanoparticle removal over a two week period. Cells which appear green were considered live and those which appear red were considered dead (indicated by white arrows). Scale bar = 100 µm. (A) An MTT assay was used to assess nanoparticle cytotoxicity by quantifying cell number over a one week period. Data is shown as an average ± standard deviation. Significantly lower differences in cell number from the control for the corresponding day are indicated by an asterisk (* = $p<0.01$). Abbreviations: citrate-stabilized (CS), poly-L-lysine (PLL). Reprinted with permission from Ricles *et al.*[34] Copyright 2011 Dove Medical Press.

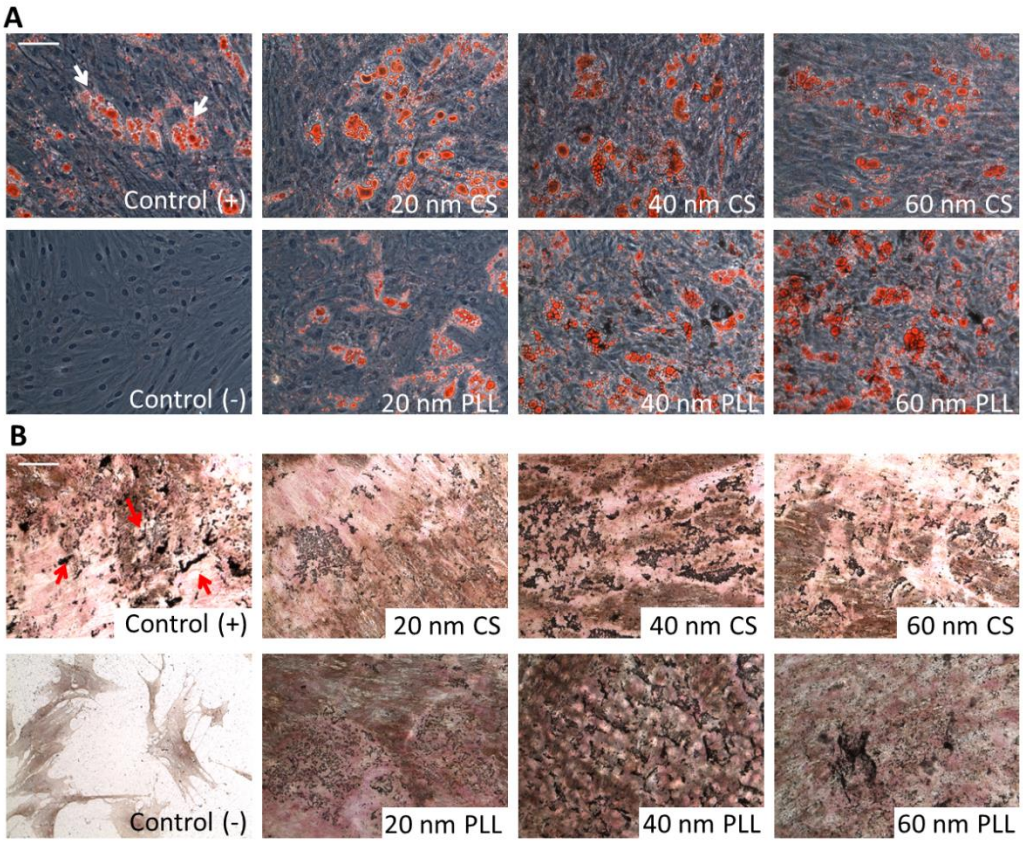

Figure 2.4: The bipotent ability of MSCs to differentiate to adipogenic and osteogenic lineages was assessed after 24 hour nanoparticle incubation. Control cells were not incubated with nanoparticles. Control (+) cells were induced to differentiate and Control (-) cells were not induced to differentiate. (A) Oil red O staining was used to assess adipogenic differentiation by staining for lipid deposits (white arrows). (B) Von Kossa staining was used to assess osteogenic differentiation by staining for calcium deposits (red arrows). Scale bar = 100 µm. Reprinted with permission from Ricles *et al.*[34] Copyright 2011 Dove Medical Press.

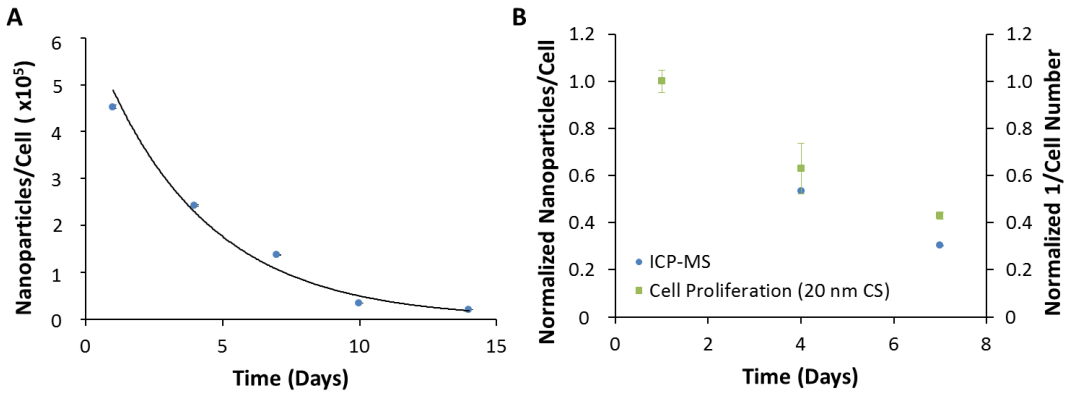

Figure 2.5: (A) Nanoparticle uptake and retention over a two week period were assessed using ICP-MS for cells incubated with 20 nm citrate-stabilized nanoparticles for 24 hours. The results are shown as the average number of nanoparticles/cell ± standard error. (B) Comparison of the normalized values for the average number of nanoparticles/cell and the inverse of cell proliferation over time for cells labeled with 20 nm citrate-stabilized nanoparticles. The results are shown as the average values ± standard deviation. Reprinted with permission from Ricles *et al.*[34] Copyright 2011 Dove Medical Press.

2.5 REFERENCES

1. Pittenger, M.F., Mackay, A.M., Beck, S.C., Jaiswal, R.K., Douglas, R., Mosca, J.D., Moorman, M.A., Simonetti, D.W., Craig, S., Marshak, D.R. Multilineage potential of adult human mesenchymal stem cells. *Science* **284**, 143-147 (1999).

2. Zhang, G., Wang, X., Wang, Z., Zhang, J., Suggs, L. A PEGylated fibrin patch for mesenchymal stem cell delivery. *Tissue Engineering* **12**, 9-19 (2006).

3. Zhang, G., Hu, Q., Braunlin, E.A., Suggs, L.J., Zhang, J. Enhancing efficacy of stem cell transplantation to the heart with a PEGylated fibrin biomatrix. *Tissue engineering. Part A* **14**, 1025-1036 (2008).

4. Zhang, G., Drinnan, C.T., Geuss, L.R., Suggs, L.J. Vascular differentiation of bone marrow stem cells is directed by a tunable three-dimensional matrix. *Acta Biomater* **6**, 3395-3403 (2010).

5. Asahara, T., Murohara, T., Sullivan, A., Silver, M., van der Zee, R., Li, T., Witzenbichler, B., Schatteman, G., Isner, J.M. Isolation of putative progenitor endothelial cells for angiogenesis. *Science* **275**, 964-967 (1997).

6. Valarmathi, M.T., Davis, J.M., Yost, M.J., Goodwin, R.L., Potts, J.D. A three-dimensional model of vasculogenesis. *Biomaterials* **30**, 1098-1112 (2009).

7. Al-Khaldi, A., Eliopoulos, N., Martineau, D., Lejeune, L., Lachapelle, K., Galipeau, J. Postnatal bone marrow stromal cells elicit a potent VEGF-dependent neoangiogenic response in vivo. *Gene Ther* **10**, 621-629 (2003).

8. Lee, Z., Dennis, J.E., Gerson, S.L. Imaging stem cell implant for cellular-based therapies. *Experimental biology and medicine* **233**, 930-940 (2008).

9. Nagesha, D., Laevsky, G.S., Lampton, P., Banyal, R., Warner, C., DiMarzio, C., Sridhar, S. In vitro imaging of embryonic stem cells using multiphoton luminescence of gold nanoparticles. *International journal of nanomedicine* **2**, 813-819 (2007).

10. D, H., M, B., P, J., V, H., Trchova, M., Likavanova, K., M, K., Hajek, M., Sykova, E. Effect of different magnetic nanoparticle coatings on the efficiency of stem cell labeling. *Journal of Magnetism and Magnetic Materials* **321**, 1539-1547 (2009).

11. Adonai, N., Nguyen, K.N., Walsh, J., Iyer, M., Toyokuni, T., Phelps, M.E., McCarthy, T., McCarthy, D.W., Gambhir, S.S. Ex vivo cell labeling with 64Cu-pyruvaldehyde-bis(N4-methylthiosemicarbazone) for imaging cell trafficking in mice with positron-emission tomography. *Proceedings of the National Academy of Sciences of the United States of America* **99**, 3030-3035 (2002).

12. Sheikh, A.Y., Wu, J.C. Molecular imaging of cardiac stem cell transplantation. *Current cardiology reports* **8**, 147-154 (2006).

13. Frangioni, J.V., Hajjar, R.J. In vivo tracking of stem cells for clinical trials in cardiovascular disease. *Circulation* **110**, 3378-3383 (2004).

14. Huang, D.M., Hsiao, J.K., Chen, Y.C., Chien, L.Y., Yao, M., Chen, Y.K., Ko, B.S., Hsu, S.C., Tai, L.A., Cheng, H.Y., Wang, S.W., Yang, C.S. The promotion of human mesenchymal stem cell proliferation by superparamagnetic iron oxide nanoparticles. *Biomaterials* **30**, 3645-3651 (2009).

15. Guzman, R., Uchida, N., Bliss, T.M., He, D., Christopherson, K.K., Stellwagen, D., Capela, A., Greve, J., Malenka, R.C., Moseley, M.E., Palmer, T.D., Steinberg, G.K. Long-term monitoring of transplanted human neural stem cells in developmental and pathological contexts with MRI. *Proceedings of the National Academy of Sciences of the United States of America* **104**, 10211-10216 (2007).

16. Ferreira, L. Nanoparticles as tools to study and control stem cells. *Journal of Cellular Biochemistry* **108**, 746-752 (2009).

17. Ferreira, L., Karp, J.M., Nobre, L., Langer, R. New opportunities: the use of nanotechnologies to manipulate and track stem cells. *Cell stem cell* **3**, 136-146 (2008).

18. Mallidi, S., Larson, T., Aaron, J., Sokolov, K., Emelianov, S. Molecular specific optoacoustic imaging with plasmonic nanoparticles. *Optics express* **15**, 6583-6588 (2007).

19. Sokolov, K., Follen, M., Aaron, J., Pavlova, I., Malpica, A., Lotan, R., Richards-Kortum, R. Real-time vital optical imaging of precancer using anti-epidermal growth factor receptor antibodies conjugated to gold nanoparticles. *Cancer research* **63**, 1999-2004 (2003).

20. Xu, M., Wang, L. Photoacoustic imaging in biomedicine. *Rev Sci Instrum* **77**, 041101 (2006).

21. Siphanto, R.I., Thumma, K.K., Kolkman, R.G., van Leeuwen, T.G., de Mul, F.F., van Neck, J.W., van Adrichem, L.N., Steenbergen, W. Serial noninvasive photoacoustic imaging of neovascularization in tumor angiogenesis. *Optics express* **13**, 89-95 (2005).

22. Lao, Y., Xing, D., Yang, S., Xiang, L. Noninvasive photoacoustic imaging of the developing vasculature during early tumor growth. *Phys Med Biol* **53**, 4203-4212 (2008).

23. Niidome, T., Yamagata, M., Okamoto, Y., Akiyama, Y., Takahashi, H., Kawano, T., Katayama, Y., Niidome, Y. PEG-modified gold nanorods with a stealth character for in vivo applications. *Journal of controlled release : official journal of the Controlled Release Society* **114**, 343-347 (2006).

24. Yang, H., Lopina, S.T., DiPersio, L.P., Schmidt, S.P. Stealth dendrimers for drug delivery: correlation between PEGylation, cytocompatibility, and drug payload. *Journal of materials science. Materials in medicine* **19**, 1991-1997 (2008).

25. Yeghiazarians, Y., Zhang, Y., Prasad, M., Shih, H., Saini, S.A., Takagawa, J., Sievers, R.E., Wong, M.L., Kapasi, N.K., Mirsky, R., Koskenvuo, J., Minasi, P., Ye, J., Viswanathan, M.N., Angeli, F.S., Boyle, A.J., Springer, M.L., Grossman, W. Injection of bone marrow cell extract into infarcted hearts results in functional improvement comparable to intact cell therapy. *Molecular therapy : the journal of the American Society of Gene Therapy* **17**, 1250-1256 (2009).

26. Liu, J., Hu, Q., Wang, Z., Xu, C., Wang, X., Gong, G., Mansoor, A., Lee, J., Hou, M., Zeng, L., Zhang, J.R., Jerosch-Herold, M., Guo, T., Bache, R.J., Zhang, J. Autologous stem cell transplantation for myocardial repair. *American journal of physiology. Heart and circulatory physiology* **287**, H501-511 (2004).

27. Fischer, D., Li, Y., Ahlemeyer, B., Krieglstein, J., Kissel, T. In vitro cytotoxicity testing of polycations: influence of polymer structure on cell viability and hemolysis. *Biomaterials* **24**, 1121-1131 (2003).

28. Ziady, A.G., Gedeon, C.R., Muhammad, O., Stillwell, V., Oette, S.M., Fink, T.L., Quan, W., Kowalczyk, T.H., Hyatt, S.L., Payne, J., Peischl, A., Seng, J.E., Moen, R.C., Cooper, M.J., Davis, P.B. Minimal toxicity of stabilized compacted DNA nanoparticles in the murine lung. *Molecular therapy : the journal of the American Society of Gene Therapy* **8**, 948-956 (2003).

29. Arbab, A.S., Bashaw, L.A., Miller, B.R., Jordan, E.K., Lewis, B.K., Kalish, H., Frank, J.A. Characterization of biophysical and metabolic properties of cells labeled with superparamagnetic iron oxide nanoparticles and transfection agent for cellular MR imaging. *Radiology* **229**, 838-846 (2003).

30. Mallidi, S., Larson, T., Tam, J., Joshi, P.P., Karpiouk, A., Sokolov, K., Emelianov, S. Multiwavelength photoacoustic imaging and plasmon resonance coupling of gold nanoparticles for selective detection of cancer. *Nano Lett* **9**, 2825-2831 (2009).

31. Durr, N.J., Larson, T., Smith, D.K., Korgel, B.A., Sokolov, K., Ben-Yakar, A. Two-photon luminescence imaging of cancer cells using molecularly targeted gold nanorods. *Nano Lett* **7**, 941-945 (2007).

32. Skala, M.C., Crow, M.J., Wax, A., Izatt, J.A. Photothermal optical coherence tomography of epidermal growth factor receptor in live cells using immunotargeted gold nanospheres. *Nano Lett* **8**, 3461-3467 (2008).

33. Gobin, A.M., Lee, M.H., Halas, N.J., James, W.D., Drezek, R.A., West, J.L. Near-infrared resonant nanoshells for combined optical imaging and photothermal cancer therapy. *Nano Lett* **7**, 1929-1934 (2007).

34. Ricles, L.M., Nam, S.Y., Sokolov, K., Emelianov, S.Y., Suggs, L.J. Function of mesenchymal stem cells following loading of gold nanotracers. *International journal of nanomedicine* **6**, 407-416 (2011).

Chapter 3: Investigation of a dissociative nanoparticle system for efficient clearance

3.1 INTRODUCTION

The ideal contrast agent for stem cell monitoring should not only be safe and nontoxic, but also have minimal transfer to non-stem cells and be efficiently cleared from the body. If the contrast agent is not efficiently cleared, it could lead to accumulation in organs and tissues, resulting in toxicity. In addition, transfer of contrast agents to non-stem cells would result in tracking the incorrect cell type, which is especially a concern when monitoring cell-based therapies.

Following intravenous delivery, nanoparticle blood residence time and the route of clearance is dependent upon the size and surface coating of the nanoparticle.[1-3] Nanoparticle retention in the blood increases with nanoparticle size, while the extent of renal clearance decreases with increasing size, as shown in Figure 3.1. The cross-over point between the two curves exists at a hydrodynamic diameter of 5-6 nm, meaning that nanoparticles within that size range are rapidly cleared from the body via renal filtration.[1-3] On the other hand, larger nanoparticles are found to be sequestered and cleared by Kupffer cells in the liver and macrophages in the spleen.[2-4] Kupffer cells and macrophages are part of the reticuloendothelial system (RES), consisting of phagocytic cells which clear debris and foreign substances from the body.[5] Renal filtration is desirable because of the intracellular catabolism associated with hepatic clearance.[2]

In addition to affecting clearance, nanoparticle size also affects cellular uptake. Chithrani *et al* found that the optimal size for nanoparticle uptake was a hydrodynamic diameter of 50 nm.[6] Smaller nanoparticles require clustering of the particles together on the surface of the membrane in order for endocytosis to take place. This can be attributed

to the free energy requirements for membrane wrapping of the nanoparticle.[6] On the other hand, particles larger than 50 nm require more membrane receptor interactions.[6,7] However, the slow diffusion kinetics of the receptors results in slow membrane wrapping time, leading to a smaller number of nanoparticles being taken up by the cell.[6]

Another ideal requirement for contrast agents for stem cell tracking is minimal transfer to non-stem cells. Other investigators have found nanoparticle transfer to macrophages *in vivo*,[8-10] resulting in the monitoring and tracking of macrophages instead of the delivered stem cell therapy. One study monitored quantum dot labeled stem cells delivered into a bone defect model.[11] However, after 7 days, fluorescent signals were observed at the contralateral sites. Histological analysis revealed that this signal was not from stem cells, but instead from macrophages, as a majority of the quantum dots in both limbs were associated with macrophages.[11] As a result, the investigators were monitoring what appeared to be stem cells, but were in fact macrophages. In another study, stem cells were labeled with superparamagnetic iron oxide particles and transduced with a fluorescent protein.[10] Longitudinal magnetic resonance (MR) imaging showed signals up to 4 weeks, whereas bioluminescence imaging showed a progressive decrease in signal over time.[10] Histological analysis revealed that most of the iron oxide nanoparticles were taken up by macrophages, accounting for the persistent MR signals.[10] It appeared that a majority of the stem cells had died, causing the decrease in bioluminescence signal. However, MR imaging is unable to distinguish viable from non-viable cells. As a result, the apoptotic stem cells were most likely endocytosed by macrophages, resulting in the MR signal to be generated from the macrophages.[10] Overall, these studies demonstrate that monitoring of stem cells using nanoparticle labeling has a drawback of not being able to distinguish the transfer of contrast agents to non-stem cells.

This study attempts to address the issue of nanoparticle transfer using a 5 nm nanoparticle contrast agent. Since cells do not readily detect and take up 5 nm gold nanoparticles, the nanoparticles were aggregated using a poly-L-lysine coating. The hypothesis is that the particles will dissociate within endosomal compartments with minimal biologic effects and will not accumulate in subsequent cell populations or in organs *in vivo*. Non-stem cells, such as macrophages, are less likely to take up nanoparticles exocytosed from MSCs which are 5 nm in diameter compared to larger nanoparticles. This is due to the fact that cells do not readily take up smaller nanoparticles (*i.e.* smaller than 50 nm) and the nanoparticles will be cleared more rapidly from the system, providing less time for macrophages to take up the nanoparticles.

3.2 MATERIALS AND METHODS

3.2.1 Cell culture

Rat mesenchymal stem cells were isolated from the bone marrow of Lewis rats (200-300 g). The femoral marrow cavity was flushed and adherent cells were collected and cultured in Dulbecco's Modified Eagle Medium (DMEM) (Invitrogen, Carlsbad, CA) supplemented with 10% fetal bovine serum (FBS), 1% glutamax, and 1% penicillin-streptomyocin. Non-adherent cells were removed after 24 hours by replacing the media. The media was then changed every two days and the cells were passaged once reaching 80% confluency. The cells were cultured under standard cell culture conditions (37°C, 5% CO2). Passage 3-7 cells were used in all studies.

3.2.2 Nanoparticle synthesis

Gold nanoparticles with a diameter of 5 nm were synthesized via citrate reduction of tetrachloroauric (III) acid ($HAuCl_4$) under reflux. Briefly, 100 mL of nanopure water was brought to boiling and 1 mL of 10 mg/mL $HAuCl_4$ was added while stirring. After 1

minute, 1 mL of 10 mg/mL sodium citrate solution was added and allowed to stir for 1 minute. Finally, 1 mL of 0.75 mg/mL of sodium borohyride in a 10 mg/mL sodium citrate solution was added and stirred for 5 minutes. The solution was then brought to room temperature. To promote aggregation of the particles, the gold nanoparticles were coated with poly-L-lysine (1-5 kD) by adding 16.57 μL of poly-L-lysine (3.33×10^{-3} M) per mL of nanoparticle solution and allowed to mix for 30 minutes. Poly-L-lysine hydrobromide (Sigma-Aldrich, St. Louis, MO) was dissolved in distilled water prior to use.

3.2.3 Nanoparticle dissociation

A dissociation study evaluating enzymatic degradation of the poly-L-lysine (PLL) linkages between nanoparticles was conducted. Nanoparticles were coated with PLL and incubated with 2.5% trypsin without EDTA. Sodium chloride (40 mM) was added to represent physiological conditions. The solutions were put on an orbital shaker and incubated at 37ºC for 72 hours. A microplate reader (BioTek) was used to obtain ultraviolet-visible spectroscopy measurements at various time points over the 72 hour time frame. At 72 hours, 10% FBS solution was added in order to evaluate if nanoparticle aggregation was affected due to adsorption of serum proteins. Nanoparticle morphology was evaluated using transmission electron microscopy (TEM). For TEM preparation, a drop of nanoparticle solution was placed on carbon coated copper 300 mesh grids (Electron Microscopy Sciences, Hatfield, Pa) which had been glow discharged. An FEI Tecnai transmission electron microscope fitted with a top mount AMT Advantage HR 1kX1k digital camera and operating at 80 kV was used to visualize the grids.

3.2.4 MSC nanoparticle labeling

Nanoparticle media was made by combining an equal volume of 5 nm PLL nanoparticles with 2x DMEM. MSCs were plated at a concentration of 5,000 cells/cm^2 and incubated with 5 nm citrate stabilized or 5 nm PLL media (200 μL/cm^2) for 24 hours. Light microscopy was used to qualitatively analyze nanoparticle uptake by MSCs. Following nanoparticle incubation, the media was removed and the cells were washed with phosphate buffered saline (PBS) to remove excess particles. The cells were then incubated with 4',6-diamidino-2-phenylindole (DAPI) (1 μg/ml) for 15 minutes, followed by PBS washes. A Leica DMI2000B microscope, equipped with a Leica DFC290 camera, was used to obtain phase contrast and dark field images. Controls consisted of cells not incubated with nanoparticles.

Inductively coupled plasma mass spectrometry (ICP-MS) was used to quantitatively analyze nanoparticle uptake by MSCs. Following nanoparticle loading, the cells were collected using trypsinization and counted. To prepare the samples for ICP-MS, all of the solutions were incubated in 300 μL of 70% nitric acid at 60ºC overnight. The solutions were then diluted to 3.7% nitric acid using ultrapure water prior to running the samples on the ICP-MS machine. Nanoparticle loading was quantified using a standard curve. Standard solutions were made by diluting AAS gold standard (Sigma-Aldrich, St. Louis, MO) in the same background solution as the samples. The number of nanoparticles per cell was calculated based on the nanoparticle dimensions and cell number.

For TEM analysis of nanoparticle endocytosis, MSCs were incubated with gold nanoparticle media for 24 hours. The cells were collected at various times points and fixed using glutaraldehyde/paraformaldehyde and osmium textroxide/potassium ferrocyanide fixatives. Cell pellets were embedded within an agar solution and

dehydrated by washing with serial concentrations of ethanol solutions, followed by treatment with 100% acetone. The pellets were then incubated in a sequential series of resin/acetone solutions and solidified in 100% resin at 60ºC for two days. The sample preparation process was accelerated using a microwave (Blowave, Pelco). The samples were then sectioned into 70 nm sections using an Ultracut UTC Ultramicrotome (Leica Microsystems, Wetzlar, Germany) and mounted onto thin bar mesh copper grids. The sections were post stained with lead citrate and viewed using a FEI Tecnai transmission electron microscope fitted with a top mount AMT Advantage HR 1kX1k digital camera and operating at 80 kV.

3.2.5 Assessment of MSC function

Cell viability was assessed following nanoparticle labeling using LIVE/DEAD viability staining and an MTS proliferation assay. LIVE/DEAD staining was performed by incubating the cells with a working solution of calcein AM (4 μm) and ethidium homodimer-1 (1 μm) for 45 minutes at 37ºC. The cells were washed with PBS and imaged using fluorescence microscopy (Leica DMI2000B microscope equipped with a Leica DFC 290 camera).

A Sigma-Aldrich MTT Cell Proliferation Assay kit was used to perform the MTT assay. Briefly, MTT reagent was added to cells at a ratio of 100 μL/mL of media. The samples were incubated for 3 hours at 37°C. The detergent reagent was then used to lyse the cells. A universal microplate reader ELX800 (Bio-Tek Instruments Inc., Winooski, VT) was used to measure the absorbance values of the samples at 562 nm and a reference wavelength of 630 nm. Control cells consisted of cells not incubated with nanoparticles. A blank sample containing no cells was used and subtracted from all measurements. Cytotoxicity was assessed over a one week period at various time points. Triplicate

samples were used and the assay was performed twice. The number of cells was calculated using a standard curve. A one-way ANOVA, followed by t-tests for multiple comparisons, was used to statistically compare the experimental conditions to the control condition at the same time point ($p<0.01$).

The ability of the cells to exhibit bipotent differentiation (*i.e.* adipogenic and osteogenic) after nanoparticle uptake was assessed for all nanoparticle conditions. Control cells consisted of cells not incubated with nanoparticles and which were induced to differentiate into the specified lineages. Negative control cells consisted of cells not incubated with nanoparticles and which were not induced to differentiate into the specified lineages.

Briefly, adipogenesis was induced by plating cells at a density of 2.1 x 10^4 cells/cm^2 and allowing the cells to grow to confluency. After the cultures reached 100% confluence, the growth media was replaced with adipogenic induction media (DMEM, 10% FBS, 1% penicillin-streptomyocin, 1% glutamax, 1 µM dexamethasone (Sigma-Aldrich, St. Louis, MO), 10 µg/mL 3-isobutyl-1-methylxanthine (Sigma-Aldrich, St. Louis, MO), 10 µg/mL insulin (Sigma-Aldrich, St. Louis, MO), and 100 µM indomethacin (Sigma-Aldrich, St. Louis, MO)). After three days, the adipogenic induction media was replaced with adipogenic maintenance media for one day (DMEM, 10% FBS, 1% penicillin-streptomyocin, 1% glutamax, 10 µg/mL insulin). Three cycles of induction/maintenance were performed, after which the cells were incubated in adipogenic maintenance media for seven days. Control cells were supplemented only with adipogenic maintenance media. Oil red O (Sigma-Aldrich, St. Louis, MO) staining was used to assess adipogenesis. The cells were fixed in 10% formalin and then incubated in 60% isopropanol for 4 minutes. The cells were then incubated in oil red O staining solution for 5 minutes, rinsed in tap water, and counterstained in hematoxylin for

1 minute. After washing with tap water, the slides were mounted and viewed under phase contrast using a Leica DMI2000B microscope equipped with a Leica DFC290 camera.

Osteogenesis was induced by plating cells at a density of 3.1 x 10^3 cells/cm^2. The cells were allowed to adhere for 24 hours, after which the media was replaced with osteogenic induction media (DMEM, 10% FBS, 1% pencillin-streptomyocin, 1% glutamax, 50 μg/mL ascorbic acid, 100 nM dexamethsone (Sigma-Aldrich, St. Louis, MO), and 10 mM beta-glycerophosphate disodium salt hydrate (Sigma-Aldrich, St. Louis, MO)). Osteogenesis was induced over a period of two weeks, after which a von Kossa staining kit (Fisher Scientific) was used to assess osteogenesis. The cells were fixed in 10% formalin and then incubated in 5% silver nitrate for 40 minutes with exposure to an ultraviolet light. The cells were washed in distilled water and then placed in 5% sodium thiosulfate for 2 minutes, after which they were rinsed in tap water and placed in nuclear fast red stain for 5 minutes. After washing with tap water, the slides were mounted and viewed under bright field using a Leica DMI2000B microscope equipped with a Leica DFC290 camera.

3.2.6 Macrophage uptake of 5 nm nanoparticles

Murine macrophages (J774A.1, ATCC) were cultured under standard cell culture conditions (37°C, 5% CO_2) in DMEM with 10% FBS. The media was changed every two days and passaged once reaching confluency. Passage 10-20 cells were used in all studies.

To assess cellular uptake of 5 nm nanoparticles by macrophages, the cells were plated at a concentration of 5,000 cells/cm^2 and incubated with 5 nm nanoparticles, 5 nm PLL nanoparticles, and 5 nm PLL nanoparticles which had been incubated with trypsin (72 hours) to promote dissociation of the particles. After 24 hours, the nanoparticle media

was removed and the cells were imaged using a Leica DMI2000B microscope equipped with a Leica DFC290 camera. The cells were then collected using a cell scrapper and counted. The absorbance spectra of the cells were measured using a microplate reader (BioTek) and normalized to the cell number.

3.2.7 MSC co-culture with macrophages

MSCs were labeled with 5 nm PLL nanoparticles as described in Section 3.2.4. The MSCs were collected via trypsinization and washed two times with PBS to remove any nanoparticle debris. MSCs were then labeled with CellTracker^{TM} Green CMFDA dye (10 μM) (Life Technologies) for 40 minutes at 37ºC, washed with PBS, and plated at 2,500 cells/cm^2 in a 12 well plate. Macrophages were collected using a cell scrapper and fluorescently labeled with CellTracker^{TM} CM-DiI (Invitrogen). The cells were incubated with CM-DiI (5 μM) at 37ºC for 8 minutes and then 4ºC for 15 minutes, washed with PBS, and co-cultured with the MSCs at a concentration of 2,500 cells/cm^2. The cells were imaged using a Leica DMI2000B microscope equipped with a Leica DFC290 camera

3.3 RESULTS AND DISCUSSION

3.3.1 *In vitro* dissociation of 5 nm nanoparticles

The enzymatic dissociation of 5 nm PLL nanoparticle aggregates was investigated using trypsin digestion, which cleaves the carboxyl side of arginine and lysine. Initially following PLL coating and prior to trypsin incubation, the nanoparticles exhibited extensive peak broadening and red shifting in the absorbance spectra (Figure 3.2A). The spectrum underwent a substantial shift over 72 hours toward the original spectrum of the 5 nm spheres, as quantified in Figure 3.2B and C. There was a slight discrepancy in the absorbance curves of the dissociated nanoparticles and the original 5 nm nanospheres, which could be attributed to the presence of some aggregates still present in solution. The

stability of the dissociated nanoparticles was demonstrated by the lack of re-aggregation following addition of FBS to the solution. TEM images of the nanosphere solutions before PLL aggregation, after PLL aggregation, following enzymatic dissociation, and after addition of FBS are shown in Figures 3.2D-G. Following PLL addition, the nanoparticles form aggregates on the size range of hundreds of nanometers. However, after enzymatic dissociation, the nanoparticles form much smaller aggregates or return to the original 5 nm nanoparticles.

3.3.2 Nanoparticle labeling and intracellular localization

Endocytosis of 5 nm primary nanoparticles (citrate-stabilized) and 5 nm PLL nanoparticles by MSCs was evaluated using phase contrast and dark field microscopy (Figure 3.3). MSCs did not endocytose the 5 nm primary nanoparticles, which coincides with other reports in the literature of cells not readily endocytosing small nanoparticles (*i.e.* much smaller than 50 nm). However, MSCs endocytosed the 5 nm PLL nanoparticles, which is most likely due to the larger size of the aggregated particles. TEM analysis of cell sections shows the nanoparticles compact and localized within endosomal compartments in the cell (Figure 3.4). It is possible that the nanoparticles formed clusters on the cell membrane and were subsequently endocytosed. However, it is also possible that the vesicles containing the endocytosed nanoparticles fused within the cells,[6] resulting in the large number of nanoparticles per vesicle. TEM analysis of cell sections at 7 and 14 days show the nanoparticles are still localized in large, compact regions within the cell. Based on this analysis, it is difficult to distinguish if the 5 nm PLL nanoparticles are still aggregated or if they are dissociated into primary nanoparticles but still localized within close proximity to each other within the endosomal compartments.

Nanoparticle retention was quantified over 14 days using ICP-MS analysis. Figure 3.5A shows the average number of nanoparticles per cell, which decreases exponentially over time from approximately $5x10^7$ nanoparticles/cell to $5x10^6$ nanoparticles/cell. Figure 3.5B compares the average number of nanoparticles/cell to the average total number of nanoparticles (both curves normalized to the day 1 data point). The curve representing the total number of nanoparticles decreases over time, suggesting that some nanoparticles are being lost due to exocytosis and not passed on to progeny. However, there is a discrepancy between the two curves at the later time points, which can attributed to the nanoparticles being passed on to progeny following cell division.

3.3.3 MSC function following labeling with 5 nm poly-L-lysine nanoparticles

Stem cell function following labeling with 5 nm PLL nanoparticles was assessed over time using LIVE/DEAD staining and an MTT proliferation assay. MSCs remained viable (Figure 3.6A) and continued to proliferate (Figure 3.6B) following nanoparticle labeling. In addition, the ability of MSCs to differentiate to osteogenic and adipogenic lineages was also investigated. Oil red O staining was used to stain fatty lipid deposits red to assess adipogenesis and von Kossa staining was used to stain calcium deposits black to assess osteogenesis. MSCs retained their bipotent ability to differentiate to adipogenic and osteogenic lineages (Figure 3.6C).

3.3.4 Macrophage interaction with 5 nm poly-L-lysine nanoparticles

Macrophages were incubated with various formulations of 5 nm nanoparticles to investigate if macrophages will endocytose the particles following exocytosis by MSCs. The different nanoparticle conditions consisted of primary 5 nm nanoparticles (citrate-stabilized), aggregated 5 nm nanoparticles (5 nm PLL), and aggregated 5 nm nanoparticles which were enzymatically dissociated (5 nm PLL dissociated). Figure 3.7A

shows dark field and bright field images of macrophages incubated with the various nanoparticle formulations. Macrophages were found not to endocytose 5 nm citrate-stabilized nanoparticles. On the other hand, macrophages endocytosed 5 nm PLL nanoparticles to a large extent, most likely due to the aggregation of the nanoparticles and the PLL coating, which promotes cellular uptake. However, macrophages also endocytosed the 5 nm nanoparticles which were enzymatically dissociated. This could be attributed to the fact that the aggregated nanoparticles are not completely dissociated to individual 5 nm nanoparticles, as shown in Figure 3.2. As a result, there were still some nanoparticle aggregates which were large enough to be detected and endocytosed by macrophages. A more quantitative analysis of nanoparticle uptake by macrophages is shown in Figure 3.7B. UV-vis measurements confirm that macrophages did not endocytose 5 nm citrate-stabilized nanoparticles. In addition, macrophages incubated with 5 nm PLL and 5 nm PLL dissociated particles exhibited absorbance spectra indicative of nanoparticle uptake. The curves were normalized by the cell number and show a 1.5 fold difference in the peak absorbance; thus macrophages endocytosed the aggregated nanoparticles to a much larger extent compared to the dissociated nanoparticles.

The 5 nm PLL nanoparticles were enzymatically dissociated using trypsin prior to incubation with macrophages. It is possible that the enzymatic dissociation using trypsin was not sufficient enough and not necessarily representative of the process occurring intracellularly within endosomes. Thus, in order to evaluate this, MSCs labeled with 5 nm PLL nanoparticles were co-cultured with macrophages. Prior to being cultured together, the cells were fluorescently labeled with CellTracker^{TM} Green CMFDA (MSCs) or CellTracker^{TM} CM-DiI (macrophages) in order to distinguish the two cell types within the culture. Dark field and bright field microscopy was used to qualitatively assess the

potential nanoparticle transfer from MSCs to macrophages. Fluorescence microscopy was used to identify the two cell types. The co-culture was evaluated daily, and by day 3 nanoparticles were evident within macrophages, as shown by the yellow circles in Figure 3.8. The nanoparticle uptake by macrophages can be attributed to nanoparticle exocytosis by MSCs followed by endocytosis of the nanoparticles by macrophages. However, it is also possible that macrophages endocytosed apoptotic MSCs containing nanoparticles. The percentage of stem cell death following therapeutic delivery is quite significant,[12,13] meaning that the possibility of infiltrating macrophages to scavenge apoptotic MSCs labeled with nanoparticles is very high. If this mechanism is occurring, then creating a dissociative nanoparticle system will not address this issue.

3.4 CONCLUSIONS

This study investigated the use of 5 nm nanoparticles as a potential labeling agent for tracking stem cells. The small size of the nanoparticles was thought to be an advantage in terms of evading transfer to non-stem cells. The nanoparticles were demonstrated to be safe and non-toxic to MSCs. *In vitro* dissociation studies demonstrated that the aggregated 5 nm PLL nanoparticles could be enzymatically dissociated over time, but nanoparticles were still found to be transferred to macrophages in co-culture experiments. While this transfer to macrophages could partially be attributed to the incomplete dissociation of the aggregated nanoparticles to primary 5 nm particles, it is also likely that macrophages were endocytosing apoptotic MSCs labeled with nanoparticles. As a result, it was concluded that the 5 nm PLL nanoparticle system did not address the issues of ensuring that contrast agent is not transferred to surrounding cells and that only MSCs are being monitored *in vivo.* Therefore, a dual nanoparticle system was developed, as outlined in Chapter 4, which is capable of tracking stem cells

following delivery *in vivo* and also monitoring macrophage infiltration and potentially the transfer of contrast agents from stem cells to macrophages.

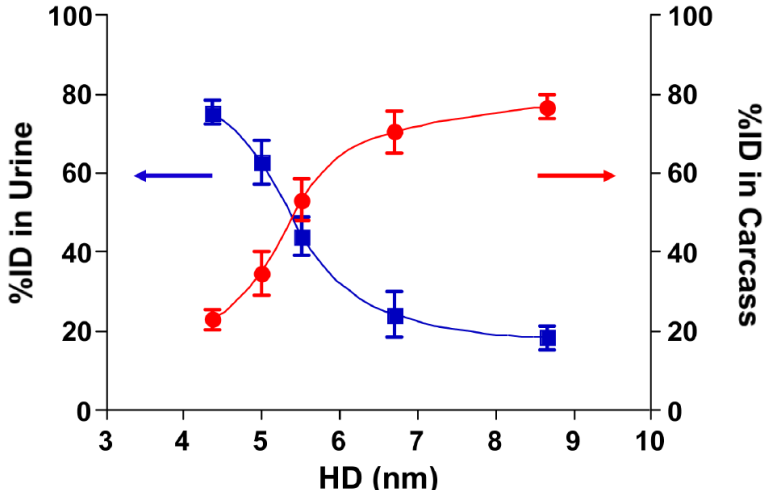

Figure 3.1: Urine excretion (blue curve) and carcass retention (red curve) of quantum dots of various hydrodynamic diameters 4 hours after intravenous injection. Reprinted with permission from Choi *et al.*[1] Copyright 2007 Nature Publishing Company.

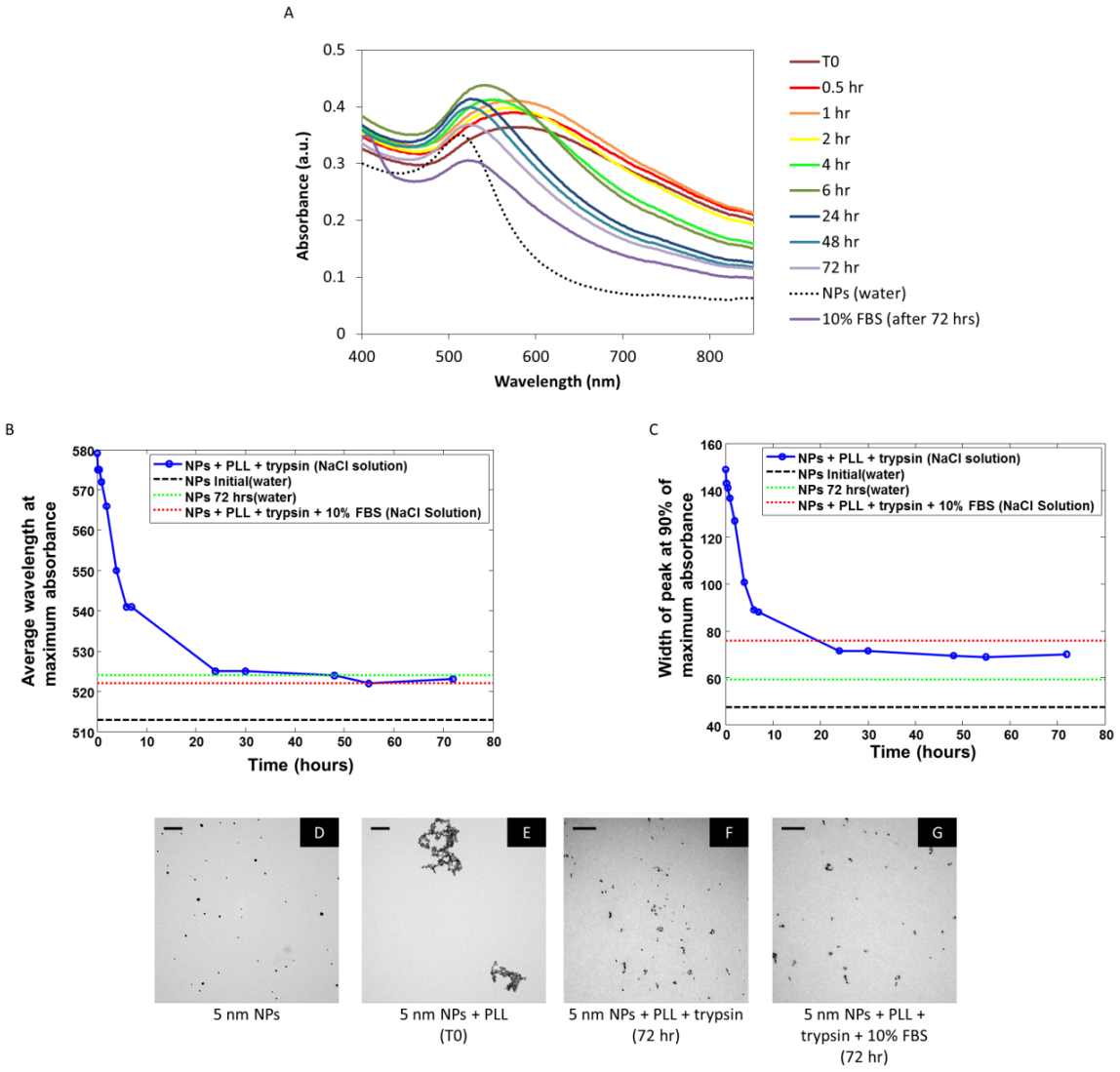

Figure 3.2: (A) Ultraviolet-visible spectroscopy of 5 nm PLL nanoparticles over time with trypsin incubation and quantification of (B) peak shifting and (C) peak broadening. Transmission electron microscopy images of (D) 5 nm citrate-stabilized nanoparticles, (E) 5 nm PLL coated nanoparticles at T0, (F) 5 nm PLL coated nanoparticles 72 hours following trypsin incubation, and (G) 5 nm PLL coated nanoparticles 72 hours following trypsin incubation with addition of 10% FBS. Scale bar = 100 nm. Abbreviations: fetal bovine serum (FBS), nanoparticles (NPs), poly-L-lysine (PLL).

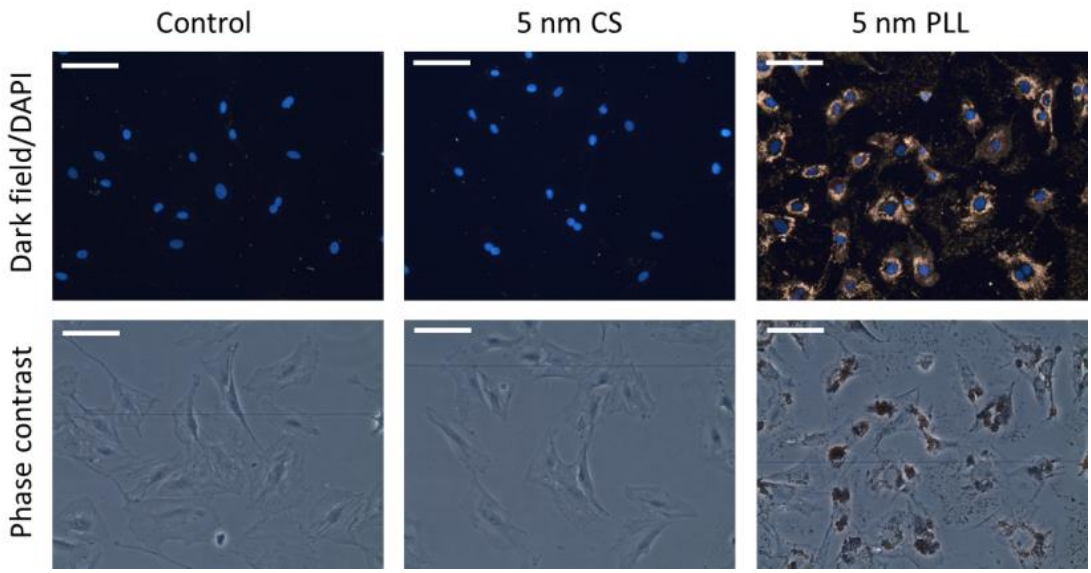

Figure 3.3: Dark field/DAPI overlay and phase contrast images of control cells (no nanoparticles) and cells incubated with 5 nm citrate-stabilized and 5 nm poly-L-lysine nanoparticles. Scale bar = 100 μm. Abbreviations: citrate-stabilized (CS), poly-L-lysine (PLL).

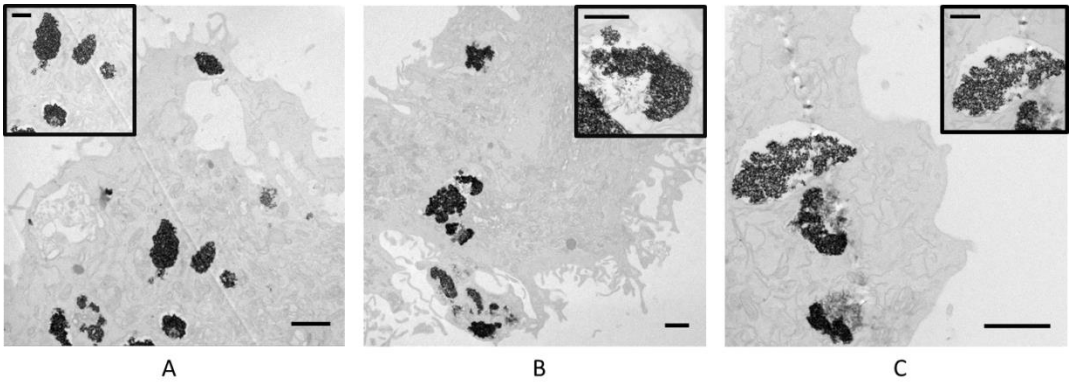

Figure 3.4: TEM images of 70 nm sections of MSCs (A) 24 hours after loading, (B) 7 days after loading, and (C) 14 days after loading with 5 nm poly-L-lysine nanoparticles. Scale bar = 1 μm. Inset scale bar = 500 nm.

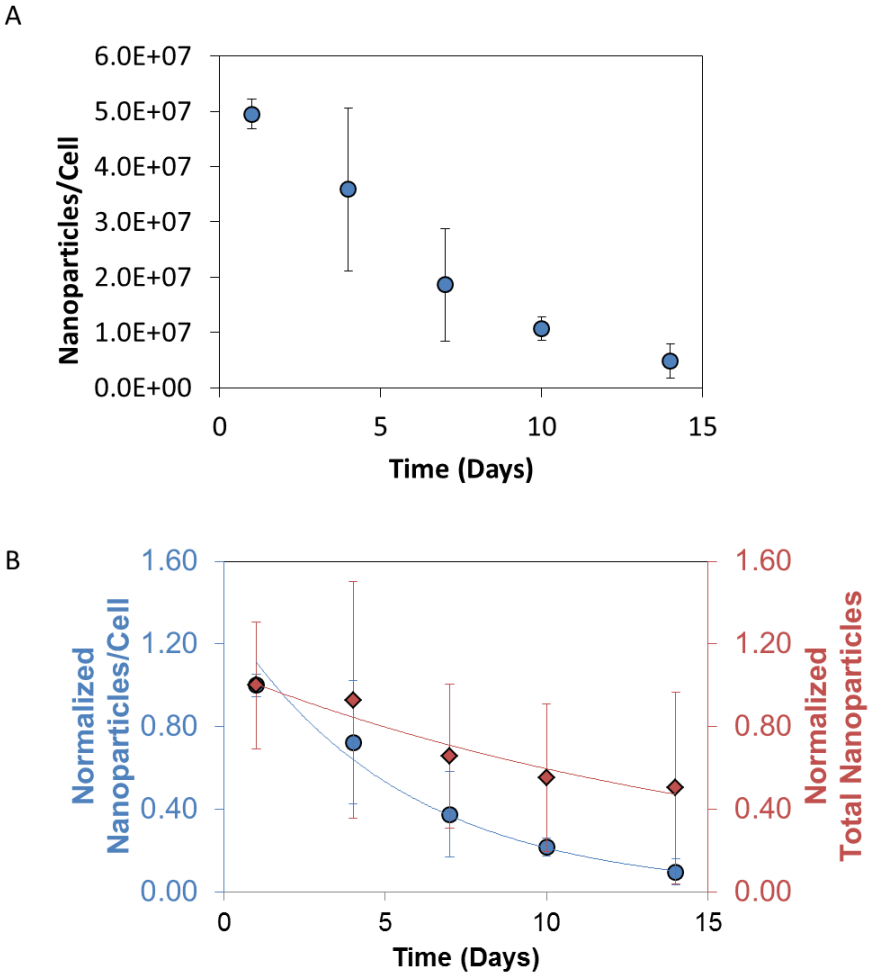

Figure 3.5: (A) Average concentration of nanoparticle loading and retention over a two week time period using inductively coupled plasma mass spectrometry. Error bars indicate standard deviation. (B) Average nanoparticle concentration compared to the total average number of nanoparticles over time. Error bars indicate standard deviation.

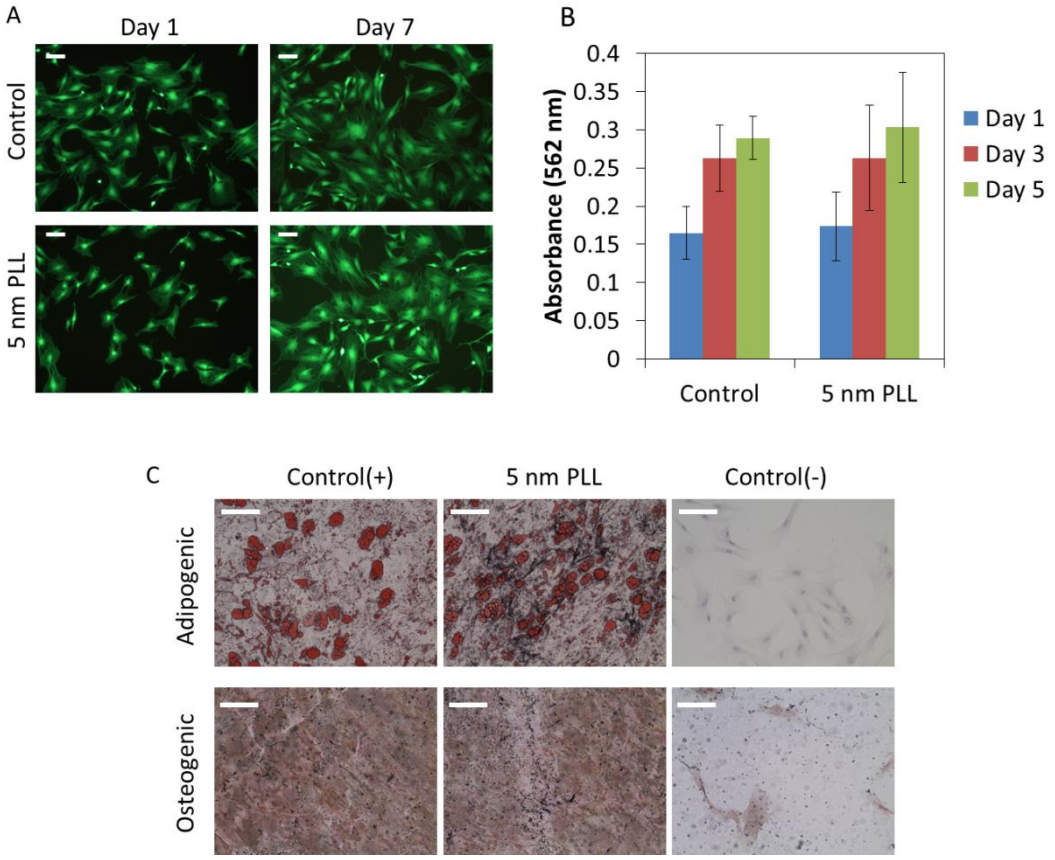

Figure 3.6: (A) LIVE/DEAD images of cells over a one week time period. Scale bars = 100 µm. (B) Cell proliferation over a one week time period was examined using an MTT cell proliferation assay. Error bars indicate standard deviation. (C) Bright field images of cells induced to differentiate to adipogenic and osteogenic lineages. Adipogenesis was assessed using oil red O staining and osteogenesis was assessed using von Kossa staining. Scale bars = 100 µm.

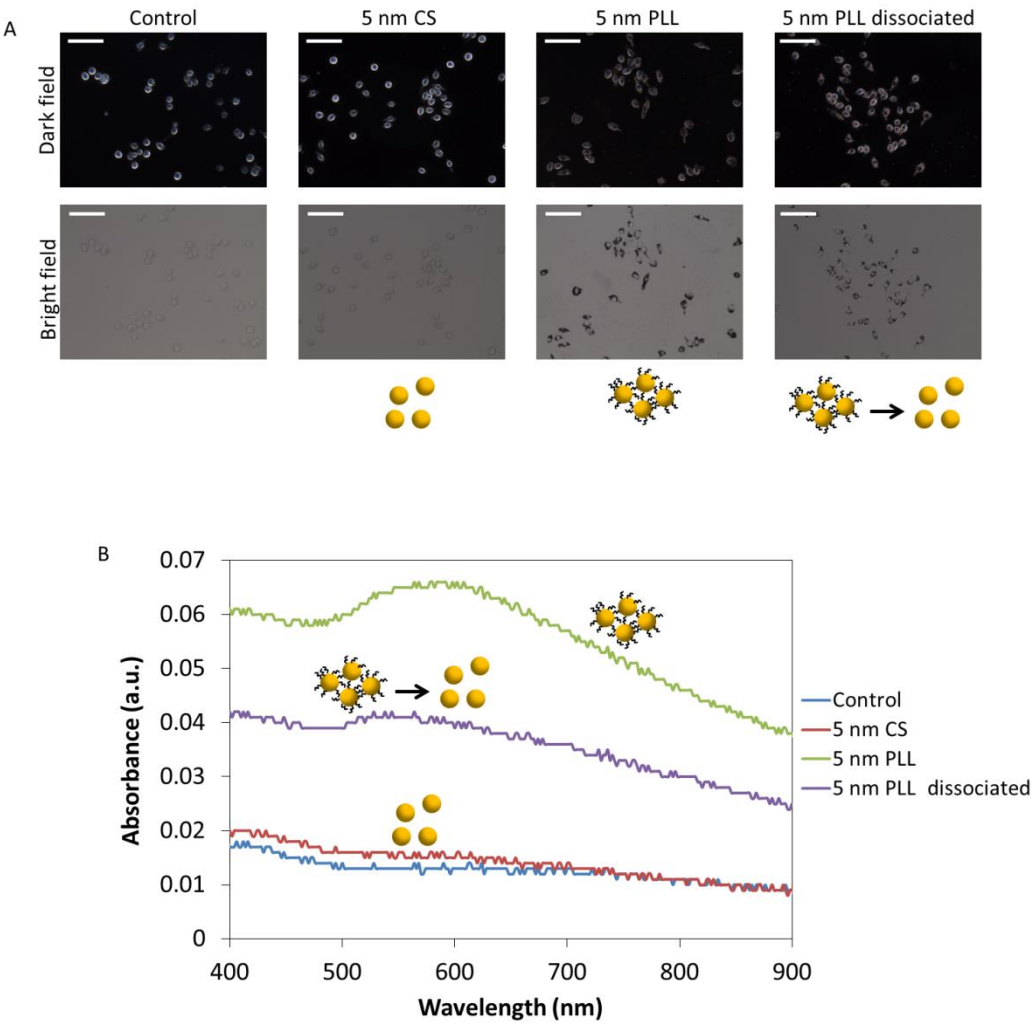

Figure 3.7: (A) Dark field and bright field microscope images of macrophages incubated with various formulations of 5 nm nanoparticles and (B) the corresponding optical absorbance spectra. Scale bar = 100 µm. Abbreviations: citrate-stabilized (CS), poly-L-lysine (PLL).

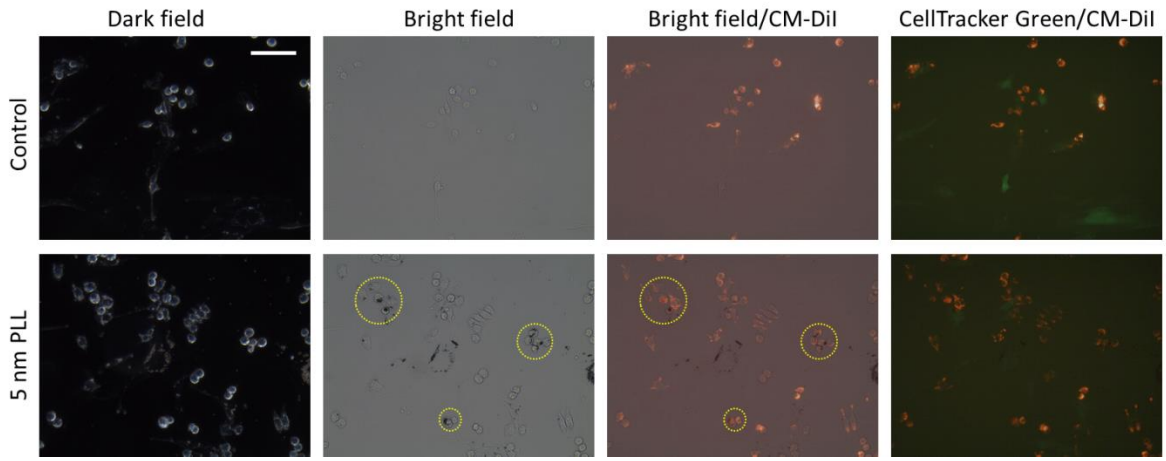

Figure 3.8: Dark field, bright field, and fluorescent microscope images of nanoparticle labeled MSCs co-cultured with macrophages. Scale bar = 100 µm. Abbreviations: poly-L-lysine (PLL).

3.5 REFERENCES

1. Choi, H.S., Liu, W., Misra, P., Tanaka, E., Zimmer, J.P., Itty Ipe, B., Bawendi, M.G., Frangioni, J.V. Renal clearance of nanoparticles. *Nat Biotechnol* **25**, 1165-1170 (2007).

2. Longmire, M., Choyke, P.L., Kobayashi, H. Clearance properties of nano-sized particles and molecules as imaging agents: considerations and caveats. *Nanomedicine* **3**, 703-717 (2008).

3. Hirn, S., Semmler-Behnke, M., Schleh, C., Wenk, A., Lipka, J., Schaffler, M., Takenaka, S., Moller, W., Schmid, G., Simon, U., Kreyling, W.G. Particle size-dependent and surface charge-dependent biodistribution of gold nanoparticles after intravenous administration. *Eur J Pharm Biopharm* **77**, 407-416 (2011).

4. Ozcan, I., Segura-Sanchez, F., Bouchemal, K., Sezak, M., Ozer, O., Guneri, T., Ponchel, G. Pegylation of poly(gamma-benzyl-L-glutamate) nanoparticles is efficient for avoiding mononuclear phagocyte system capture in rats. *International journal of nanomedicine* **5**, 1103-1111 (2010).

5. Cowan, M.K. Microbiology : a systems approach, Edn. 3rd. (McGraw-Hill, New York, NY; 2012).

6. Chithrani, B.D., Chan, W.C. Elucidating the mechanism of cellular uptake and removal of protein-coated gold nanoparticles of different sizes and shapes. *Nano Lett* **7**, 1542-1550 (2007).

7. Jiang, W., Kim, B.Y.S., Rutka, J.T., Chan, W.C.W. Nanoparticle-mediated cellular response is size-dependent. *Nature Nanotechnology* **3**, 145-150 (2008).

8. Amsalem, Y., Mardor, Y., Feinberg, M.S., Landa, N., Miller, L., Daniels, D., Ocherashvilli, A., Holbova, R., Yosef, O., Barbash, I.M., Leor, J. Iron-oxide labeling and outcome of transplanted mesenchymal stem cells in the infarcted myocardium. *Circulation* **116**, I38-45 (2007).

9. Dupont, K.M., Sharma, K., Stevens, H.Y., Boerckel, J.D., Garcia, A.J., Guldberg, R.E. Human stem cell delivery for treatment of large segmental bone defects. *Proceedings of the National Academy of Sciences of the United States of America* **107**, 3305-3310 (2010).

10. Li, Z., Suzuki, Y., Huang, M., Cao, F., Xie, X., Connolly, A.J., Yang, P.C., Wu, J.C. Comparison of reporter gene and iron particle labeling for tracking fate of human embryonic stem cells and differentiated endothelial cells in living subjects. *Stem Cells* **26**, 864-873 (2008).

11. Homan, K., Shah, J., Gomez, S., Gensler, H., Karpiouk, A., Brannon-Peppas, L., Emelianov, S. Silver nanosystems for photoacoustic imaging and image-guided therapy. *Journal of Biomedical Optics* **15**, 021316 (2010).

12. Suga, H., Glotzbach, J., Sorkin, M., Longaker, M., Gurtner, G. Paracrine mechanism of angiogenesis in adipose-derived stem cell transplantation. *Annals of Plastic Surgery* **72**, 234-241 (2014).

13. Robey, T.E., Saiget, M.K., Reinecke, H., Murry, C.E. Systems approaches to preventing transplanted cell death in cardiac repair. *J Mol Cell Cardiol* **45**, 567-581 (2008).

Chapter 4: Optimization of a dual nanoparticle system for *in vivo* monitoring of mesenchymal stem cells and macrophages

4.1 INTRODUCTION

Stem cell therapy shows great potential to treat a large variety of diseases, including cardiovascular diseases, which are the number one cause of death globally.[1] In particular, bone-marrow-derived mesenchymal stem cells (MSCs) are advantageous in that they possess angiogenic properties, are easily obtained in large numbers and expandable in culture, and are part of the ischemic response.[1] Numerous preclinical and clinical trials have investigated the therapeutic benefits of stem cell therapy for cardiovascular diseases. However, advances in the field of stem cell therapy have been limited by the inability to track administered cells,[2] which would provide information concerning cell engraftment and persistence, mechanisms of vascular regeneration, and the role of MSCs in vascular repair.

Conventional methods for assessing the biological mechanisms underlying disease states and potential therapies rely on postmortem histology, which only offers endpoint measurements and requires a large number of animals to be sacrificed in order to produce statistically significant results. A more ideal cell tracking method would involve using noninvasive longitudinal imaging to monitor cells. Towards this end, many contrast agents are currently being investigated to label cells for cell tracking purposes, including reporter genes,[3-6] radionuclides,[6-8] fluorescent probes,[9-11] and nanoparticles[4,8,12-14]. Nanoparticles, such as quantum dots, iron oxide nanoparticles, and plasmonic nanoparticles (gold and silver), offer many advantages over other contrast agents. For example, nanoparticles can be optimized to promote cellular uptake through shape, size, and surface coating modification[12,15-19] and allow for long-term monitoring of cells[12-14,20]. However, viable and non-viable cells cannot be distinguished using nanoparticle contrast

agents. As a result, it is not possible to detect if a cell is dead and has been endocytosed by macrophages, leading to a transfer of contrast agent from the labeled cells to macrophages. Other investigators have found nanoparticle transfer to macrophages,[4,21,22] resulting in the monitoring and tracking of macrophages instead of the stem cell therapy.

Thus, the goal of this study is to develop a nanoparticle system which is capable of tracking stem cells following delivery *in vivo* and also monitoring macrophage infiltration. Macrophages are known to have key roles in wound healing and vascular regeneration[23-26] and to be influenced by and exert paracrine effects on stem cells, including MSCs[27-29]. The nanoparticle system will consist of gold plasmonic nanoparticles. Gold nanoparticles can be synthesized in various shapes and sizes and their absorption characteristics can be tuned to maximally absorb in the near-infrared region, where the absorption from endogenous tissue is the lowest. Gold nanoparticles are also non-toxic to cells in certain formulations[12,30,31] and exhibit surface plasmon resonance, which contributes to their superior optical absorption properties,[32,33] making them ideal contrast agents for photoacoustic imaging[20,34]. Figure 4.1 shows the outline of the dual nanoparticle system consisting of gold nanorods to label MSCs and gold nanospheres to label macrophages. This system is delivered within a 3D PEGylated fibrin gel, which promotes the angiogenic potential of MSCs and leads to tubular network formation within the gels, as demonstrated by previous work in our lab.[35] The gold nanorods were selected because these particles maximally absorb in the near-infrared region. On the other hand, gold nanospheres maximally absorb in the visible light region (520 nm), but plasmon coupling following nanosphere endocytosis by cells leads to peak broadening. Thus, the gold nanospheres will only be detected using photoacoustic imaging when they are endocytosed by macrophages and imaged within the tissue optical window of 650-1000 nm. To evaluate this nanoparticle system, various *in vitro* assays were performed,

including labeling of cells with the nanoparticles and the assessment of cell function and viability following nanoparticle labeling. In addition, *in vitro* and *in vivo* photoacoustic imaging experiments were performed to assess the feasibility of monitoring the two cell types. Histological analysis and mass spectrometry were also performed to verify the *in vivo* photoacoustic imaging results. This study has important implications for cell tracking and the role of MSCs and macrophages in vascular regeneration.

4.2 MATERIALS AND METHODS

4.2.1 Cell culture

Rat mesenchymal stem cells were isolated from the bone marrow of Lewis rats (200-300 g). The femoral marrow cavity was flushed and adherent cells were collected and cultured in Dulbecco's Modified Eagle Medium (DMEM) (Invitrogen, Carlsbad, CA) supplemented with 10% fetal bovine serum (FBS), 1% glutamax, and 1% penicillin-streptomyocin. Non-adherent cells were removed after 24 hours by replacing the media. The media was then changed every two days and the cells were passed once reaching 80% confluency. The cells were cultured under standard cell culture conditions (37°C, 5% CO_2). Passage 3-7 cells were used in all studies.

Murine macrophages (J774A.1, ATCC) were cultured under standard cell culture conditions (37°C, 5% CO_2) in DMEM with 10% FBS. The media was changed every two days and passaged once reaching 80% confluency. Passage 10-20 cells were used in all studies.

4.2.2 Nanoparticle synthesis

Spherical gold nanoparticle seeds (20 nm in diameter) were synthesized by heating 100 mL of distilled (DI) water to 100°C and adding 1 mL of 10 mg/mL gold(III) chloride hydrate ($HAuCl_4$). Then, 5 mL of 10 mg/mL sodium citrate dissolved in DI

water was added and the reaction was allowed to cool to room temperature. Gold nanoparticles 50 nm in diameter were synthesized by mixing 7.5 mL of 10 mg/mL $HAuCl_4$, 15.61 mL of 0.2 M ammonium hydroxylamine, 750 mL of DI water, and 50 nm of seed solution while stirring. The surface of the gold nanoparticles was coated with methoxy-polyethylene glycol-thiol (mPEG-SH) at a concentration of 0.1 mM and allowed to react for 30 minutes on a shaker, followed by centrifugal filtration (Amicon ultra-15, Millipore) to remove residual PEG.

Gold nanorods (NRs) were synthesized via seed mediated growth as previously described.[36,37] Briefly, the seed solution was synthesized by mixing 5 mL of cetyl trimethylammonium bromide (CTAB) (0.2 M) with 5 mL of $HAuCl_4$ (0.5 mM) while stirring vigorously. Then 0.6 mL of ice cold sodium borohydride ($NaBH_4$) was added to the solution. The growth solution was prepared by mixing 380 mL of 0.2 M CTAB, 8 mL of 0.01 M silver nitrate ($AgNO_3$), and 40 mL of 0.01 M $HAuCl_4$ while stirring at 30°C. Then 4.4 mL of 0.1 M ascorbic acid ($C_6H_8O_6$) was added drop wise, resulting in a color change from yellow to colorless. To produce NRs, 0.958 mL of gold nanoseeds were added to the growth solution and allowed to stir for 3 minutes. The solution was allowed to age overnight, centrifuged twice at 14000 rcf for 45 minutes, and resuspended in ultrafiltrated (18 MΩcm, Thermo Scientific Barnstead Diamond water purification systems) deionized water.

The NR surface was modified by replacing CTAB with mPEG-SH through ligand exchange. Briefly, an equal volume of mPEG-SH (0.2 mM) was added to the gold NR solution, sonicated for 1 minute, and allowed to react overnight. Excess PEG was removed by centrifugal filtration (Amicon ultra-15, Millipore) at 2000 rcf for 10 minutes. Finally, a layer of silica was deposited on the surface of the PEG modified NRs through a modified Stöber method, as previously described.[38-40] Under vigorous stirring, 2 mL of

PEGylated NRs was added to 3 mL of isopropanol, followed by 1.2 mL of tetraethyl orthosilica (TEOS) (3%) in isopropanol and 1.2 mL of ammonium hydroxide (8.4%) in isopropanol. The reaction was allowed to mix for 2 hours, followed by centrifugal filtration at 500 rcf for 15 minutes, twice. The NRs were then coated with a layer of poly-L-lysine (5 kD; Sigma-Aldrich) at a concentration of 0.833 mM and allowed to react for 2 hours, followed by centrifugation at 3000 rcf for 10 minutes and then 5000 rcf for 7 minutes.

The size of the nanoparticles was characterized using transmission electron microscope (TEM) analysis and dynamic light scattering (DLS), and the surface charge was characterized using zeta potential measurements. For TEM preparation, a drop of nanoparticle solution was placed on carbon coated copper 300 mesh grids (Electron Microscopy Sciences, Hatfield, Pa) which had been glow discharged. An FEI Tecnai transmission electron microscope fitted with a top mount AMT Advantage HR 1kX1k digital camera and operating at 80 kV was used to assess NR size and morphology. Chemical analysis of the silica coating on the NR surface was performed by imaging the grids using the TEM mode of a Hitachi S5500 FESEM operated at 30 kV and equipped with an energy dispersive spectrometer (EDS). ImageJ analysis was used to quantify the size of the NRs and thickness of the silica coating (n = 100). A DelsaNano (Beckman Coulter, Inc., Brea, CA) was used for DLS analysis of spherical nanoparticles. Nanoparticle solutions were loaded into a cuvette and readings were taken at a temperature of 25°C. For size measurements, 5 repetitions were performed for each nanoparticle solution with 60 readings per repetition. A Zetasizer Nano ZS (Malvern) was used to measure the zeta potential of nanoparticle solutions. A total of 3 measurements, with 15 repetitions, were collected at a temperature of 25°C.

4.2.3 Nanoparticle labeling of cells

Gold nanosphere media was made following PEGylation of 50 nm nanospheres. The nanospheres were sterile filtered using a 0.22 μm filter, centrifuged in a centrifugal filter tube (Amicon ultra-15, Millipore) at 3000 rcf for 5 minutes, and resuspended in cell culture media at a concentration of approximately 10^{12} NPs/mL. Gold NR media was made following PLL coating of silica NRs. The NRs were sterile filtered using a 0.22 μm filter and centrifuged at 3000 rcf for 10 minutes. The supernatant was then centrifuged at 5000 rcf for 7 minutes. The NRs were resuspended in cell culture media at a concentration of approximately 10^{12} NRs/mL. Macrophages were incubated with nanosphere media (200 μL/cm^2) and MSCs were incubated with NR media (200 μL/cm^2) for 24 hours.

Bright field and dark field microscopy was used to qualitatively analyze nanoparticle uptake by macrophages and MSCs. Following nanoparticle incubation, the media was removed and the cells were washed with phosphate buffered saline (PBS) to remove excess particles. The cells were then incubated with DAPI (1 μg/ml) for 15 minutes, followed by PBS washes. A Leica DMI2000B microscope, equipped with a Leica DFC290 camera, was used to obtain bright field and dark field images. Controls consisted of cells not incubated with nanoparticles.

Inductively coupled plasma mass spectrometry (ICP-MS) was used to quantitatively analyze nanoparticle uptake by macrophages and MSCs in 2D, as well as by macrophages in 3D PEGylated fibrin gels. The PEGylated fibrin gels were synthesized as described below and contained 50,000 cells/mL and 10^{12} NPs/mL. Following nanoparticle loading in 2D, the cells were collected using trypsinization and counted. To collect the cells in 3D, the gels were digested by incubation with 500 μL of bovine pancreatic trypsin (5 mg/mL in 0.9% sodium chloride) per 1 mL of gel for 1 hour.

The reaction was quenched with serum containing media and the solution was filtered with a 70 μm and 40 μm cell strainer and centrifuged at 600 rcf for 7 minutes to collect the cells. To prepare the samples for ICP-MS, all of the solutions were incubated in 300 μL of 70% nitric acid at 60ºC overnight. The solutions were then diluted to 3.7% nitric acid using ultrapure water prior to running the samples on the ICP-MS machine. The samples containing MSCs incubated with 50 nm gold nanospheres were prepared for ICP-MS analysis by heating the samples at 150ºC and bringing them to dryness. The samples were then resuspended in 200 μL of aqua regia and further diluted with 2% HCl. Nanoparticle loading was quantified using a standard curve. Standard solutions were made by diluting AAS gold standard (Sigma-Aldrich, St. Louis, MO) in the same background solution as the samples. The number of nanoparticles per cell was calculated based on the nanoparticle dimensions and cell number.

For TEM analysis of nanoparticle endocytosis, MSCs were incubated with gold NR media for 24 hours. The cells were collected and fixed using glutaraldehyde/paraformaldehyde and osmium textroxide/potassium ferrocyanide fixatives. Cell pellets were embedded within an agar solution and dehydrated by washing with serial concentrations of ethanol solutions, followed by treatment with 100% acetone. The pellets were then incubated in a sequential series of resin/acetone solutions and solidified in 100% resin at 60ºC for two days. The sample preparation process was accelerated using a microwave (Blowave, Pelco). The samples were then sectioned into 70 nm sections using an Ultracut UTC Ultramicrotome (Leica Microsystems, Wetzlar, Germany) and mounted onto thin bar mesh copper grids. The sections were post stained with lead citrate and viewed using a FEI Tecnai transmission electron microscope fitted with a top mount AMT Advantage HR 1kX1k digital camera and operating at 80 kV.

MSCs and macrophages were co-cultured in a 3D PEGylated fibrin gel to investigate the nanoparticle system in a 3D environment. PEGylated fibrin gels were synthesized as described below and contained 25,000 MSCs/mL; 50,000 macrophages/mL; and 10^{14} NPs/mL. The gels were made in 12 well transwell plates with 8.0 μm pore sizes and were incubated at 37°C in MSC growth media.

4.2.4 Stability of nanorod silica coating

The stability of the silica coating on the nanorods following MSC endocytosis was evaluated using TEM and EDS analysis. MSCs were labeled with silica NRs and collected immediately. In order to collect the endocytosed NRs, the cells were then lysed with RIPA buffer (Santa Cruz Biotechnology) supplemented with PMSF, protease inhibitor cocktail, and sodium orthovanadate. The samples were incubated in lysis buffer for 30 minutes and homogenized by passing the samples through a 21G needle ten times at 4ºC. The samples were then centrifuged at 3200 x g for 10 minutes and the supernatant collected. The samples were washed with water and centrifuged again to concentrate the nanorods (3200 x g for 10 minutes). A drop of nanoparticle solution was then placed on carbon coated copper 300 mesh grids (Electron Microscopy Sciences, Hatfield, Pa) which had been glow discharged. Control conditions consisted of silica NRs exposed to the RIPA lysis buffer and silica NRs which were not exposed to the RIPA lysis buffer. The grids were then imaged using the TEM mode of a Hitachi S5500 FESEM operating at 30 kV and equipped with an energy dispersive spectrometer (EDS).

4.2.5 Cell viability

Cell viability was assessed following nanoparticle labeling using LIVE/DEAD viability staining and an MTS proliferation assay. LIVE/DEAD staining was performed by incubating the cells with a working solution of calcein AM (4 μm) and ethidium

homodimer-1 (1 μm) for 45 minutes at 37ºC. The cells were washed with PBS and imaged using fluorescence microscopy (Leica DMI2000B microscope equipped with a Leica DFC 290 camera).

Cell proliferation following nanoparticle labeling was assessed using MTS. Cells were incubated with DMEM media containing 20% MTS solution for 4 hours at 37ºC. The supernatant was collected and the absorbance value measured at 490 nm (n=3). A blank sample containing no cells was subtracted from all measurements.

The maintenance of cell function in 3D PEGylated fibrin gels was assessed after laser irradiation by examining cell morphology and tubular network formation. Difunctional succinimidyl glutarate PEG (8 mg/mL in PBS without calcium; NOF America) was added to fibrinogen (80 mg/mL in PBS without calcium; Sigma) in a 1:1 volume ratio, and the reaction was allowed to take place at room temperature for 3-5 minutes. An equal volume of MSCs as the fibrinogen and PEG mixture was then added at a concentration of 200,000 cells/mL. Gels with either NR labeled MSCs or unlabeled MSCs were made. The reaction then underwent gelation by adding an equal volume solution of thrombin (25 U/mL in 40 mM $CaCl_2$; CalBiochem). The final concentrations in the gel were 10 mg/mL of fibrinogen; 1 mg/mL of SG-PEG-SG; 50,000 cells/mL; and 12.5 U/mL of thrombin. The gels were made in 4 well chambered coverglass slides (Laboratory-Tek II; Nalge Nunc) and incubated at 37°C in MSC growth media.

The gels were irradiated at various time points (day 1, 4, and 7) using a 800 nm laser with a fluence of 10 mJ/cm^2 for 100 pulses. Control conditions consisted of the same gel formulations without laser irradiation. At day 7, the cells were stained with calcein AM (10 μM) and 3D z-stacks were taken using a Leica SP2 AOBS confocal microscope (10x magnification; 512x512 resolution). The images covered approximately

1 mm with a step size of approximately 3 μm. The 3D images were reconstructed using ImageJ.

4.2.6 *In vitro* photoacoustic imaging

A tissue mimicking phantom with varying ratios of NR labeled MSCs and nanosphere labeled macrophages was prepared for combined ultrasound and photoacoustic (US/PA) imaging. The bottom layer of the phantom consisted of gelatin (8% by weight; Sigma-Aldrich) with 15 μm diameter silica particles (0.2% by weight; Sigma-Aldrich) for ultrasonic scattering. The cell inclusions (20 μL) were placed on top of the bottom layer and consisted of gelatin mixed with cells. Each cell inclusion had a total of 10,000 cells.

Photoacoustic signals were captured using the Vevo LAZR system (VisualSonics, Inc.) including a tunable laser as well as a 40 MHz array transducer combined with an optical fiber bundle to deliver the laser pulses. RF signals were acquired for laser wavelengths ranging from 680-970 nm and with a laser fluence of 5-15 mJ/cm^2. The transducer was mechanically scanned along the tissue mimicking phantom to obtain 3D photoacoustic information. The signals exported from the imaging system were post-processed for beamforming, laser fluence compensation, image reconstruction, and signal quantification. For spectral analysis, the quantified photoacoustic signals were used to calculate the ratio of the NR labeled MSCs and the nanosphere labeled macrophages in each voxel by comparison to weighted sums of their optical absorption spectrum. Then, the estimated ratios in the voxels were averaged to calculate the overall cell ratio for whole inclusions.

4.2.7 Ischemic injury and *in vivo* photoacoustic imaging

Animal handling and care followed the recommendations of the National Institutes of Health (NIH) guidelines for the care and use of laboratory animals. All protocols were approved by the Animal Care Committee at the University of Texas at Austin. Lewis rats (11 weeks) weighing 250-300 g were used. Rats were anesthetized using isoflurane (0.5-2%) infused with oxygen (2 L/min). A femoral artery ligation was performed in Lewis rats (11 weeks, male) to induce hind limb ischemia. Through a small incision on the medial side of the thigh, the femoral artery of a single hind limb was separated from the nearby nerve and vein and ligated immediately distal to the inferior epigastric artery and proximal to the branch point of the popliteal and saphenous arteries using Prolene 5-0 sutures. The ligated segment was then excised and the skin incision closed with interrupted sutures. The animal was allowed to recover overnight and the following day (about 24 hours later), MSCs were injected intramuscularly into the gastrocnemius muscle of the ligated limb. PEGylated fibrin injections were prepared by combining difunctional succinimidyl glutarate PEG (4 mg/mL in PBS without calcium; NOF America) to fibrinogen (40 mg/mL in PBS without calcium; Sigma) in a 1:1 volume ratio. An equal volume of MSCs labeled with gold NRs was mixed with the PEGylated fibrinogen solution in a 1:1 volume ratio at a concentration of $13x10^6$ cells/mL. Next, 50 nm PEGylated gold nanospheres was added to the cell/PEGylated fibrin solution at a concentration of 10^{14} NPs/mL. The solution was then loaded into a 23 G needle syringe, followed by an equal volume of thrombin (25 U/mL in 40 mM $CaCl_2$). The solution was mixed thoroughly within the syringe and the gel solution (300 uL) was injected into the gastrocnemius of the rat. The final concentrations in the gel were 5 mg/mL of fibrinogen; 0.5 mg/mL of SG-PEG-SG; $3.33x10^6$ cells/mL; and 12.5 U/mL of thrombin. Prior to delivery, MSCs were fluorescently labeled with CellTracker™ CM-DiI (Invitrogen). The

cells were incubated with CM-DiI (15 μM) at 37ºC for 8 minutes and then 4ºC for 15 minutes, washed with PBS, and resuspended in DMEM.

Ultrasound and photoacoustic signals were captured using the Vevo LAZR (VisualSonics, Inc.) system. A 40 MHz array transducer incorporated with a fiber bundle was submerged in a water bath, and the rat hind limb was coupled through a transparent film at the bottom of the water bath. RF signals were acquired for laser wavelengths ranging from 680-970 nm and with a laser fluence of 5-10 mJ/cm^2. Post-processing was the same as that for the *in vitro* photoacoustic. The processed photoacoustic and spectroscopic images were overlaid with ultrasound images using a user-defined threshold of the photoacoustic signals.

4.2.8 Histology

At the terminal endpoint of the study, animals were sacrificed and the gastrocnemius muscles were isolated, embedded in optimal cutting temperature (OCT) compound, submerged in liquid nitrogen-cooled isopentane, and stored at -80ºC until further processing. The samples were cut into 12 μm thick sections using a cryostat and placed onto positively charged microscope slides. The tissue sections were fixed in 10% formalin for 15 minutes. Imunohistochemical and histochemical staining were subsequently performed.

For immunostaining, the slides were incubated in 0.125% trypsin solution for 20 minutes at 37ºC. They were then permeabilized in 0.5% Triton X-100 in TBST for 30 minutes and blocked in 10% normal goat serum for 1 hour. The slides were incubated overnight at 4ºC in the primary antibody (1:50 dilution in 2.5% normal goat serum) (ED1; Millipore), followed by incubation with a fluorescence-conjugated secondary antibody (1:200 in 2.5% normal goat serum) (Alexa Fluor 488 Goat Anti-Mouse

Immunoglobulin G; Life Technologies). As a negative control, normal immunoglobulin G was used instead of the primary antibody. The samples were counterstained with DAPI (5 ug/mL) for 15 minutes, mounted, and viewed using a fluorescence microscope (DMI2000B; Leica)

TUNEL staining was performed with the APO-BrdU TUNEL Assay Kit (Invitrogen). The slides were incubated in 0.125% trypsin for 20 minutes at 37ºC, followed by permeabilization in 0.5% Triton X-100 for 30 minutes. The slides were then incubated with TdT and BrdUTP for 2 hours at 37ºC. Alexa Fluor 488 dye-labeled anti-BrdU antibody was applied for 30 minutes. The slides were then counterstained with DAPI (5 ug/mL) for 15 minutes, mounted, and viewed using a fluorescence microscope (DMI2000B; Leica).

4.2.9 Fluorescence-activated cell sorting of macrophages

Seven days following intramuscular injection of nanorod labeled or unlabeled MSCs and nanospheres within PEGylated fibrin, animals were sacrificed and the gastrocnemius muscle was isolated. The muscle samples were finely minced and incubated in 1% collagenase in DMEM for 1 hour at 37ºC under constant agitation. Samples were then filtered through cell strainers (40 μm and 70 μm), washed with PBS, and blocked for 30 minutes in fluorescence-activated cell sorting (FACS) buffer (1% BSA in PBS + 1% sodium azide). Samples were then incubated with primary antibody (1:50; ED1; Millipore) in FACS buffer for 45 minutes, washed, and incubated in secondary antibody (1:50; Alexa Fluor 488 Goat Anti-Mouse Immunoglobulin G; Life Technologies) for 45 minutes. Next, samples were fixed in 4% neutral buffered formalin for 15 minutes, washed, and resuspended in PBS. Samples were then sorted for macrophages using a FACSAria flow cytometer. Following sorting, samples were

digested for ICP-MS analysis. The cells were collected by centrifuging at 270 x g for 5 minutes and resuspended in a small volume of aqua regia solution. The samples were heated at 150ºC and brought to dryness. They were then resuspended in 250 µL of aqua regia and further diluted with ultrapure water to give an HCl concentration of 5%. A standard curve was used to quantify the amount of gold in the cells by diluting AAS gold standard (Sigma-Aldrich, St. Louis, MO) in the same background solution as that of the cell solutions. The data was quantified by calculating the mass of gold per macrophage.

4.3 RESULTS AND DISCUSSION

4.3.1 Nanoparticle characterization

The size, shape, and surface charge of gold NRs and nanospheres were characterized using ultraviolet-light spectroscopy (UV-vis), TEM analysis, DLS, and zeta potential measurements. The absorbance spectra of gold NRs had a peak around 750 nm, which red shifted 20 nm following silica coating and an additional 8 nm following poly-L-lysine (PLL) coating (Figure 4.2A). Zeta potential measurements confirmed the sequential coatings were deposited on the NRs (Figure 4.2A), as the surface charge was +40 mV for CTAB coated NRs, -0.61 mV for PEG coated NRs, -30.37 mV for silica coated NRs, and +26 mV for PLL coated NRs. Using TEM analysis, the size of the NRs was measured as 55.63 ± 9.14 x 15.59 ± 3.45 nm, with a silica coating thickness of 25.04 ± 3.06 nm (Figure 4.2A). Energy dispersive spectrometry (EDS) confirmed silica coating of the gold nanorods (Figure 4.3). The 50 nm spherical nanoparticles had an absorbance peak around 520 nm (Figure 4.2B), with a red shift of a few nm following PEG coating. TEM analysis confirmed the spherical shape of the particles and DLS measured the hydrodynamic diameter of the particles as being 50.4 nm with a polydispersity index of 0.044 (Figure 4.2B). Zeta potential measurements demonstrated that the nanospheres had

a negative surface charge (-46.07 mV), which became closer to neutral (-8.41 mV) following PEG coating (Figure 4.2B).

4.3.2 Nanoparticle labeling of cells

MSCs were incubated with PLL silica NRs and the uptake by the cells was qualitatively analyzed using microscopy and quantitatively analyzed using ICP-MS. Dark field microscopy demonstrated nanoparticle labeling of MSCs as evident by the yellow/green color of the cells as compared to control cells (Figure 4.4A, C). In addition, dark nanoparticle aggregates within cells were visible under bright field (Figure 4.4B, D). Figure 4.5 shows TEM images of MSCs incubated with nanorods and verifies the nanorods were endocytosed by the cells and are localized within endosomal compartments. Others have seen similar endocytosis and packaging of gold nanoparticles within stem cells.[30] ICP-MS analysis quantified the number of nanorods per MSC as 1.89 ± 0.877 x 10^5 nanorods/cell (Figure 4.6A). This large extent of extent of cellular uptake of the nanorods can be attributed in part to both the silica coating, providing a more spherical shape to the particle which is more conducive for cellular uptake,[16,17,41] and the PLL surface coating, which is commonly used as a transfection agent and has been used to promote cellular uptake of iron oxide nanoparticles[42-44].

Macrophages were incubated with 50 nm PEGylated gold nanospheres and dark field and bright field microscopy demonstrated a large extent of uptake by the cells (Figure 4.4G, H) as compared to control cells (Figure 4.4E, F). In addition, MSCs were incubated with the same nanoparticles and there was no evident uptake by the cells (Figure 4.4I, J), which was verified by ICP-MS measurements (Figure 4.6B). The reason MSCs did not uptake these particles can be attributed to the PEG surface coating, which passivates the particles and gives them a neutral charge, leading to minimal detection and

uptake by cells.[41,45] Macrophages, on the other hand, are characterized by their high rate of nonspecific uptake, and thus endocytose these particles to a large extent.[46] Over time the mPEG-SH layer is slowly displaced by serum proteins, leading to preferential uptake by macrophages.[47,48] Thus, 50 nm PEGylated gold nanospheres can be used as a contrast agent to preferentially label macrophages and identify the infiltration of macrophages *in vivo*. ICP-MS measurements quantified the number of gold nanospheres per macrophage as 6.76 ± 1.68 x 10^3 nanospheres/cell in 2D culture (Figure 4.6B). The macrophages were also cultured in 3D PEGylated fibrin gels containing gold nanospheres in order to more closely resemble the *in vivo* scenario in which macrophages will infiltrate the ischemic area and come in contact with nanospheres delivered within a 3D hydrogel. The number of gold nanospheres per macrophage in 3D culture as measured with ICP-MS was 4.38 ± 1.63 x 10^3 nanospheres/cell. These measurements took into account the fact that gold nanospheres not endocytosed by cells could still be entrapped in the gels. As a result, gels containing only gold nanospheres were used as a blank and subtracted from the 3D cell measurements.

Co-culture of the MSCs and macrophages within a 3D PEGylated fibrin gel showed that nanorod labeled MSCs formed tubular networks in the gels after 7 days. Macrophages maintained a rounded morphology within the gel and started to endocytose nanoparticles. Figure 3.7 shows the co-culture system, with nanoparticle labeled macrophages circled in yellow.

4.3.3 Stability of nanorod silica coating

TEM analysis of MSCs which had endocytosed NRs suggested that the silica coating on the NR was no longer present. In addition, the peak broadening of the UV-vis spectra of cells labeled with NRs also supported this claim. As a result, a study was

conducted to confirm if the silica coating was still present on the NRs following endocytosis. It is a possibility that the silica coating was not visible in the TEM images because the electron density of silica is approximately the same as the resin in which the cells were embedded for sectioning.[49] To overcome this issue, the cells were lysed following NR endocytosis and the particles were separated out of solution and imaged on a TEM grid. EDS analysis was performed to chemically analyze the particles and the presence of silicon on the outer surface. Figure 4.8A and 4.8B show the TEM and EDS analysis, respectively, of silica NRs. The EDS analysis shows gold in green and the silicon in red, and the quantitative analysis indicates a large peak representing silicon. On the other hand, NRs which were isolated following MSC endocytosis (Figure 4.8D-F) show many NRs without the presence of a silica layer and there appears to be dispersed silica in the background. Also, quantitative analysis shows a dramatic decline in the silicon peak. To confirm the buffer solution used to lyse the cells did not affect the NRs, silica NRs which were incubated with the lysis buffer solution were also evaluated (Figure 4.8G-I). The results demonstrate that the lysis buffer did not affect the NRs, as the silica layer is still present.

Potential mechanisms for the silica degradation could potentially be the acidic pH within the endosomal compartment. However, studies in which silica NRs were incubated in various acidic solutions suggested this was not the case. On the other hand, it is possible that serum proteins are penetrating the porous silica layer and displacing the silica layer.[47] One study found that degradation of silica nanoparticles took place in the cytoplasm and lysosomes of HUVECs, followed by exocytosis of the excess silica into the cell culture media.[50] The authors were unsure as to the mechanisms responsible for the degradation, but attribute the intracellular environment (including pH and hydrolytic enzymes) as the main factor.[50]

The degradation of the silica layer could have important implications. For example, photoacoustic imaging can be affected, as the silica provides thermal stability to the nanorods[40] and also causes an enhancement in the photoacoustic signal produced by the nanorods[51]. In addition, the degradation of the silica layer could be taken advantage of for multimodal applications related to drug/gene delivery, where the molecule to be released could be loaded into the silica layer and the NR could provide imaging contrast for monitoring purposes.

4.3.4 Cell viability and function following nanoparticle labeling

LIVE/DEAD staining and an MTS proliferation assay were used to assess cell viability following nanoparticle labeling. Nanoparticle cytotoxicity is dependent upon the size, shape, and surface coating of the nanoparticles. In particular, CTAB, a surfactant used during nanorod synthesis and which forms a bilayer on the surface of the nanorod, is especially cytotoxic to cells, and thus removing or displacing CTAB is necessary to reduce the cytotoxic effects.[31,52,53] Following labeling of MSCs with silica coated NRs, MSCs were viable up to 5 days and continued to proliferate, with no significant reduction in cell proliferation compared to the control cells (Figure 4.9A, B). Labeling of macrophages with 50 nm PEGylated gold nanospheres did not affect cell proliferation or viability (Figure 4.9C, D) compared to controls.

The maintenance of MSC tubular network formation within 3D PEGylated fibrin gels was assessed following nanorod labeling and laser irradiation. This was performed to verify the process of photoacoustic imaging did not affect the cells' ability to form tubular networks. MSCs without NR labeling or laser irradiation formed extensive tubular networks within the gels, and this network formation was maintained following NR labeling (Figure 4.10A, B). The gels were also irradiated with an 800 nm laser to

ensure photoacoustic imaging did not affect cell function. Both non-labeled cells and NR labeled cells continued to form networks following laser irradiation (Figure 4.10C, D). These results demonstrate that the cells maintain their function of forming tubular networks following NR labeling and photoacoustic imaging.

4.3.5 *In vitro* photoacoustic imaging of nanoparticle labeled cells

In vitro photoacoustic imaging of nanosphere labeled macrophages and NR labeled MSCs was performed to evaluate the feasibility of distinguishing and quantifying the two cell types using photoacoustic imaging. The two cell types were mixed in various ratios and Figure 4.11A shows the spectroscopic results in which the 100% macrophage inclusion was identified as having 50 nm PEGylated nanospheres (red) and the 100% MSC inclusion was identified as having NRs (green). A transition from nanospheres to NRs is evident as the concentration of macrophages decreases and of MSCs increases. These results demonstrate that the two cell types can be distinguished based on labeling with different nanoparticles, even when they are in close proximity. In addition, the ratios of the two cell types were calculated based on the photoacoustic imaging results (Figure 4.11B), with the predicted cell ratios being a very good estimate of the actual cell ratios in the inclusions. Thus, photoacoustic imaging can be used in combination with the dual nanoparticle system presented here to quantify the ratios of cells within a region. This data would be important for *in vivo* applications to quantify the infiltration of macrophages and the persistence of MSCs following delivery.

4.3.6 *In vivo* photoacoustic imaging of nanoparticle labeled cells

The dual nanoparticle system (consisting of NR labeled MSCs and nanospheres) was intramuscularly injected within PEGylated fibrin gel into the gastrocnemius of a rat following an ischemic injury. Combined ultrasound and photoacoustic imaging (US/PA)

obtained at 800 nm shows a high photoacoustic signal located within the gastrocnemius muscle (Figure 4.12A), which persisted until day 7. Spectroscopic analysis attributes the photoacoustic signal to NRs (shown in green) immediately after the injection on day 0. Over time, the contribution from 50 nm PEGylated nanospheres increases (shown in red), and there is a 20% relative increase in signal attributed to the nanospheres from day 0 to day 7 (Figure 4.12C). The ratio of the two nanoparticle types was quantified, as shown in Figure 4.12B. This increase in signal from nanospheres can be attributed to infiltration of macrophages following the ischemic injury and subsequent endocytosis of the PEGylated nanospheres by the cells. The endocytosis of the nanospheres by macrophages leads to plasmon coupling of the particles,[46] as demonstrated by the peak shift in Figure 4.1, and thus an increase in photoacoustic signal within the range of wavelengths which were used for imaging (680-970 nm). A majority of the infiltrating macrophages are localized around the delivered hydrogel system containing MSCs. This could be attributed in part to the fact that the nanospheres were delivered within the gel system containing the MSCs, and thus the nanoparticles which were available for phagocytosis by the macrophages were already localized in close proximity to the stem cells. In addition, others have shown that macrophages have important roles in wound healing and angiogenesis,[24,54,55] with stem cells and macrophages potentially undergoing some sort of synergistic crosstalk to further promote the regeneration process. MSCs have been shown to secrete not only angiogenic factors, but also factors which influence macrophage function.[27,56,57] Furthermore, others have found that macrophages are frequently associated with endothelial cells during the process of angiogenesis.[58] In addition, chemotactic signals secreted from apoptotic stem cells could also promote macrophage migration to the area. Stem cell death following delivery for therapeutic purposes is a common issue,[59,60] and thus it would not be surprising if macrophages are entering the

area to scavenge apoptotic MSCs. Thus, one of the advantages of this dual nanoparticle system is the ability to distinguish the two cell types *in vivo,* providing information about the interaction between stem cells and macrophage. Such information could include if macrophages are phagocytosing MSCs, leading to a transfer of contrast agent from MSCs to macrophages. Based on our imaging system, we would designate transfer of contrast agent from MSCs to macrophages if there is co-localization of the nanosphere and nanorod signal.

Histological analysis of the muscle sample following sacrifice at day 7 shows the presence of injected MSCs (fluorescently pre-labeled with CM-DiI) distributed throughout the muscle fibers (Figure 4.13A). In addition, the presence of nanoparticles within the cells is evident under bright field. TUNEL staining was performed to assess cell apoptosis following injection. The TUNEL staining in Figure 4.13B shows a large extent of cell death within the injection region corresponding to the delivered MSCs. It has been largely reported in the literature that only a small proportion of stem cells survive following delivery.[57,61,62] Immunostaining for macrophages (ED1) in Figure 4.13C shows macrophage infiltration within the muscle and in particularly close proximity to the injected MSCs, which were fluorescently labeled with CM-DiI prior to delivery. The ED1 immunostaining data supports the *in vivo* photoacoustic imaging results, which shows the presence of macrophages on day 7 surrounding the injected MSCs.

4.3.7 Fluorescence-activated cell sorting of macrophages

Macrophages were sorted from gastrocnemius muscle 7 days following injection. ICP-MS analysis confirmed that macrophages endocytosed gold nanoparticles within the muscle (Figure 4.14). To confirm that macrophages were not just endocytosing MSCs

labeled with gold NRs, a condition consisting of unlabeled MSCs was used. In this condition gold was also detected within isolated macrophages, confirming that macrophages are endocytosing the gold nanospheres.

4.4 CONCLUSIONS

This study demonstrated the use of a dual nanoparticle system to monitor stem cells following delivery and to detect the presence of infiltrating macrophages to a wound area. Cellular uptake of the nanoparticles was qualitatively and quantitatively assessed *in vitro* using microscopy and mass spectrometry, respectively. In addition, the viability and function of the cells was maintained following nanoparticle labeling. An *in vitro* phantom imaging experiment verified that the two cell types could be distinguished and quantified using photoacoustic imaging. The stem cells were also successfully monitored following intramuscular injection into a hind limb ischemia model, and the increased infiltration of macrophages into the area was quantified over time. Histological analysis of macrophages confirmed the photoacoustic imaging results, and mass spectrometry analysis confirmed that the macrophages had endocytosed gold nanoparticles, and specifically gold nanospheres. These results represent important advancements in monitoring stem cells for therapeutic purposes and distinguishing the delivered cells from infiltrating immune cells, which also have important roles in the wound healing response.

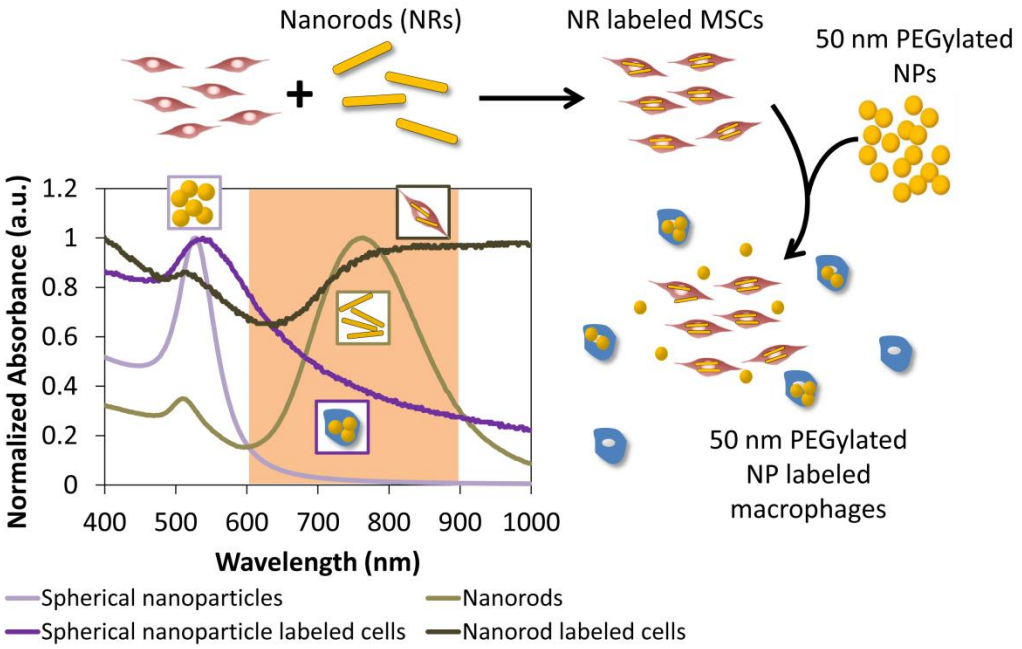

Figure 4.1: Outline of the dual nanoparticle system for labeling MSCs with gold nanorods and macrophages with spherical gold nanospheres. The nanoparticles exhibit different optical absorption characteristics following endocytosis by cells and can thus be distinguished when imaged within the tissue optical window (highlighted wavelength region).

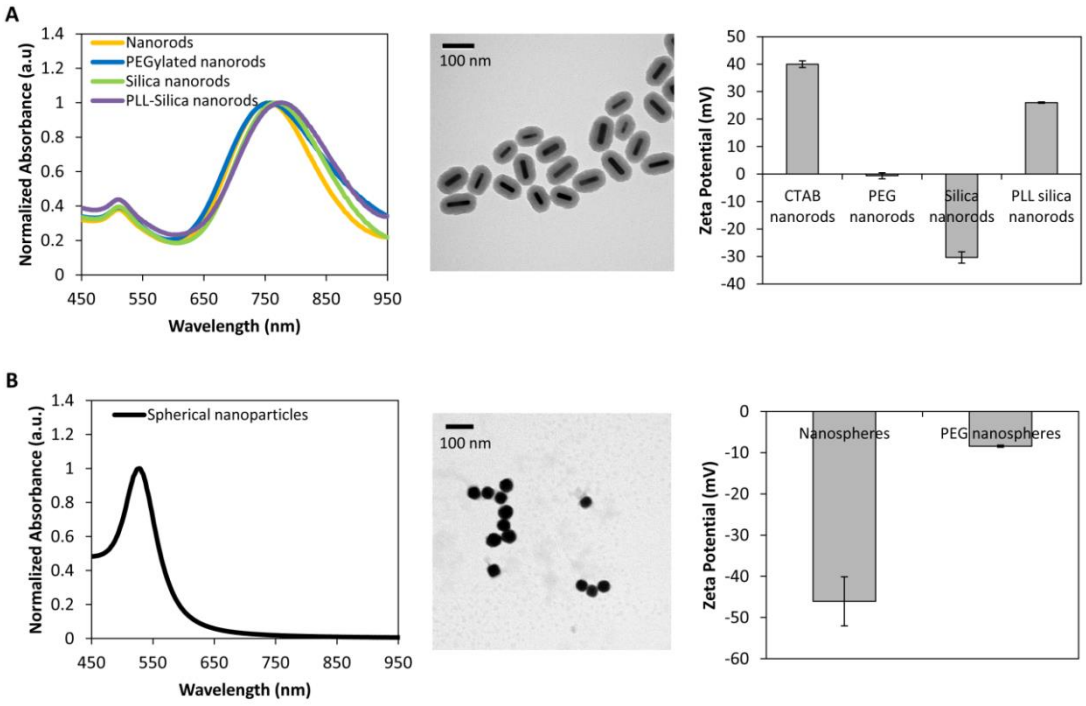

Figure 4.2: Characterization of (A) gold nanorods and (B) nanospheres using ultraviolet-light spectroscopy, transmission electron microscopy, and zeta potential analysis.

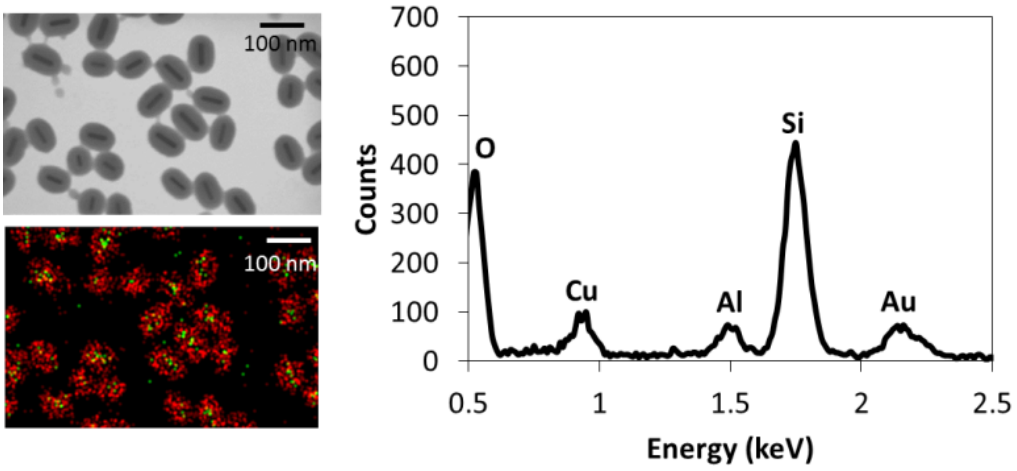

Figure 4.3: Analysis of silica coated gold nanorods using transmission electron microscopy and energy dispersive spectrometry (red – silicon; green – gold).

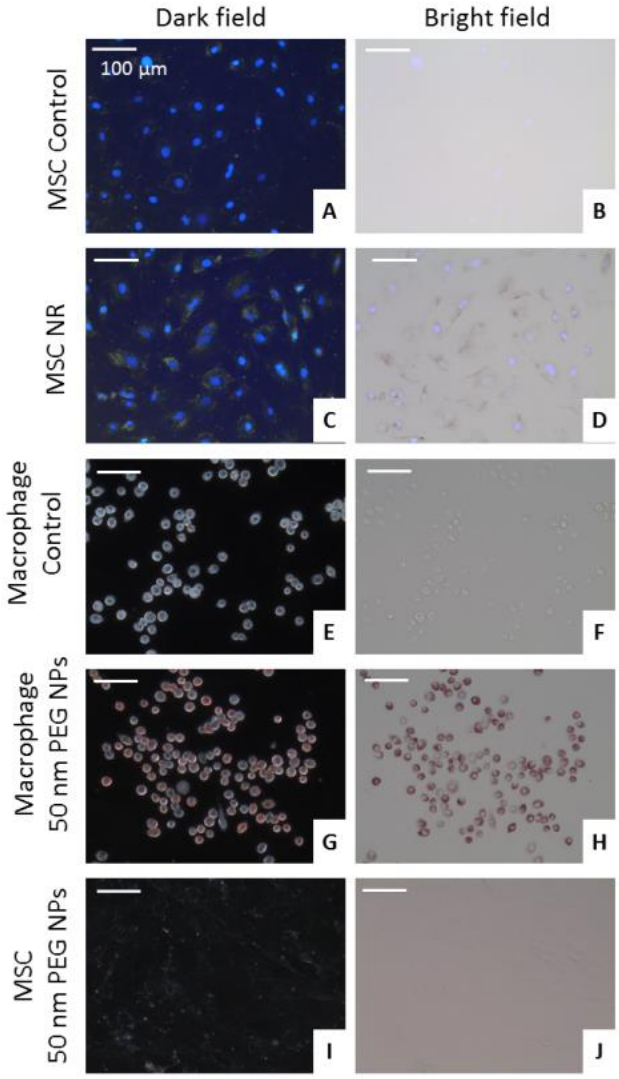

Figure 4.4: Assessment of nanoparticle labeling of cells using dark field and bright field microscopy. Control MSCs are shown in (A) and (B) and nanorod labeled MSCs are shown in (C) and (D). Images are overlaid with DAPI fluorescence images. Control macrophages are shown in (E) and (F) and nanosphere labeled macrophages are shown in (G) and (H). MSCs incubated with 50 nm PEGylated nanospheres are shown in (I) and (J).

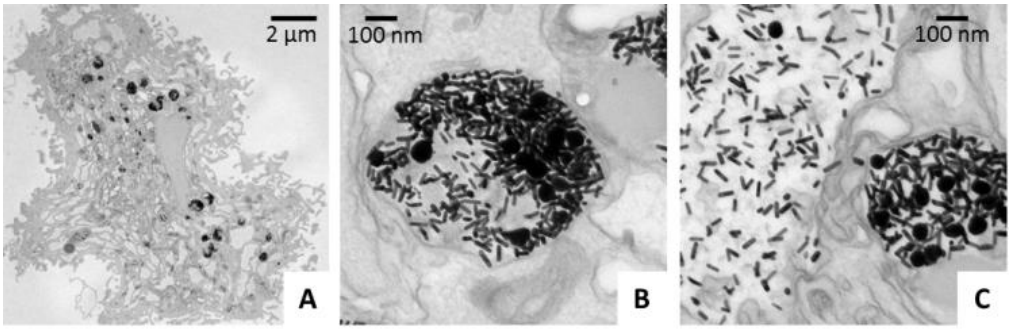

Figure 4.5: Transmission electron microscope images of 70 nm cell sections demonstrating endocytosis of nanorods by MSCs and localization within membrane bound compartments.

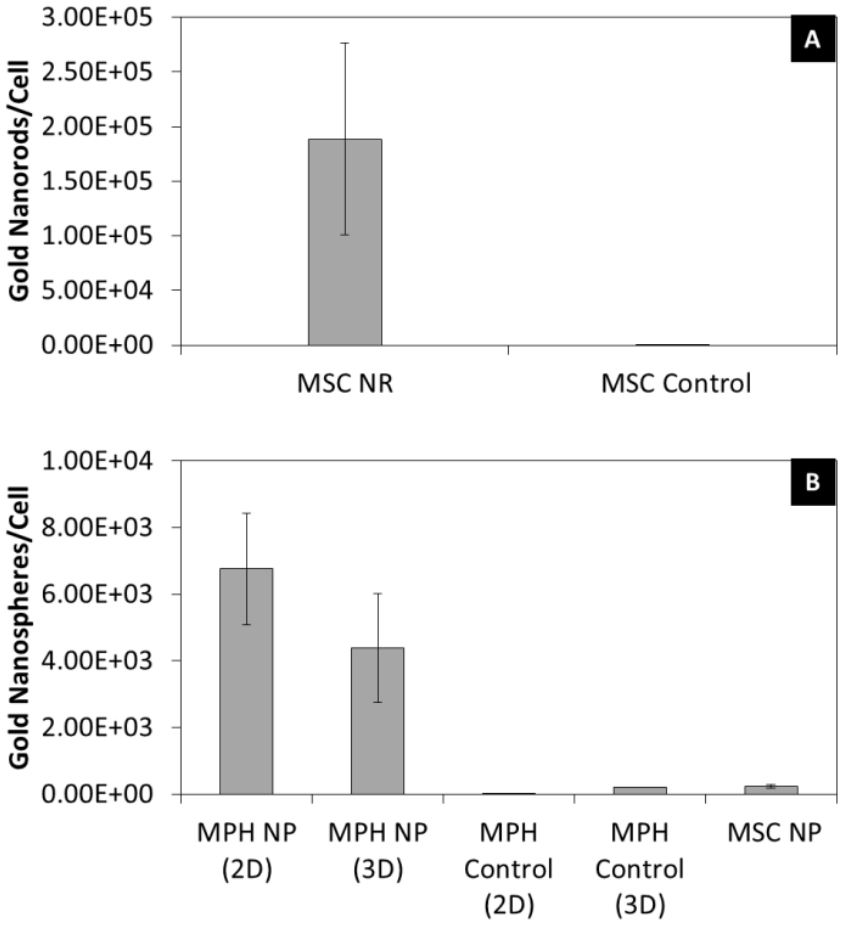

Figure 4.6: Quantification of (A) nanorod labeling of MSCs and (B) nanosphere labeling of macrophages and MSCs using inductively coupled plasma mass spectrometry. Abbreviations: macrophage (MPH), mesenchymal stem cell (MSC), nanorod (NR), nanosphere (NP).

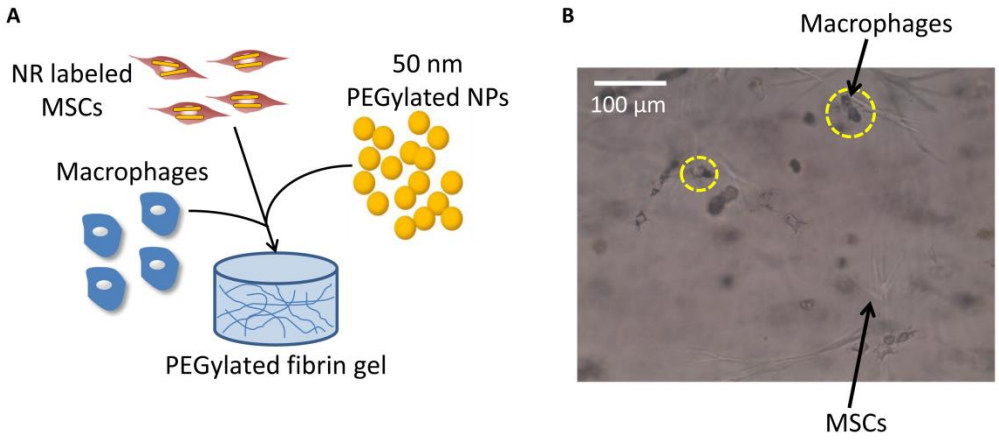

Figure 4.7: (A) Schematic showing a 3D co-culture system of nanorod labeled MSCs, macrophages, and nanospheres within a PEGylated fibrin gel. (B) Bright field microscopy demonstrating nanoparticle uptake by macrophages within the gels (yellow circles).

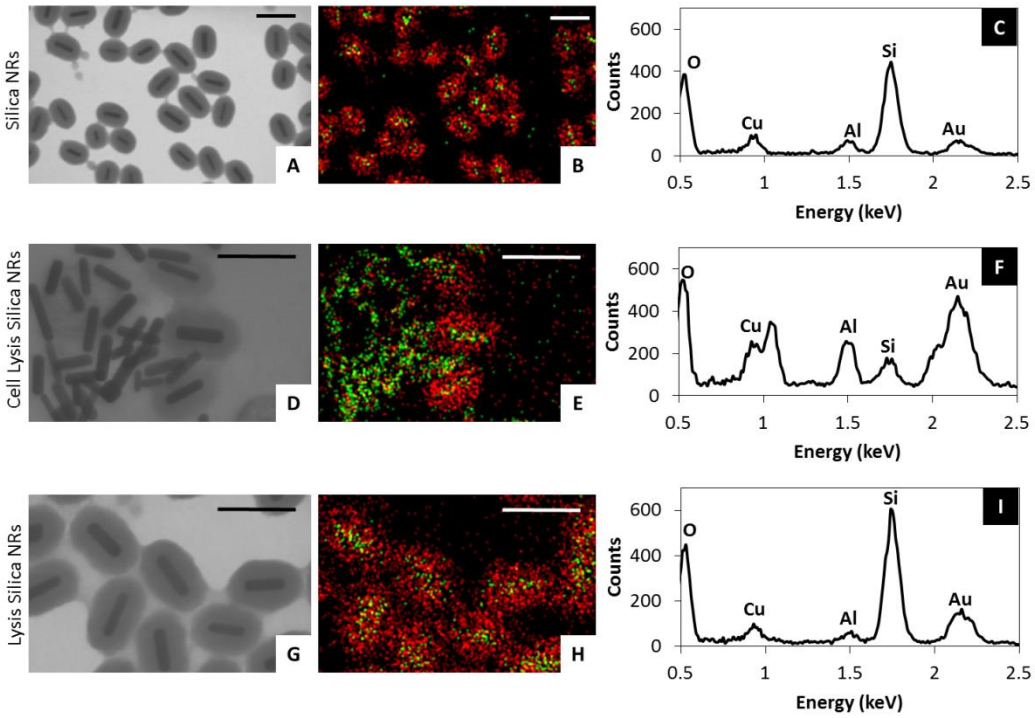

Figure 4.8: Evaluation of the stability of the nanorod silica coating following cellular endocytosis using TEM and EDS analysis (red – silicon; green – gold).

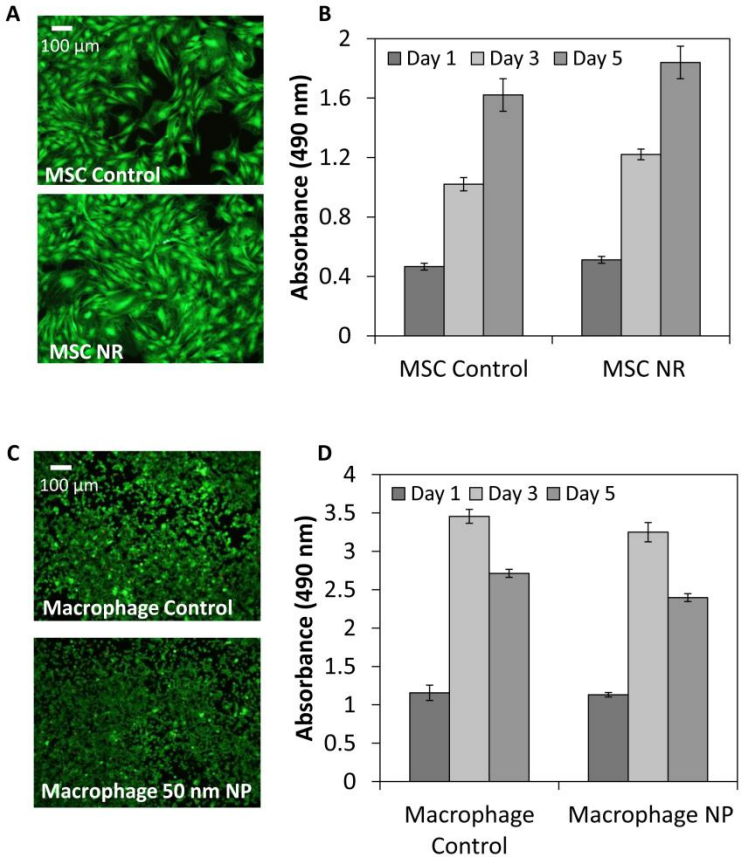

Figure 4.9: LIVE/DEAD staining of (A) control and nanorod labeled MSCs and (C) control and 50 nm PEGylated nanosphere labeled macrophages at day 5. MTS assay of (B) control and nanorod labeled MSCs and (D) control and 50 nm PEGylated nanosphere labeled macrophages to assess cell proliferation.

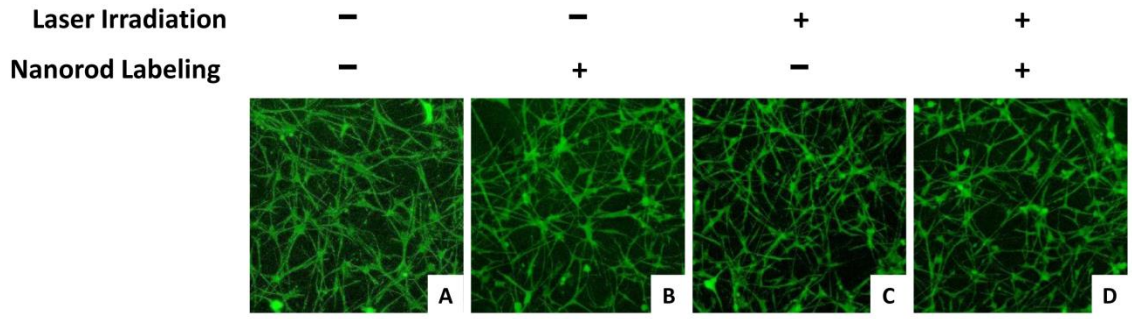

Figure 4.10: 3D stacks of tubular network formation within PEGylated fibrin gels for (A. C) unlabeled and (B, D) NR labeled MSCs with (A, B) no laser irradiation or (C, D) laser irradiation.

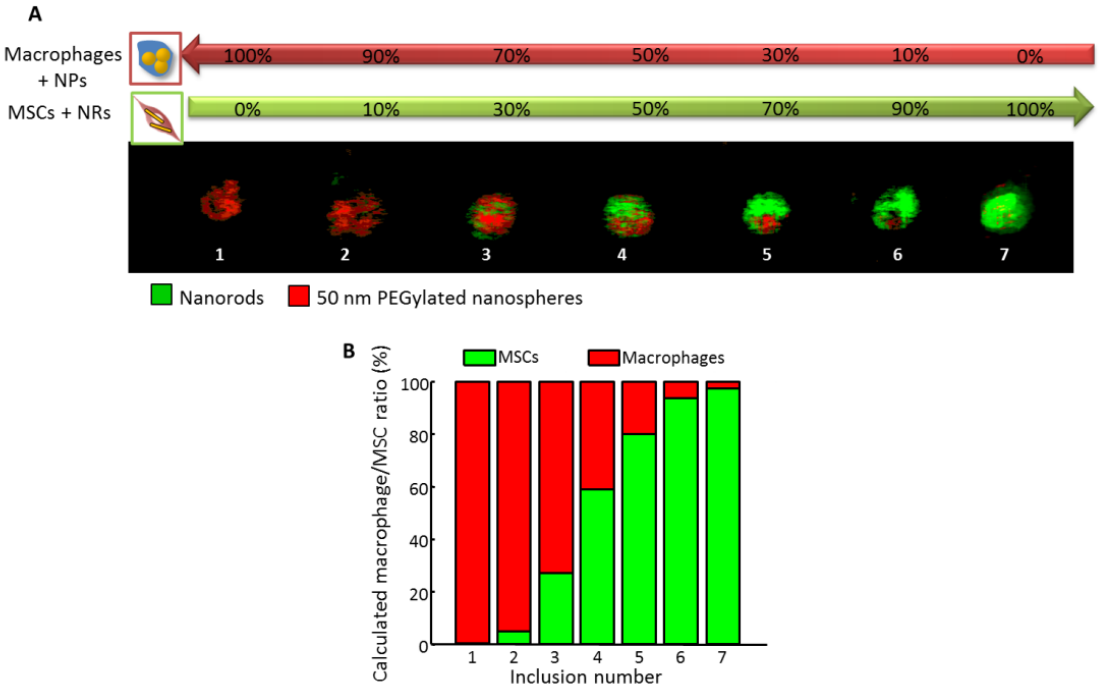

Figure 4.11: (A) Spectroscopic *in vitro* photoacoustic imaging of nanosphere labeled macrophages (red) and nanorod labeled MSCs (green) mixed in various ratios. (B) Quantification of the ratio of the two cell types based on the photoacoustic imaging results.

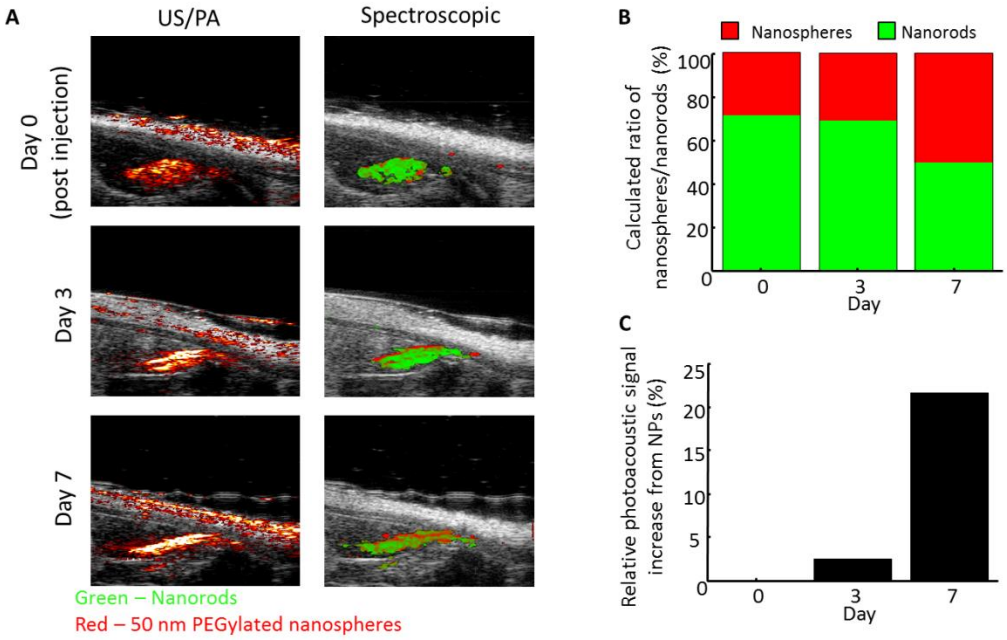

Figure 4.12: (A) Longitudinal ultrasound/photoacoustic imaging (800 nm) and spectroscopic photoacoustic imaging of NR labeled MSCs and nanospheres injected within PEGylated fibrin gel into the gastrocnemius. (B) Calculated ratio of nanospheres and nanorods. (C) Quantification of the relative photoacoustic signal increase attributed to nanospheres compared to day 0.

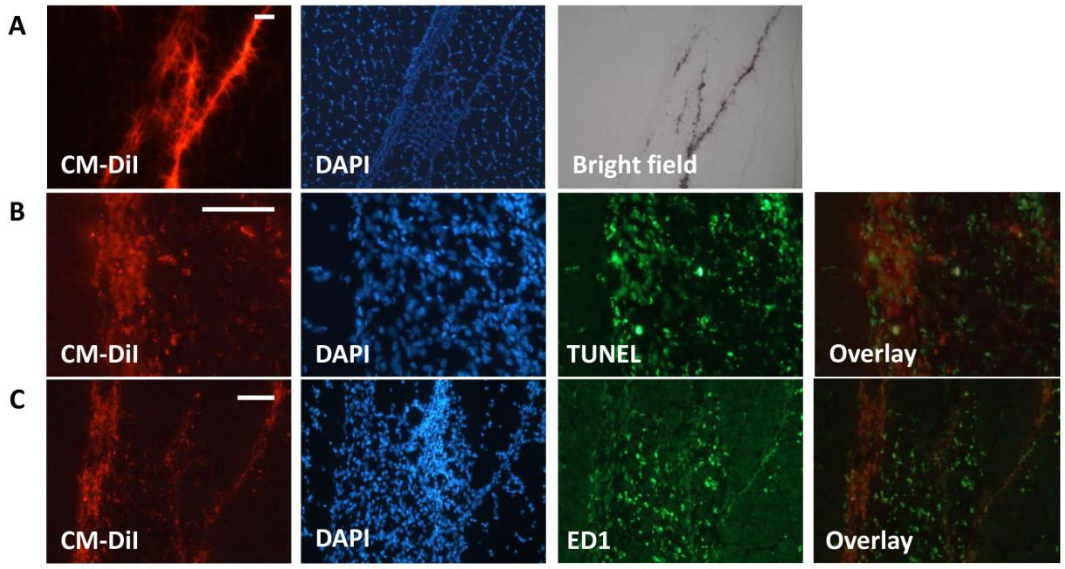

Figure 4.13: (A) Fluorescent microscopy of muscle sections demonstrates the distribution of CM-DiI labeled MSCs throughout the muscle fibers. Bright field microscopy shows the localization of nanoparticles within the cells. (B) TUNEL staining demonstrates MSC death following injection. (C) Immunostaining for ED1 cell surface marker demonstrates macrophage infiltration. Scale bars = 50 μm.

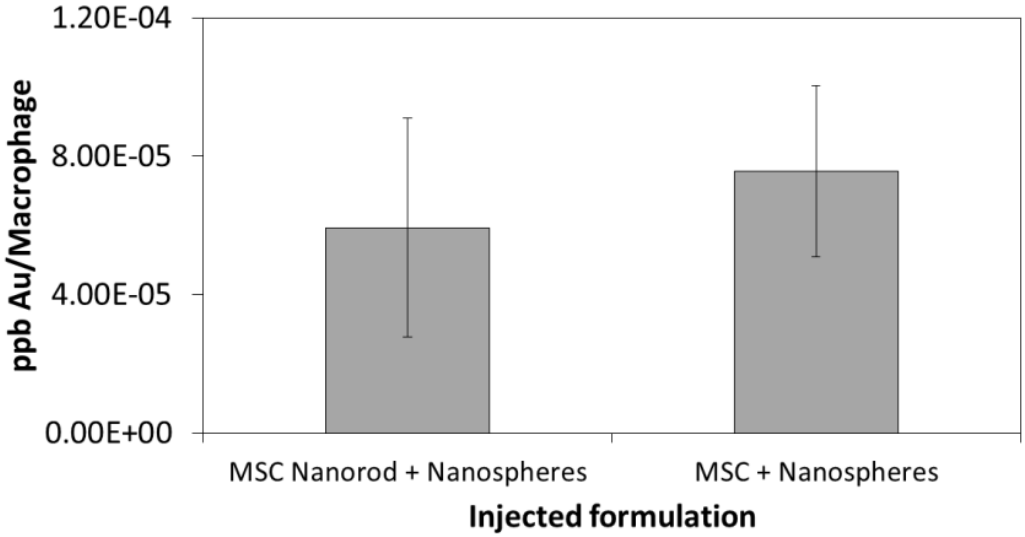

Figure 4.14: Inductively coupled plasma mass spectrometry analysis to quantify nanoparticle labeling of macrophages isolated from gastrocnemius. Test conditions included nanorod labeled and unlabeled MSCs delivered in combination with nanospheres.

4.5 REFERENCES

1. Copland, I.B. Mesenchymal stromal cells for cardiovascular disease. *J Cardiovasc Dis Res* **2**, 3-13 (2011).

2. Taghavi, S., Duran, J.M., George, J.C. Stem cell therapy for peripheral arterial disease: a review of clinical trials. *Stem Cell Studies* **1**, 105-114 (2011).

3. Cao, F., Lin, S., Xie, X., Ray, P., Patel, M., Zhang, X., Drukker, M., Dylla, S.J., Connolly, A.J., Chen, X., Weissman, I.L., Gambhir, S.S., Wu, J.C. In vivo visualization of embryonic stem cell survival, proliferation, and migration after cardiac delivery. *Circulation* **113**, 1005-1014 (2006).

4. Li, Z., Suzuki, Y., Huang, M., Cao, F., Xie, X., Connolly, A.J., Yang, P.C., Wu, J.C. Comparison of reporter gene and iron particle labeling for tracking fate of human embryonic stem cells and differentiated endothelial cells in living subjects. *Stem Cells* **26**, 864-873 (2008).

5. van Laake, L.W., Passier, R., Monshouwer-Kloots, J., Verkleij, A.J., Lips, D.J., Freund, C., den Ouden, K., Ward-van Oostwaard, D., Korving, J., Tertoolen, L.G., van Echteld, C.J., Doevendans, P.A., Mummery, C.L. Human embryonic stem cell-derived cardiomyocytes survive and mature in the mouse heart and transiently improve function after myocardial infarction. *Stem cell research* **1**, 9-24 (2007).

6. Barbash, I.M., Chouraqui, P., Baron, J., Feinberg, M.S., Etzion, S., Tessone, A., Miller, L., Guetta, E., Zipori, D., Kedes, L.H., Kloner, R.A., Leor, J. Systemic delivery of bone marrow-derived mesenchymal stem cells to the infarcted myocardium - Feasibility, cell migration, and body distribution. *Circulation* **108**, 863-868 (2003).

7. Hofmann, M., Wollert, K.C., Meyer, G.P., Menke, A., Arseniev, L., Hertenstein, B., Ganser, A., Knapp, W.H., Drexler, H. Monitoring of bone marrow cell homing into the infarcted human myocardium. *Circulation* **111**, 2198-2202 (2005).

8. Kraitchman, D.L., Tatsumi, M., Gilson, W.D., Ishimori, T., Kedziorek, D., Walczak, P., Segars, W.P., Chen, H.H., Fritzges, D., Izbudak, I., Young, R.G., Marcelino, M., Pittenger, M.F., Solaiyappan, M., Boston, R.C., Tsui, B.M., Wahl, R.L., Bulte, J.W. Dynamic imaging of allogeneic mesenchymal stem cells trafficking to myocardial infarction. *Circulation* **112**, 1451-1461 (2005).

9. Daldrup-Link, H.E., Rudelius, M., Metz, S., Piontek, G., Pichler, B., Settles, M., Heinzmann, U., Schlegel, J., Oostendorp, R.A., Rummeny, E.J. Cell tracking with gadophrin-2: a bifunctional contrast agent for MR imaging, optical imaging, and fluorescence microscopy. *European journal of nuclear medicine and molecular imaging* **31**, 1312-1321 (2004).

10. Xiong, T., Zhang, Z., Liu, B.F., Zeng, S., Chen, Y., Chu, J., Luo, Q. In vivo optical imaging of human adenoid cystic carcinoma cell metastasis. *Oral oncology* **41**, 709-715 (2005).

11. Kawada, H., Fujita, J., Kinjo, K., Matsuzaki, Y., Tsuma, M., Miyatake, H., Muguruma, Y., Tsuboi, K., Itabashi, Y., Ikeda, Y., Ogawa, S., Okano, H., Hotta, T., Ando, K., Fukuda, K. Nonhematopoietic mesenchymal stem cells can be mobilized and differentiate into cardiomyocytes after myocardial infarction. *Blood* **104**, 3581-3587 (2004).

12. Ricles, L.M., Nam, S.Y., Sokolov, K., Emelianov, S.Y., Suggs, L.J. Function of mesenchymal stem cells following loading of gold nanotracers. *International journal of nanomedicine* **6**, 407-416 (2011).

13. Guzman, R., Uchida, N., Bliss, T.M., He, D., Christopherson, K.K., Stellwagen, D., Capela, A., Greve, J., Malenka, R.C., Moseley, M.E., Palmer, T.D., Steinberg, G.K. Long-term monitoring of transplanted human neural stem cells in developmental and pathological contexts with MRI. *Proceedings of the National Academy of Sciences of the United States of America* **104**, 10211-10216 (2007).

14. Lin, S., Xie, X., Patel, M.R., Yang, Y.H., Li, Z., Cao, F., Gheysens, O., Zhang, Y., Gambhir, S.S., Rao, J.H., Wu, J.C. Quantum dot imaging for embryonic stem cells. *BMC Biotechnol* **7**, 67 (2007).

15. Chung, E., Ricles, L.M., Stowers, R.S., Nam, S.Y., Emelianov, S.Y., Suggs, L.J. Multifunctional nanoscale strategies for enhancing and monitoring blood vessel regeneration. *Nano Today* **7**, 514-531 (2012).

16. Chithrani, B.D., Chan, W.C. Elucidating the mechanism of cellular uptake and removal of protein-coated gold nanoparticles of different sizes and shapes. *Nano Lett* **7**, 1542-1550 (2007).

17. Chithrani, B.D., Ghazani, A.A., Chan, W.C. Determining the size and shape dependence of gold nanoparticle uptake into mammalian cells. *Nano Lett* **6**, 662-668 (2006).

18. Kubinova, S., Sykova, E. Nanotechnologies in regenerative medicine. *Minimally invasive therapy & allied technologies : MITAT : official journal of the Society for Minimally Invasive Therapy* **19**, 144-156 (2010).

19. Lu, C.W., Hung, Y., Hsiao, J.K., Yao, M., Chung, T.H., Lin, Y.S., Wu, S.H., Hsu, S.C., Liu, H.M., Mou, C.Y., Yang, C.S., Huang, D.M., Chen, Y.C. Bifunctional magnetic silica nanoparticles for highly efficient human stem cell labeling. *Nano Lett* **7**, 149-154 (2007).

20. Nam, S.Y., Ricles, L.M., Suggs, L.J., Emelianov, S.Y. In vivo ultrasound and photoacoustic monitoring of mesenchymal stem cells labeled with gold nanotracers. *PLoS One* **7**, e37267 (2012).

21. Amsalem, Y., Mardor, Y., Feinberg, M.S., Landa, N., Miller, L., Daniels, D., Ocherashvilli, A., Holbova, R., Yosef, O., Barbash, I.M., Leor, J. Iron-oxide labeling and outcome of transplanted mesenchymal stem cells in the infarcted myocardium. *Circulation* **116**, I38-45 (2007).

22. Dupont, K.M., Sharma, K., Stevens, H.Y., Boerckel, J.D., Garcia, A.J., Guldberg, R.E. Human stem cell delivery for treatment of large segmental bone defects. *Proceedings of the National Academy of Sciences of the United States of America* **107**, 3305-3310 (2010).

23. Sunderkotter, C., Steinbrink, K., Goebeler, M., Bhardwaj, R., Sorg, C. Macrophages and angiogenesis. *J Leukoc Biol* **55**, 410-422 (1994).

24. Chazaud, B., Brigitte, M., Yacoub-Youssef, H., Arnold, L., Gherardi, R., Sonnet, C., Lafuste, P., Chretien, F. Dual and beneficial roles of macrophages during skeletal muscle regeneration. *Exercise and sport sciences reviews* **37**, 18-22 (2009).

25. Mahdavian Delavary, B., van der Veer, W.M., van Egmond, M., Niessen, F.B., Beelen, R.H. Macrophages in skin injury and repair. *Immunobiology* **216**, 753-762 (2011).

26. Wynn, T.A., Chawla, A., Pollard, J.W. Macrophage biology in development, homeostasis and disease. *Nature* **496**, 445-455 (2013).

27. Kim, J., Hematti, P. Mesenchymal stem cell-educated macrophages: a novel type of alternatively activated macrophages. *Exp Hematol* **37**, 1445-1453 (2009).

28. Anton, K., Banerjee, D., Glod, J. Macrophage-associated mesenchymal stem cells assume an activated, migratory, pro-inflammatory phenotype with increased IL-6 and CXCL10 secretion. *PLoS One* **7**, e35036 (2012).

29. Chen, L., Tredget, E.E., Wu, P.Y., Wu, Y. Paracrine factors of mesenchymal stem cells recruit macrophages and endothelial lineage cells and enhance wound healing. *PLoS One* **3**, e1886 (2008).

30. Chung, E., Nam, S.Y., Ricles, L.M., Emelianov, S.Y., Suggs, L.J. Evaluation of gold nanotracers to track adipose-derived stem cells in a PEGylated fibrin gel for dermal tissue engineering applications. *International journal of nanomedicine* **8**, 325-336 (2013).

31. Alkilany, A.M., Murphy, C.J. Toxicity and cellular uptake of gold nanoparticles: what we have learned so far? *J Nanopart Res* **12**, 2313-2333 (2010).

32. Jain, P.K., El-Sayed, M.A. Plasmonic coupling in noble metal nanostructures. *Chemical Physics Letters* **487**, 153-164 (2010).

33. Hore, M.J.A., Composto, R.J. Nanorod Self-Assembly for Tuning Optical Absorption. *Acs Nano* **4**, 6941-6949 (2010).

34. Mallidi, S., Larson, T., Tam, J., Joshi, P.P., Karpiouk, A., Sokolov, K., Emelianov, S. Multiwavelength photoacoustic imaging and plasmon resonance coupling of gold nanoparticles for selective detection of cancer. *Nano Lett* **9**, 2825-2831 (2009).

35. Zhang, G., Drinnan, C.T., Geuss, L.R., Suggs, L.J. Vascular differentiation of bone marrow stem cells is directed by a tunable three-dimensional matrix. *Acta Biomater* **6**, 3395-3403 (2010).

36. Jana, N.R., Gearheart, L., Murphy, C.J. Seed-mediated growth approach for shape-controlled synthesis of spheroidal and rod-like gold nanoparticles using a surfactant template. *Advanced Materials* **13**, 1389-1393 (2001).

37. Nikoobakht, B., El-Sayed, M.A. Preparation and growth mechanism of gold nanorods (NRs) using seed-mediated growth method. *Chemistry of Materials* **15**, 1957-1962 (2003).

38. Stober, W., Fink, A., Bohn, E. Controlled Growth of Monodisperse Silica Spheres in Micron Size Range. *Journal of Colloid and Interface Science* **26**, 62-& (1968).

39. Lu, Y., Yin, Y.D., Mayers, B.T., Xia, Y.N. Modifying the surface properties of superparamagnetic iron oxide nanoparticles through a sol-gel approach. *Nano Lett* **2**, 183-186 (2002).

40. Chen, Y.S., Frey, W., Kim, S., Homan, K., Kruizinga, P., Sokolov, K., Emelianov, S. Enhanced thermal stability of silica-coated gold nanorods for photoacoustic imaging and image-guided therapy. *Optics express* **18**, 8867-8878 (2010).

41. Arnida, Janat-Amsbury, M.M., Ray, A., Peterson, C.M., Ghandehari, H. Geometry and surface characteristics of gold nanoparticles influence their biodistribution and uptake by macrophages. *European journal of pharmaceutics and biopharmaceutics : official journal of Arbeitsgemeinschaft fur Pharmazeutische Verfahrenstechnik e.V* **77**, 417-423 (2011).

42. Albukhaty, S., Naderi-Manesh, H., Tiraihi, T. In vitro labeling of neural stem cells with poly-L-lysine coated super paramagnetic nanoparticles for green fluorescent protein transfection. *Iranian biomedical journal* **17**, 71-76 (2013).

43. Nayerossadat, N., Maedeh, T., Ali, P.A. Viral and nonviral delivery systems for gene delivery. *Advanced biomedical research* **1**, 27 (2012).

44. Horák, D., Babič, M., Jendelová, P., Herynek, V., Trchova, M., Likavanova, K., M, K., Hajek, M., Sykova, E. Effect of different magnetic nanoparticle coatings on the efficiency of stem cell labeling. *Journal of Magnetism and Magnetic Materials* **321**, 1539-1547 (2009).

45. Mallidi, S., Larson, T., Aaron, J., Sokolov, K., Emelianov, S. Molecular specific optoacoustic imaging with plasmonic nanoparticles. *Optics express* **15**, 6583-6588 (2007).

46. Wang, B., Yantsen, E., Larson, T., Karpiouk, A.B., Sethuraman, S., Su, J.L., Sokolov, K., Emelianov, S.Y. Plasmonic intravascular photoacoustic imaging for detection of macrophages in atherosclerotic plaques. *Nano Lett* **9**, 2212-2217 (2009).

47. Larson, T.A., Joshi, P.P., Sokolov, K. Preventing protein adsorption and macrophage uptake of gold nanoparticles via a hydrophobic shield. *ACS nano* **6**, 9182-9190 (2012).

48. Walkey, C.D., Olsen, J.B., Guo, H., Emili, A., Chan, W.C. Nanoparticle size and surface chemistry determine serum protein adsorption and macrophage uptake. *J Am Chem Soc* **134**, 2139-2147 (2012).

49. Jokerst, J.V., Thangaraj, M., Kempen, P.J., Sinclair, R., Gambhir, S.S. Photoacoustic imaging of mesenchymal stem cells in living mice via silica-coated gold nanorods. *ACS nano* **6**, 5920-5930 (2012).

50. Zhai, W., He, C., Wu, L., Zhou, Y., Chen, H., Chang, J., Zhang, H. Degradation of hollow mesoporous silica nanoparticles in human umbilical vein endothelial cells. *Journal of biomedical materials research. Part B, Applied biomaterials* **100**, 1397-1403 (2012).

51. Chen, Y.S., Frey, W., Kim, S., Kruizinga, P., Homan, K., Emelianov, S. Silica-Coated Gold Nanorods as Photoacoustic Signal Nanoamplifiers. *Nano Lett* **11**, 348-354 (2011).

52. Alkilany, A.M., Nagaria, P.K., Hexel, C.R., Shaw, T.J., Murphy, C.J., Wyatt, M.D. Cellular Uptake and Cytotoxicity of Gold Nanorods: Molecular Origin of Cytotoxicity and Surface Effects. *Small* **5**, 701-708 (2009).

53. Niidome, T., Yamagata, M., Okamoto, Y., Akiyama, Y., Takahashi, H., Kawano, T., Katayama, Y., Niidome, Y. PEG-modified gold nanorods with a stealth character for in vivo applications. *J Control Release* **114**, 343-347 (2006).

54. Arnold, L., Henry, A., Poron, F., Baba-Amer, Y., van Rooijen, N., Plonquet, A., Gherardi, R.K., Chazaud, B. Inflammatory monocytes recruited after skeletal muscle injury switch into antiinflammatory macrophages to support myogenesis. *The Journal of experimental medicine* **204**, 1057-1069 (2007).

55. Novak, M.L., Koh, T.J. Phenotypic transitions of macrophages orchestrate tissue repair. *Am J Pathol* **183**, 1352-1363 (2013).

56. Chen, L.W., Tredget, E.E., Wu, P.Y.G., Wu, Y.J. Paracrine Factors of Mesenchymal Stem Cells Recruit Macrophages and Endothelial Lineage Cells and Enhance Wound Healing. *PLoS One* **3** (2008).

57. Hu, X.Y., Yu, S.P., Fraser, J.L., Lu, Z.Y., Ogle, M.E., Wang, J.A., Wei, L. Transplantation of hypoxia-preconditioned mesenchymal stem cells improves infarcted heart function via enhanced survival of implanted cells and angiogenesis. *Journal of Thoracic and Cardiovascular Surgery* **135**, 799-808 (2008).

58. Nucera, S., Biziato, D., De Palma, M. The interplay between macrophages and angiogenesis in development, tissue injury and regeneration. *International Journal of Developmental Biology* **55**, 495-503 (2011).

59. Robey, T.E., Saiget, M.K., Reinecke, H., Murry, C.E. Systems approaches to preventing transplanted cell death in cardiac repair. *J Mol Cell Cardiol* **45**, 567-581 (2008).

60. Suga, H., Glotzbach, J., Sorkin, M., Longaker, M., Gurtner, G. Paracrine mechanism of angiogenesis in adipose-derived stem cell transplantation. *Annals of Plastic Surgery* **72**, 234-241 (2014).

61. Toma, C., Pittenger, M.F., Cahill, K.S., Byrne, B.J., Kessler, P.D. Human mesenchymal stem cells differentiate to a cardiomyocyte phenotype in the adult murine heart. *Circulation* **105**, 93-98 (2002).

62. Zhang, M., Methot, D., Poppa, V., Fujio, Y., Walsh, K., Murry, C.E. Cardiomyocyte grafting for cardiac repair: Graft cell death and anti-death strategies. *J Mol Cell Cardiol* **33**, 907-921 (2001).

Chapter 5: *In vitro* hypoxic modulation of mesenchymal stem cells and the resulting effects on macrophage function for ischemic tissue repair

5.1 INTRODUCTION

Mesenchymal stem cells (MSCs) possess regenerative properties[1-7] and have the potential to differentiate into various cell and tissue types[6]. It has been suggested that these pro-regenerative properties can be enhanced when MSCs are exposed to a hypoxic environment.[8-12] MSCs naturally reside in a hypoxic environment (2-6%) within the bone marrow cavity.[8,13-15] However, following an ischemic injury, where the oxygen level drops below 2%, MSCs have been shown to produce improved angiogenic responses.[8-12] In comparison to other cell types, MSCs can withstand a severely hypoxic environment (less than 2% O_2) for at least 48 hours, as they are able to derive the bulk of their ATP from glycolysis.[13] In addition to upregulated expression of pro-angiogenic and pro-survival factors under hypoxia,[9-11,16,17] MSCs also secrete factors which influence other cell types, including endothelial cells and macrophages,[18,19] potentially leading to improved tissue regeneration[20-22].

Many different cell types participate in the wound healing response (including fibroblasts, macrophages, and endothelial cells), and the dynamic interplay and synergistic effects of these cell types is essential in order for effective wound healing to occur. Macrophages are known to have key roles in wound healing processes and to participate in angiogenesis and skeletal muscle repair. The role of macrophages include: clearing damaged tissue; releasing cytokines to promote wound healing through recruitment, proliferation, and differentiation of other cell types; and altering the extracellular matrix to produce a more conducive environment for proper tissue regeneration.[23,24] In addition, dynamic changes in macrophage populations (from pro-inflammatory to regenerative) are essential for efficient wound healing.[25]

Macrophages support wound healing by enhancing angiogenesis. Specifically, macrophages secrete proteases (*e.g.* matrix metalloproteinases (MMPs)) which degrade and alter the extracellular matrix and also growth factors and monokines (*e.g.* transforming growth factor (TGF)-α and -β, granulocyte macrophage colony-stimulating factor (GM-CSF), vascular endothelial growth factor (VEGF), interleukin (IL)-1 and -6, and tumor necrosis factor (TNF)-α) which influence endothelial cell migration and proliferation.[24,26]

Macrophages also have important roles in the regeneration of skeletal muscle following an injury. Monocytes are recruited to the injured muscle within 24 hours following an injury[20,27,28] and total impairment of recruitment of monocytes to damaged skeletal muscle during this time period prevents muscle repair[20,22,28]. The monocytes become activated to macrophages and, as a result of cytokines expressed during Th1-driven inflammatory responses, such as interferon-γ (IFN-γ) and TNF-α,[21,27] are polarized to an M1, or pro-inflammatory, phenotype. M1 macrophages secrete pro-inflammatory cytokines such as TNF-α and IL-1β, clear damaged tissue by phagocytosing necrotic debris, and release cytokines that stimulate myoblast proliferation.[20,27] Approximately 1-3 days following M1 activation, the macrophages switch their phenotype to an M2 phenotype,[20,27,28] which is known to have a more "regenerative" role compared to M1 pro-inflammatory macrophages[29]. Conversion into an anti-inflammatory macrophage population is necessary for complete wound repair, as anti-inflammatory macrophages promote myoblast differentiation and fusion in skeletal muscle.[20-22,27] M2 macrophages are activated by Th2 cytokines such as interleukin (IL)-4, IL-10, and IL-13.[21,27] M2 macrophages secrete anti-inflammatory cytokines, including TGF-β and IL-10. M2 macrophages are often divided into subclasses, which consist of M2a, M2b, and M2c phenotypes.[30-33] Macrophages are stimulated to an M2a phenotype by IL-4 and IL-13 and

are thought to promote wound-healing[31] and participate in the later stages of angiogenesis, with high production of PDGF-BB[30]. M2b macrophages are stimulated by LPS and IL-1β and are thought to have an immunoregulatory role.[23,31] M2c macrophages are stimulated by TGF-β and IL-10 and have been shown to participate in matrix deposition and tissue remodeling, with high levels of MMP secretion.[23,30]

Taking into account the role of hypoxia and macrophage function in wound healing, this study evaluates the effect of an *in vitro* hypoxic environment on MSC function and phenotype and the resulting interaction with macrophages. It has been demonstrated that MSC therapy significantly affects macrophage subpopulations and wound repair.[34] However, the effect of environmental cues on the interaction between the two cell types is not well understood, specifically within a wound healing environment. Many have implemented hypoxic pre-conditioning methods in order to improve stem cell survival and enhance the wound healing response of MSCs following delivery within an ischemic site.[10] While hypoxic pre-conditioned stem cells have shown improvements in heart functional recovery[10] and skeletal muscle and liver regeneration,[9,35] the resulting immunomodulatory effects of stem cells is not well understood. The results of this study would provide insights about the mechanisms taking place during the wound healing response when utilizing stem cell therapy and the potential benefits of a hypoxic environment on stem cell function.

5.2 MATERIALS AND METHODS

5.2.1 Human mesenchymal stem cell culture

Bone marrow-derived human mesenchymal stem cells (hMSCs) (Lonza, Walkersville, MD) were cultured in Dulbecco's Modified Eagle Medium (DMEM) (Invitrogen, Carlsbad, CA) supplemented with 10% fetal bovine serum (FBS), 1%

glutamax, and 1% penicillin-streptomycin. The cell culture media was changed every 2-3 days. Cells were passaged using 0.25% trypsin/EDTA (Lonza), collected by centrifugation at 600 x g for 7 minutes, and counted with trypan blue exclusion. For all experiments, cells were seeded at a density of 5,000 cells/cm^2. Cells were grown under standard cell culture conditions (37°C, 5% CO_2). Passage 5-8 hMSCs were used in this study.

Human pre-macrophage-like (monocyte) cell line, U-937 cells (CRL-1593.2™) (ATCC), were cultured in suspension in RPMI-1650 growth media supplemented with 10% FBS and 1% penicillin-streptomycin. For macrophage differentiation, 100 nM of 12-O-Tetradecanoylphorbol-13-Acetate (TPA) (Cell Signaling Technology) was added to the growth media and the cells were cultured for 48 hours.

5.2.2 Cell culture under hypoxic and normoxic conditions

Human MSCs were plated at a concentration of 20,000 cells/cm^2 in growth media (10% FBS) and allowed to adhere overnight under normal cell culture conditions (20% O_2, 5% CO_2). Following overnight incubation, the media was replaced with serum free cell culture media following washing with phosphate buffered saline (PBS) without calcium and magnesium. The cells were placed in either a normoxic (20% O_2) or a hypoxic (1% or 2% O_2) environment for 48 hours. The media was collected every 24 hours and replaced with serum free media. The media was stored at -80ºC until further analysis. In addition, stem cells were also cultured in 2% O_2 for 72 hours and the media was collected for the macrophage proliferation study.

For the co-culture experiments, stem cells were seeded in 6 well transwell inserts (8 μm pore size) at a concentration of 20,000 cells/cm^2 in DMEM containing 10% FBS and cultured under standard cell culture conditions overnight to allow for adherence. U-

937 cells which were TPA treated for 48 hours were seeded in 6 well plates at a concentration of 400,000 cells/well in RPMI media containing 10% FBS and cultured under standard cell culture conditions overnight to allow for adherence. Following overnight culture, the media was removed from both cell types and replaced with serum free DMEM (1 mL) or 10% FBS (3 mL) containing RPMI media for stem cells and macrophages, respectively. The transwell inserts containing stem cells were transferred to the 6 well plates containing the macrophages. The co-cultured cells were then incubated under normoxic or 1% hypoxic conditions for 48 hours, after which the media was collected and RNA was isolated. In addition, cell proliferation was quantified for both cell types using a CellTiter 96® Aqueous One Solution Cell Proliferation Assay (MTS) (Promega) as described in section 5.2.3. Macrophage only conditions were also used as controls.

5.2.3 Cell proliferation

The effect of hypoxic culture on stem cell proliferation was assessed following culture in serum free media for 48 hours. Cells were collected by trypsinization and diluted 1:10 with serum free media. CellTiter 96® Aqueous One Solution Cell Proliferation Assay (MTS) (Promega) was used to measure the cell metabolic activity. MTS solution (20% v/v, 200 µl) was added to the cell suspension (1 mL) and allowed to incubate for 4 hours under standard cell culture conditions (5% CO_2 at 37ºC). After 4 hours, the cell media was collected and the absorbance levels at 490 nm were measured using a microplate reader (BioTek). The metabolic activity of macrophages cultured with MSC conditioned media (2% hypoxia for 72 hours) for 24 hours was similarly measured. In addition, the metabolic activity of MSCs and macrophages co-cultured under 1% hypoxia for 48 hours was also measured. For the co-culture proliferation studies, MSCs

and macrophages were co-cultured using 12 well inserts (8 μm pore size). Macrophages were not TPA treated prior to culture.

5.2.4 HIF-1α protein analysis

A DuoSet ELISA (R&D Systems) was used to detect HIF-1α expression following 6 hour incubation of stem cells under 2% hypoxia. Cell protein was collected by lysing cells with RIPA buffer (Santa Cruz Biotechnology) supplemented with PMSF, protease inhibitor cocktail, and sodium orthovanadate. The cells were incubated with lysis buffer for 30 minutes and homogenized by passing the samples through a 21G needle ten times at 4ºC. The cell lysates were then centrifuged at 14,000 x g for 20 minutes (at 4ºC) and the supernatant collected. The samples were then concentrated using a 10kD centrifugal filter (Millipore) by centrifuging at 10,000 x g for 5 minutes and the samples were retrieved by inverting the centrifugal column in a microcentrifuge tube and centrifuging at 1,000 x g for 2 minutes.

The ELISA plate was prepared and the samples were processed according to the manufacturer's directions. Briefly, the samples were added to the ELISA plate and allowed to incubate for 2 hours at room temperature. The plate was then washed with washing buffer. The detection antibody was added to the plate and incubated for 2 hours at room temperature. Following washing with the washing buffer, Streptavidin-HRP was added and incubated for 20 minutes. The plate was washed again and the substrate solution was added and incubated for 20 minutes. Finally, the stop solution was added to each well and the optical density was measured at 540 nm and subtracted from readings at 450 nm to calculate the concentration of protein.

5.2.5 Gene analysis

RNA was isolated from cells using an RNeasy Mini Kit (Qiagen) and QIAshredder (Qiagen) according to the manufacturer's directions. Reverse transcription was performed to convert the RNA to cDNA by combining 500 ng of RNA with reagents in the High-Capacity cNDA Reverse Transcription Kit (Life Tech) (10x RT buffer, 25x dNTP mix, 10x RT random primers, MultiScribe™ Reverse Transcriptase, and nuclease-free water) according to the manufacturer's directions. The cDNA was diluted by combining with nuclease-free water in a 1:1 volume ratio. PCR samples were prepared by combining cDNA with 2X TaqMan® Fast Universal PCR Master Mix-no AmpErase® UNG (Life Tech), specific gene expression assays (Life Tech), and DNase-free water. Real-time PCR was performed using a ViiA™ 7 machine (Life Tech) with a polymerization cycle of 43. Relative gene expression was calculated using a delta-delta-Ct method by normalizing with gene levels of beta-actin or GAPDH and further normalizing with normoxic conditions. For stem cell gene analysis, RNA was collected from MSCs cultured under hypoxia (1% or 2%) or co-cultured with macrophages for 48 hours. For macrophage gene analysis, RNA was collected from TPA treated U-937 cells cultured with MSC conditioned media or co-cultured with MSCs. Positive control conditions consisted of treating macrophages with the following cytokines: M1 – LPS (100 ng/ml) and IFN-γ (20 ng/ml); M2a – IL-4 (20 ng/ml) and IL-13 (20 ng/ml); M2c – IL-10 (50 ng/ml).

5.2.6 Protein analysis

Protein was collected by lysing cells with RIPA buffer (Santa Cruz Biotechnology) supplemented with PMSF, protease inhibitor cocktail, and sodium orthovanadate. The cells were incubated with lysis buffer for 30 minutes and homogenized by passing the samples through a 21G needle ten times at 4ºC. The cell

lysates were then centrifuged at 14,000 x g for 20 minutes (at 4ºC) and the supernatant collected. The samples were then concentrated using a 10kD centrifugal filter (Millipore) by centrifuging at 10,000 x g for 5 minutes and the samples were retrieved by inverting the centrifugal column in a microcentrifuge tube and centrifuging at 1,000 x g for 2 minutes.

Sodium dodecyl sulfate-polyacrylamide gel electrophoresis (SDS-PAGE) was performed on a 10% Mini-PROTEAN® TGX™ Precast gel (Bio-Rad Laboratories) at room temperature for 1 h at 100 V using a Mini-Protein cell system (Bio-Rad, Hercules, CA). The total protein content was quantified using a BCA assay and each sample was boiled with an equal volume of 2x Laemmli sample buffer at a ratio of 1:1. Equal amounts of total protein (25 μg) were loaded into each well of the gel. Following SDS-PAGE, proteins were transferred to a PVDF membrane (1 hr at 100 V) and blocked with 5% milk in 0.1% Tween-20 in TBS (TBST) for 1 h. Membranes were incubated in primary antibodies in 5% milk solution at 4ºC overnight (HSP70 1:1000, beta actin 1:1000), followed by incubation with the secondary antibody in 5% milk solution at room temperature for 1 h (goat anti-mouse 1:2000, goat anti-rabbit 1:2000). Chemiluminescent substrate (SuperSignal West Dura Extended Substrate, Pierce) was used to visualize immunoblotted protein bands. The membranes were imaged using FluorChem Q (ProteinSimple) and signal quantification was analyzed using AlphaView software.

5.2.7 Macrophage migration

U-937 monocyte cells were fluorescently pre-labeled by collecting the cells, washing with PBS, and incubating with calcein AM (4 μM in PBS) at 37ºC for 30 minutes. The cells were then washed with PBS and resuspended in serum free RPMI media. The cells (100,000 cells in 75 μL for the 2% conditioned media and 60,000 cells

in 75 μL for the 1% conditioned media) were placed in the top well of a 96 transwell insert (8 μm pore size) (Corning Life Sciences) and the conditioned media (50 μL of concentrated conditioned media + 200 μL of serum free RPMI media) was placed in the bottom of the transwell plate. To quantify cell migration, the fluorescence intensity was measured (excitation: 485 nm; emission: 520 nm) at designated time points using a BioTek plate reader, and the cell number was calculated using a standard curve.

5.2.8 Soluble factor secretion

Enzyme-linked immunosorbent analysis (ELISA) was used to analyze VEGF secretion of MSCs under normoxic and hypoxic conditions. Media was collected from MSCs cultured under 1% hypoxia or from co-culture of macrophages and MSCs cultured under 1% hypoxia. A Quantikine ELISA Kit (R&D Systems) against human VEGF was used according to the manufacturer's instructions. Briefly, the samples were added to the ELISA plate (diluted 1:40 in assay diluent) and incubated for 2 hours at room temperature. The samples were aspirated and the plate was washed with washing buffer. VEGF Conjugate was added to each well and incubated for 2 hours. The plate was washed and the substrate solution was added and incubated for 20 minutes. Finally, the stop solution was added to each well and the optical density was measured at 450 nm, using a wavelength correction at 540 nm. Protein concentrations were normalized to the cell number, as determined using an MTS assay.

Cell culture media was analyzed using a RayBio® Custom C-Series Human Array as a broad-spectrum screen for secreted factors. The factors which were analyzed included: bFGF, IFN-γ, IGF-1, IL-1α, IL-1β, IL1-Ra, IL-4, IL-6, IL-8, IL-10, IL-13, MCP-1, MMP-1, MMP-2, MMP-9, PDGF-1, SDF-1, and TGF-β. Triplicate samples were combined for analysis. The membranes were incubated with the media samples overnight

at 4ºC, followed by addition of biotinylated antibody and HRP-conjugated streptavidin reagents for 2 hours each at 4ºC. The chemiluminscent signal was imaged using FluorChem Q (ProteinSimple) and signal quantification was analyzed using AlphaView software. A heatmap was generated using the JMP software.

5.2.9 Statistical analysis

All test groups consisted of a sample number of 3. Statistical analysis was performed using student t-tests with a p value of 0.05.

5.3 RESULTS AND DISCUSSION

5.3.1 MSC function under 2% hypoxia

In order to evaluate the effect of a hypoxic environment on stem cell function, bone marrow-derived mesenchymal stem cells were cultured under 2% hypoxia. The expression of HIF-1α protein was assessed after 6 hour hypoxic culture (Figure 5.1A). HIF-1α is known to be upregulated in response to hypoxia and the downstream effects of the HIF-1α pathway include pro-angiogenic and pro-survival mechanisms.[11] Also, the degree of stabilization of HIF-1α has been shown to be inversely proportional to the oxygen concentration.[36] There was a significant upregulation of HIF-1α protein under hypoxic conditions compared to normoxic conditions. In addition, the expression of heat shock protein (HSP) 70 was upregulated in MSCs, although not significantly, following 48 hour hypoxic culture (Figure 5.1B). Stem cell proliferation was significantly increased under hypoxia, with MSCs showing a 1.8 fold increase (Figure 5.2A). Others have found that MSCs cultured under hypoxia (ranging from 1-5% oxygen) displayed an early start of the exponential growth phase and decreased population doubling time, resulting in faster proliferation.[13,15,37-39] MSCs cultured under hypoxia were also found to exhibit a larger shortening of telomere length, which was related with the high proliferation rate.[15]

On the other hand, some studies found that hypoxia did not cause faster proliferation of MSCs, but instead extended the duration of their proliferation.[8,13,40] In addition to enhanced cell proliferation, hypoxic culture has been found to increase the differentiation efficiency of MSCs.[13,15,40]

Gene analysis was performed to evaluate phenotypic changes in MSCs following 2% hypoxic culture. As shown in Figure 5.2B, MSCs showed a significant downregulation in SMA and upregulation in PECAM compared to normoxic culture. MSCs also exhibited an upregulation in MMP2 and VEGF under hypoxia, although not significantly. MSCs are known to express pericyte markers such as SMA,[41,42] and it is evident that MSCs undergo a phenotypic change under hypoxia, with upregulation of endothelial cell markers. Gene analysis data suggests the cells are transitioning from a pericyte-like phenotype to an endothelial-like phenotype, with upregulation of PECAM (endothelial marker), VEGF (promotes angiogenesis), and MMP2 (facilitates matrix degradation). However, additional morphological and protein analysis is necessary to confirm the transition of hypoxic cultured MSCs towards an endothelial phenotype.

5.3.2 Influence of MSC conditioned media (2% hypoxia) on macrophages

U-937 monocytes were cultured with conditioned media collected from stem cells cultured under normoxia and 2% hypoxia. Following 48 hour incubation with conditioned media, U-937 proliferation was evaluated. Monocytes cultured with MSC normoxic and hypoxic conditioned media had substantially enhanced cell proliferation compared to the serum free condition (Figure 5.3A), although there was no difference between the MSC hypoxia and normoxia conditioned media. Thus, under normoxic culture conditions MSCs secrete factors which are mitogenic for monocytes, but this effect is not significantly enhanced within hypoxic environments.

The chemoattractive effects of MSC conditioned media on macrophages was evaluated using a modified Boyden's assay (Figure 5.3B). Conditioned media from MSCs cultured under 2% hypoxia did not exhibit significant chemoattractive effects compared to normoxic conditions. Others have seen chemoattractive effects of MSCs cultured under hypoxia, with enhanced monocyte migration after 2 hours compared to control media.[18] However, differences in culture conditions and experimental design could potentially be the cause for these differences between this study and studies by others. Specifically, Chen *et al*[18] cultured MSCs under a much more severe hypoxic environment (0.5% O_2 for 24 hours) compared to our study and saw some differences in macrophage migration. Thus, it is possible that MSCs secrete more chemoattractive factors for macrophages under more severe hypoxic conditions.

Evaluation of macrophage phenotype along the M1/M2 spectrum was performed using gene analysis. Positive control conditions consisted of treating macrophages with certain cytokines to induce changes towards a specific macrophage phenotype (M0, M1, M2a, or M2c). The markers chosen for the M1 and M2 subclasses were selected based on the literature.[23,30,43] The data (Figure 5.4) shows that CCR7 identified M1 macrophages, arginase-1 (Arg1) identified M2 (specifically M2a) macrophages, and CD163 identified M2c macrophages. CD206 is identified as an M2a phenotypic marker.[30] However, gene analysis did not show a substantial upregulation of CD206 for M2a macrophages. This could potentially be attributed to the fact that the concentrations of cytokines used to induce differentiation were not high enough, or the time point of analysis (24 hours) was not optimal. Analysis of macrophages incubated with normoxic or hypoxic conditioned media showed there were not substantial changes in macrophage phenotype. While trends showed an upregulation in M2c, this change was not significant. As a result, it was

concluded that conditioned media collected from MSCs cultured under 2% hypoxia did not significantly influence macrophage phenotype.

5.3.3 MSC function under 1% hypoxia

Typically within the wound environment cells encounter hypoxic conditions less than 2% O_2. Thus, the effect of a more severe hypoxic environment (1% O_2) on stem cell function was evaluated. Under more severe hypoxic culture, stem cells showed a dramatic upregulation in cell proliferation, with a 3.16 fold increase compared to normoxic culture (Figure 5.5A). Gene analysis was performed to evaluate phenotypic changes in MSCs following 1% hypoxic culture (Figure 5.5B). MSCs showed a significant downregulation in SMA and an even more dramatic upregulation of VEGF compared to 2% hypoxia. MSCs also exhibited an upregulation in MMP2 and downregulation in PECAM under 1% hypoxia, although not significantly. Similar to the 2% hypoxic conditions, this data suggest a transition from a pericyte phenotype to an angiogenic promoting phenotype.

5.3.4 Influence of MSC conditioned media (1% hypoxia) on macrophages

Migration of U-937 monocytes with conditioned media from MSCs cultured under 1% hypoxia was evaluated using the same method as for the 2% hypoxia media. Based on the 2% hypoxia migration study, we hypothesized that the optimal chemotactic effect would be during the earlier time points following incubation with the conditioned media. As a result, more early time points were evaluated for the 1% hypoxia case. However, conditioned media from MSCs cultured under 1% hypoxia did not exhibit significant chemoattractive effects compared to normoxic conditions (Figure 5.6). It is possible that MSCs are secreting factors which are chemoattractive for macrophages, but they are in such low concentration and thus do not significantly influence macrophage

migration. It is also possible that MSCs might have more significant chemotactic effects on macrophages under a more severe hypoxic environment (<1% O_2).[18]

Macrophage phentoyope was evaluated using gene analysis (Figure 5.7). Similar to the 2% conditioned media, the 1% conditioned media also did not elicit substantial phenotypic changes in macrophages. It is possible that the MSCs were not secreting high enough concentrations of cytokines to elicit a response from macrophages. In addition, the co-culture of macrophages and MSCs may be necessary in order to produce synergistic effects and allow for cross-talk between the two cell types and enhanced paracrine and autocrine effects.[19,44,45]

5.3.5 MSC soluble factor secretion under severe (1%) hypoxia

Analysis of the soluble factors secreted by MSCs under 1% hypoxia was performed using a cytokine array (Figure 5.8). Of the 18 factors analyzed, only 5 were detectable (IL-6, MCP-1, bFGF, MMP-1, and IL-8). Under hypoxia MSCs secreted higher levels of IL-6. Although IL-6 is traditionally considered to be a pro-inflammatory cytokine, it is necessary for complete wound healing to occur,[19,46] as demonstrated by the lack of wound healing in IL-6 deficient mouse,[46] and is also considered pro-angiogenic. MMP-1 and bFGF are also factors which are important for angiogenesis, but there were minimal differences in secretion levels of these factors under hypoxia versus normoxia. IL-8 and MCP-1 are chemokines which drive the infiltration of neutrophils and macrophages to the wound area following an injury.[47] Although these factors were slightly upregulated under hypoxia, the migration results in Figure 5.6 demonstrate they were not secreted in a high enough concentration to elicit a response from macrophages.

The secretion of VEGF was quantified using an ELISA (Figure 5.9). MSCs cultured under 1% hypoxia secreted significantly higher amounts of VEGF compared to

normoxic conditions. However, when normalizing by the cell number, there was not a significant difference between normoxic and hypoxic conditions. This suggests that the total amount of VEGF is increased as a result of the increase in cell number, and not necessarily due to the increased secretion of VEGF per cell. Other investigators who have seen upregulated secretion of VEGF by MSCs under hypoxia only reported total VEGF and did not normalize by cell number.[9,48-52] Some have reported upregulated VEGF secretion per cell, but in this case both secreted and intracellular VEGF were quantified,[53] which is in contrast to our study in which only secreted VEGF was quantified. However, VEGF gene expression analysis of MSCs under 1% hypoxia showed a significant upregulation compared to normoxia (Figure 5.5B), which suggests that on the cellular level VEGF is upregulated in terms of gene expression, but not for protein, at the 48 hour time point.

5.3.6 Cross-talk between MSCs and macrophages within a hypoxic environment

Previous studies have demonstrated that stem cells can potentially have an influence on macrophage function and phenotype, essentially producing "mesenchymal stem cell-educated macrophages".[19,44,45]. Kim *et al* showed that co-culture of stem cells and macrophages produced more dramatic results in terms of influencing macrophages.[19] As a result, the co-culture of MSCs and macrophages under hypoxic (1% O_2) and normoxic conditions was evaluated. The co-culture was performed using a transwell insert and the cells were separated and analyzed following incubation. Analysis of MSC function showed a significant upregulation in cell proliferation (2.8 fold increase) under hypoxia compared to normoxia (Figure 5.10A), similar to that seen for the 2% and 1% hypoxia experiments in sections 5.3.1 and 5.3.3, respectively. Gene expression analysis of MSCs co-cultured with macrophages again showed a downregulation of SMA under

hypoxia. In addition, all of the endothelial and angiogenic markers were upregulated under hypoxia, including significant upregulation of PECAM and VEGF (Figure 5.10B).

Macrophages co-cultured with MSCs under hypoxia had significantly higher proliferation compared to normoxic co-culture (Figure 5.11). In addition, macrophages cultured alone under hypoxia (not with MSCs) had significantly higher proliferation compared to normoxic conditions. Interestingly, it appears that MSCs enhance the proliferation of macrophages when cultured under hypoxia, as evident when comparing macrophages co-cultured with MSCs and macrophages cultured alone under hypoxia. Macrophage proliferation is influenced by macrophage colony-stimulating factor, granulocyte-macrophage colony-stimulating factor, and IL-3.[54-56] However, additional analysis and quantification of the production of these cytokines under normoxia and hypoxia are needed.

Phenotypic changes of macrophages co-cultured with MSCs were also analyzed (Figure 5.12) and compared to macrophages cultured alone. Gene expression analysis showed a significant increase in CCR7, an M1 marker, for both co-cultured macrophages and macrophages alone under hypoxia. Arg1 expression, an M2 marker, was significantly increased for the co-cultured macrophages and significantly decreased for the macrophages alone under hypoxia. The other markers (CD206 and CD163) did not show significant changes. Taking the ratio of M1/M2 (CCR7/Arg1) showed a significant shift towards an M1 phenotype for macrophages cultured alone under hypoxia. On the other hand, macrophages co-cultured with MSCs under hypoxia were not stimulated towards an M1 phenotype and showed a trend towards an M2 phenotype, although it was not significant. Others have seen changes in macrophage function in response to hypoxia. Most notably, macrophages cultured under hypoxia showed upregulation of pro-angiogenic factors, including VEGF.[57,58] However, the phenotypic changes induced by

hypoxia is more differential and is dependent upon the duration and extent of hypoxia, the cell type and source, and previous priming of the macrophages (such as with LPS).[57,59] In general, hypoxia is found to lead to the release of inflammatory cytokines, including TNF-α, IL-1, IL-6, and iNOS,[57,58,60] and some have claimed hypoxia is a stimulus for M1 activation[57,60,61]. It has also been suggested that the initial immune response to hypoxia is an exaggerated inflammatory stage, with secretion of pro-inflammatory factors.[57,59] This acute response is then followed by the release of anti-inflammatory cytokines.[57] The shift between these two phases is most likely due to external factors, including neighboring cells. Our results support this statement, in that macrophages cultured alone show an enhanced M1 response, whereas macrophages co-cultured with MSCs do not shift towards an M1 phenotype.

5.3.7 Effect of hypoxia and culture conditions on soluble factor secretion

Soluble factor secretion of macrophages and MSCs co-cultured under 1% hypoxia was analyzed using a cytokine array (Figure 5.13). Of the 18 factors analyzed, only 5 were detectable (IL-6, MCP-1, IL-10, MMP-1, and IL-8). For the co-culture condition, IL-10 and MMP-1 production was increased under hypoxia compared to normoxia, while IL-6 production was slightly decreased. IL-10 is an anti-inflammatory cytokine which activates macrophages to an M2 phenotype (specifically M2c)[21,27] and is also secreted by M2 macrophages[23,30]. There was a slight increase in MCP-1 secretion under hypoxia and a decrease in secretion of IL-8. For the macrophages cultured alone under hypoxia, there was an increase in the production of IL-6 and IL-10 and of the pro-angiogenic factor MMP-1. There was a decrease in MCP-1 and IL-8 under hypoxia.

When comparing the differences in soluble factor secretion between the two culture conditions under normoxia, it was found that production of IL-6 and IL-10 were

increased for the co-culture system (Figure 5.14). It has been shown co-culture of macrophages and MSCs leads to enhanced secretion of IL-10 by macrophages and of IL-6 by both cell types.[19,44,45] Under hypoxia, it was found that production of IL-6, MCP-1, IL-10, MMP-1, and IL-8 were enhanced for the co-culture system. IL-8 and MCP-1 are chemotactic factors for macrophages, and thus future studies could include analyzing the effect of conditioned media collected from co-cultured MSCs and macrophages on macrophage migration. Overall, these results demonstrate that culturing MSCs with macrophages under hypoxia leads to enhanced secretion of pro-angiogenic and anti-inflammatory cytokines.

Others have demonstrated that MSCs influence macrophages, either through direct culture or soluble factor secretion, to express higher levels of CD206, increased production of IL-10 and IL-6, and decreased production of IL-12 and TNFα.[19,44] These trends hold true for the current study, as analysis of the soluble factors secreted from the co-culture of MSCs and macrophages showed higher levels of IL-6 and IL-10 compared to macrophages alone. However, the cell source *(i.e.* MSCs or macrophages) of the soluble factors is not known in the co-culture system. With that said, MSCs cultured with macrophage conditioned media have also been shown to have increased IL-6 production.[45] Although IL-6 is essential in the wound healing process[19,46,62] and is usually considered to be pro-inflammatory, it can also play an anti-inflammatory role by potentially regulating the levels of pro-inflammatory cytokines such as IL-1 and TNFα[63]. Furthermore, M2b macrophages express high levels of IL-6.[19]

In addition, the co-culture of MSCs and macrophages resulted in enhanced VEGF secretion under 1% hypoxia (Figure 5.15), although it was not significant. Thus, even under normoxia, the combination of MSCs and macrophages leads to upregulated expression of VEGF which is not further enhanced under hypoxia. This is in contrast to

MSCs cultured alone (Figure 5.9), in which there were lower basal levels of VEGF expression under normoxia which was significantly upregulated under hypoxia. The VEGF secretion can be attributed to both the MSCs and the macrophages and the co-culture of the two cell types. When comparing the co-culture condition to macrophages cultured alone for the 1% hypoxia, there was a significant increase in VEGF secretion for the co-culture condition under hypoxia. This could be due to the paracrine and autocrine effects of the stem cells and macrophages being cultured together, as both cell types have been demonstrated to secrete VEGF.

5.4 CONCLUSIONS

This study investigated the effect of a hypoxic environment on MSCs and the subsequent effects on the interaction between MSCs and macrophages. Various culture conditions were analyzed, including mild (2% O_2) and severe (1% O_2) hypoxia, as well as culture of macrophages with MSCs or MSC conditioned media. MSCs exhibited a stress response under hypoxia, with upregulation of pathways (HIF-1α and HSP70) which are pro-angiogenic and pro-survival. Quantitative analysis showed increased expression of angiogenic and endothelial factors under mild hypoxia, with an enhanced expression under severe hypoxia. Culturing macrophages with MSC conditioned media did not result in enhanced macrophage proliferation compared to normoxic conditions, although it appeared that MSCs are secreting factors even under normoxic conditions which sustain macrophage proliferation. However, co-culturing MSCs with macrophages under hypoxia did lead to a significant upregulation in macrophage proliferation, demonstrating the need for cross-talk between the two cell types. In addition, significant changes in macrophage phenotype only occurred when the cells were co-cultured with MSCs, with macrophages not shifting towards an M1 phenotype. Analysis of cytokine secretion under the various

culture conditions (conditioned media and co-culture) showed that for MSCs cultured under severe hypoxia, secretion of IL-6 was substantially upregulated under hypoxia, while other chemoattractive (MCP-1 and IL-8) and pro-angiogenic (MMP-1) cytokines were slightly upregulated. In addition, total VEGF secretion was significantly higher for MSCs cultured under hypoxia compared to normoxia. On the other hand, analysis of the co-culture condition compared to macrophages alone showed substantial upregulation in pro-angiogenic and anti-inflammatory cytokines under hypoxia, including IL-6, MCP-1, IL-10, MMP-1, and IL-8. Although IL-6 is sometimes considered to be pro-inflammatory, it has important roles in wound healing. Total VEGF secretion was significantly higher for the co-cultured cells compared to macrophages only under both normoxic and hypoxic conditions. Overall this study provides insights into the response of MSCs and macrophages to hypoxia and the essential cross-talk between the two cell types.

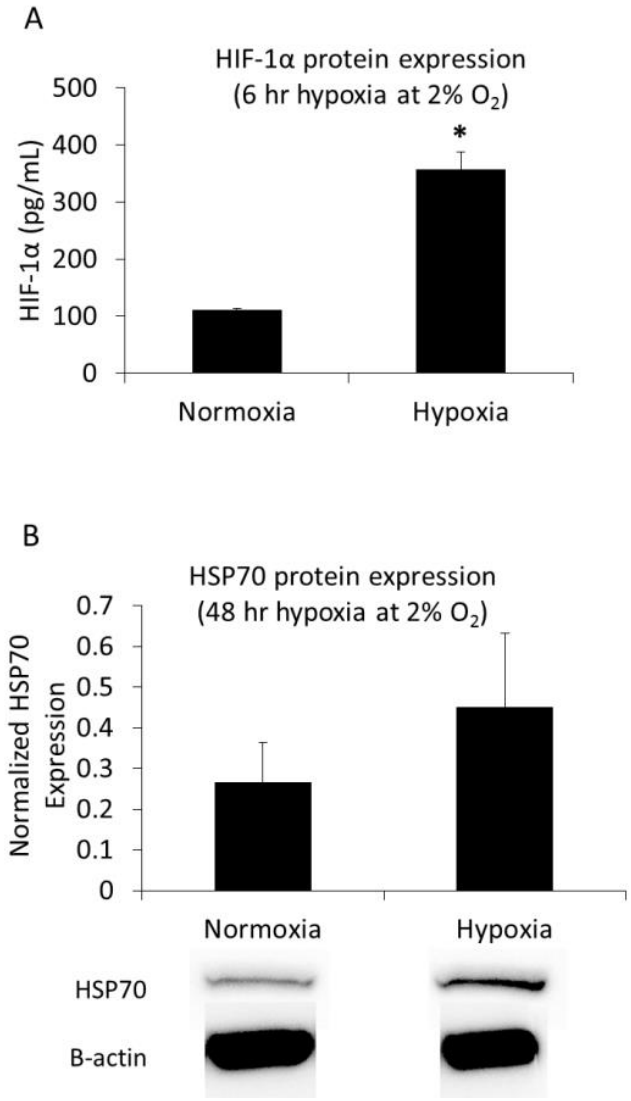

Figure 5.1: Quantification of (A) HIF-1α and (B) HSP70 protein expression by MSCs in response to 2% hypoxia. (* = $p<0.05$ compared to normoxia)

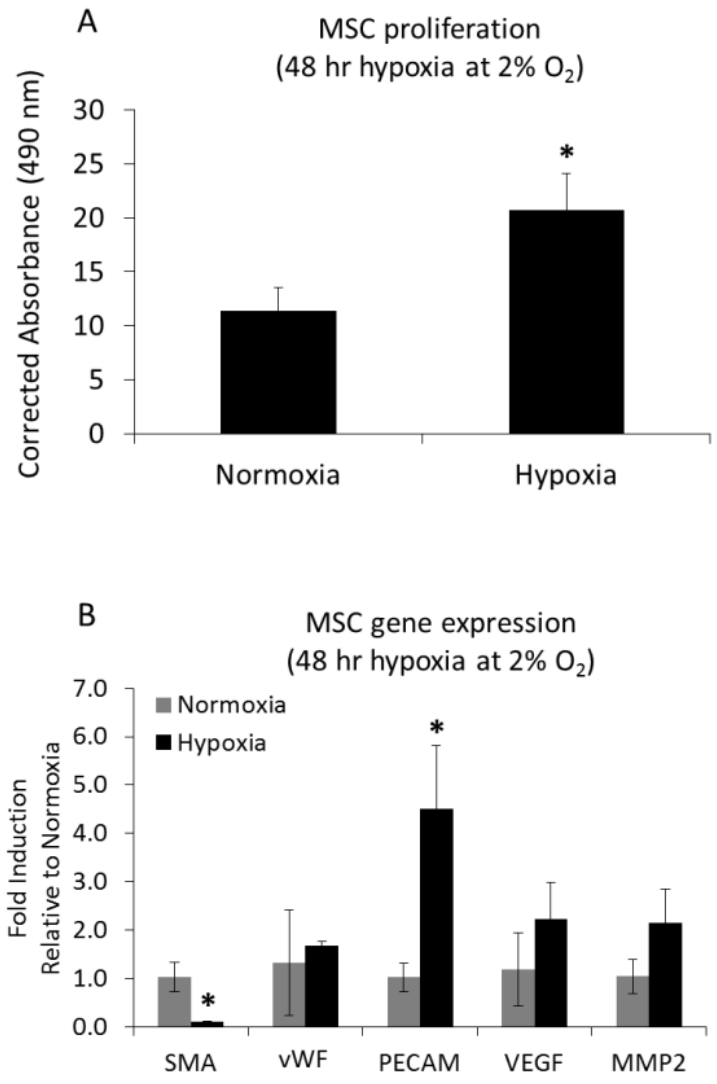

Figure 5.2: (A) MSC proliferation and (B) gene expression after 48 hour culture under normoxic or 2% hypoxic conditions. (* = $p<0.05$ compared to normoxia)

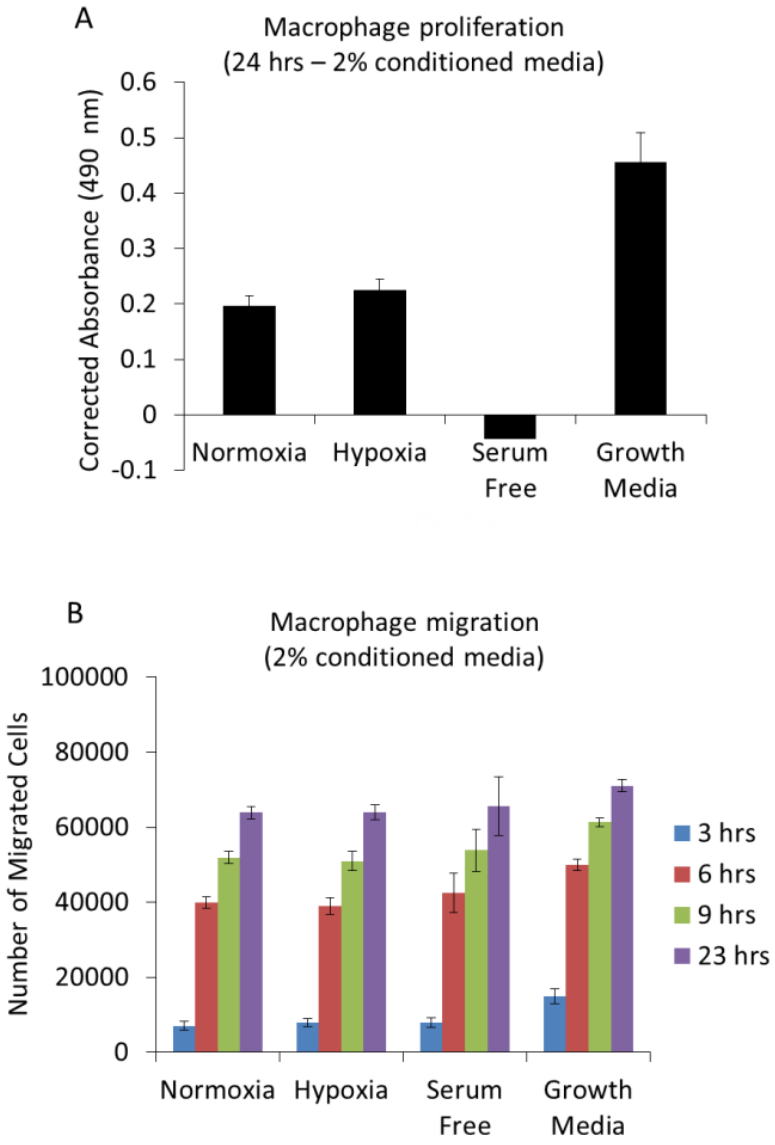

Figure 5.3: Effect of 2% hypoxic MSC conditioned media on (A) macrophage proliferation and (B) macrophage migration.

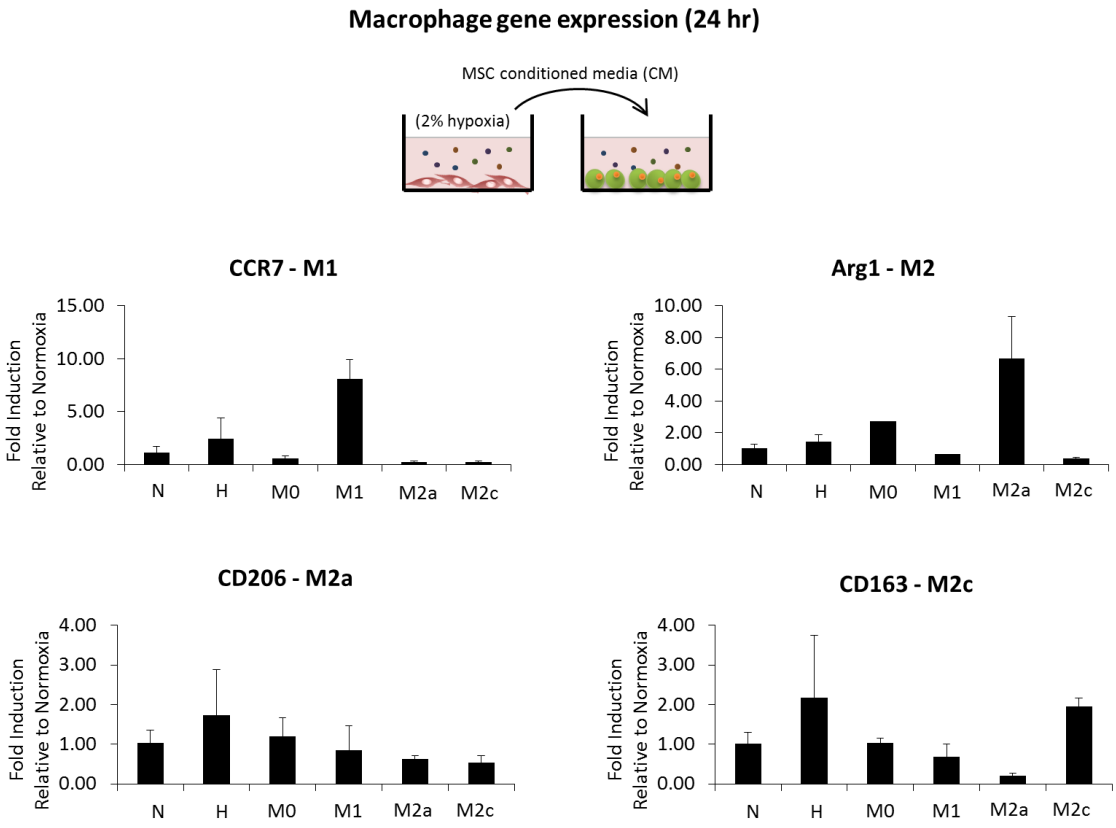

Figure 5.4: Phenotype analysis of macrophages following 24 hour culture with 2% hypoxic MSC conditioned media. Abbreviations: normoxia (N), hypoxia (H).

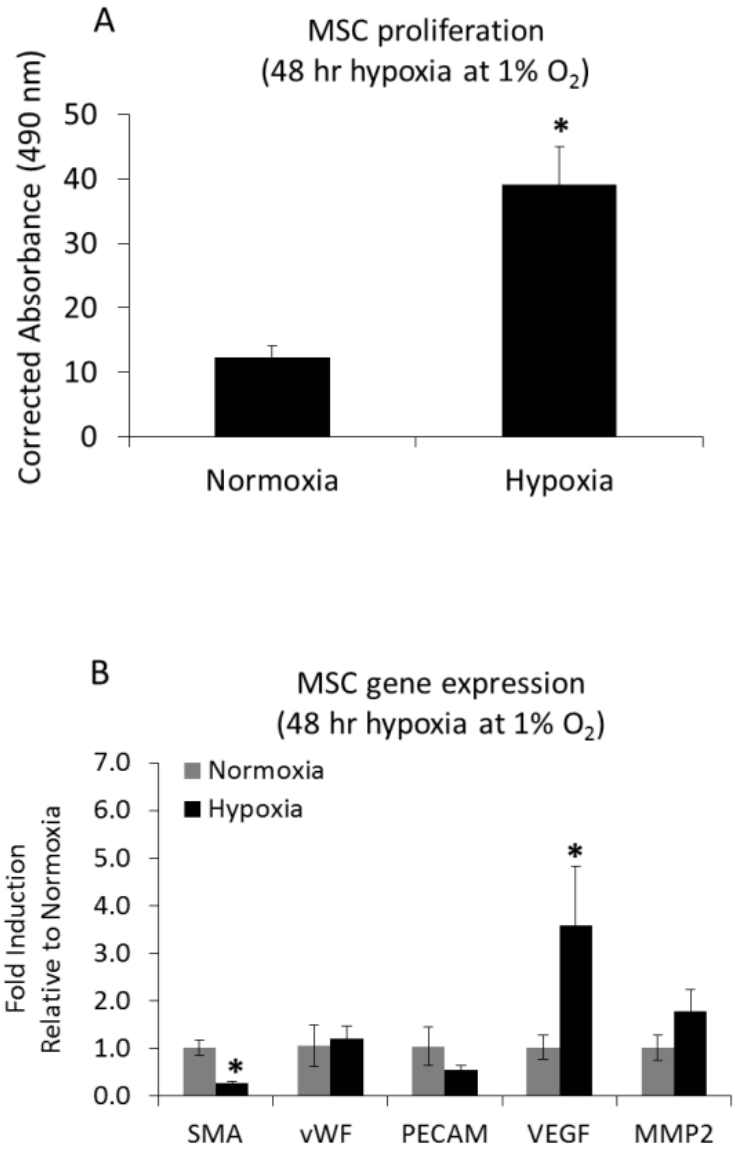

Figure 5.5: (A) MSC proliferation and (B) gene expression after 48 hour culture under normoxic or 1% hypoxic conditions. (* = $p<0.05$ compared to normoxia)

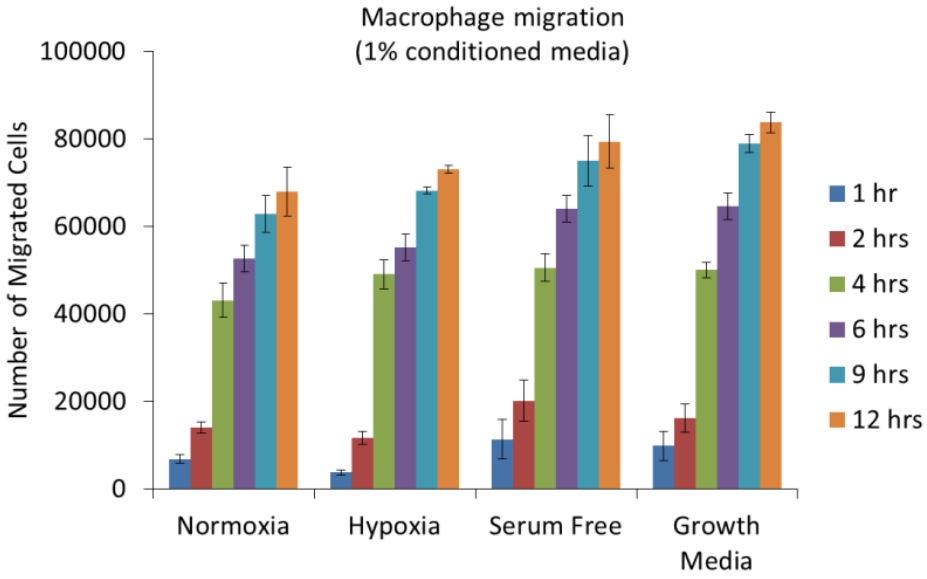

Figure 5.6: Effect of 1% hypoxic MSC conditioned media on macrophage migration.

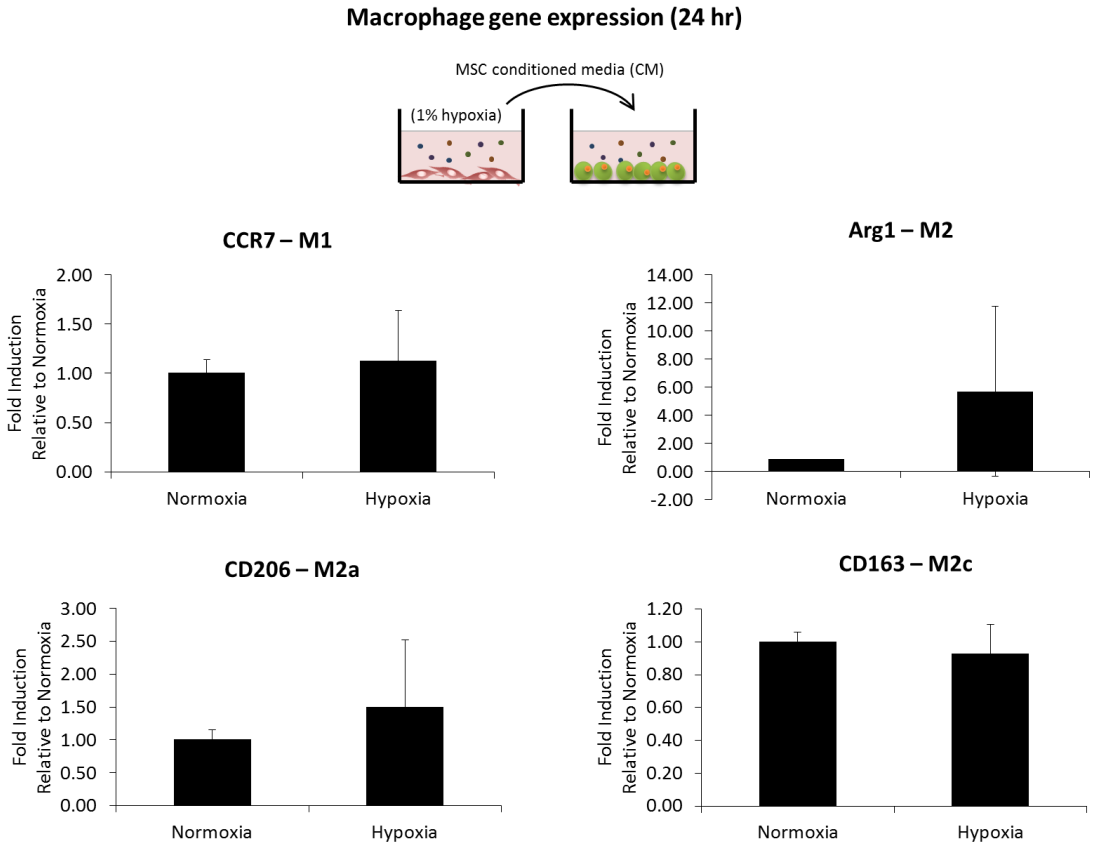

Figure 5.7: Phenotype analysis of macrophages following 24 hour culture with 2% hypoxic MSC conditioned media.

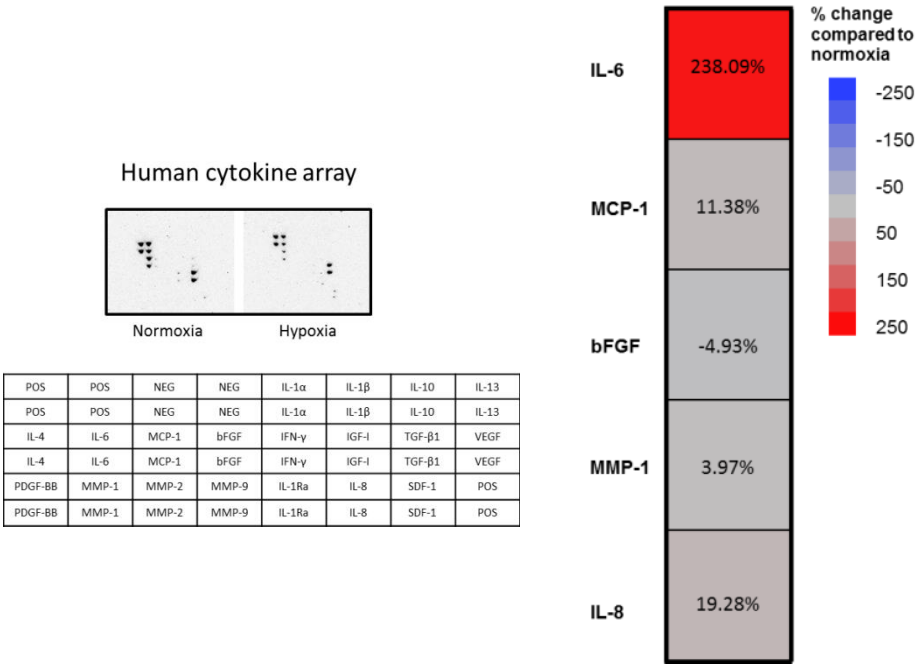

Figure 5.8: Secretion of various factors by MSCs analyzed by human cytokine membrane array following 1% hypoxic culture.

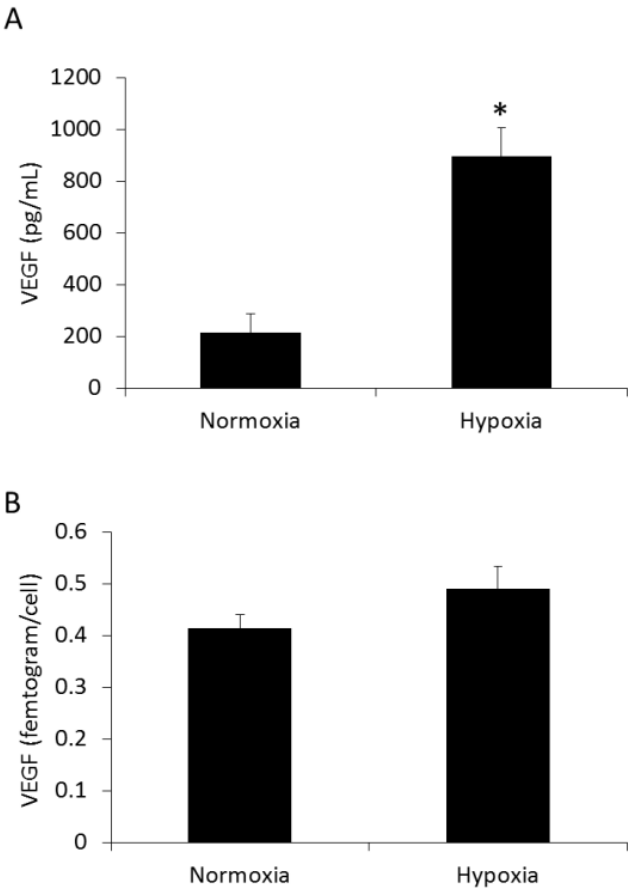

Figure 5.9: VEGF secretion of MSCs cultured 1% hypoxia. (* = $p<0.05$ compared to normoxia).

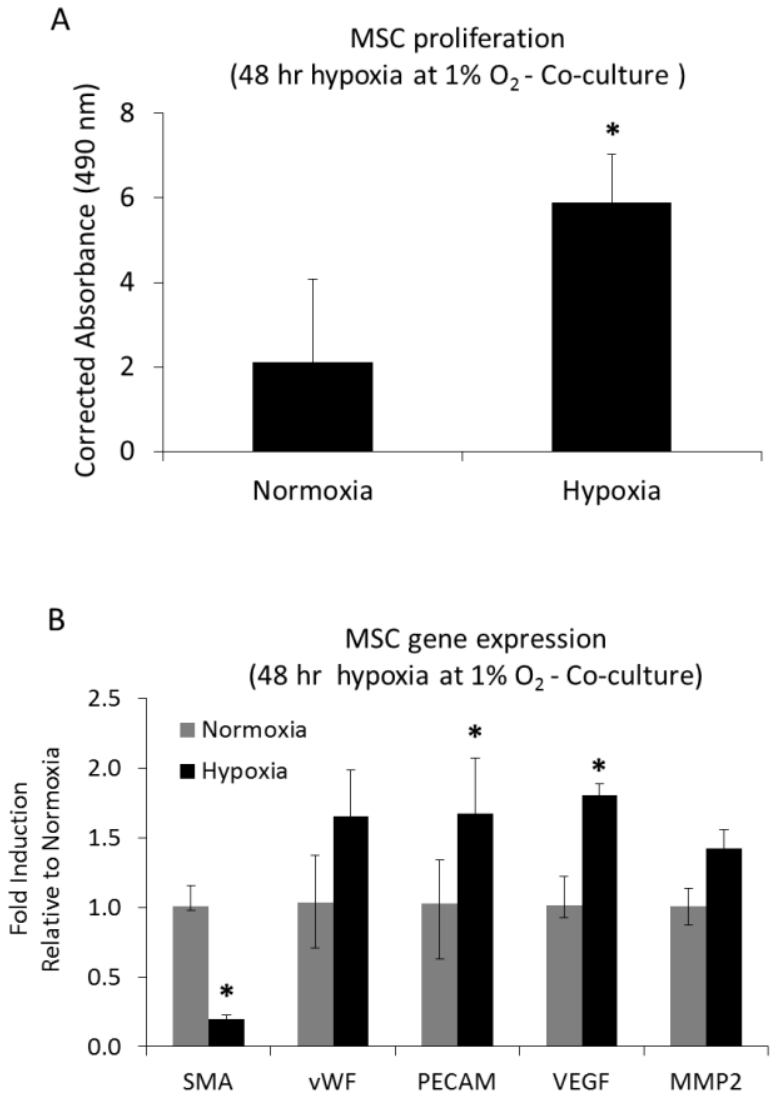

Figure 5.10: (A) MSC proliferation and (B) gene expression after 48 hour co-culture with macrophages under normoxic or 1% hypoxic conditions. (* = $p<0.05$ compared to normoxia)

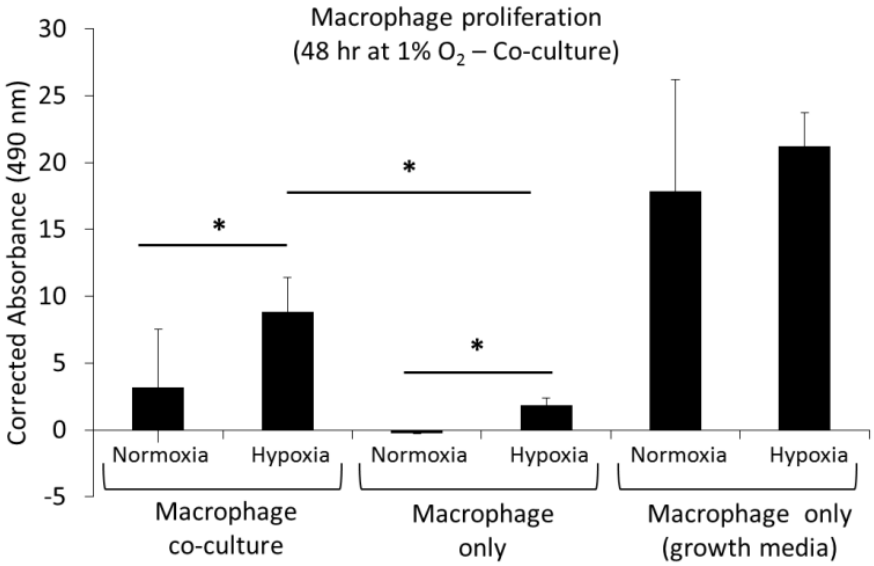

Figure 5.11: Macrophage proliferation following 48 hour culture under normoxia or 1% hypoxia. Macrophages were either cultured individually or co-cultured with MSCs. Macrophages cultured alone with 10% FBS containing media (growth media) was used as a positive control. (* = $p<0.05$)

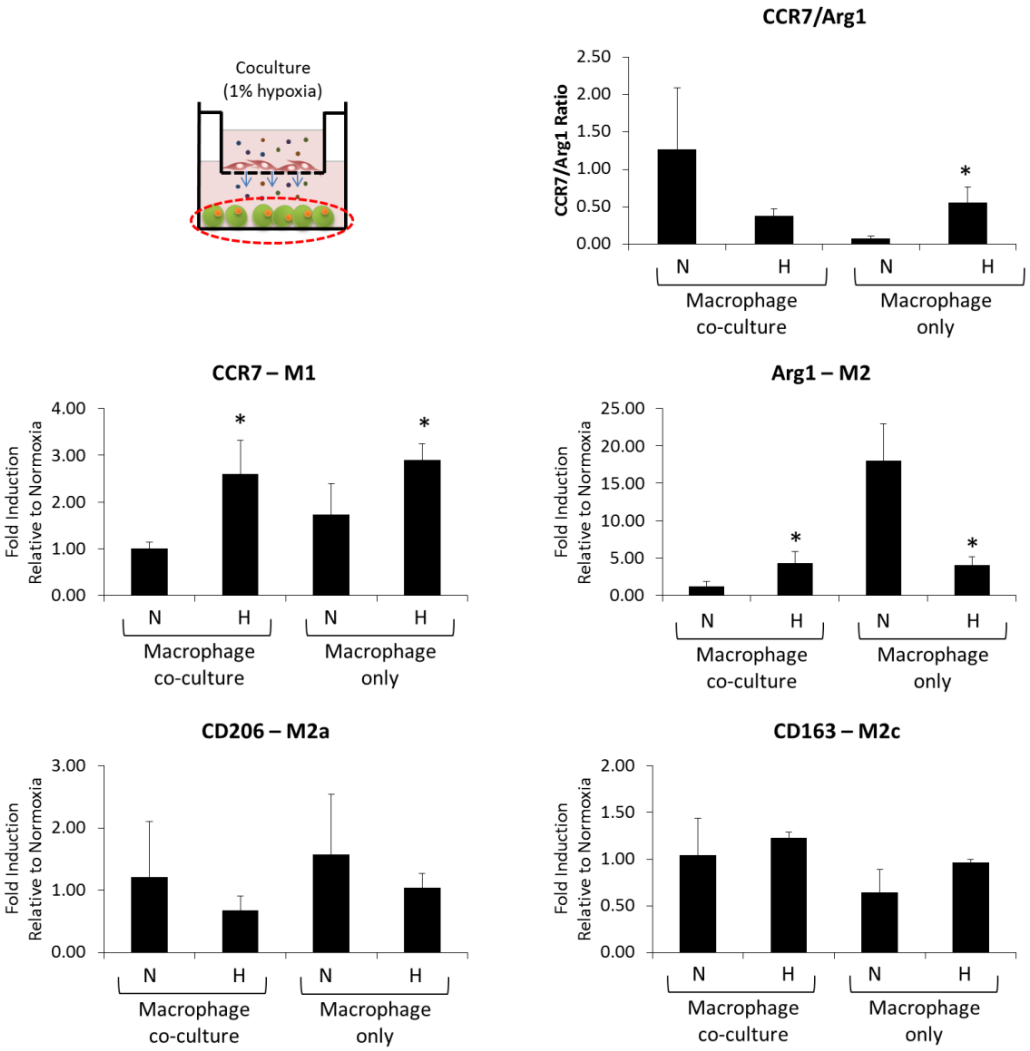

Figure 5.12: Phenotype analysis of macrophages under 1% hypoxia following either 24 hour co-culture with MSCs or cultured alone. (* = $p<0.05$ compared to normoxia). Abbreviations: normoxia (N), hypoxia (H).

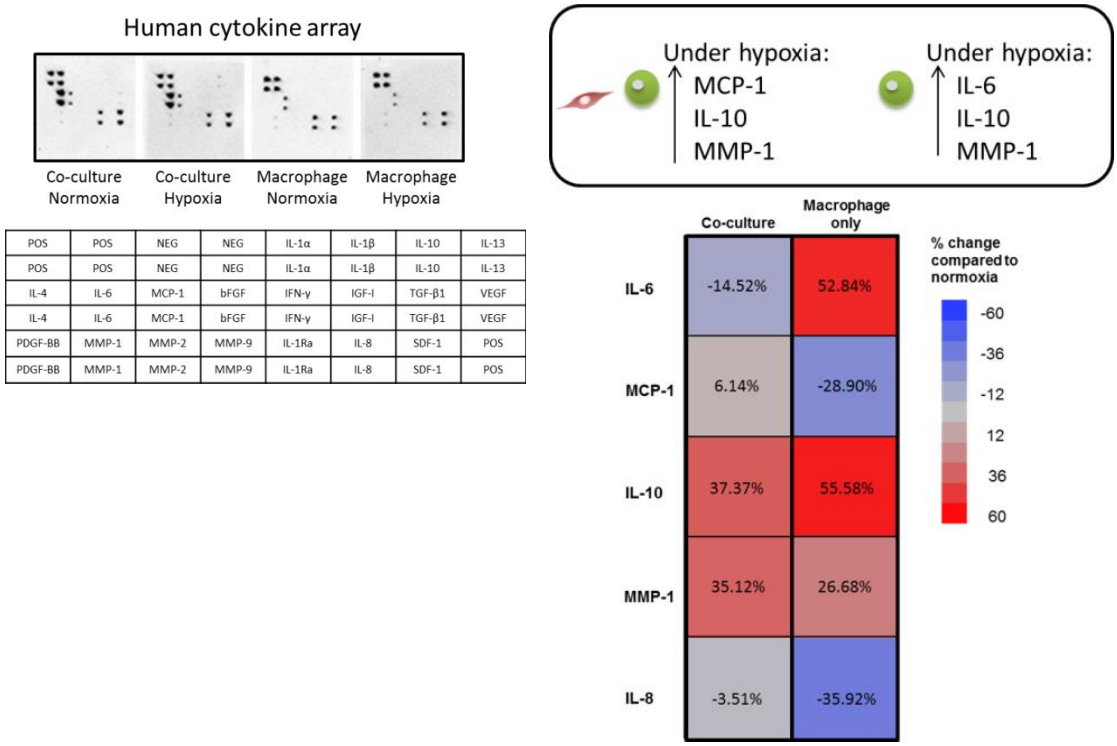

Figure 5.13: Effect of hypoxic culture (1% O_2) on secretion of various factors by co-cultured MSCs and macrophages or macrophages cultured alone, analyzed by human cytokine membrane array. Data is normalized to normoxic condition.

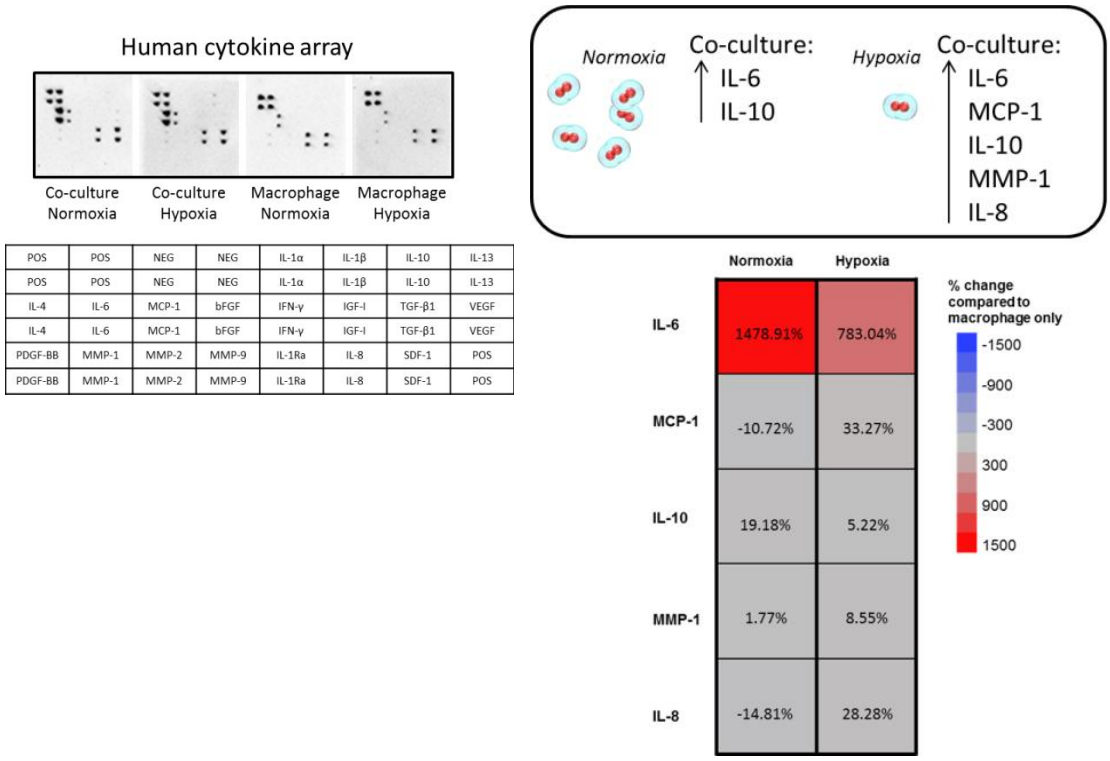

Figure 5.14: Effect of culture condition (co-cultured MSCs and macrophages or macrophages cultured alone) on secretion of various factors under normoxia or 1% hypoxia, analyzed by human cytokine membrane array. Data is normalized to macrophage only condition.

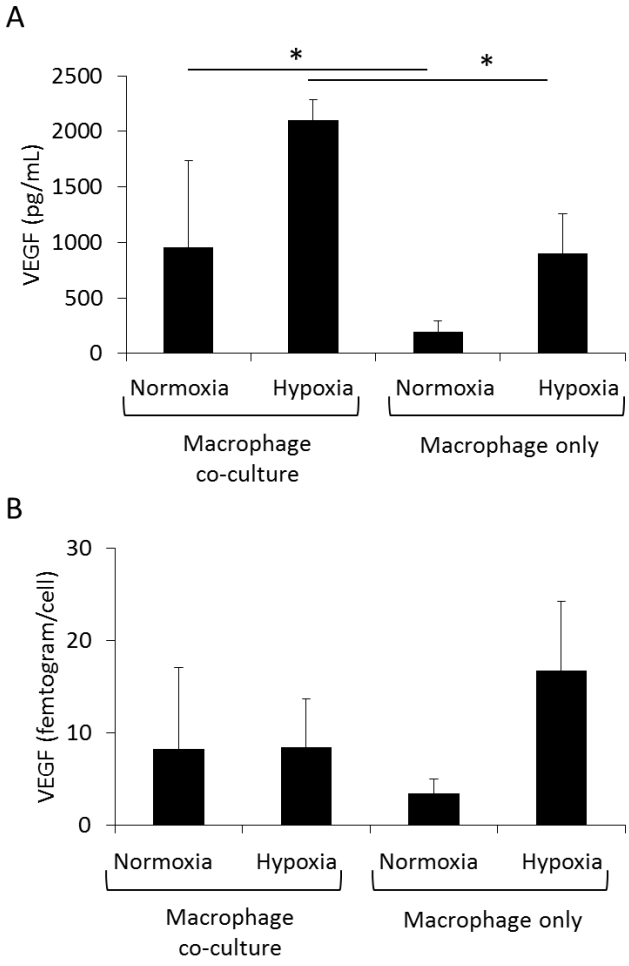

Figure 5.15: VEGF secretion of co-cultured MSCs and macrophages under 1% hypoxia. (* = $p<0.05$)

5.5 REFERENCES

1. Aranguren, X.L., McCue, J.D., Hendrickx, B., Zhu, X.H., Du, F., Chen, E., Pelacho, B., Penuelas, I., Abizanda, G., Uriz, M., Frommer, S.A., Ross, J.J., Schroeder, B.A., Seaborn, M.S., Adney, J.R., Hagenbrock, J., Harris, N.H., Zhang, Y., Zhang, X., Nelson-Holte, M.H., Jiang, Y., Billiau, A.D., Chen, W., Prosper, F., Verfaillie, C.M., Luttun, A. Multipotent adult progenitor cells sustain function of ischemic limbs in mice. *J Clin Invest* **118**, 505-514 (2008).

2. Ikenaga, S., Hamano, K., Nishida, M., Kobayashi, T., Li, T.S., Kobayashi, S., Matsuzaki, M., Zempo, N., Esato, K. Autologous bone marrow implantation induced angiogenesis and improved deteriorated exercise capacity in a rat ischemic hindlimb model. *The Journal of surgical research* **96**, 277-283 (2001).

3. Kinnaird, T., Stabile, E., Burnett, M.S., Epstein, S.E. Bone-marrow-derived cells for enhancing collateral development: mechanisms, animal data, and initial clinical experiences. *Circulation research* **95**, 354-363 (2004).

4. Kinnaird, T., Stabile, E., Burnett, M.S., Shou, M., Lee, C.W., Barr, S., Fuchs, S., Epstein, S.E. Local delivery of marrow-derived stromal cells augments collateral perfusion through paracrine mechanisms. *Circulation* **109**, 1543-1549 (2004).

5. Copland, I.B. Mesenchymal stromal cells for cardiovascular disease. *J Cardiovasc Dis Res* **2**, 3-13 (2011).

6. Appasani, K., Appasani, R.K. Stem cells & regenerative medicine : from molecular embryology to tissue engineering. (Humana Press, New York; 2011).

7. Lawall, H., Bramlage, P., Amann, B. Stem cell and progenitor cell therapy in peripheral artery disease. A critical appraisal. *Thromb Haemost* **103**, 696-709 (2010).

8. Grayson, W.L., Zhao, F., Izadpanah, R., Bunnell, B., Ma, T. Effects of hypoxia on human mesenchymal stem cell expansion and plasticity in 3D constructs. *Journal of cellular physiology* **207**, 331-339 (2006).

9. Hoffmann, J., Glassford, A.J., Doyle, T.C., Robbins, R.C., Schrepfer, S., Pelletier, M.P. Angiogenic effects despite limited cell survival of bone marrow-derived mesenchymal stem cells under ischemia. *The Thoracic and cardiovascular surgeon* **58**, 136-142 (2010).

10. Hu, X., Yu, S.P., Fraser, J.L., Lu, Z., Ogle, M.E., Wang, J.A., Wei, L. Transplantation of hypoxia-preconditioned mesenchymal stem cells improves infarcted heart function via enhanced survival of implanted cells and angiogenesis. *J Thorac Cardiov Sur* **135**, 799-808 (2008).

11. Muscari, C., Giordano, E., Bonafe, F., Govoni, M., Pasini, A., Guarnieri, C. Priming adult stem cells by hypoxic pretreatments for applications in regenerative medicine. *Journal of biomedical science* **20**, 63 (2013).

12. Yang, D., Wang, W., Li, L., Peng, Y., Chen, P., Huang, H., Guo, Y., Xia, X., Wang, Y., Wang, H., Wang, W.E., Zeng, C. The relative contribution of paracine effect versus direct differentiation on adipose-derived stem cell transplantation mediated cardiac repair. *PLoS One* **8**, e59020 (2013).

13. Das, R., Jahr, H., van Osch, G.J., Farrell, E. The role of hypoxia in bone marrow-derived mesenchymal stem cells: considerations for regenerative medicine approaches. *Tissue engineering. Part B, Reviews* **16**, 159-168 (2010).

14. Lonne, M., Lavrentieva, A., Walter, J.G., Kasper, C. Analysis of oxygen-dependent cytokine expression in human mesenchymal stem cells derived from umbilical cord. *Cell and tissue research* **353**, 117-122 (2013).

15. Dos Santos, F., Andrade, P.Z., Boura, J.S., Abecasis, M.M., da Silva, C.L., Cabral, J.M. Ex vivo expansion of human mesenchymal stem cells: a more effective cell proliferation kinetics and metabolism under hypoxia. *Journal of cellular physiology* **223**, 27-35 (2010).

16. Meirelles Lda, S., Fontes, A.M., Covas, D.T., Caplan, A.I. Mechanisms involved in the therapeutic properties of mesenchymal stem cells. *Cytokine & growth factor reviews* **20**, 419-427 (2009).

17. Chen, L., Xu, Y.B., Zhao, J.L., Zhang, Z.Q., Yang, R.H., Xie, J.L., Liu, X.S., Qi, S.H. Conditioned Medium from Hypoxic Bone Marrow-Derived Mesenchymal Stem Cells Enhances Wound Healing in Mice. *PLoS One* **9** (2014).

18. Chen, L., Tredget, E.E., Wu, P.Y., Wu, Y. Paracrine factors of mesenchymal stem cells recruit macrophages and endothelial lineage cells and enhance wound healing. *PLoS One* **3**, e1886 (2008).

19. Kim, J., Hematti, P. Mesenchymal stem cell-educated macrophages: a novel type of alternatively activated macrophages. *Exp Hematol* **37**, 1445-1453 (2009).

20. Chazaud, B., Brigitte, M., Yacoub-Youssef, H., Arnold, L., Gherardi, R., Sonnet, C., Lafuste, P., Chretien, F. Dual and beneficial roles of macrophages during skeletal muscle regeneration. *Exercise and sport sciences reviews* **37**, 18-22 (2009).

21. Kharraz, Y., Guerra, J., Mann, C.J., Serrano, A.L., Munoz-Canoves, P. Macrophage Plasticity and the Role of Inflammation in Skeletal Muscle Repair. *Mediators of Inflammation* (2013).

22. Novak, M.L., Koh, T.J. Phenotypic transitions of macrophages orchestrate tissue repair. *Am J Pathol* **183**, 1352-1363 (2013).

23. Mantovani, A., Sica, A., Sozzani, S., Allavena, P., Vecchi, A., Locati, M. The chemokine system in diverse forms of macrophage activation and polarization. *Trends in Immunology* **25**, 677-686 (2004).

24. Sunderkotter, C., Steinbrink, K., Goebeler, M., Bhardwaj, R., Sorg, C. Macrophages and angiogenesis. *J Leukoc Biol* **55**, 410-422 (1994).

25. Ploeger, D.T., Hosper, N.A., Schipper, M., Koerts, J.A., de Rond, S., Bank, R.A. Cell plasticity in wound healing: paracrine factors of M1/ M2 polarized macrophages influence the phenotypical state of dermal fibroblasts. *Cell communication and signaling : CCS* **11**, 29 (2013).

26. Mahdavian Delavary, B., van der Veer, W.M., van Egmond, M., Niessen, F.B., Beelen, R.H. Macrophages in skin injury and repair. *Immunobiology* **216**, 753-762 (2011).

27. Tidball, J.G. Inflammatory processes in muscle injury and repair. *American journal of physiology. Regulatory, integrative and comparative physiology* **288**, R345-353 (2005).

28. Arnold, L., Henry, A., Poron, F., Baba-Amer, Y., van Rooijen, N., Plonquet, A., Gherardi, R.K., Chazaud, B. Inflammatory monocytes recruited after skeletal muscle injury switch into antiinflammatory macrophages to support myogenesis. *The Journal of experimental medicine* **204**, 1057-1069 (2007).

29. Swirski, F.K., Nahrendorf, M. Macrophage-stem cell crosstalk after myocardial infarction. *J Am Coll Cardiol* **62**, 1902-1904 (2013).

30. Spiller, K.L., Anfang, R.R., Spiller, K.J., Ng, J., Nakazawa, K.R., Daulton, J.W., Vunjak-Noyakovic, G. The role of macrophage phenotype in vascularization of tissue engineering scaffolds. *Biomaterials* **35**, 4477-4488 (2014).

31. Mosser, D.M., Edwards, J.P. Exploring the full spectrum of macrophage activation. *Nature Reviews Immunology* **8**, 958-969 (2008).

32. Gordon, S. Alternative activation of macrophages. *Nature Reviews Immunology* **3**, 23-35 (2003).

33. Murray, P.J., Wynn, T.A. Protective and pathogenic functions of macrophage subsets. *Nature Reviews Immunology* **11**, 723-737 (2011).

34. Ben-Mordechai, T., Holbova, R., Landa-Rouben, N., Harel-Adar, T., Feinberg, M.S., Abd Elrahman, I., Blum, G., Epstein, F.H., Silman, Z., Cohen, S., Leor, J. Macrophage Subpopulations Are Essential for Infarct Repair With and Without Stem Cell Therapy. *J Am Coll Cardiol* **62**, 1890-1901 (2013).

35. Yu, J., Yin, S., Zhang, W., Gao, F., Liu, Y., Chen, Z., Zhang, M., He, J., Zheng, S. Hypoxia preconditioned bone marrow mesenchymal stem cells promote liver regeneration in a rat massive hepatectomy model. *Stem cell research & therapy* **4**, 83 (2013).

36. Ivanovic, Z. Hypoxia or in situ normoxia: The stem cell paradigm. *Journal of cellular physiology* **219**, 271-275 (2009).

37. Carrancio, S., Lopez-Holgado, N., Sanchez-Guijo, F.M., Villaron, E., Barbado, V., Tabera, S., Diez-Campelo, M., Blanco, J., San Miguel, J.F., Del Canizo, M.C. Optimization of mesenchymal stem cell expansion procedures by cell separation and culture conditions modification. *Exp Hematol* **36**, 1014-1021 (2008).

38. D'Ippolito, G., Diabira, S., Howard, G.A., Roos, B.A., Schiller, P.C. Low oxygen tension inhibits osteogenic differentiation and enhances stemness of human MIAMI cells. *Bone* **39**, 513-522 (2006).

39. Ren, H., Cao, Y., Zhao, Q., Li, J., Zhou, C., Liao, L., Jia, M., Cai, H., Han, Z.C., Yang, R., Chen, G., Zhao, R.C. Proliferation and differentiation of bone marrow stromal cells under hypoxic conditions. *Biochemical and biophysical research communications* **347**, 12-21 (2006).

40. Tsai, C.C., Chen, Y.J., Yew, T.L., Chen, L.L., Wang, J.Y., Chiu, C.H., Hung, S.C. Hypoxia inhibits senescence and maintains mesenchymal stem cell properties through down-regulation of E2A-p21 by HIF-TWIST. *Blood* **117**, 459-469 (2011).

41. Charbord, P., Lerat, H., Newton, I., Tamayo, E., Gown, A.M., Singer, J.W., Herve, P. The cytoskeleton of stromal cells from human bone marrow cultures resembles that of cultured smooth muscle cells. *Exp Hematol* **18**, 276-282 (1990).

42. Kinner, B., Zaleskas, J.M., Spector, M. Regulation of smooth muscle actin expression and contraction in adult human mesenchymal stem cells. *Experimental cell research* **278**, 72-83 (2002).

43. Martinez, F.O., Gordon, S., Locati, M., Mantovani, A. Transcriptional profiling of the human monocyte-to-macrophage differentiation and polarization: New molecules and patterns of gene expression. *J Immunol* **177**, 7303-7311 (2006).

44. Eggenhofer, E., Hoogduijn, M.J. Mesenchymal stem cell-educated macrophages. *Transplantation research* **1**, 12 (2012).

45. Anton, K., Banerjee, D., Glod, J. Macrophage-associated mesenchymal stem cells assume an activated, migratory, pro-inflammatory phenotype with increased IL-6 and CXCL10 secretion. *PLoS One* **7**, e35036 (2012).

46. Gallucci, R.M., Simeonova, P.P., Matheson, J.M., Kommineni, C., Guriel, J.L., Sugawara, T., Luster, M.I. Impaired cutaneous wound healing in interleukin-6-deficient and immunosuppressed mice. *Faseb J* **14**, 2525-2531 (2000).

47. Engelhardt, E., Toksoy, A., Goebeler, M., Debus, S., Brocker, E.B., Gillitzer, R. Chemokines IL-8, GROalpha, MCP-1, IP-10, and Mig are sequentially and differentially expressed during phase-specific infiltration of leukocyte subsets in human wound healing. *Am J Pathol* **153**, 1849-1860 (1998).

48. Hung, S.C., Pochampally, R.R., Chen, S.C., Hsu, S.C., Prockop, D.J. Angiogenic effects of human multipotent stromal cell conditioned medium activate the PI3K-Akt pathway in hypoxic endothelial cells to inhibit apoptosis, increase survival, and stimulate angiogenesis. *Stem Cells* **25**, 2363-2370 (2007).

49. Zwezdaryk, K.J., Coffelt, S.B., Figueroa, Y.G., Liu, J., Phinney, D.G., LaMarca, H.L., Florez, L., Morris, C.B., Hoyle, G.W., Scandurro, A.B. Erythropoietin, a hypoxia-regulated factor, elicits a pro-angiogenic program in human mesenchymal stem cells. *Exp Hematol* **35**, 640-652 (2007).

50. Potier, E., Ferreira, E., Andriamanalijaona, R., Pujol, J.P., Oudina, K., Logeart-Avramoglou, D., Petite, H. Hypoxia affects mesenchymal stromal cell osteogenic differentiation and angiogenic factor expression. *Bone* **40**, 1078-1087 (2007).

51. Crisostomo, P.R., Wang, Y., Markel, T.A., Wang, M., Lahm, T., Meldrum, D.R. Human mesenchymal stem cells stimulated by TNF-alpha, LPS, or hypoxia produce growth factors by an NF kappa B- but not JNK-dependent mechanism. *Am J Physiol Cell Physiol* **294**, C675-682 (2008).

52. Razban, V., Lotfi, A.S., Soleimani, M., Ahmadi, H., Massumi, M., Khajeh, S., Ghaedi, M., Arjmand, S., Najavand, S., Khoshdel, A. HIF-1alpha Overexpression Induces Angiogenesis in Mesenchymal Stem Cells. *Biores Open Access* **1**, 174-183 (2012).

53. Beckermann, B.M., Kallifatidis, G., Groth, A., Frommhold, D., Apel, A., Mattern, J., Salnikov, A.V., Moldenhauer, G., Wagner, W., Diehlmann, A., Saffrich, R., Schubert, M., Ho, A.D., Giese, N., Buchler, M.W., Friess, H., Buchler, P., Herr, I. VEGF expression by mesenchymal stem cells contributes to angiogenesis in pancreatic carcinoma. *Br J Cancer* **99**, 622-631 (2008).

54. Comalada, M., Xaus, J., Sanchez, E., Valledor, A.F., Celada, A. Macrophage colony-stimulating factor-, granulocyte-macrophage colony-stimulating factor-, or IL-3-dependent survival of macrophages, but not proliferation, requires the expression of p21(Waf1) through the phosphatidylinositol 3-kinase/Akt pathway. *European Journal of Immunology* **34**, 2257-2267 (2004).

55. Zhang, L., Wang, Y., Xiao, F., Wang, S., Xing, G., Li, Y., Yin, X., Lu, K., Wei, R., Fan, J., Chen, Y., Li, T., Xie, P., Yuan, L., Song, L., Ma, L., Ding, L., He, F. CKIP-1 regulates macrophage proliferation by inhibiting TRAF6-mediated Akt activation. *Cell research* **24**, 742-761 (2014).

56. Otero, K., Turnbull, I.R., Poliani, P.L., Vermi, W., Cerutti, E., Aoshi, T., Tassi, I., Takai, T., Stanley, S.L., Miller, M., Shaw, A.S., Colonna, M. Macrophage colony-stimulating factor induces the proliferation and survival of macrophages via a pathway involving DAP12 and beta-catenin. *Nature Immunology* **10**, 734-743 (2009).

57. Lewis, J.S., Lee, J.A., Underwood, J.C., Harris, A.L., Lewis, C.E. Macrophage responses to hypoxia: relevance to disease mechanisms. *J Leukoc Biol* **66**, 889-900 (1999).

58. Murdoch, C., Muthana, M., Lewis, C.E. Hypoxia regulates macrophage functions in inflammation. *J Immunol* **175**, 6257-6263 (2005).

59. Rahat, M.A., Bitterman, H., Lahat, N. Molecular mechanisms regulating macrophage response to hypoxia. *Front Immunol* **2**, 45 (2011).

60. Albina, J.E., Henry, W.L., Jr., Mastrofrancesco, B., Martin, B.A., Reichner, J.S. Macrophage activation by culture in an anoxic environment. *J Immunol* **155**, 4391-4396 (1995).

61. Duffield, J.S. The inflammatory macrophage: a story of Jekyll and Hyde. *Clin Sci (Lond)* **104**, 27-38 (2003).

62. Lin, Z.Q., Kondo, T., Ishida, Y., Takayasu, T., Mukaida, N. Essential involvement of IL-6 in the skin wound-healing process as evidenced by delayed wound healing in IL-6-deficient mice. *J Leukoc Biol* **73**, 713-721 (2003).

63. Xing, Z., Gauldie, J., Cox, G., Baumann, H., Jordana, M., Lei, X.F., Achong, M.K. IL-6 is an antiinflammatory cytokine required for controlling local or systemic acute inflammatory responses. *J Clin Invest* **101**, 311-320 (1998).

Chapter 6: Therapeutic contribution of mesenchymal stem cells following an ischemic injury

6.1 INTRODUCTION

Peripheral artery disease (PAD) is a growing health concern in the United States, with 8-10 million people being affected by the disease.[1] Intermittent claudication is an early, moderate manifestation of the disease and is characterized by leg pain and muscle weakness.[1,2] However, PAD can quickly develop into critical limb ischemia, which is a more chronic and severe problem.[1,2] Critical limb ischemia often results in tissue infection, death, and potentially amputation because the resting metabolic needs of the tissue are not met by the available blood supply.[1,2] Although current revascularization therapies (including bypass surgery and balloon angioplasty) may provide some benefit to patients, not all patients are eligible for such procedures.[1-4] Major limb amputation is often necessary if revascularization therapy is not possible, or was not successful.[3,4]

Many have investigated the use of angiogenic gene and protein therapy as an alternative revascularization strategy.[2,5,6] Although gene and protein strategies have shown some success in preclinical animal models, there have not been significant improvements in clinical studies.[5,6] This could potentially be attributed to the fact that the ischemic wound healing response is very complex, and thus delivering the correct genes/proteins is very difficult,[5,6] especially when taking into account necessary temporal release kinetics and concentration gradients. As a result, cell-based approaches are an attractive therapy option because the cells can supply the necessary cytokines and growth factors necessary to promote, as well as support, vascular regeneration.[2] In addition, the use of multipotent stem cells, such as bone marrow-derived mesenchymal stem cells

(MSCs), could provide the advantage of replacing compromised tissue in addition to generating blood vessels.[2]

This study evaluated the use of bone marrow-derived mesenchymal stem cells as a therapy for peripheral arterial disease. A rat model of acute hind limb ischemia was used in which the femoral artery was ligated and excised. MSCs were intramuscularly delivered within a PEGylated fibrin biomatrix following ischemia. The PEGylated fibrin delivery system offers many advantages, including retaining MSCs at the delivery site. In addition, fibrin is a natural component of the wound healing response and has been demonstrated to have angiogenic properties.[7,8] To evaluate the therapeutic contribution, restoration of blood flow and muscle function were evaluated. Histological analysis was also performed to evaluate tissue architecture and blood vessel formation. The results of this study have important implications pertaining to alternative cell-based therapies for ischemic and cardiovascular diseases.

6.2. MATERIALS AND METHODS

6.2.1 Ischemic injury

Animal handling and care followed the recommendations of the National Institutes of Health (NIH) guidelines for the care and use of laboratory animals. All protocols were approved by the Animal Care Committee at the University of Texas at Austin. Lewis rats (11 weeks) weighing 250-300 g were used. To induce hind limb ischemia, femoral artery ligation in Lewis rats (11 weeks, male) was performed. Rats were anesthetized using isoflurane (0.5-2%) infused with oxygen (2 L/min). Through a small incision on the medial side of the thigh, the femoral artery of a single hind limb was separated from the nearby nerve and vein and ligated immediately distal to the inferior epigastric artery and proximal to the branch point of the popliteal and saphenous arteries

using Prolene 5-0 sutures (Figure 6.1). The ligated segment (~0.5 cm) was then excised and the skin incision closed with interrupted sutures. The animal was allowed to recover overnight and the following day (about 24 hours later) therapy was delivered.

6.2.2 Syringe viability study

Cell viability following injection within PEGylated fibrin gels was evaluated using a LIVE/DEAD stain. PEGylated fibrin injections were prepared by combining difunctional succinimidyl glutarate PEG (4 mg/mL in PBS without calcium; NOF America) with fibrinogen (40 mg/mL in PBS without calcium; Sigma) in a 1:1 volume ratio. An equal volume of rat MSCs (passage 5) was mixed with the PEGylated fibrin solution in a 1:1 volume ratio at a concentration of $2x10^5$ cells/mL. The solution was then loaded into a 23G needle syringe, followed by an equal volume of thrombin (25 U/mL in 40 mM $CaCl_2$). The solution was mixed thoroughly within the syringe and the gel solution (500 μL) was injected into a 24 well plate. The final concentrations in the gel were 5 mg/mL of fibrinogen; 0.5 mg/mL of SG-PEG-SG; $5x10^5$ cells/mL; and 12.5 U/mL of thrombin. A gel which was formed in the well plate and not injected through a syringe was used as a positive control. The gels were stored at 37ºC in MSC growth media. Twenty four hours following the injection, the cells were stained with a LIVE/DEAD stain to assess cell viability. Briefly, the media was removed and the gels were washed with PBS for 15 minutes. The PBS washes were repeated for a total of 90 minutes. The gels were then incubated in a LIVE/DEAD stain solution consisting of 10 μM calcein and 10 μM ethidium homodimer for 1 hour at 37ºC. The stain was removed and the gels were washed with PBS, fixed in 10% formalin for 20 minutes, washed with PBS, and imaged on a Leica DMI2000B microscope equipped with a Leica DFC290

camera. Gels incubated with methanol prior to staining were used as a dead control condition.

6.2.3 PEGylated fibrin gel delivery of MSCs

MSCs were injected intramuscularly into the gastrocnemius muscle of the ligated limb. PEGylated fibrin injections were prepared by combining difunctional succinimidyl glutarate PEG (4 mg/mL in PBS without calcium; NOF America) with fibrinogen (40 mg/mL in PBS without calcium; Sigma) in a 1:1 volume ratio. An equal volume of MSCs was mixed with the PEGylated fibrin solution in a 1:1 volume ratio at a concentration of $13x10^6$ cells/mL. The solution was then loaded into a 23G needle syringe, followed by an equal volume of thrombin (25 U/mL in 40 mM $CaCl_2$). The solution was mixed thoroughly within the syringe and the gel solution (300 μL) was injected into the gastrocnemius of the rat. The final concentrations in the gel were 5 mg/mL of fibrinogen; 0.5 mg/mL of SG-PEG-SG; $3.33x10^6$ cells/mL; and 12.5 U/mL of thrombin. Other treatment groups consisted of no treatment, PEGylated fibrin gel, and MSCs. For the PEGylated fibrin gel treatment, 300 μL of PEGylated fibrin gel was injected into the lateral gastrocnemius muscle, with the cell portion replaced by 10% FBS containing DMEM. For the MSC treatment, 300 μL of MSCs ($3.33x10^6$ cells/mL) suspended in 10% FBS containing DMEM was injected into the lateral gastrocnemius muscle. Prior to delivery, MSCs were fluorescently labeled with CellTracker™ CM-DiI (Invitrogen). The cells were incubated with CM-DiI (15 μM) at 37ºC for 8 minutes and then 4ºC for 15 minutes, washed with PBS, and resuspended in DMEM.

6.2.4 Blood flow measurements

Thermal infrared imaging was performed to evaluate blood flow to the ischemic hind limbs. Rats were anesthetized using isoflurane (0.5-2%) infused with oxygen (2

L/min) and imaged with an FLIR A325sc camera. The rats were put in the prone position, with the dorsal side up and the ventral side down. The hind limbs were imaged for a total of 3 minutes, acquiring a total of 180 frames. The images were acquired and processed using FLIR ExaminIR. The difference between the average temperature of the ischemic and control contralateral limb were used for quantification.

6.2.5 Force production measurements

Force production measurements of the lateral gastrocnemius muscle were conducted on all treatment groups with sample size of 5. The gastrocnemius muscle was surgically isolated from the surrounding tissue and innervation to the medial gastrocnemius muscle was removed. The Achilles tendon was secured to the lever arm of a dual-mode servomotor (Aurora Scientific Model 310B). The muscle was stimulated using a stimulator (A-M Systems Model 2100) with electrodes applied to the tibial nerve. The optimal length, or the length which produced the maximal twitch force, was determined by stimulating the muscle at 0.5 Hz. The maximal peak tetanic tension was measured by stimulating the muscle at the optimal length at a frequency of 150 Hz and the minimal voltage required to elicit a maximal response. Between each contraction there was a 2 minute period of rest. The temperature of the muscle was maintained with a heating lamp throughout the duration of the study. At the end of the study, the animal was sacrificed and the lateral gastrocnemius muscle was isolated. The muscle mass and muscle length were measured in order to calculate the cross sectional area (Equation 1), where Q is the fiber angle from the mid-line (19º). The fiber length is calculated by multiplying the muscle length by 0.38 (fiber length/muscle length ratio for the gastrocnemius), and the density of skeletal muscle is 1.056 g/cm^3. The specific tension

was calculated using Equation 2. The specific tension was normalized to the contralateral control (% of contralateral control).

$$Cross\ sectional\ area = \frac{muscle\ mass\ (mg) * \cos Q}{fiber\ length\ (mm) * density\ (\frac{g}{cm^3})} \quad (1)$$

$$Specific\ tension = \frac{maximal\ peak\ tetanic\ tension\ (N)}{cross\ sectional\ area\ (cm^2)} \quad (2)$$

6.2.6 Histology

At the terminal endpoint of the study, animals were sacrificed and the gastrocnemius muscles were isolated, embedded in optimal cutting temperature (OCT) compound, submerged in liquid nitrogen-cooled isopentane, and stored at -80ºC until further processing. The samples were cut into 12 µm thick sections using a cryostat and placed onto positively charged microscope slides. The tissue sections were fixed in 10% formalin for 15 minutes. Hematoxylin and eosin (H&E) and imunohistochemical staining were subsequently performed.

For H&E staining, the slides were fixed in 10% formalin for 15 minutes, followed by rinsing with PBS. The sections were then incubated in Mayer's hematoxylin solution (Electron Microscopy Sciences) for 15 minutes and rinsed in running tap water for 15 minutes. The sections were then dipped in Scott's bluing solution for 30 seconds, rinsed in distilled water for 30 seconds, and incubated in 95% ethanol for 30 seconds. The samples were then transferred into Eosin Y solution (Sigma-Aldrich) for 1 minute followed by serial washes in 95% ethanol, 100% ethanol, and xylene for 2 minutes each. The slides were then mounted with Cytoseal Mounting Media (Thermo Scientific) and viewed with a DMI2000B Leica microscope.

For immunohistochemistry, the slides were fixed in 10% formalin for 15 minutes, followed by rinsing with PBS. The sections were then incubated in 0.125% trypsin solution for 20 minutes at 37ºC. They were then incubated in 0.3% hydrogen peroxide solution for 5 minutes, permeabilized in 0.5% Triton X-100 in TBST for 30 minutes, and blocked in 2.5% horse serum for 1 hour. The slides were incubated overnight at 4ºC in the primary antibody (1:100 dilution in 2.5% horse serum) (SMA; Abcam). Following overnight incubation, the sections were incubated with ImmPRESS (rat absorbed mouse IgG) solution (Vector Laboratories) for 30 minutes and then ImmPACT DAB peroxidase substrate (Vector Laboratories) for 5 minutes. The sections were counterstained with hematoxylin QS (Vector Laboratories), rinsed with running tap water, incubated in serial concentration of ethanol (95% and 100%) and xylene for 2 minutes each, and mounted. The SMA positive area and the number of SMA positive vessels were quantified using ImageJ.

6.2.7 Statistical analysis

All test groups consisted of a sample number of 5. Statistical analysis was performed using student t-tests with a p value of 0.05.

6.3 RESULTS AND DISCUSSION

6.3.1 Assessment of MSC viability following syringe injection

The *in vivo* delivery of the stem cells via syringe injection was evaluated to determine if this delivery method was feasible and did not damage MSCs. It has been demonstrated that MSCs can survive and maintain phenotypic and functional characteristics following passage through a needle as small as 26G.[9] In addition, the encapsulation of MSCs within a hydrogel system, such as PEGylated fibrin, may serve as a protective barrier to minimize cell death as a result of delivery via syringe injection.[10]

Cell viability following injection within PEGylated fibrin gel was evaluated *in vitro* using a LIVE/DEAD stain. Stem cells which were passed through a 23G needle did not undergo cell death, as demonstrated by the large extent of viable cells (Figure 6.2). Control conditions consisted of cells encapsulated within a PEGylated fibrin gel which had not been passed through a syringe, and a dead control for staining purposes.

6.3.2 Perfusion of ischemic tissue

Quantification of blood vessel formation in the treatment groups was performed using smooth muscle actin (SMA) staining (Figure 6.3). Quantification of the SMA positive area showed no differences between treatment groups on day 7, but significantly enhanced blood vessel formation for the PEGylated fibrin gel and MSCs + PEGylated fibrin gel groups on day 14. Quantification of the total number of SMA positive vessels produced similar results, with significantly enhanced blood vessel formation for the PEGylated fibrin gel on day 14 and MSCs + PEGylated fibrin gel group on days 7 and 14. Fibrin has a high affinity for various growth factors and cytokines (including pro-angiogenic factors such as VEGF,[11] IGF,[12] and TGF-β[13]) and supports angiogenesis and tissue repair.[14] This could account for the enhanced blood vessel formation in the PEGylated fibrin gel treatment group.

Reperfusion of the ischemic hind limb was indirectly evaluated using thermal infrared imaging and calculating the temperature difference between the ischemic limb and contralateral control. Thermal infrared imaging has been demonstrated to be an accurate tool to assess circulatory changes and thus reperfusion of ischemic tissue.[15,16] On day 14 there were significant improvements in reperfusion of the ischemic hind limb for the PEGylated fibrin gel and MSCs + PEGylated fibrin gel treatment groups (Figure 6.4).

6.3.3 Functional recovery of ischemic tissue

In order to evaluate the localization and distribution of MSCs following injection, the cells were fluorescently labeled prior to delivery. Figure 6.5 shows the distribution of the cells for the MSC and MSC + PEGylated fibrin gel groups at day 7 and day 14. The cells are distributed throughout the muscle fibers and are present until day 14. However, as evidenced in Figure 4.13B, a majority of the cells are most likely no longer viable, especially at day 14.

Tissue necrosis is typically evaluated histologically by the presence of multi-cellular infiltrates and muscle fibers which are inhomogeneous in size, hypereosinophilic, and devoid of nuclei.[17] Histological analysis of all treatment groups on day 7 and day 14 showed no evidence of inflammation or necrosis, even for the no treatment group (Figure 6.6). This lack of tissue damage is likely due to the fact that the rat underused the ligated limb following surgery and also that collateral flow was sufficient to provide blood to the tissue, especially at later time points.[18-20] Subjecting the rats to more physical activity following surgery has been shown to exacerbate the adverse effects of ischemia because of impaired limb blood flow capacity with stress,[21] with enhanced capillary endothelial swelling and white blood cell activation.[18,22] Along the same lines, reperfusion of ischemic tissue results in oxidative stress caused by the generation of reactive oxygen species, resulting in extensive tissue damage.[12,23-25]

Functional recovery of the ischemic tissue was evaluated using force production measurements (Figure 6.7). Functional assessments (quantified as the % of contralateral control) at day 7 showed a significant improvement in specific tension ($p<0.05$) for the MSC (81.03 ± 6.35%) treatment group compared to no treatment (66.50 ± 3.10%). The MSC + PEGylated fibrin gel treatment group had an average specific tension of 76.63 ± 15.26%, which was not a significant improvement compared to the no treatment group.

Day 14 measurements showed significant improvement in specific tension ($p<0.05$) for MSCs + PEGylated fibrin gel (91.26 ± 4.06%) compared to no treatment (67.11 ± 9.40%). MSC and PEGylated fibrin gel treatment groups did not have significant improvements in force production, with specific tension values of 71.74 ± 9.21% and 68.12 ± 6.23%, respectively. We hypothesize that the MSC + PEGylated fibrin gel group led to significant improvements in force production because the MSCs are contributing to functional recovery and restoration of the ischemic tissue. However, the PEGylated fibrin gel microenvironment appears to modulate the MSCs, as the MSC only treatment group did not have significant improvements in force production at day 14. The gel assists in retaining the MSCs at the delivery site, allowing the cells to contribute to skeletal muscle regeneration either through differentiation or paracrine effects. In addition, the gel could be acting as a depot to collect cytokines and growth factors, either released endogenously or from the delivered MSCs. This in turn could impart autocrine and paracrine effects on the MSCs and surrounding cells. Also, the hypoxic microenvironment of the ischemic tissue and the PEGylated fibrin gel could be modulating stem cell function, as outlined in Chapter 5. In particular, the interaction of MSCs with infiltrating macrophages could modulate macrophage function, inducing changes in macrophage phenotype necessary for skeletal muscle regeneration.[26-29]

Interestingly, although the ischemia model investigated here did not appear to result in any damage when evaluated histologically (such as cell infiltration and necrosis), functional deficits still occurred. Others have seen functional deficits in hind limb ischemia models using femoral artery ligation with no corresponding histological evidence of inflammatory cell infiltration, fibrosis, or edema.[18,30-32] The results presented here are in agreement with these other studies, in which consistent, moderate ischemia is

associated with less severe inflammation and necrosis compared to acute, severe ischemia.[18,30-32]

6.4 CONCLUSIONS

This study investigated the use of mesenchymal stem cell therapy for ischemic injury. MSCs delivered within a PEGylated fibrin gel contributed to significant improvements in blood vessel formation and blood flow, as well as functional recovery of the ischemic limb, on day 14. None of the other treatment groups (MSCs or PEGylated fibrin gel) exhibited such significant improvements. Thus, the results demonstrate that MSCs delivered in combination with PEGylated fibrin gel is a promising therapy for treatment of ischemic diseases. This therapeutic mechanism could be attributed to the stem cells themselves, which secrete pro-angiogenic factors and recruit other cell types for wound healing, as well as the gel microenvironment. The recruitment and interaction with macrophages could also potentially be a contributing factor, as macrophages have been found to participate in angiogenesis and wound healing and to accumulate around growing collaterals.[33-35] Not only will the gel alter the microenvironment for the delivered stem cells, but it also acts as a depot for released cytokines and growth factors and is a natural component of the wound healing response.

While this model of hind limb ischemia did not result in tissue necrosis, as assessed histologically, functional deficits still occurred. It has been demonstrated that the severity of ischemic injury, and the extent of arteriogenesis, is dependent upon the species and strain of the animal used.[17,36] Thus, future studies could implement a more severe ischemia model, potentially using a disease animal model which is more representative of the patient population suffering from peripheral artery disease.

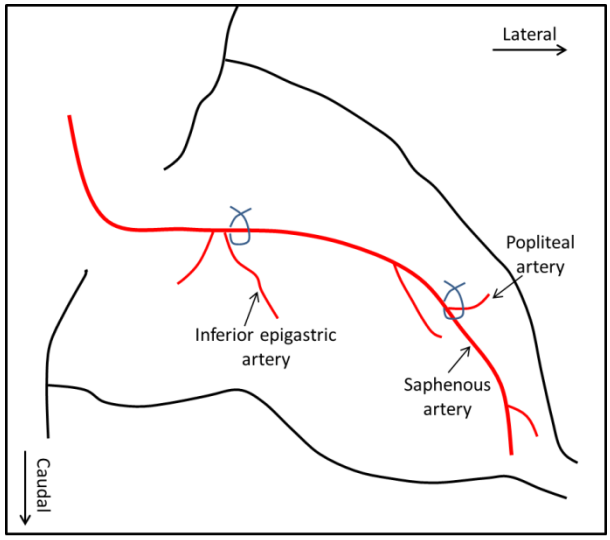

Figure 6.1: Schematic illustrating the sites of ligation immediately distal to the inferior epigastric artery and proximal to the branch point of the popliteal and saphenous arteries.

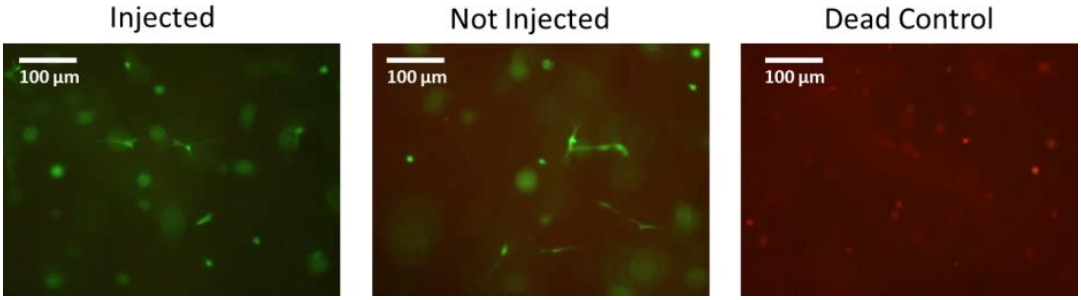

Figure 6.2: *In vitro* MSC viability following injection within a PEGylated fibrin gel. Scale bar = 100 µm.

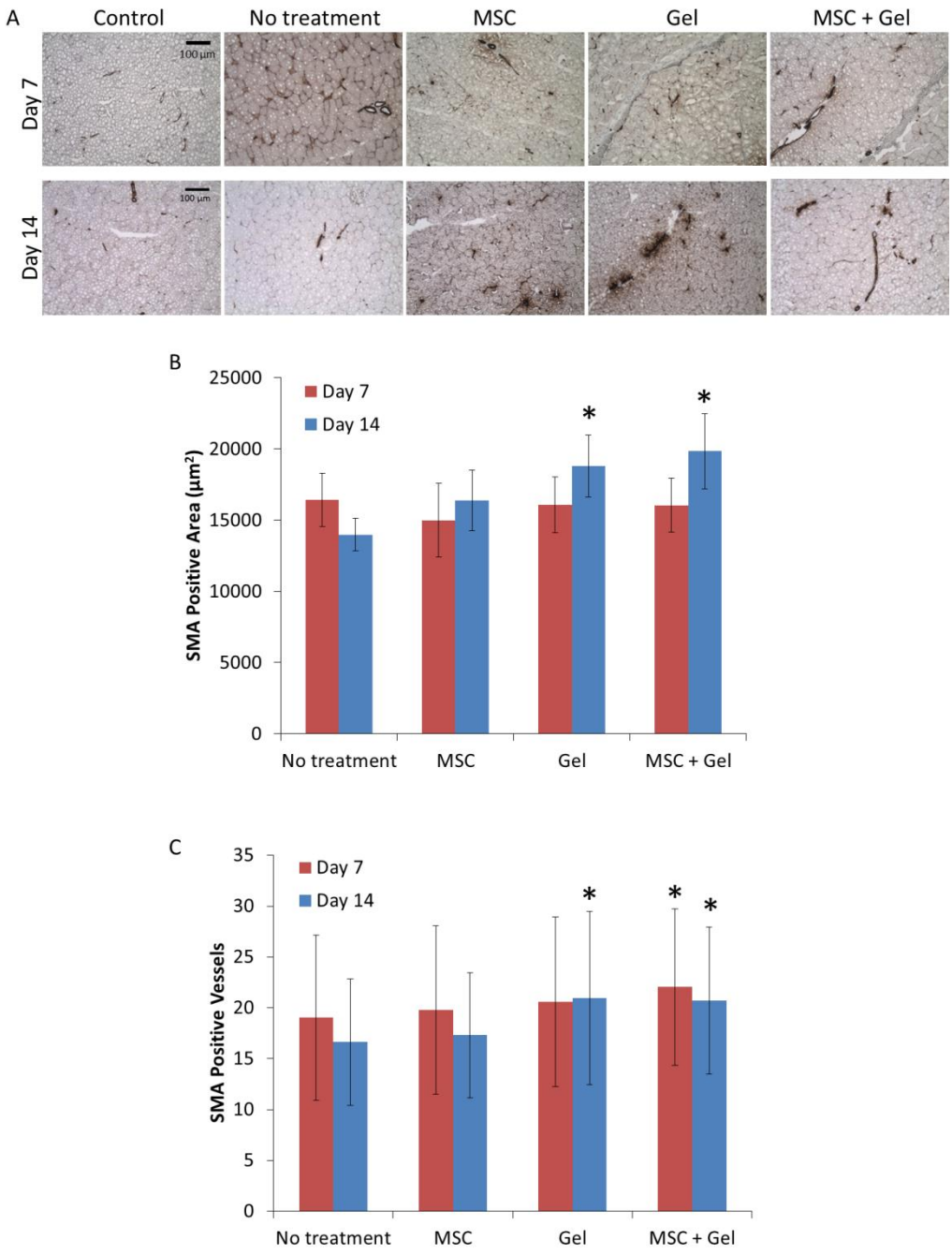

Figure 6.3: (A) Smooth muscle actin (SMA) staining of ischemic muscles with various treatments, and contralateral control, at day 7 and 14. Quantification of (B) SMA positive area and (C) the number of SMA positive vessels. (* = $p<0.05$ compared to no treatment)

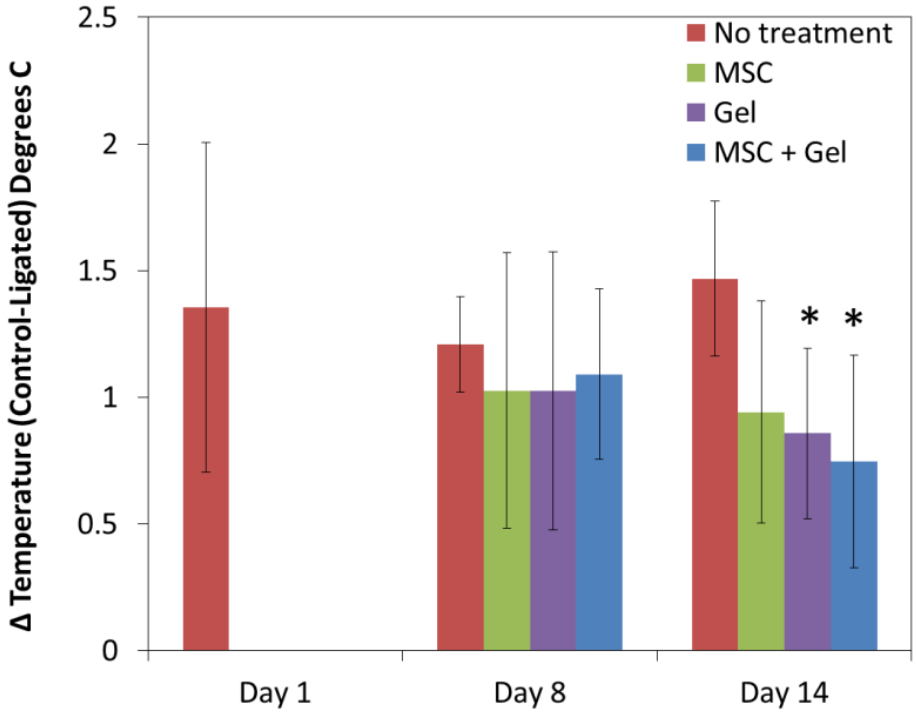

Figure 6.4: Evaluation of blood flow to ischemic hind limbs using thermal infrared imaging. (* = $p<0.05$ compared to no treatment)

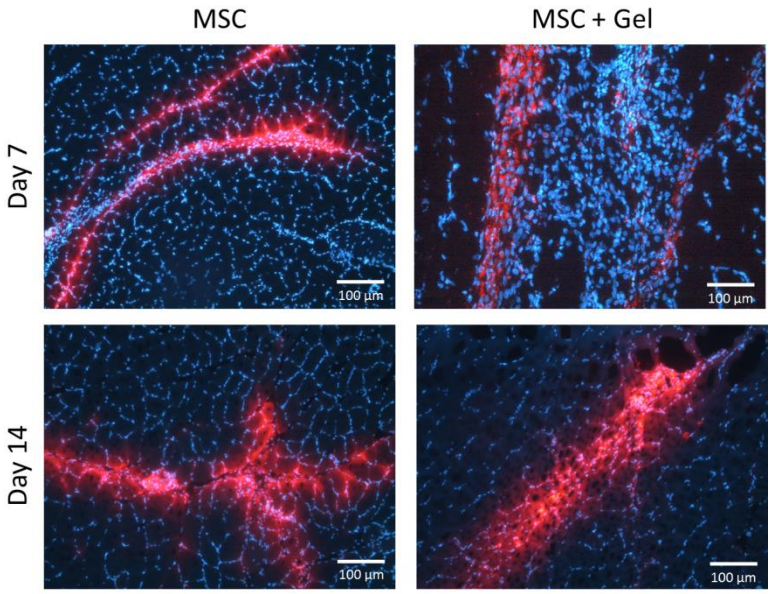

Figure 6.5: MSC localization and distribution within the muscle following injection for MSC and MSC + PEGylated fibrin gel groups on days 7 and 14. MSCs are shown in red (CM-DiI) and cell nuclei are shown in blue (DAPI). Scale bar = 100 µm.

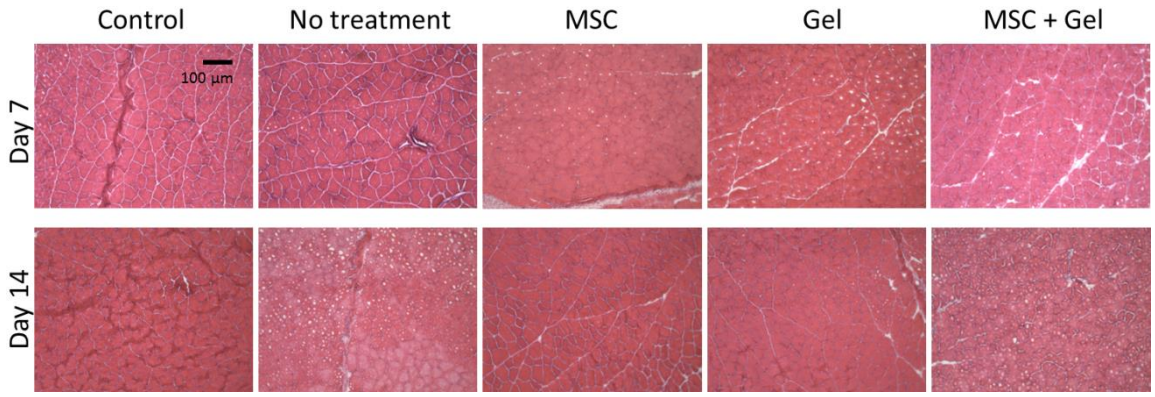

Figure 6.6: Hematoxylin and eosin staining of ischemic muscles with various treatments, and contralateral control, at day 7 and 14. Scale bar = 100 µm.

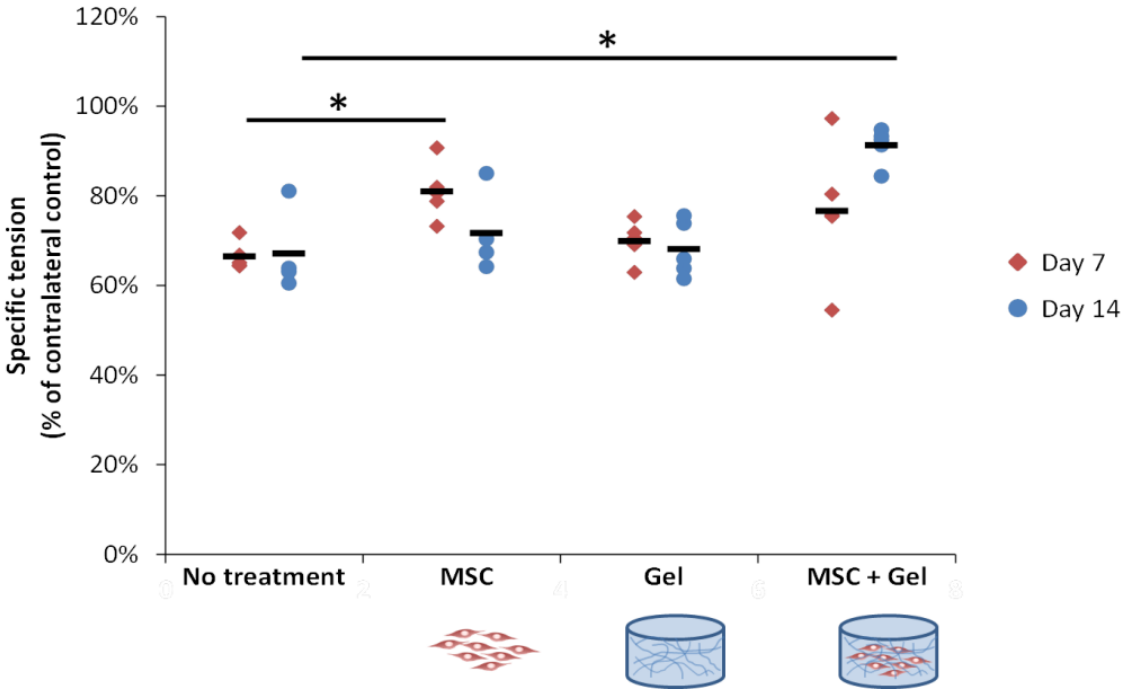

Figure 6.7: Maximum force production measurements of the lateral gastrocnemius 7 and 14 days following treatment. Black lines indicate mean values for each treatment group. (* = $p<0.05$ compared to no treatment)

6.5 REFERENCES

1. Creager, M.A. Medical management of peripheral arterial disease. Cardiol Rev 9, 238-245 (2001).

2. Aranguren, X.L., McCue, J.D., Hendrickx, B., Zhu, X.H., Du, F., Chen, E., Pelacho, B., Penuelas, I., Abizanda, G., Uriz, M., Frommer, S.A., Ross, J.J., Schroeder, B.A., Seaborn, M.S., Adney, J.R., Hagenbrock, J., Harris, N.H., Zhang, Y., Zhang, X., Nelson-Holte, M.H., Jiang, Y., Billiau, A.D., Chen, W., Prosper, F., Verfaillie, C.M., Luttun, A. Multipotent adult progenitor cells sustain function of ischemic limbs in mice. J Clin Invest 118, 505-514 (2008).

3. Lawall, H., Bramlage, P., Amann, B. Stem cell and progenitor cell therapy in peripheral artery disease. A critical appraisal. Thromb Haemost 103, 696-709 (2010).

4. Taghavi, S., Duran, J.M., George, J.C. Stem cell therapy for peripheral arterial disease: a review of clinical trials. Stem Cell Studies 1, 105-114 (2011).

5. Epstein, S.E., Fuchs, S., Zhou, Y.F., Baffour, R., Kornowski, R. Therapeutic interventions for enhancing collateral development by administration of growth factors: basic principles, early results and potential hazards. Cardiovascular research 49, 532-542 (2001).

6. Kinnaird, T., Stabile, E., Burnett, M.S., Lee, C.W., Barr, S., Fuchs, S., Epstein, S.E. Marrow-derived stromal cells express genes encoding a broad spectrum of arteriogenic cytokines and promote in vitro and in vivo arteriogenesis through paracrine mechanisms. Circulation research 94, 678-685 (2004).

7. Mosesson, M.W. Fibrinogen and fibrin structure and functions. J Thromb Haemost 3, 1894-1904 (2005).

8. Zhang, G., Drinnan, C.T., Geuss, L.R., Suggs, L.J. Vascular differentiation of bone marrow stem cells is directed by a tunable three-dimensional matrix. Acta Biomater 6, 3395-3403 (2010).

9. Mamidi, M.K., Singh, G., Husin, J.M., Nathan, K.G., Sasidharan, G., Zakaria, Z., Bhonde, R., Majumdar, A.S., Das, A.K. Impact of passing mesenchymal stem cells through smaller bore size needles for subsequent use in patients for clinical or cosmetic indications. J Transl Med 10, 229 (2012).

10. Aguado, B.A., Mulyasasmita, W., Su, J., Lampe, K.J., Heilshorn, S.C. Improving viability of stem cells during syringe needle flow through the design of hydrogel cell carriers. Tissue engineering. Part A 18, 806-815 (2012).

11. Sahni, A., Francis, C.W. Vascular endothelial growth factor binds to fibrinogen and fibrin and stimulates endothelial cell proliferation. Blood 96, 3772-3778 (2000).

12. Hammers, D.W., Sarathy, A., Pham, C.B., Drinnan, C.T., Farrar, R.P., Suggs, L.J. Controlled release of IGF-I from a biodegradable matrix improves functional recovery of skeletal muscle from ischemia/reperfusion. Biotechnol Bioeng 109, 1051-1059 (2012).

13. Stowers, R.S., Drinnan, C.T., Chung, E.N., Suggs, L.J. Mesenchymal stem cell response to TGF-beta 1 in both 2D and 3D environments. Biomaterials Science 1, 860-869 (2013).

14. Shaikh, F.M., Callanan, A., Kavanagh, E.G., Burke, P.E., Grace, P.A., McGloughlin, T.M. Fibrin: a natural biodegradable scaffold in vascular tissue engineering. Cells Tissues Organs 188, 333-346 (2008).

15. Madonna, R., Delli Pizzi, S., Di Donato, L., Mariotti, A., Di Carlo, L., D'Ugo, E., Teberino, M.A., Merla, A., Tartaro, A., De Caterina, R. Non-invasive in vivo detection of peripheral limb ischemia improvement in the rat after adipose tissue-derived stromal cell transplantation. Circ J 76, 1517-1525 (2012).

16. Merla, A., Di Romualdo, S., Di Donato, L., Proietti, M., Salsano, F., Romani, G.L. Combined thermal and laser Doppler imaging in the assessment of cutaneous tissue perfusion. Conference proceedings : ... Annual International Conference of the IEEE Engineering in Medicine and Biology Society. IEEE Engineering in Medicine and Biology Society. Conference 2007, 2630-2633 (2007).

17. Limbourg, A., Korff, T., Napp, L.C., Schaper, W., Drexler, H., Limbourg, F.P. Evaluation of postnatal arteriogenesis and angiogenesis in a mouse model of hind-limb ischemia. Nature protocols 4, 1737-1746 (2009).

18. Brown, M.D., Kent, J., Kelsall, C.J., Milkiewicz, M., Hudlicka, O. Remodeling in the microcirculation of rat skeletal muscle during chronic ischemia. Microcirculation 10, 179-191 (2003).

19. Milkiewicz, M., Hudlicka, O., Shiner, R., Egginton, S., Brown, M.D. Vascular endothelial growth factor mRNA and protein do not change in parallel during non-inflammatory skeletal muscle ischaemia in rat. The Journal of physiology 577, 671-678 (2006).

20. Peck, M.A., Crawford, R.S., Abularrage, C.J., Patel, V.I., Conrad, M.F., Yoo, J.H., Watkins, M.T., Albadawi, H. A functional murine model of hindlimb demand ischemia. Ann Vasc Surg 24, 532-537 (2010).

21. Waters, R.E., Terjung, R.L., Peters, K.G., Annex, B.H. Preclinical models of human peripheral arterial occlusive disease: implications for investigation of therapeutic agents. J Appl Physiol 97, 773-780 (2004).

22. Anderson, S.I., Hudlicka, O., Brown, M.D. Capillary red blood cell flow and activation of white blood cells in chronic muscle ischemia in the rat. The American journal of physiology 272, H2757-2764 (1997).

23. Blaisdell, F.W. The pathophysiology of skeletal muscle ischemia and the reperfusion syndrome: a review. Cardiovascular surgery 10, 620-630 (2002).

24. Dorweiler, B., Pruefer, D., Andrasi, T.B., Maksan, S.M., Schmiedt, W., Neufang, A., Vahl, C.F. Ischemia-reperfusion injury - Pathophysiology and clinical implications. European Journal of Trauma and Emergency Surgery 33, 600-612 (2007).

25. Gute, D.C., Ishida, T., Yarimizu, K., Korthuis, R.J. Inflammatory responses to ischemia and reperfusion in skeletal muscle. Molecular and cellular biochemistry 179, 169-187 (1998).

26. Chazaud, B., Brigitte, M., Yacoub-Youssef, H., Arnold, L., Gherardi, R., Sonnet, C., Lafuste, P., Chretien, F. Dual and beneficial roles of macrophages during skeletal muscle regeneration. Exercise and sport sciences reviews 37, 18-22 (2009).

27. Kharraz, Y., Guerra, J., Mann, C.J., Serrano, A.L., Munoz-Canoves, P. Macrophage Plasticity and the Role of Inflammation in Skeletal Muscle Repair. Mediators of Inflammation (2013).

28. Novak, M.L., Koh, T.J. Phenotypic transitions of macrophages orchestrate tissue repair. Am J Pathol 183, 1352-1363 (2013).

29. Tidball, J.G. Inflammatory processes in muscle injury and repair. American journal of physiology. Regulatory, integrative and comparative physiology 288, R345-353 (2005).

30. Milkiewicz, M., Hudlicka, O., Shiner, R., Egginton, S., Brown, M.D. Vascular endothelial growth factor mRNA and protein do not change in parallel during non-inflammatory skeletal muscle ischaemia in rat. J Physiol-London 577, 671-678 (2006).

31. Tang, G.L., Chang, D.S., Sarkar, R., Wang, R., Messina, L.M. The effect of gradual or acute arterial occlusion on skeletal muscle blood flow, arteriogenesis, and inflammation in rat hindlimb ischemia. J Vasc Surg 41, 312-320 (2005).

32. Yang, Z., von Ballmoos, M.W., Diehm, N., Baumgartner, I., Kalka, C., Di Santo, S. Call for a reference model of chronic hind limb ischemia to investigate therapeutic angiogenesis. Vascular pharmacology 51, 268-274 (2009).

33. Mahdavian Delavary, B., van der Veer, W.M., van Egmond, M., Niessen, F.B., Beelen, R.H. Macrophages in skin injury and repair. Immunobiology 216, 753-762 (2011).

34. Sunderkotter, C., Steinbrink, K., Goebeler, M., Bhardwaj, R., Sorg, C. Macrophages and angiogenesis. J Leukoc Biol 55, 410-422 (1994).

35. Moldovan, L., Moldovan, N.I. Role of monocytes and macrophages in angiogenesis. Exs, 127-146 (2005).

36. Helisch, A., Wagner, S., Khan, N., Drinane, M., Wolfram, S., Heil, M., Ziegelhoeffer, T., Brandt, U., Pearlman, J.D., Swartz, H.M., Schaper, W. Impact of mouse strain differences in innate hindlimb collateral vasculature. Arterioscl Throm Vas 26, 520-526 (2006).

Chapter 7: Conclusions and future work

7.1 SUMMARY OF PRESENT FINDINGS AND CONCLUSIONS

Cardiovascular diseases are the leading cause of death globally,[1] and the mortality rate is expected to continue to rise over the next 30 years[2,3]. Despite advances in revascularization procedures, many patients do not respond well to currently available treatments, or are not even eligible for these therapies, due partially to co-morbidities.[4] However, cell-based therapies have been shown to be a promising alternative, with preclinical and clinical trials using bone marrow-derived mesenchymal stem cells demonstrating improved outcomes.[5] Furthermore, incorporating biomaterial delivery systems can be beneficial for cell-based therapies by increasing the rate of cell retention and altering cell function to promote healing.

The objective of this thesis was to evaluate the use of bone marrow-derived mesenchymal stem cells delivered within a PEGylated fibrin gel biomatrix for revascularization therapies. This evaluation included designing nanoparticle contrast agents for tracking stem cells *in vivo* using noninvasive imaging techniques; assessing the influence of hypoxia on MSCs and the resulting interactions with endogenous cell types; and demonstrating the extent of neovascularization and functional recovery within a hind limb ischemia model. Specifically, Chapters 2 and 3 investigated the potential application of nanoparticle contrast agents for stem cell monitoring. Chapter 2 demonstrated that gold nanoparticles of various sizes and surface coatings are safe labeling agents for stem cells, as cell function and viability were not affected. Chapter 3 attempted to explore the development of a nanoparticle system which would dissociate within endosomal compartments with minimal biologic effects and not accumulate in subsequent cell populations or in organs *in vivo*. This system consisted of 5 nm nanoparticles which were aggregated using a poly-L-lysine coating to promote cellular uptake. However, this

nanoparticle system proved to not be ideal, as the nanoparticles were found to be transferred to macrophages. As a result, this prompted further investigation into a nanoparticle system which also monitored infiltration of macrophages, both to detect the transfer of contrast agents from MSCs to non-stem cells, as well as to potentially evaluate the therapeutic contribution of macrophages to wound healing. This dual nanoparticle system is outlined in Chapter 4. This nanoparticle system was safe in terms of maintaining cell viability and function. In addition, the system preferentially labeled the cells of interest (either macrophages or MSCs), allowing the distinction between the two cell types using photoacoustic imaging (both *in vitro* and *in vivo*). Histological analysis and cell sorting confirmed the labeling of macrophages with nanoparticles within a hind limb ischemia model.

The motivation for monitoring macrophage infiltration was two-fold: to help distinguish the transfer of contrast agents to non-stem cells and also to evaluate the infiltration of macrophages following injury as part of the wound healing response. Macrophages have been shown to have important functions in tissue repair, including skeletal muscle, cardiac muscle, and vascular regeneration. Chapter 5 evaluated the interaction between MSCs and macrophages, specifically in relation to an *in vivo* ischemic injury environment. MSCs naturally reside within a hypoxic environment and have been shown to produce improved angiogenic responses following an ischemic injury.[6-10] Chapter 5 demonstrated influence of an *in vitro* hypoxic environment on MSCs and found MSCs undergo a stress response to mild (2%) or severe (1%) hypoxia. Specifically, MSCs exhibited increased cell proliferation and upregulation of pro-angiogenic and anti-apoptotic factors. In addition, the role of macrophages in wound healing and angiogenesis was evaluated, with emphasis on the interaction between MSCs and macrophages. It was found that culturing macrophages with MSC conditioned media

did not have immunomodulatory effects. However, co-culturing MSCs and macrophages led to changes in both cell types, including soluble factor secretion and phenotypic changes.

Finally, the therapeutic effects of MSCs delivered within a PEGylated fibrin gel were evaluated using a hind limb ischemia model. While the PEGylated fibrin gel itself seemed to impart some angiogenic effects, delivering MSCs in combination a PEGylated fibrin gel were found to enhance vascular formation, perfusion of the ischemic limb, and functional recovery of the tissue.

7.2 FUTURE DIRECTIONS

This thesis focused on demonstrating the feasibility of labeling MSCs with gold nanoparticles for cell tracking. However, one of the drawbacks of using gold nanoparticles as cell tracking agents is the inability to distinguish viable from nonviable cells. While the dual nanoparticle system presented in this thesis partially addressed this issue, the system is not able to definitively determine if the MSCs are viable, but instead only if macrophages infiltrated the area and endocytosed the MSCs. Thus, a major contribution to the field would be to design a gold nanoparticle contrast agent which is capable of monitoring MSCs noninvasively using photoacoustic imaging and also determine if the cells are viable or changing function (*e.g.* differentiating to another cell type). Such a system could involve a caspase-degradable nanoparticle system which is activated following cell death, leading to changes in the optical absorption characteristics of the particles, and thus the photoacoustic signal.

Investigation of silica coated gold nanorods revealed that the silica coating is no longer present on the nanorod surface following cellular endocytosis. Further investigation is needed to elucidate the mechanisms responsible for the degradation of the

silica layer, including the time course of the degradation process. Possible mechanisms for the silica degradation could be penetration of serum proteins into the porous silica coating or the intracellular environment (including pH and hydrolytic enzymes). Obtaining a better understanding of the degradation mechanisms could also contribute to the design of a multimodal system, in which drugs/genes are loaded into the silica layer and released at the site of interest as a result of silica degradation. The gold nanoparticles would serve as an imaging contrast agent for monitoring purposes.

The interaction between MSCs and other cell types, specifically macrophages, is essential for wound healing to occur. This work demonstrated that MSCs are responsive to a hypoxic environment, with the expression of more pro-regenerative characteristics. In addition, this work also showed that macrophages are influenced by MSCs, especially when the interaction between the two cell types occurs within a hypoxic environment. However, more extensive studies on the interaction between MSCs and macrophages can be conducted. For example, in order to more precisely characterize macrophage phenotype along the M1/M2 spectrum, additional markers for M1 (*e.g.* CXCL9/10/11/19 and indoleamine-pyrrole 2,3 dioxygenase (IDO)) and M2 (*e.g.* CCL13/18, prostaglandin E2 (PGE2), and insulin-like growth factor 1 (IGF-1)) should be analyzed. Other analysis techniques could also be incorporated for phenotype classification, such as intracellular staining and fluorescence-activated cell sorting. Also, this work focused on the interaction between MSCs and macrophages within a 2D environment. However, in order to more closely resemble the *in vivo* scenario, it would be beneficial to study the interaction between the cell types within a 3D environment, such as the PEGylated fibrin gels. Also, translating these studies to an *in vivo* situation would be beneficial, such as evaluating the changes in macrophage phenotype within the ischemic tissue treated with MSCs in combination with PEGylated fibrin gel.

Lastly, more accurate models of peripheral artery disease are necessary to test the effectiveness of stem cell therapy in humans. The work presented here used a femoral artery ligation to induce hind limb ischemia in a rodent model. However, the extensive collateral network within the rat hind limb, and the lack of exercise following the injury, limited the damage to the tissue. In addition, this is an acute model of ischemia, which is not necessarily representative of the gradual onset of peripheral artery disease which occurs in humans. Also, many patients with peripheral artery disease have existing co-morbidities, such as diabetes, and thus the use of a diseased animal model would be a more relevant model. Finally, many patients have to undergo multiple revascularization procedures because of restenosis or reclotting of the vessel. However, revascularization induces reperfusion injury. Thus a more clinically relevant model may be a patient who has had an acute ischemic event and is postoperative to a revascularization procedure. Taken together, a more optimal animal model would involve a diseased rodent model which has undergone gradual onset of ischemia and experienced a reperfusion event.

7.4 REFERENCES

1. Copland, I.B. Mesenchymal stromal cells for cardiovascular disease. *J Cardiovasc Dis Res* **2**, 3-13 (2011).

2. Mathers, C.D., Loncar, D. Projections of global mortality and burden of disease from 2002 to 2030. *PLoS medicine* **3**, e442 (2006).

3. Organization, W.H. (World Health Organization, Geneva, Switzerland; 2011).

4. Creager, M.A. Medical management of peripheral arterial disease. *Cardiol Rev* **9**, 238-245 (2001).

5. Lawall, H., Bramlage, P., Amann, B. Stem cell and progenitor cell therapy in peripheral artery disease. A critical appraisal. *Thromb Haemost* **103**, 696-709 (2010).

6. Muscari, C., Giordano, E., Bonafe, F., Govoni, M., Pasini, A., Guarnieri, C. Priming adult stem cells by hypoxic pretreatments for applications in regenerative medicine. *Journal of biomedical science* **20**, 63 (2013).

7. Grayson, W.L., Zhao, F., Izadpanah, R., Bunnell, B., Ma, T. Effects of hypoxia on human mesenchymal stem cell expansion and plasticity in 3D constructs. *Journal of cellular physiology* **207**, 331-339 (2006).

8. Hu, X., Yu, S.P., Fraser, J.L., Lu, Z., Ogle, M.E., Wang, J.A., Wei, L. Transplantation of hypoxia-preconditioned mesenchymal stem cells improves infarcted heart function via enhanced survival of implanted cells and angiogenesis. *J Thorac Cardiov Sur* **135**, 799-808 (2008).

9. Hoffmann, J., Glassford, A.J., Doyle, T.C., Robbins, R.C., Schrepfer, S., Pelletier, M.P. Angiogenic effects despite limited cell survival of bone marrow-derived mesenchymal stem cells under ischemia. *The Thoracic and cardiovascular surgeon* **58**, 136-142 (2010).

10. Yang, D., Wang, W., Li, L., Peng, Y., Chen, P., Huang, H., Guo, Y., Xia, X., Wang, Y., Wang, H., Wang, W.E., Zeng, C. The relative contribution of paracine effect versus direct differentiation on adipose-derived stem cell transplantation mediated cardiac repair. *PLoS One* **8**, e59020 (2013).

Bibliography

Adonai, N., K. N. Nguyen, et al. (2002). "Ex vivo cell labeling with 64Cu-pyruvaldehyde-bis(N4-methylthiosemicarbazone) for imaging cell trafficking in mice with positron-emission tomography." Proceedings of the National Academy of Sciences of the United States of America 99(5): 3030-3035.

Aguado, B. A., W. Mulyasasmita, et al. (2012). "Improving viability of stem cells during syringe needle flow through the design of hydrogel cell carriers." Tissue engineering. Part A 18(7-8): 806-815.

Al-Khaldi, A., N. Eliopoulos, et al. (2003). "Postnatal bone marrow stromal cells elicit a potent VEGF-dependent neoangiogenic response in vivo." Gene therapy 10(8): 621-629.

Albukhaty, S., H. Naderi-Manesh, et al. (2013). "In vitro labeling of neural stem cells with poly-L-lysine coated super paramagnetic nanoparticles for green fluorescent protein transfection." Iranian biomedical journal 17(2): 71-76.

Alkilany, A. M. and C. J. Murphy (2010). "Toxicity and cellular uptake of gold nanoparticles: what we have learned so far?" J Nanopart Res 12(7): 2313-2333.

Alkilany, A. M., P. K. Nagaria, et al. (2009). "Cellular Uptake and Cytotoxicity of Gold Nanorods: Molecular Origin of Cytotoxicity and Surface Effects." Small 5(6): 701-708.

Almany, L. and D. Seliktar (2005). "Biosynthetic hydrogel scaffolds made from fibrinogen and polyethylene glycol for 3D cell cultures." Biomaterials 26(15): 2467-2477.

Amann, B., C. Luedemann, et al. (2009). "Autologous bone marrow cell transplantation increases leg perfusion and reduces amputations in patients with advanced critical limb ischemia due to peripheral artery disease." Cell transplantation 18(3): 371-380.

Amsalem, Y., Y. Mardor, et al. (2007). "Iron-oxide labeling and outcome of transplanted mesenchymal stem cells in the infarcted myocardium." Circulation 116(11 Suppl): I38-45.

Anderson, S. I., O. Hudlicka, et al. (1997). "Capillary red blood cell flow and activation of white blood cells in chronic muscle ischemia in the rat." The American journal of physiology 272(6 Pt 2): H2757-2764.

Anton, K., D. Banerjee, et al. (2012). "Macrophage-associated mesenchymal stem cells assume an activated, migratory, pro-inflammatory phenotype with increased IL-6 and CXCL10 secretion." Plos One 7(4): e35036.

Aoki, T., H. Kataoka, et al. (2007). "Macrophage-derived matrix metalloproteinase-2 and-9 promote the progression of cerebral aneurysms in rats." Stroke 38(1): 162-169.

Appasani, K. and R. K. Appasani (2011). Stem cells & regenerative medicine : from molecular embryology to tissue engineering. New York, Humana Press.

Aranguren, X. L., J. D. McCue, et al. (2008). "Multipotent adult progenitor cells sustain function of ischemic limbs in mice." J Clin Invest 118(2): 505-514.

Arbab, A. S., L. A. Bashaw, et al. (2003). "Characterization of biophysical and metabolic properties of cells labeled with superparamagnetic iron oxide nanoparticles and transfection agent for cellular MR imaging." Radiology 229(3): 838-846.

Arnida, M. M. Janat-Amsbury, et al. (2011). "Geometry and surface characteristics of gold nanoparticles influence their biodistribution and uptake by macrophages." European journal of pharmaceutics and biopharmaceutics : official journal of Arbeitsgemeinschaft fur Pharmazeutische Verfahrenstechnik e.V 77(3): 417-423.

Arnold, L., A. Henry, et al. (2007). "Inflammatory monocytes recruited after skeletal muscle injury switch into antiinflammatory macrophages to support myogenesis." The Journal of experimental medicine 204(5): 1057-1069.

Asahara, T., T. Murohara, et al. (1997). "Isolation of putative progenitor endothelial cells for angiogenesis." Science 275(5302): 964-967.

Barbash, I. M., P. Chouraqui, et al. (2003). "Systemic delivery of bone marrow-derived mesenchymal stem cells to the infarcted myocardium - Feasibility, cell migration, and body distribution." Circulation 108(7): 863-868.

Bartsch, T., M. Brehm, et al. (2007). "Transplantation of autologous mononuclear bone marrow stem cells in patients with peripheral arterial disease (the TAM-PAD study)." Clinical research in cardiology : official journal of the German Cardiac Society 96(12): 891-899.

Basciano, L., C. Nemos, et al. (2011). "Long term culture of mesenchymal stem cells in hypoxia promotes a genetic program maintaining their undifferentiated and multipotent status." BMC cell biology 12: 12.

Beckermann, B. M., G. Kallifatidis, et al. (2008). "VEGF expression by mesenchymal stem cells contributes to angiogenesis in pancreatic carcinoma." British journal of cancer 99(4): 622-631.

Ben-Mordechai, T., R. Holbova, et al. (2013). "Macrophage Subpopulations Are Essential for Infarct Repair With and Without Stem Cell Therapy." Journal of the American College of Cardiology 62(20): 1890-1901.

Benoit, E., T. F. O'Donnell, Jr., et al. (2011). "The role of amputation as an outcome measure in cellular therapy for critical limb ischemia: implications for clinical trial design." Journal of translational medicine 9: 165.

Bhirde, A., J. Xie, et al. (2011). "Nanoparticles for cell labeling." Nanoscale 3(1): 142.

Blaisdell, F. W. (2002). "The pathophysiology of skeletal muscle ischemia and the reperfusion syndrome: a review." Cardiovascular surgery 10(6): 620-630.

Brown, M. D., J. Kent, et al. (2003). "Remodeling in the microcirculation of rat skeletal muscle during chronic ischemia." Microcirculation 10(2): 179-191.

Cao, F., S. Lin, et al. (2006). "In vivo visualization of embryonic stem cell survival, proliferation, and migration after cardiac delivery." Circulation 113(7): 1005-1014.

Caplan, A. I. (2009). "Why are MSCs therapeutic? New data: new insight." Journal of Pathology 217(2): 318-324.

Carrancio, S., N. Lopez-Holgado, et al. (2008). "Optimization of mesenchymal stem cell expansion procedures by cell separation and culture conditions modification." Experimental hematology 36(8): 1014-1021.

Charbord, P., H. Lerat, et al. (1990). "The cytoskeleton of stromal cells from human bone marrow cultures resembles that of cultured smooth muscle cells." Experimental hematology 18(4): 276-282.

Chazaud, B., M. Brigitte, et al. (2009). "Dual and beneficial roles of macrophages during skeletal muscle regeneration." Exercise and sport sciences reviews 37(1): 18-22.

Chen, L., E. E. Tredget, et al. (2008). "Paracrine factors of mesenchymal stem cells recruit macrophages and endothelial lineage cells and enhance wound healing." Plos One 3(4): e1886.

Chen, L., Y. B. Xu, et al. (2014). "Conditioned Medium from Hypoxic Bone Marrow-Derived Mesenchymal Stem Cells Enhances Wound Healing in Mice." Plos One 9(4).

Chen, P., S. Mwakwari, et al. (2008). "Gold nanoparticles: From nanomedicine to nanosensing." Nanotechnology, Science and Applications: 45-66.

Chen, Y. S., W. Frey, et al. (2010). "Enhanced thermal stability of silica-coated gold nanorods for photoacoustic imaging and image-guided therapy." Optics express 18(9): 8867-8878.

Chen, Y. S., W. Frey, et al. (2011). "Silica-Coated Gold Nanorods as Photoacoustic Signal Nanoamplifiers." Nano Letters 11(2): 348-354.

Chithrani, B. D. and W. C. Chan (2007). "Elucidating the mechanism of cellular uptake and removal of protein-coated gold nanoparticles of different sizes and shapes." Nano Letters 7(6): 1542-1550.

Chithrani, B. D., A. A. Ghazani, et al. (2006). "Determining the size and shape dependence of gold nanoparticle uptake into mammalian cells." Nano Letters 6(4): 662-668.

Chochola, M., R. Pytlik, et al. (2008). "Autologous intra-arterial infusion of bone marrow mononuclear cells in patients with critical leg ischemia." International angiology : a journal of the International Union of Angiology 27(4): 281-290.

Choi, H. S., W. Liu, et al. (2007). "Renal clearance of nanoparticles." Nature Biotechnology 25(10): 1165-1170.

Chung, E., S. Y. Nam, et al. (2013). "Evaluation of gold nanotracers to track adipose-derived stem cells in a PEGylated fibrin gel for dermal tissue engineering applications." International journal of nanomedicine 8: 325-336.

Chung, E., L. M. Ricles, et al. (2012). "Multifunctional nanoscale strategies for enhancing and monitoring blood vessel regeneration." Nano Today 7(6): 514-531.

Cobellis, G., A. Silvestroni, et al. (2008). "Long-term effects of repeated autologous transplantation of bone marrow cells in patients affected by peripheral arterial disease." Bone marrow transplantation 42(10): 667-672.

Comalada, M., J. Xaus, et al. (2004). "Macrophage colony-stimulating factor-, granulocyte-macrophage colony-stimulating factor-, or IL-3-dependent survival of macrophages, but not proliferation, requires the expression of p21(Waf1) through the phosphatidylinositol 3-kinase/Akt pathway." European Journal of Immunology 34(8): 2257-2267.

Copland, I. B. (2011). "Mesenchymal stromal cells for cardiovascular disease." J Cardiovasc Dis Res 2(1): 3-13.

Cowan, M. K. (2012). Microbiology : a systems approach. New York, NY, McGraw-Hill.

Creager, M. A. (2001). "Medical management of peripheral arterial disease." Cardiol Rev 9(4): 238-245.

Crisostomo, P. R., Y. Wang, et al. (2008). "Human mesenchymal stem cells stimulated by TNF-alpha, LPS, or hypoxia produce growth factors by an NF kappa B- but not JNK-dependent mechanism." American journal of physiology. Cell physiology 294(3): C675-682.

D'Ippolito, G., S. Diabira, et al. (2006). "Low oxygen tension inhibits osteogenic differentiation and enhances stemness of human MIAMI cells." Bone 39(3): 513-522.

Daldrup-Link, H. E., M. Rudelius, et al. (2004). "Cell tracking with gadophrin-2: a bifunctional contrast agent for MR imaging, optical imaging, and fluorescence microscopy." European journal of nuclear medicine and molecular imaging 31(9): 1312-1321.

Das, R., H. Jahr, et al. (2010). "The role of hypoxia in bone marrow-derived mesenchymal stem cells: considerations for regenerative medicine approaches." Tissue engineering. Part B, Reviews 16(2): 159-168.

Dikovsky, D., H. Bianco-Peled, et al. (2006). "The effect of structural alterations of PEG-fibrinogen hydrogel scaffolds on 3-D cellular morphology and cellular migration." Biomaterials 27(8): 1496-1506.

Dorweiler, B., D. Pruefer, et al. (2007). "Ischemia-reperfusion injury - Pathophysiology and clinical implications." European Journal of Trauma and Emergency Surgery 33(6): 600-612.

Dos Santos, F., P. Z. Andrade, et al. (2010). "Ex vivo expansion of human mesenchymal stem cells: a more effective cell proliferation kinetics and metabolism under hypoxia." Journal of cellular physiology 223(1): 27-35.

Dupont, K. M., K. Sharma, et al. (2010). "Human stem cell delivery for treatment of large segmental bone defects." Proceedings of the National Academy of Sciences of the United States of America 107(8): 3305-3310.

Durdu, S., A. R. Akar, et al. (2006). "Autologous bone-marrow mononuclear cell implantation for patients with Rutherford grade II-III thromboangiitis obliterans." Journal of vascular surgery 44(4): 732-739.

Durr, N. J., T. Larson, et al. (2007). "Two-photon luminescence imaging of cancer cells using molecularly targeted gold nanorods." Nano Lett 7(4): 941-945.

Eggenhofer, E. and M. J. Hoogduijn (2012). "Mesenchymal stem cell-educated macrophages." Transplantation research 1(1): 12.

Emelianov, S. Y., P. C. Li, et al. (2009). "Photoacoustics for molecular imaging and therapy." Physics today 62(8): 34-39.

Engelhardt, E., A. Toksoy, et al. (1998). "Chemokines IL-8, GROalpha, MCP-1, IP-10, and Mig are sequentially and differentially expressed during phase-specific infiltration of leukocyte subsets in human wound healing." The American journal of pathology 153(6): 1849-1860.

Epstein, S. E., S. Fuchs, et al. (2001). "Therapeutic interventions for enhancing collateral development by administration of growth factors: basic principles, early results and potential hazards." Cardiovascular research 49(3): 532-542.

Ferreira, L. (2009). "Nanoparticles as tools to study and control stem cells." Journal of Cellular Biochemistry 108(4): 746-752.

Ferreira, L., J. Karp, et al. (2008). "New Opportunities: The Use of Nanotechnologies to Manipulate and Track Stem Cells." Cell Stem Cell 3(2): 136-146.

Fischer, D., Y. Li, et al. (2003). "In vitro cytotoxicity testing of polycations: influence of polymer structure on cell viability and hemolysis." Biomaterials 24(7): 1121-1131.

Frangioni, J. V. and R. J. Hajjar (2004). "In vivo tracking of stem cells for clinical trials in cardiovascular disease." Circulation 110(21): 3378-3383.

Frisdal, E., E. Teiger, et al. (2000). "Increased expression of gelatinases and alteration of basement membrane in rat soleus muscle following femoral artery ligation." Neuropathology and Applied Neurobiology 26(1): 11-21.

Gallucci, R. M., P. P. Simeonova, et al. (2000). "Impaired cutaneous wound healing in interleukin-6-deficient and immunosuppressed mice." FASEB journal : official publication of the Federation of American Societies for Experimental Biology 14(15): 2525-2531.

Ghosh, P., G. Han, et al. (2008). "Gold nanoparticles in delivery applications." Advanced Drug Delivery Reviews 60(11): 1307-1315.

Gobin, A. M., M. H. Lee, et al. (2007). "Near-infrared resonant nanoshells for combined optical imaging and photothermal cancer therapy." Nano letters 7(7): 1929-1934.

Gordon, S. (2003). "Alternative activation of macrophages." Nature Reviews Immunology 3(1): 23-35.

Goshima, K. R., J. L. Mills, et al. (2004). "A new look at outcomes after infrainguinal bypass surgery: Traditional reporting standards systematically underestimate the expenditure of effort required to attain limb salvage." Journal of vascular surgery 39(2): 330-335.

Grayson, W. L., F. Zhao, et al. (2006). "Effects of hypoxia on human mesenchymal stem cell expansion and plasticity in 3D constructs." Journal of cellular physiology 207(2): 331-339.

Gute, D. C., T. Ishida, et al. (1998). "Inflammatory responses to ischemia and reperfusion in skeletal muscle." Molecular and cellular biochemistry 179(1-2): 169-187.

Guzman, R., N. Uchida, et al. (2007). "Long-term monitoring of transplanted human neural stem cells in developmental and pathological contexts with MRI." Proceedings of the National Academy of Sciences of the United States of America 104(24): 10211-10216.

Hammers, D. W., A. Sarathy, et al. (2012). "Controlled release of IGF-I from a biodegradable matrix improves functional recovery of skeletal muscle from ischemia/reperfusion." Biotechnol Bioeng 109(4): 1051-1059.

Hardman, R. (2006). "A toxicologic review of quantum dots: toxicity depends on physicochemical and environmental factors." Environmental health perspectives 114(2): 165-172.

Helisch, A., S. Wagner, et al. (2006). "Impact of mouse strain differences in innate hindlimb collateral vasculature." Arteriosclerosis Thrombosis and Vascular Biology 26(3): 520-526.

Heo, J. H., J. Lucero, et al. (1999). "Matrix metalloproteinases increase very early during experimental focal cerebral ischemia." Journal of Cerebral Blood Flow and Metabolism 19(6): 624-633.

Higashi, Y., M. Kimura, et al. (2004). "Autologous bone-marrow mononuclear cell implantation improves endothelium-dependent vasodilation in patients with limb ischemia." Circulation 109(10): 1215-1218.

Hirn, S., M. Semmler-Behnke, et al. (2011). "Particle size-dependent and surface charge-dependent biodistribution of gold nanoparticles after intravenous administration." European journal of pharmaceutics and biopharmaceutics : official journal of Arbeitsgemeinschaft fur Pharmazeutische Verfahrenstechnik e.V 77(3): 407-416.

Hoffmann, J., A. J. Glassford, et al. (2010). "Angiogenic effects despite limited cell survival of bone marrow-derived mesenchymal stem cells under ischemia." The Thoracic and cardiovascular surgeon 58(3): 136-142.

Hofmann, M., K. C. Wollert, et al. (2005). "Monitoring of bone marrow cell homing into the infarcted human myocardium." Circulation 111(17): 2198-2202.

Homan, K., J. Shah, et al. (2010). "Silver nanosystems for photoacoustic imaging and image-guided therapy." Journal of Biomedical Optics 15(2): 021316.

Horák, D., M. Babič, et al. (2009). "Effect of different magnetic nanoparticle coatings on the efficiency of stem cell labeling." Journal of Magnetism and Magnetic Materials 321(10): 1539-1547.

Hore, M. J. A. and R. J. Composto (2010). "Nanorod Self-Assembly for Tuning Optical Absorption." Acs Nano 4(11): 6941-6949.

Hu, X., S. P. Yu, et al. (2008). "Transplantation of hypoxia-preconditioned mesenchymal stem cells improves infarcted heart function via enhanced survival of implanted cells and angiogenesis." The Journal of Thoracic and Cardiovascular Surgery 135(4): 799-808.

Huang, D. M., J. K. Hsiao, et al. (2009). "The promotion of human mesenchymal stem cell proliferation by superparamagnetic iron oxide nanoparticles." Biomaterials 30(22): 3645-3651.

Huang, P. H., Y. H. Chen, et al. (2009). "Matrix Metalloproteinase-9 Is Essential for Ischemia-Induced Neovascularization by Modulating Bone Marrow-Derived Endothelial Progenitor Cells." Arteriosclerosis Thrombosis and Vascular Biology 29(8): 1179-U1158.

Hung, S. C., R. R. Pochampally, et al. (2007). "Angiogenic effects of human multipotent stromal cell conditioned medium activate the PI3K-Akt pathway in hypoxic endothelial cells to inhibit apoptosis, increase survival, and stimulate angiogenesis." Stem cells 25(9): 2363-2370.

Hunt, S. A., W. T. Abraham, et al. (2005). "ACC/AHA 2005 Guideline Update for the Diagnosis and Management of Chronic Heart Failure in the Adult: a report of the American College of Cardiology/American Heart Association Task Force on Practice Guidelines (Writing Committee to Update the 2001 Guidelines for the Evaluation and Management of Heart Failure): developed in collaboration with the American College of Chest Physicians and the International Society for Heart and Lung Transplantation: endorsed by the Heart Rhythm Society." Circulation 112(12): e154-235.

Iafrati, M. D., J. W. Hallett, et al. (2011). "Early results and lessons learned from a multicenter, randomized, double-blind trial of bone marrow aspirate concentrate in critical limb ischemia." Journal of vascular surgery 54(6): 1650-1658.

Idei, N., J. Soga, et al. (2011). "Autologous bone-marrow mononuclear cell implantation reduces long-term major amputation risk in patients with critical limb ischemia: a comparison of atherosclerotic peripheral arterial disease and Buerger disease." Circulation. Cardiovascular interventions 4(1): 15-25.

Ikenaga, S., K. Hamano, et al. (2001). "Autologous bone marrow implantation induced angiogenesis and improved deteriorated exercise capacity in a rat ischemic hindlimb model." The Journal of surgical research 96(2): 277-283.

Ishida, A., Y. Ohya, et al. (2005). "Autologous peripheral blood mononuclear cell implantation for patients with peripheral arterial disease improves limb ischemia." Circulation journal : official journal of the Japanese Circulation Society 69(10): 1260-1265.

Ivanovic, Z. (2009). "Hypoxia or in situ normoxia: The stem cell paradigm." Journal of cellular physiology 219(2): 271-275.

Jain, P. K. and M. A. El-Sayed (2010). "Plasmonic coupling in noble metal nanostructures." Chemical Physics Letters 487(4-6): 153-164.

Jana, N. R., L. Gearheart, et al. (2001). "Seed-mediated growth approach for shape-controlled synthesis of spheroidal and rod-like gold nanoparticles using a surfactant template." Advanced Materials 13(18): 1389-1393.

Jiang, W., B. Y. S. Kim, et al. (2008). "Nanoparticle-mediated cellular response is size-dependent." Nature Nanotechnology 3(3): 145-150.

Johnson, C., H. J. Sung, et al. (2004). "Matrix metalloproteinase-9 is required for adequate angiogenic revascularization of ischemic tissues - Potential role in capillary branching." Circulation research 94(2): 262-268.

Jokerst, J. V., M. Thangaraj, et al. (2012). "Photoacoustic imaging of mesenchymal stem cells in living mice via silica-coated gold nanorods." ACS nano 6(7): 5920-5930.

Kawada, H., J. Fujita, et al. (2004). "Nonhematopoietic mesenchymal stem cells can be mobilized and differentiate into cardiomyocytes after myocardial infarction." Blood 104(12): 3581-3587.

Kharraz, Y., J. Guerra, et al. (2013). "Macrophage Plasticity and the Role of Inflammation in Skeletal Muscle Repair." Mediators of Inflammation.

Kim, J. and P. Hematti (2009). "Mesenchymal stem cell-educated macrophages: a novel type of alternatively activated macrophages." Experimental hematology 37(12): 1445-1453.

Kinnaird, T., E. Stabile, et al. (2004). "Bone-marrow-derived cells for enhancing collateral development: mechanisms, animal data, and initial clinical experiences." Circulation research 95(4): 354-363.

Kinnaird, T., E. Stabile, et al. (2004). "Marrow-derived stromal cells express genes encoding a broad spectrum of arteriogenic cytokines and promote in vitro and in vivo arteriogenesis through paracrine mechanisms." Circulation research 94(5): 678-685.

Kinnaird, T., E. Stabile, et al. (2004). "Local delivery of marrow-derived stromal cells augments collateral perfusion through paracrine mechanisms." Circulation 109(12): 1543-1549.

Kinner, B., J. M. Zaleskas, et al. (2002). "Regulation of smooth muscle actin expression and contraction in adult human mesenchymal stem cells." Experimental cell research 278(1): 72-83.

Kraitchman, D. L., M. Tatsumi, et al. (2005). "Dynamic imaging of allogeneic mesenchymal stem cells trafficking to myocardial infarction." Circulation 112(10): 1451-1461.

Kraitchman, D. L. and J. C.-M. Wu (2012). Stem cell labeling for delivery and tracking using noninvasive imaging. Boca Raton, CRC Press/Taylor & Francis.

Kubinová, Š. and E. Syková (2010). "Nanotechnologies in regenerative medicine." Minimally Invasive Therapy & Allied Technologies 19(3): 144-156.

Lao, Y., D. Xing, et al. (2008). "Noninvasive photoacoustic imaging of the developing vasculature during early tumor growth." Physics in medicine and biology 53(15): 4203-4212.

Larson, T. A., P. P. Joshi, et al. (2012). "Preventing protein adsorption and macrophage uptake of gold nanoparticles via a hydrophobic shield." ACS nano 6(10): 9182-9190.

Lawall, H., P. Bramlage, et al. (2010). "Stem cell and progenitor cell therapy in peripheral artery disease. A critical appraisal." Thromb Haemost 103(4): 696-709.

Lee, Z., J. E. Dennis, et al. (2008). "Imaging stem cell implant for cellular-based therapies." Experimental biology and medicine 233(8): 930-940.

Lévy, R., U. Shaheen, et al. (2010). "Gold nanoparticles delivery in mammalian live cells: a critical review." Nano Reviews 1(0).

Li, S. C., L. M. Tachiki, et al. (2010). "A biological global positioning system: considerations for tracking stem cell behaviors in the whole body." Stem cell reviews 6(2): 317-333.

Li, Z., Y. Suzuki, et al. (2008). "Comparison of reporter gene and iron particle labeling for tracking fate of human embryonic stem cells and differentiated endothelial cells in living subjects." Stem cells 26(4): 864-873.

Li, Z., H. Wei, et al. (2010). "Expression and secretion of interleukin-1beta, tumour necrosis factor-alpha and interleukin-10 by hypoxia- and serum-deprivation-stimulated mesenchymal stem cells." The FEBS journal 277(18): 3688-3698.

Limbourg, A., T. Korff, et al. (2009). "Evaluation of postnatal arteriogenesis and angiogenesis in a mouse model of hind-limb ischemia." Nature protocols 4(12): 1737-1746.

Lin, S., X. Xie, et al. (2007). "Quantum dot imaging for embryonic stem cells." BMC Biotechnol 7: 67.

Lin, Z. Q., T. Kondo, et al. (2003). "Essential involvement of IL-6 in the skin wound-healing process as evidenced by delayed wound healing in IL-6-deficient mice." Journal of leukocyte biology 73(6): 713-721.

Liu, J., Q. Hu, et al. (2004). "Autologous stem cell transplantation for myocardial repair." American journal of physiology. Heart and circulatory physiology 287(2): H501-511.

Longmire, M., P. L. Choyke, et al. (2008). "Clearance properties of nano-sized particles and molecules as imaging agents: considerations and caveats." Nanomedicine 3(5): 703-717.

Lonne, M., A. Lavrentieva, et al. (2013). "Analysis of oxygen-dependent cytokine expression in human mesenchymal stem cells derived from umbilical cord." Cell and tissue research 353(1): 117-122.

Losordo, D. W., M. R. Kibbe, et al. (2012). "A randomized, controlled pilot study of autologous CD34+ cell therapy for critical limb ischemia." Circulation. Cardiovascular interventions 5(6): 821-830.

Lu, C. W., Y. Hung, et al. (2007). "Bifunctional magnetic silica nanoparticles for highly efficient human stem cell labeling." Nano letters 7(1): 149-154.

Lu, Y., Y. D. Yin, et al. (2002). "Modifying the surface properties of superparamagnetic iron oxide nanoparticles through a sol-gel approach." Nano letters 2(3): 183-186.

Madonna, R., S. Delli Pizzi, et al. (2012). "Non-invasive in vivo detection of peripheral limb ischemia improvement in the rat after adipose tissue-derived stromal cell transplantation." Circulation journal : official journal of the Japanese Circulation Society 76(6): 1517-1525.

Mahdavian Delavary, B., W. M. van der Veer, et al. (2011). "Macrophages in skin injury and repair." Immunobiology 216(7): 753-762.

Mallidi, S., T. Larson, et al. (2007). "Molecular specific optoacoustic imaging with plasmonic nanoparticles." Optics express 15(11): 6583-6588.

Mallidi, S., T. Larson, et al. (2009). "Multiwavelength Photoacoustic Imaging and Plasmon Resonance Coupling of Gold Nanoparticles for Selective Detection of Cancer." Nano Letters 9(8): 2825-2831.

Mamidi, M. K., G. Singh, et al. (2012). "Impact of passing mesenchymal stem cells through smaller bore size needles for subsequent use in patients for clinical or cosmetic indications." Journal of translational medicine 10: 229.

Mantovani, A., A. Sica, et al. (2004). "The chemokine system in diverse forms of macrophage activation and polarization." Trends in Immunology 25(12): 677-686.

Martinez, F. O., S. Gordon, et al. (2006). "Transcriptional profiling of the human monocyte-to-macrophage differentiation and polarization: New molecules and patterns of gene expression." Journal of Immunology 177(10): 7303-7311.

Mathers, C. D. and D. Loncar (2006). "Projections of global mortality and burden of disease from 2002 to 2030." PLoS medicine 3(11): e442.

Meirelles Lda, S., A. M. Fontes, et al. (2009). "Mechanisms involved in the therapeutic properties of mesenchymal stem cells." Cytokine & growth factor reviews 20(5-6): 419-427.

Merla, A., S. Di Romualdo, et al. (2007). "Combined thermal and laser Doppler imaging in the assessment of cutaneous tissue perfusion." Conference proceedings : ... Annual International Conference of the IEEE Engineering in Medicine and Biology Society. IEEE Engineering in Medicine and Biology Society. Conference 2007: 2630-2633.

Michalet, X. (2005). "Quantum Dots for Live Cells, in Vivo Imaging, and Diagnostics." Science 307(5709): 538-544.

Milkiewicz, M., O. Hudlicka, et al. (2006). "Vascular endothelial growth factor mRNA and protein do not change in parallel during non-inflammatory skeletal muscle ischaemia in rat." The Journal of physiology 577(Pt 2): 671-678.

Moldovan, L. and N. I. Moldovan (2005). "Role of monocytes and macrophages in angiogenesis." EXS(94): 127-146.

Mosesson, M. W. (2005). "Fibrinogen and fibrin structure and functions." J Thromb Haemost 3(8): 1894-1904.

Mosser, D. M. and J. P. Edwards (2008). "Exploring the full spectrum of macrophage activation." Nature Reviews Immunology 8(12): 958-969.

Muhs, B. E., G. Plitas, et al. (2003). "Temporal expression and activation of matrix metalloproteinases-2, -9, and membrane type 1-matrix metalloproteinase following acute hindlimb ischemia." The Journal of surgical research 111(1): 8-15.

Muller-Borer, B. J., M. C. Collins, et al. (2007). "Quantum dot labeling of mesenchymal stem cells." J Nanobiotechnology 5: 9.

Murray, P. J. and T. A. Wynn (2011). "Protective and pathogenic functions of macrophage subsets." Nature Reviews Immunology 11(11): 723-737.

Muscari, C., E. Giordano, et al. (2013). "Priming adult stem cells by hypoxic pretreatments for applications in regenerative medicine." Journal of biomedical science 20: 63.

Nagesha, D., G. S. Laevsky, et al. (2007). "In vitro imaging of embryonic stem cells using multiphoton luminescence of gold nanoparticles." International journal of nanomedicine 2(4): 813-819.

Nam, S. Y., L. M. Ricles, et al. (2012). "In vivo ultrasound and photoacoustic monitoring of mesenchymal stem cells labeled with gold nanotracers." Plos One 7(5): e37267.

Nayerossadat, N., T. Maedeh, et al. (2012). "Viral and nonviral delivery systems for gene delivery." Advanced biomedical research 1: 27.

Niidome, T., M. Yamagata, et al. (2006). "PEG-modified gold nanorods with a stealth character for in vivo applications." Journal of controlled release : official journal of the Controlled Release Society 114(3): 343-347.

Nikoobakht, B. and M. A. El-Sayed (2003). "Preparation and growth mechanism of gold nanorods (NRs) using seed-mediated growth method." Chemistry of Materials 15(10): 1957-1962.

Novak, M. L. and T. J. Koh (2013). "Phenotypic transitions of macrophages orchestrate tissue repair." The American journal of pathology 183(5): 1352-1363.

Nucera, S., D. Biziato, et al. (2011). "The interplay between macrophages and angiogenesis in development, tissue injury and regeneration." International Journal of Developmental Biology 55(4-5): 495-503.

Organization, W. H. (2011). Global status report on noncommunicable diseases 2010. Geneva, Switzerland, World Health Organization.

Otero, K., I. R. Turnbull, et al. (2009). "Macrophage colony-stimulating factor induces the proliferation and survival of macrophages via a pathway involving DAP12 and beta-catenin." Nature Immunology 10(7): 734-743.

Ozcan, I., F. Segura-Sanchez, et al. (2010). "Pegylation of poly(gamma-benzyl-L-glutamate) nanoparticles is efficient for avoiding mononuclear phagocyte system capture in rats." International journal of nanomedicine 5: 1103-1111.

Peck, M. A., R. S. Crawford, et al. (2010). "A functional murine model of hindlimb demand ischemia." Ann Vasc Surg 24(4): 532-537.

Pittenger, M. F., A. M. Mackay, et al. (1999). "Multilineage potential of adult human mesenchymal stem cells." Science 284(5411): 143-147.

Ploeger, D. T., N. A. Hosper, et al. (2013). "Cell plasticity in wound healing: paracrine factors of M1/ M2 polarized macrophages influence the phenotypical state of dermal fibroblasts." Cell communication and signaling : CCS 11(1): 29.

Potier, E., E. Ferreira, et al. (2007). "Hypoxia affects mesenchymal stromal cell osteogenic differentiation and angiogenic factor expression." Bone 40(4): 1078-1087.

Powell, R. J., A. J. Comerota, et al. (2011). "Interim analysis results from the RESTORE-CLI, a randomized, double-blind multicenter phase II trial comparing expanded autologous bone marrow-derived tissue repair cells and placebo in patients with critical limb ischemia." Journal of vascular surgery 54(4): 1032-1041.

Razban, V., A. S. Lotfi, et al. (2012). "HIF-1alpha Overexpression Induces Angiogenesis in Mesenchymal Stem Cells." BioResearch open access 1(4): 174-183.

Ren, H., Y. Cao, et al. (2006). "Proliferation and differentiation of bone marrow stromal cells under hypoxic conditions." Biochemical and biophysical research communications 347(1): 12-21.

Ricles, L. M., S. Y. Nam, et al. (2011). "Function of mesenchymal stem cells following loading of gold nanotracers." International journal of nanomedicine 6: 407-416.

Robbins, S. L., V. Kumar, et al. (2010). Robbins and Cotran pathologic basis of disease. Philadelphia, PA, Saunders/Elsevier.

Robey, T. E., M. K. Saiget, et al. (2008). "Systems approaches to preventing transplanted cell death in cardiac repair." Journal of molecular and cellular cardiology 45(4): 567-581.

Roemeling-van Rhijn, M., F. K. Mensah, et al. (2013). "Effects of Hypoxia on the Immunomodulatory Properties of Adipose Tissue-Derived Mesenchymal Stem cells." Frontiers in immunology 4: 203.

Rundhaug, J. E. (2005). "Matrix metalloproteinases and angiogenesis." Journal of Cellular and Molecular Medicine 9(2): 267-285.

Sahni, A. and C. W. Francis (2000). "Vascular endothelial growth factor binds to fibrinogen and fibrin and stimulates endothelial cell proliferation." Blood 96(12): 3772-3778.

Saito, Y., K. Sasaki, et al. (2007). "Effect of autologous bone-marrow cell transplantation on ischemic ulcer in patients with Buerger's disease." Circulation journal : official journal of the Japanese Circulation Society 71(8): 1187-1192.

Schroeder, T. (2008). "Imaging stem-cell-driven regeneration in mammals." Nature 453(7193): 345-351.

Shaikh, F. M., A. Callanan, et al. (2008). "Fibrin: a natural biodegradable scaffold in vascular tissue engineering." Cells Tissues Organs 188(4): 333-346.

Sheikh, A. and J. Wu (2006). "Molecular Imaging of Cardiac Stem Cell Transplantation." Current Cardiology Reports 8(2): 147-154.

Siphanto, R. I., K. K. Thumma, et al. (2005). "Serial noninvasive photoacoustic imaging of neovascularization in tumor angiogenesis." Optics express 13(1): 89-95.

Skala, M. C., M. J. Crow, et al. (2008). "Photothermal optical coherence tomography of epidermal growth factor receptor in live cells using immunotargeted gold nanospheres." Nano letters 8(10): 3461-3467.

So, M. K., C. Xu, et al. (2006). "Self-illuminating quantum dot conjugates for in vivo imaging." Nat Biotechnol 24(3): 339-343.

Sokolov, K., M. Follen, et al. (2003). "Real-time vital optical imaging of precancer using anti-epidermal growth factor receptor antibodies conjugated to gold nanoparticles." Cancer research 63(9): 1999-2004.

Solanki, A., J. Kim, et al. (2008). "Nanotechnology for Regenerative Medicine: Nanomaterials for Stem Cell Imaging." Nanomedicine 3(4): 567-578.

Spiller, K. L., R. R. Anfang, et al. (2014). "The role of macrophage phenotype in vascularization of tissue engineering scaffolds." Biomaterials 35(15): 4477-4488.

Stober, W., A. Fink, et al. (1968). "Controlled Growth of Monodisperse Silica Spheres in Micron Size Range." Journal of Colloid and Interface Science 26(1): 62-&.

Stowers, R. S., C. T. Drinnan, et al. (2013). "Mesenchymal stem cell response to TGF-beta 1 in both 2D and 3D environments." Biomaterials Science 1(8): 860-869.

Suga, H., J. Glotzbach, et al. (2014). "Paracrine mechanism of angiogenesis in adipose-derived stem cell transplantation." Annals of Plastic Surgery 72(2): 234-241.

Suh, J. S., J. Y. Lee, et al. (2009). "Efficient labeling of mesenchymal stem cells using cell permeable magnetic nanoparticles." Biochemical and Biophysical Research Communications 379(3): 669-675.

Sunderkotter, C., K. Steinbrink, et al. (1994). "Macrophages and angiogenesis." Journal of Leukocyte Biology 55(3): 410-422.

Swirski, F. K. and M. Nahrendorf (2013). "Macrophage-stem cell crosstalk after myocardial infarction." Journal of the American College of Cardiology 62(20): 1902-1904.

Taghavi, S., J. M. Duran, et al. (2011). "Stem cell therapy for peripheral arterial disease: a review of clinical trials." Stem Cell Studies 1(e17): 105-114.

Tang, G. L., D. S. Chang, et al. (2005). "The effect of gradual or acute arterial occlusion on skeletal muscle blood flow, arteriogenesis, and inflammation in rat hindlimb ischemia." Journal of vascular surgery 41(2): 312-320.

Taylor, P. M. (2007). "Biological matrices and bionanotechnology." Philosophical transactions of the Royal Society of London. Series B, Biological sciences 362(1484): 1313-1320.

Tidball, J. G. (2005). "Inflammatory processes in muscle injury and repair." American journal of physiology. Regulatory, integrative and comparative physiology 288(2): R345-353.

Toma, C., M. F. Pittenger, et al. (2002). "Human mesenchymal stem cells differentiate to a cardiomyocyte phenotype in the adult murine heart." Circulation 105(1): 93-98.

Tsai, C. C., Y. J. Chen, et al. (2011). "Hypoxia inhibits senescence and maintains mesenchymal stem cell properties through down-regulation of E2A-p21 by HIF-TWIST." Blood 117(2): 459-469.

Valarmathi, M. T., J. M. Davis, et al. (2009). "A three-dimensional model of vasculogenesis." Biomaterials 30(6): 1098-1112.

van Laake, L. W., R. Passier, et al. (2007). "Human embryonic stem cell-derived cardiomyocytes survive and mature in the mouse heart and transiently improve function after myocardial infarction." Stem cell research 1(1): 9-24.

Vu, T. H., J. M. Shipley, et al. (1998). "MMP-9/gelatinase B is a key regulator of growth plate angiogenesis and apoptosis of hypertrophic chondrocytes." Cell 93(3): 411-422.

Walkey, C. D., J. B. Olsen, et al. (2012). "Nanoparticle size and surface chemistry determine serum protein adsorption and macrophage uptake." Journal of the American Chemical Society 134(4): 2139-2147.

Walter, D. H., H. Krankenberg, et al. (2011). "Intraarterial administration of bone marrow mononuclear cells in patients with critical limb ischemia: a randomized-start, placebo-controlled pilot trial (PROVASA)." Circulation. Cardiovascular interventions 4(1): 26-37.

Wang, B., E. Yantsen, et al. (2009). "Plasmonic intravascular photoacoustic imaging for detection of macrophages in atherosclerotic plaques." Nano letters 9(6): 2212-2217.

Wang, L., Z. G. Zhang, et al. (2006). "Matrix metalloproteinase 2 (MMP2) and MMP9 secreted by erythropoietin-activated endothelial cells promote neural progenitor cell migration." Journal of Neuroscience 26(22): 5996-6003.

Wang, L. V. and S. Hu (2012). "Photoacoustic tomography: in vivo imaging from organelles to organs." Science 335(6075): 1458-1462.

Waters, R. E., R. L. Terjung, et al. (2004). "Preclinical models of human peripheral arterial occlusive disease: implications for investigation of therapeutic agents." J Appl Physiol 97(2): 773-780.

Wynn, T. A., A. Chawla, et al. (2013). "Macrophage biology in development, homeostasis and disease." Nature 496(7446): 445-455.

Xing, Z., J. Gauldie, et al. (1998). "IL-6 is an antiinflammatory cytokine required for controlling local or systemic acute inflammatory responses." The Journal of clinical investigation 101(2): 311-320.

Xiong, T., Z. Zhang, et al. (2005). "In vivo optical imaging of human adenoid cystic carcinoma cell metastasis." Oral oncology 41(7): 709-715.

Xu, M. and L. Wang (2006). "Photoacoustic imaging in biomedicine." Review of Scientific Instruments 77(4): 041101.

Yang, D., W. Wang, et al. (2013). "The relative contribution of paracine effect versus direct differentiation on adipose-derived stem cell transplantation mediated cardiac repair." Plos One 8(3): e59020.

Yang, H., S. T. Lopina, et al. (2008). "Stealth dendrimers for drug delivery: correlation between PEGylation, cytocompatibility, and drug payload." Journal of materials science. Materials in medicine 19(5): 1991-1997.

Yang, Z., M. W. von Ballmoos, et al. (2009). "Call for a reference model of chronic hind limb ischemia to investigate therapeutic angiogenesis." Vascular pharmacology 51(4): 268-274.

Yeghiazarians, Y., Y. Zhang, et al. (2009). "Injection of bone marrow cell extract into infarcted hearts results in functional improvement comparable to intact cell therapy." Molecular therapy : the journal of the American Society of Gene Therapy 17(7): 1250-1256.

Yu, J., S. Yin, et al. (2013). "Hypoxia preconditioned bone marrow mesenchymal stem cells promote liver regeneration in a rat massive hepatectomy model." Stem cell research & therapy 4(4): 83.

Zhai, W., C. He, et al. (2012). "Degradation of hollow mesoporous silica nanoparticles in human umbilical vein endothelial cells." Journal of biomedical materials research. Part B, Applied biomaterials 100(5): 1397-1403.

Zhang, G., C. T. Drinnan, et al. (2010). "Vascular differentiation of bone marrow stem cells is directed by a tunable three-dimensional matrix." Acta Biomater 6(9): 3395-3403.

Zhang, G., Q. Hu, et al. (2008). "Enhancing efficacy of stem cell transplantation to the heart with a PEGylated fibrin biomatrix." Tissue engineering. Part A 14(6): 1025-1036.

Zhang, G., X. Wang, et al. (2006). "A PEGylated fibrin patch for mesenchymal stem cell delivery." Tissue Engineering 12(1): 9-19.

Zhang, L., Y. Wang, et al. (2014). "CKIP-1 regulates macrophage proliferation by inhibiting TRAF6-mediated Akt activation." Cell research 24(6): 742-761.

Zhang, M., D. Methot, et al. (2001). "Cardiomyocyte grafting for cardiac repair: Graft cell death and anti-death strategies." Journal of Molecular and Cellular Cardiology 33(5): 907-921.

Zhang, Y., S. Thorn, et al. (2008). "Collagen-based matrices improve the delivery of transplanted circulating progenitor cells: development and demonstration by ex vivo radionuclide cell labeling and in vivo tracking with positron-emission tomography." Circulation. Cardiovascular imaging 1(3): 197-204.

Ziady, A. G., C. R. Gedeon, et al. (2003). "Minimal toxicity of stabilized compacted DNA nanoparticles in the murine lung." Molecular therapy : the journal of the American Society of Gene Therapy 8(6): 948-956.

Zwezdaryk, K. J., S. B. Coffelt, et al. (2007). "Erythropoietin, a hypoxia-regulated factor, elicits a pro-angiogenic program in human mesenchymal stem cells." Experimental hematology 35(4): 640-652.

Vita

Laura Michelle Ricles was born in Berkeley, California. She graduated from Liberty High School in Bethlehem, Pennsylvania in 2005. In May 2009 she graduated with highest honors from Lehigh University with a Bachelor of Science in bioengineering and a minor in business. She entered graduate school in the fall of 2009 at The University of Texas at Austin, where she joined Dr. Laura Suggs' Laboratory for Cardiovascular Tissue Engineering and Dr. Stanislav Emelianov's Ultrasound Imaging and Therapeutics Research Laboratory in the Department of Biomedical Engineering. During her graduate career, Laura was awarded a National Science Foundation Graduate Research Fellowship. Her research focused on the evaluation of stem cell therapy for cardiovascular diseases and incorporated the use of tissue engineering, regenerative medicine, and nanotechnology.

Permanent email address: laura.ricles@utexas.edu

This dissertation was typed by the author.